UNIVERSIDADE DE LISBOA
INSTITUTO SUPERIOR TÉCNICO

Integrated Modelling for Water Management in Reservoirs and Watersheds

David Armando Costa Brito

Supervisor: Doctor Ramiro Joaquim de Jesus Neves

Thesis approved in public session to obtain the PhD Degree in Environmental Engineering

Jury final classification: Pass with Distinction

Jury

Chairperson: Doctor António Jorge Gonçalves de Sousa, Instituto Superior Técnico, Universidade de Lisboa

Members of the Committee:

Doctor Luís Filipe Tavares Ribeiro, Instituto Superior Técnico, Universidade de Lisboa

Doctor Ramiro Joaquim de Jesus Neves, Instituto Superior Técnico, Universidade de Lisboa

Doctor Pedro Manuel Hora Santos Coelho, Faculdade de Ciências e Tecnologia, Universidade Nova de Lisboa

Doctor Rodrigo de Almada Cardoso Proença de Oliveira, Instituto Superior Técnico, Universidade de Lisboa

Doctor Rui José Raposo Rodrigues, Laboratório Nacional de Engenharia Civil

2017

Para a Beatriz

Abstract

Historically, numerical model development was always in the forefront of computer power increase, being able to overcome previous limitations in the physics (reducing numerical simplifications) and in the spatial extent (increasing number of computation points) of the problem to solve.

The developments achieved made possible to represent with high detail: i) complex aquifer dynamics, ii) river expansion and contraction, iii) surface water flooding including urban areas, iv) crop growth cycle management, v) biological and chemical driven processes (trophic networks, organic matter processes, soil salinization, soil nutrients sortion-dessortion, etc.).

However, most of the time, the complex numerical models in one field of study rely on assumptions in boundary conditions from other fields (e.g. infiltration, aquifer recharge, river inflows, lateral groundwater inflows, urban drainage inflows and outflows, etc.

The thesis hypothesis is that integrated state-of-the art approaches can solve this problem by combining in one numerical framework the best knowledge of each area describing the main processes and explicitly describing the fluxes between mediums not having to make assumptions in boundary conditions.

The thesis objectives are to i) show integration examples suited to solve specific environmental problems that verify the hypothesis and ii) integrate the best knowledge in each field of study in a state-of-the-art open source framework to be able to continuously improve with time.

Such a system is being developed in MOHID framework with MOHID Land, a distributed, physically based, variable time step model that solves mass and momentum conservation equations in integral form applying to finite volumes, including 2D surface runoff an 1D river network solving St. Venant Equations, 3D ground water flow solving Richards equation both in saturated and non saturated media. This model integrates in his structure state-of-the-art coupling with SWAT crop growth model, RZWQM biological driven and PHREEQC chemical driven soil dynamics, and river/reservoir water quality models from WASP, CE-QUAL-W2 and ERSEM models.

In the thesis several examples are presented to test the hypothesis that the integration approach works and is consistent in 3 different scales: i) micro scale of urban watershed in Póvoa de Santa Iria using MOHID Land and SWMM models coupled in real time to manage urban floods; ii) small scale in super eutrophic reservoir Enxoé using SWAT, MOHID Land and CE-QUAL-W2 models (coupled offline) to represent actual situation and test management scenarios and iii) large scale in Iberia Peninsula to forecast conditions for estuary and coastal models to improve forecasted fresh water inputs that can impact local circulations and water quality.

The articles presented showed that the integration approach was core to i) represent Enxoé long-term and short-term processes that have both influence the reservoir dynamics; ii) represent surface water-drainage system interactions that influence hydraulic behaviour and originated floods in Póvoa e Santa Iria and iii) represent best forecast conditions to coastal areas that take into consideration all hydrology and biogeochemical interactions in upstream watersheds.

The work presented here built the backbone of a state-of-the-art numerical system that has the main processes associated to hydrology, hydraulics, soil and river water quality (biological and chemical driven) and it has the potential to be a starting point for future fine-tuning and validation that can result in several research projects and PhD thesis.

Keywords: watershed, reservoir, integrated modelling, MOHID Land, water management.

Resumo

Historicamente, o desenvolvimento de modelo numérico tem estado na vanguarda do aumento da capacidade de computação, sendo capaz de superar as limitações impostas na física (reduzindo as simplificações numéricas) e na extensão espacial (aumentando o número de pontos de cálculo) do problema a resolver.

Os desenvolvimentos alcançados tornaram possível representar com elevado detalhe: i) a complexa dinâmica dos aquíferos, ii) a expansão e contração da rede de drenagem natural, iii) inundações, incluindo em áreas urbanas, iv) gestão do ciclo das culturas agrícolas, v) processos biológicos e químicos (redes tróficas, processos associados à matéria orgânica, salinização do solo, nutrientes do solo, adsorção e dessorção, etc.).

No entanto, na maioria das vezes, os modelos numéricos complexos num campo de estudo dependem de suposições nas condições de fronteira de outras áreas (por exemplo, a infiltração, recarga do aquífero, caudais superficial e subterrâneo afluente aos rios, entradas e saídas das redes de drenagem artificias, etc.

A hipótese da tese é que as abordagens estado-da-arte integradas podem resolver problemas ambientais complexos e o "problema da condição de fronteira" através da combinação numa estrutura numérica do melhor conhecimento de cada área que descreva os principais processos e explicitamente os fluxos entre os meios e não tendo que fazer suposições nas condições de fronteira.

Os objetivos da tese são i) mostrar exemplos de integração adequados para resolver os problemas ambientais específicos e ii) integrar o melhor conhecimento em cada área de estudo numa estrutura estado-da-arte e de código aberto para ser capaz de melhorar continuamente com o tempo.

Esse sistema está a ser desenvolvido na estrutura MOHID com o MOHID Land, um modelo distribuído, de base física, com passo de tempo variável que resolve equações de conservação de massa e momento na forma integral aplicada a volumes finitos, incluindo o escoamento superficial em 2D e uma rede fluvial 1D resolvendo as equações de St. Venant, escoamento subterrâneo 3D resolvendo a equação de Richards tanto em meio saturado como não saturado. Este modelo integra na sua estrutura o acoplamento estado-da-arte com o modelo de

crescimento de vegetação do modelo SWAT, as reações biológicas no solo do modelo RZWQM e reações químicas do modelo PHREEQC, e os modelos de qualidade da água do rio / reservatório do modelo WASP, CE-QUAL-W2 e ERSEM.

Na tese vários exemplos são apresentados para testar a hipótese de que a abordagem de integração funciona e é consistente em 3 escalas diferentes: i) micro escala de bacia urbana na Póvoa de Santa Iria utilizando o modelo MOHID Land e modelo SWMM acoplado em tempo real para gerir inundações urbanas; ii) de pequena escala no reservatório super-eutrófico Enxoé utilizando os modelos SWAT, MOHID Land e CE-QUAL-W2 (acoplamento off-line) para representar a situação atual e testar cenários de gestão, e iii) grande escala na Península Ibérica para prever condições de fronteira nos modelos de estuário e modelos costeiros de modo a melhorar as previsões das afluências que podem afetar as circulações locais e qualidade da água.

Os artigos apresentados mostraram que a abordagem de integração foi fundamental para i) representar os processos de curto e longo prazo no Enxoé que influenciam a dinâmica do reservatório; ii) representar as interações entre a rede de drenagem natural e a do sistema de drenagem urbano que influenciam o comportamento hidráulico e originaram inundações na Póvoa de Santa Iria e iii) representar as condições de previsão mais completas para as zonas costeiras que têm em consideração a hidrologia e interações biogeoquímicas nas bacias hidrográficas a montante.

O trabalho apresentado aqui construiu a espinha dorsal de um sistema numérico estado-da-arte que resolve os principais processos associados à hidrologia, hidráulica, qualidade da água no solo e na água superficial (com origem biológica e/ou química) e tem o potencial para ser um ponto de partida para futura afinação e validação, que pode resultar em vários projetos de investigação e teses de doutoramento.

Palavras-chave: bacia hidrográfica, albufeira, modelação integrada, MOHID Land, gestão da água.

Contents

List of Figures

List of Tables

1 Introduction

1.1 Context and thesis structure

The candidate finished is graduation in Environmental Engineering in 2005 with his dissertation at Maretec – Tecnologias Marítimas from Instituto Superior Técnico (IST), in modelling wind waves in Tagus Estuary and its effect on sediment resuspension. He started working as a researcher at the same group in the same year in a new field, modelling fresh water hydrodynamics, by developing also a “fresh” model, MOHID Land. From 2005 to 2014, he participated in several national and European research projects that allowed him to implement and develop several watershed and reservoirs models, contributing at the end to the knowledge included in his MOHID Land developments. In 2014, he started working in an IST spin-off named Action Modulers where still maintained the development of MOHID models and turned to delivering cutting-edge modelling web and desktop Graphical User Interfaces. The present thesis is the combination of work developed in both workplaces (3 articles from IST and 1 from Action Modulers) and that will carry on in to the future.

The thesis presents the following structure:

- Chapter 1– Introduction chapters developing the rationale, the hypothesis driven from the rationale and the objectives proposed.
- Chapter 2 – Describing the methodology and materials used to test the hypothesis.
- Chapter 3 - Application Articles where the hypothesis are tested.
- Chapter 4 – Presenting a description of candidate work on MOHID Land models and in the above application articles.
- Chapter 5 – Conclusions from the articles, revisiting hypothesis and thesis possible reach and recommendations.

Next chapter will start to create the context on watershed integrated modelling, the state-of-the-art and the opportunities found that are the basis for the thesis hypothesis and objectives.

1.2 State of the art

Water quantity and quality problems in the past decades have followed the increasingly anthropogenic pressures on growing urban areas and agriculture automation (increasing production with fertilizer and pesticide applications). Concentrated pressures in inland waters and increased water demand (for consumption and irrigation) took to over exploration of fresh water wells and the construction of artificial reservoirs (EEA, 2009) close to the demand (high pressure areas) increasing water quality degradation risk.

With the increasing pressure on water bodies (coastal areas, reservoirs, rivers) water quantity and quality started to be an issue and the origin of the problem in the fresh water part of the water cycle (that generates the loads to the water bodies) was thoroughly studied. In fact water and property transport in the land part of the cycle became in the last years an object of study related mainly to eutrophication, aquifer contamination, irrigation and soil salinization, river and water mass quality assessment, following European Union directions as Nitrates Directive, WWTP Directive, Water Framework Directive, etc.

Because of the complexity of the analysis in terms of water transport in the watershed (perennial or temporary surface flow in rivers, irregular surface flow in runoff, saturated and unsaturated flow in porous media) and in nutrient/contaminant cycles (fertilization, aquifer contamination, point sources discharges, biological mineralization of organic matter, primary production), ended with the problems being studied by separate teams and in separate mediums. As so, hydrologists and biologists focused their study in the river, hydro geologists specialized in aquifers and in unsaturated flow, biologists looked also for soil activity, agronomists studied crop cycles and agricultural practices, etc.

The need to solve water quantity and quality problems and the increased computational capacity, led to the development of mathematical models capable of describing the main processes affecting water and nutrient/contaminants transport/transformation. While hydrology and water quality studies were carried at least centuries ago (e.g. Perrault description on water cycle and Streeter–Phelps equation for dissolved oxygen), taking into account the development of computational capacity, first mature numerical models for watershed appeared in the 50's - 60´s making the focus on water - the called rainfall-runoff modelling – (Donigian and Imhoff, 2002), and in the 70´s water quality has started to be integrated at the same scale, focusing in the soil loss and nutrient and pesticide export to the river (Horn et al. 2004).

Model development followed the team's field of study specialization, encountering different degrees of detail on each process depending on the focus of the teams work. Examples of models developed to study mainly water and property leaching from soil are Hydrus (Šimůnek et al. 2008) and RZWQM (Ma et al., 2000). These models are plot scale models for soil (farm scale), from USDA laboratories that focus on soil water and solute leaching (e.g. from agriculture practices) including detailed biologic and chemical property transformation. Hydrus hydraulics and water quality model reflects the team knowledge on soil water movement, salinization and cation exchange capacity (e.g. Ramos et al., 2011, Grünberger et al., 2008). While in Hydrus, crop or vegetation growth are not explicitly simulated, RZWQM, focuses more on crop and agricultural practices effect on solute and agro-chemical leaching, simulating explicitly crop growth and agricultural practices incorporating the group knowledge mainly about corn, soybean, maize and wheat cycles (e.g. Cameira et al., 2007, Ma et al., 2006)

The increasing complexity of soil water utilizations beside crop growth (including pumping or hazard material disposal) led to the developments of detailed 3D models describing aquifer and unsaturated media and interactions with solute transport as Modflow (Harbaugh et al., 2000). Modflow is a USGS 3D groundwater flow model within confined/unconfined aquifer including effect of water drainage, wells and river drainage. It is a widespread very detailed model for aquifer areas and the inputs from surface or river boundary conditions (aquifer vertical and lateral fluxes) have to be defined (e.g. by other models).

The complexity of the fresh water problems integrating human activities (crop management, point sources), soil water and surface water led to the development of integrated models for the watershed scale. As an example SWAT (Neitsch et al., 2005) model is a semi-distributed watershed model focused on land management at reach or basin scale in which a big effort and knowledge was putted in the crop database (with growth parameters of around 100 species) and vegetation growth model both developed under the knowledge of the Grassland laboratory in USDA. SWAT model divides the watershed into subareas that are assumed to be homogeneous in their hydrologic response (Hydrologic Response Units), uses a daily time step and infiltration or groundwater flow is computed based on empiric or semi-empiric formulations (as the SCS rainfall-runoff curves or soil-shallow aquifer-river transfer times). The relative straightforward formulation allows the model to produce in reasonable time (minutes or hours) simulations of decades in large watersheds (up to 10 000 Km^2 – e.g. Jayakrishnan et al. 2005).

On the other end, some watershed models were developed suited specifically to events with small time steps in order to simulate floods and usually suspended solids transport as ANSWERS (Beasley & Huggins, 1982). This type of models focus is usually in small flashy regime watersheds where a large percentage of annual material exported (suspended sediment, organic matter, nutrients) to downstream water bodies may be transported in a few episodic floods and usually only simulate short events.

With the increasing computational capacity and numerical modelling knowledge, in the last decade, physically based, distributed and continuous models at a watershed scale were able to compete (in computation time) with the empirical or lumped formulations. MIKE SHE (Refsgaard and Storm, 2005) from Dutch Hydraulic Institute and SHETRAN (Ewen et al., 2000) from Newcastle University have the same common origin from SHE (Systém Hydrologyque Europeen) and are a reference in a generation of physically based, integrated, distributed watershed models. SHETRAN and MIKE SHE use a continuity approach between mediums (surface water, sub-surface, and aquifer), a grid for spatial discretization and physically driven equations (St. Venant's equations for surface flow, Richards equation for groundwater) as MOHID Land, but the spatial method to solve equations is finite differences in these models and finite volumes in MOHID Land. MIKE Flood is a commercial package using existing Danish Hydraulic Institute (DHI) 1D river MIKE Hydro River and 2D overland flow MIKE 21 where also full St. Venant equations are solved, using finite differences (DHI, 2007). Similar approach is followed by Delft3D model (from Deltares) that although is widely used in coastal areas, is also applied for flood studies making use of St. Venant equations with finite differences.

On urban drainage systems, one of the most widely used, open-source urban drainage system model is SWMM (Storm Water Management Model from US Environment Protection Agency described in Rossman 2016) that solves both hydrology (simple sub-watersheds volume model to estimate inputs to drainage system) and hydraulics in a complex system of pipes, channels, storage/treatment devices, pumps, and regulators. The model can solve the complete St. Venant equations for free surface and pressurized gravity driven flow. MIKE Urban is a commercial package using existing DHI MOUSE and MIKE 1D where also complete St Venant equations are used. This type of models need the explicit definition of watershed boundary conditions (lateral and drainage inflow) and usually are solved in a simplistic manner (e.g. SWMM with Curve Number or Green-Ampt for the watershed infiltration) or need the link to other models that increases complexity for the end-user.

Models evolved in specific fields of study and in general have a big degree of complexity in the field subject of their developers but lack integration in other components, leading to either being lumped in space (need the definition of boundary conditions), limited in time (small time steps suited only for events or big time steps that filter sub-hourly processes), or simplified in some processes (empirical or semi-empirically formulations). Moreover, finite volumes (as used by

MOHID Land), in the past years have been the dominating approach for discretization of the equations (in opposition to finite differences for instance used by SHE, MIKE or Delft3D) because of its greater geometric flexibility, and the way it more easily lends itself to error analysis (Thomee, 2001). Finite volumes applies integral form of conservation equation integrated to control volumes where the integral of the divergence is the integral of a flux over the boundary (control volume flux can be computed by the fluxes through its surfaces) while finite differences considers infinitesimal volumes. The finite volumes approach assures mass conservations and is easier to interpret and troubleshoot which is one of the advantages of MOHID Land in relation to similar software, in an open-source perspective, where a wide range of developers explore, edit and debug the model. The open-source approach followed by MOHID Land is advantageous to users/developers that can use it as a learning tool, adapt it to its needs and contribute to/benefit from the community new developments and advantageous to the model itself since is tested, validated and spread to a higher audience than the original developers.

MOHID Land is a physically based, distributed, continuous, with variable time step model that tries to take advantage of the effort and knowledge brought to light by the previous modelling work and overcome some of the gaps found, producing a physically based formulation that can be applied to study water and property transport (e.g. nutrients, pesticides, other contaminants, etc.) from plot scales to complete complex watersheds and from events (hourly or sub-hourly processes) to yearly time scales (variable time step) maintaining mass conservation. For urban drainage systems that are not described by the model, MOHID Land can be dynamically linked to SWMM model in order to provide high detail surface interaction (inflows to sewer system by street gutter and manhole outflows routing on surface that can eventually be an inflow downstream).

MOHID Land is a product of the integration of the knowledge in several areas from water transport (surface and groundwater, evapotranspiration), property transport and transformation (numerical methods, chemical and biological reactions,

erosion/deposition, vegetation growth), and its modular structure allows the readily coupling to other formulations without changing previous code.
MOHID Land is an open source model[1] under development and users are suggested to do implementation/validation but also invited for code developing, coupling models that are needed for a specific purpose, and making it more suitable for a wider range of applications.

The opportunities found in literature review, lacking mature open-source full integrated frameworks to respond to complex hydrodynamics and water quality problems, driven the current thesis and carved its hypothesis and objectives, that are defined next.

1.3 Hypothesis and Objectives

As described in previous chapter, the complex behaviour and interactions between surface, sub-surface and groundwater fluxes in watersheds and waterbodies, with biogeochemical cycles and urban interaction with natural systems, suggests that:

- the integrated modelling approach using the capabilities of several state-of-the art formulations is suited to describe/quantify the actual state of such complex systems and to produce useful water quality management scenarios.
- the integration of such complex formulations in a single, open-source modelling framework is possible without the need to simplify processes or linkage between domains of study. In addition, it should continuously evolve with new processes and computational technologies in an open community.

In order to test the hypothesis, the objectives of the thesis are:

---
[1] https://github.com/Mohid-Water-Modelling-System

- Integrate several models or components, offline or online, to solve complex watershed/reservoir environmental problems and provide useful management solutions to water quantity and quality.
- Develop an open-source mathematical model framework that can integrate all the created state-of-the-art knowledge about watershed hydrology and water quality processes (MOHID Land) that will be able to continuously improve with time in an open-source philosophy.

The models and modelling methodology to answer how to fulfil the thesis objectives are presented next.

2 Material & Methods

This chapter describes first the main modelling approach followed by the thesis and since MOHID Land model is not fully described in its several components in bibliography (detailed description exists for the river model, Trancoso et al., 2009), the next chapters will give a general insight of the main processes and main equations used.

This chapter will also cover a general succinct description of other numerical models and field data used in the thesis.

2.1 Approach

The current thesis describes the implementation of several numerical models to describe different components of the complex natural system and tries to focus on the creation of an integrated numerical framework that gathers the state-of-the-art knowledge on all these fields of study. This tool is MOHID Land model: a tool not as an ending point but a starting one, with the main backbone of hydrological and water quality processes, with minimized boundary conditions assumptions, open for improvement.

One key aspect for integrated modelling is related to field data integration since field data give insights to processes description and verify model accuracy, models on the other hand, fill field data and knowledge gaps and give insights on best field data effort, and so on. However, the focus of the thesis is on model integration and MOHID Land model development under that scope.

With that in mind, five modelling applications were selected to verify the hypothesis about the advantage of the integration capability and ultimately to provide knowledge for MOHID Land developments (Table 1).

One application (Chapter 0) shows the integration of MOHID Land model that describe surface water (rivers, streams and runoff) with SWMM model that describe drainage systems (domestic and pluvial) in a online fashion (running simultaneously) to depict the cause of urban floods and test management scenarios to reduce them. This is small-scale (watersheds around 1 km^2) urban watershed where flow changes are of the order of minutes and concentration times are lower than 1 hour. This example shows the need for an integrated approach since in flooding situation, surface water routed on streets influences hydraulic pressure on the urban system and outflow from manholes can be routed in surface and create an inflow to the urban system elsewhere (via street gutters) that can cause flood underestimations if the urban system model is run standalone. MOHID Land was developed for the scope of urban implementations to be OpenMI compliant (able to be linked with other OpenMI compliant models) and to prepare for SWMM linkage (e.g. computes total inflow to sewer system and receives outflow from it to be routed on surface). This application allowed to test the model performance against high frequency field data (usually not available in public field data repositories or difficult to support via research projects) but is needed to evaluate model ability to simulate very fast flood progression.

Three applications (Chapter 3.1, 0 and 0) show the modelling integration approach with different models (SWAT, MOHID Land and CE-QUAL-W2) to depict the origin of Enxoé reservoir highest trophic state in Portugal where the watershed is small with extensive agriculture and no important point sources (usually these constraints do not pose water quality problems). The first application with SWAT model tries to estimate the watershed input loads to the reservoir in a 30-year period to depict the average annual order of magnitude of nutrient loads to the reservoir. Since Enxoé floods occur in sub-daily intervals (couple of hours) and SWAT uses a daily time step, also MOHID Land model was applied for identifying the flood role on nutrient loads. At the time, MOHID Land property transport and water quality processes were in development, so only the hydrodynamics part was used, and nutrient loads were computed with both traditional and flood sampling data that was deployed specifically for the purpose (Enxoé was an ungauged watershed). Finally, CE-QUAL-W2 model was coupled with SWAT model (to receive input loads for the entire reservoir life) and MOHID Land model results were used to assess the order of the reservoir internal sediment phosphorus load. This is a small to medium size watershed with around 60 km^2 and where concentration times are of around a few hours, with intense flash floods. These examples show the value added of integrating several models where besides to represent the reservoir inputs allows to depict different time scale of the process and with cross validation, the causes for under/overestimations. The author experience with SWAT model implementation, made possible to develop MOHID Land vegetation module in the scope of this thesis, as it was adapted from SWAT.

The last application (Chapter 3.5) describes the MOHID Land operationalisation for Iberian Peninsula and Western Iberia, with not only hydrology but also water quality processes in soil and river and property transport in all mediums what represents the full model capabilities (partially developed during this thesis). Most of national rivers are unmonitored (or monitoring is not systematic) and the integrated impact of all river fresh water sources in the coastal area is still unknown. As so, the objective was to integrate the full water cycle both in land and in coastal areas, providing the best available forecast from inland and solve the river boundary condition problem for coastal models. This application simulates watersheds of the order of 100 000 km^2 (e.g. Douro and Tagus in Portugal and Spain and Ebro in Spain, etc.) and where concentration times are the order of days and results are compared to field data in Tagus and Mondego (highly reservoir managed vs low managed river). The integration is key for the costal model implementations since produces a dynamic forecast of inland inputs (e.g. during high flow season or just a local intense event) that is not described by climatological approaches. All of the MOHID Land developments described in this thesis (e.g. vegetation growth, property transport, property transformation in soil and river) were implemented in this application that is operational since 2010[2]

[2] http://forecast.maretec.org

Table 1 – Description of the main applications to verify the thesis hypothesis

Application /Chapter	Location	Problem to Solve	Watershed Scale	Temporal Scale	Integration Type	Why Integration needed	MOHID Land Benefit
3.4	Póvoa Santa Iria, 10km West from Lisbon	Urban Floods	~1km^2	Minutes	Watershed model (MOHID Land) and urban drainage model (SWMM) running at the same time and exchanging information in real-time	Urban drainage and surface water dynamics depend on each other (water floods out at manholes, routes in surface and flows in in gutters)	MOHID Land developments for OpenMI compliance and to SWMM linkage and hydrodynamics evaluated in flash urban floods with high frequency data.
3.1-3.3	Enxoé, 200km Southeast from Lisbon	Eutrophication	~100km^2	Hours	Watershed model (SWAT) and reservoir model (CE-QUAL-W2) linked offline.	Allows estimating input loads and to test management scenarios in the watershed and their impact on the reservoir.	MOHID Land coupled with SWAT vegetation model and hydrodynamics evaluated in flash natural floods with flood sampling.
3.5	Iberia Peninsula	River Influence on Coastal Zones	~100 000km^2	Days	Watershed model (MOHID Land) and coastal model (MOHI Water) as linked offline.	Need for dynamic boundary conditions in coastal models to predict fresh water impact in coastal systems	MOHID Land property transport and water quality developments and hydrodynamics and water quality evaluated for large scale with public monitoring network.

It was described above the thesis applications that try to verify the hypothesis. Below are described the tools used to implement those applications (models and field data). MOHID Land, a centre part of the thesis as knowledge aggregator, is described next in more detail, from a historic perspective, to how is structured and the equations used, type of inputs/outputs, etc.

2.2 MOHID Land model

2.2.1 MOHID Framework

In the early 80's MOHID model gave its first steps as 1D model applied in an Portuguese estuary called Sado (with forcing tide and river inflow) and evolved for 2D simulations in coastal areas (Neves, 1985). MOHID capabilities were successfully enlarged to Boussinesq waves (Silva, 1992), water quality (Portela, 1996), tridimensional flows (Martins, 2000), oil dispersion, plume dispersion, sediment transport and consolidation, producing a tool for modelling surface water bodies (MOHID Water) that was applied to large variety of scales and challenges (www.mohid.com).

In the early 00's with the release of the Water Framework Directive, an integrative perspective was thrown to the table and talking about water quality meant an integration effort to study water cycle from the raindrops up to the reservoirs/coastal bodies. In this framework MOHID Water started to be applied to freshwater reservoirs and MOHID Land gave its first steps starting with soil water dynamics in 3D (Chambel et. al., 2000) and on top of that runoff flow and river network dynamics were developed (Trancoso et. al., 2009) allowing the simulation of watershed water cycle in which Trancão catchment in Tagus estuary located in Portugal and the Vène River in the French Mediterranean coast (Obermann, 2007) are examples.

The MOHID Modelling System has been constructed using an object-oriented approach to facilitate integration of new processes and models. The numerical algorithms are based on the finite volume approach, a flux-driven strategy that facilitates the coupling of different processes and allows conservation of mass and momentum.

MOHID is programmed in ANSI FORTRAN 95, a language where object creation is not achieved by class instantiation but through module instantiation (Braunschweig et al., 2004). The modular and object-oriented approach of MOHID makes that further developments can take advantage of these existing modules, limiting the requirements for new coding (e.g. adding new formulations or new processes is easily scalable and easy to connect/disconnect via keywords, allowing user-friendly customization). This structure has allowed that contrasting fields as numerical analysis, hydrology, hydraulics, agronomy, civil engineering, biology, biogeochemistry be present in one single umbrella that is MOHID. And that will be able to continue to incorporate new features (new process, new technology).

2.2.2 MOHID Land Structure

MOHID Land is divided in 4 main compartments or mediums (atmosphere, porous media, surface land and river) and water moves through the mediums based on mass and momentum balance equations (Figure 1).

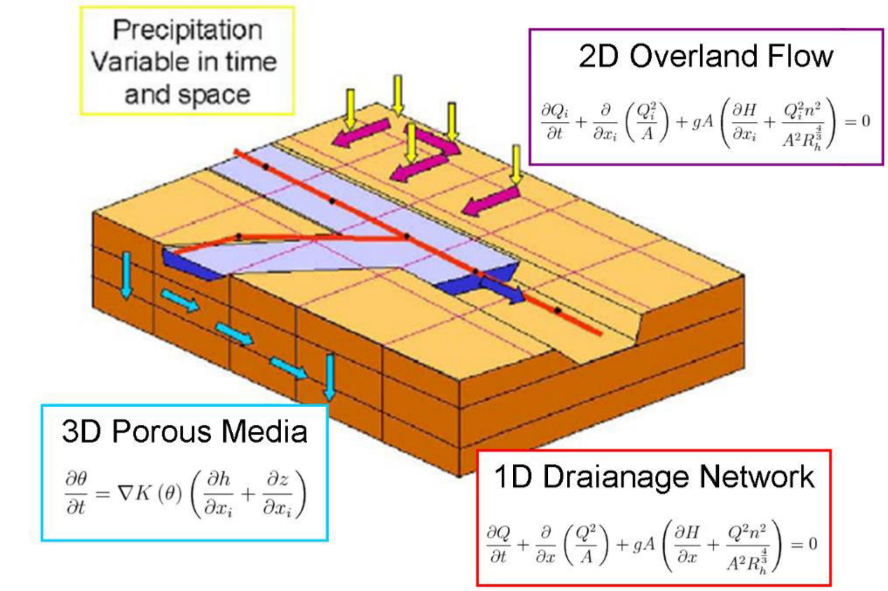

Figure 1 – MOHID Land compartments, fluxes and main equations – yellow for atmosphere and precipitation flux, blue for porous media, purple for surface runoff and red for drainage network.

The atmosphere is not explicitly simulated in MOHID Land but gives boundary conditions to the model (precipitation, solar radiation, wind, etc.) that can be space and time variant. Surface land is described by a 2D horizontal grid (may be constant or variable grid) based on digital elevation model (DTM). The porous media is a 3D domain with same horizontal grid as surface and vertical grid that may have constant or variable layer thickness, and river is a 1D domain that is defined from DTM and reaches exist between surface cell nodes (centres).

As understood from the above, the model uses a finite volume approach (control volume) for all the domain and state variables like water content, volume, property concentration are defined for the cell centre (assuming homogeneous concentration inside control volume) and velocities are defined for cell faces (assuming homogeneous velocity along the face of the control volume).

For each compartment exists two levels of computation modules: i) level 1 modules that solve water flow and ii) level 2 modules that manage properties (property transport using velocities from level 1 modules, and property transformation). Vegetation and Drainage Network have both water and properties computation. One module exists (Basin) to manage the information between modules (as an interface module) from different compartments and levels (Figure 2). Exists a third level of modules that do not depend on geometry (0D) to transform properties (organic matter mineralization, nitrification, denitrification, chemical reactions, phytoplankton trophic relations, etc.) and can be called by any of the modules that handle properties (level 2). 0D modules are transversal to MOHID framework and can be used by both MOHID Water and MOHID Land models.

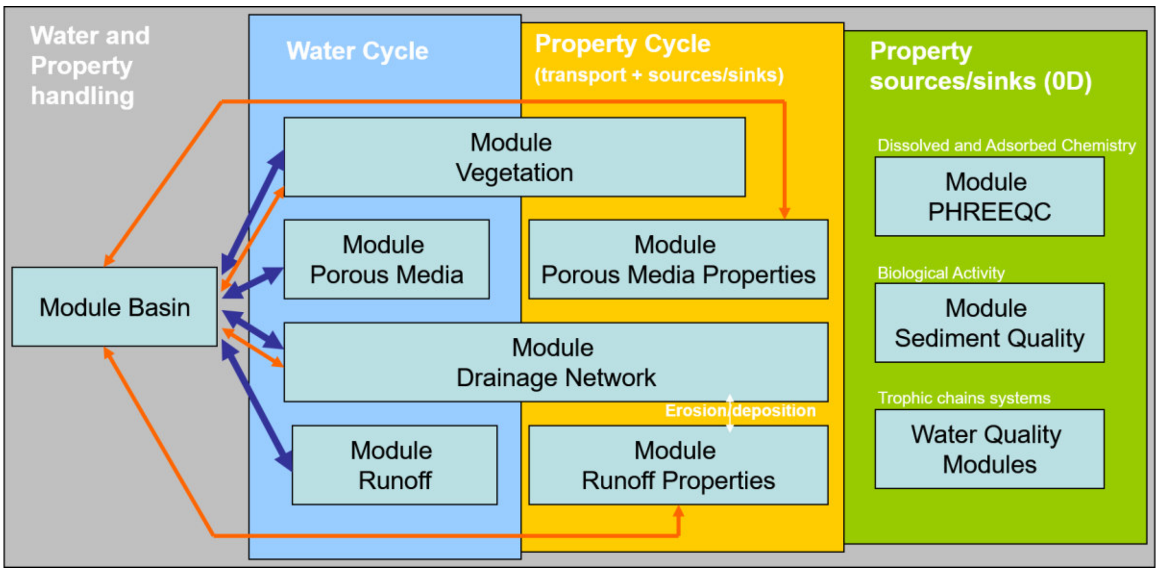

Figure 2 – MOHID Land module information fluxes in water balance (blue arrows) and property balance (orange arrows). In addition, 0D modules for property sources and sinks (controlled by property modules) are presented.

MOHID Land has introduced in MOHID framework the concept of variable time step since processes change rate is different if water passes through a porous media (velocities of the order of 1E-5 m/s or less), or in the order of units of cm/s or m/s when passing through land surface or river. As so, each compartment flow module has its own convergence iteration (until small volume variation is accomplished, local time step is reduced) and time step decreases when the rate of variation of water volume is high (usually during rain events) and increases when the change is small (during drought) and the lowest of the modules is the global model time step.

2.2.3 Governing Equations

It will be presented in next chapters the main equations for i) water transport; ii) properties transport.

All the equations are based in simple balance to a control volume where accumulation rate of one property β inside the volume is equal to the property flux balance (advection and diffusion) through the surfaces plus sources minus sinks of the property inside the volume (Equation 1):

$$\frac{d}{dt}\iiint(\beta)\,dvol + \iint(\beta\,(\vec{v}\cdot\vec{n}))\,dA = \iint(\gamma\,(\vec{\nabla}\beta\cdot\vec{n}))\,dA + [Sources - Sinks]$$

Equation 1 – Mass Conservation equation to one control volume for a generic property.

where β is any generic constituent (M/L^3), *v* is velocity (L/T), γ is diffusivity (L^2/T) and *n* the normal to the volume surface.

The generic property transported may be momentum (β is water density) or any given property (e.g. nitrate).

2.2.3.1 Water Cycle

The water cycle description will start in atmosphere with precipitation and leaf interception to define the water that reaches the ground. This initial infiltration column is used by Porous media (in conjunction with vegetation evapotranspiration) to simulate ground water flow and update effective infiltration. The remainder water in surface (if any) is routed in surface runoff. Both ground water and runoff fluxes with river are computed and added/extracted from river where finally the river flow is computed (Figure 3).

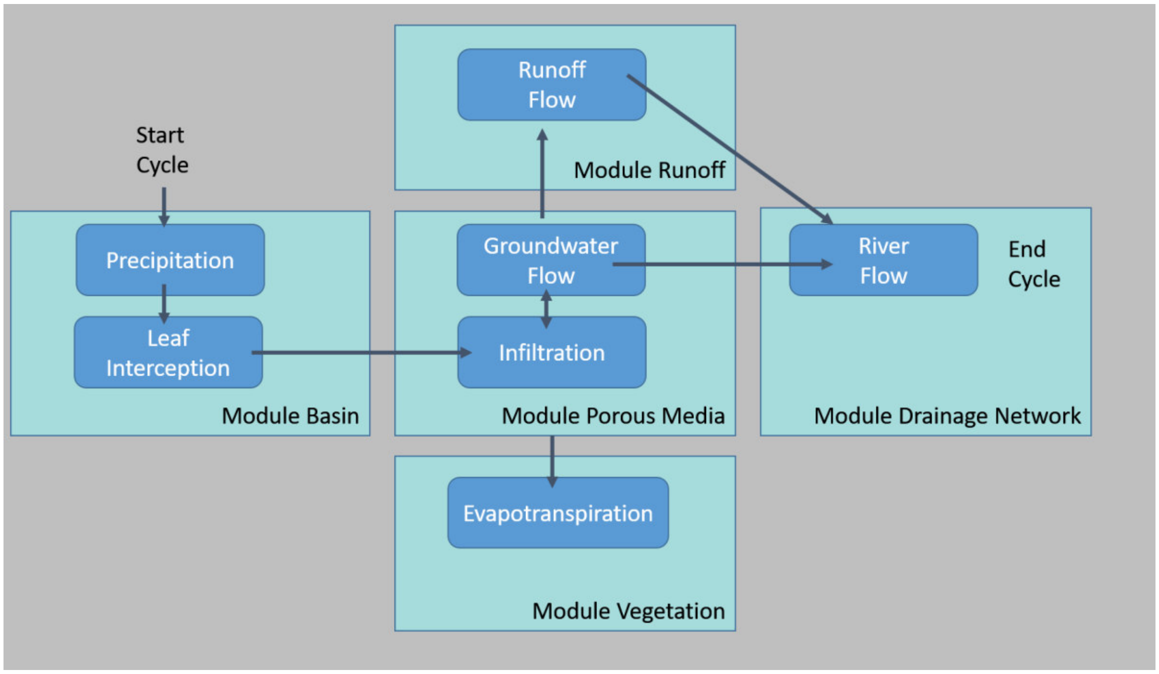

Figure 3 – MOHID Land Water cycle sequence in terms of modules and processes computed.

The river component and specific model equations will not be detailed as it was done in Trancoso et al., 2009. Succinctly, the river component solves St. Venant equations in 1D (similar as described below for runoff, in 2D) and property transport and erosion/deposition algorithms are also similar to the description that will be done in next chapters.

2.2.3.1.1 Atmosphere forcing

Atmosphere handles boundary conditions for precipitation, solar radiation, wind, relative humidity and can be of the type i) constant, ii) time series; iii) variable in space (grid) and invariant in time; iv) variable in space (grid) and variable in time. MOHID Land can be coupled to atmosphere models like MM5[3], WRF[4] from National Center for Atmospheric Research (NCAR) and the National Oceanic and

[3] http://www.mmm.ucar.edu/mm5/

[4] http://www.wrf-model.org

Atmospheric Administration in USA, via using/converting theirs outputs as inputs to MOHID Land.

2.2.3.1.2 Leaf Interception and Infiltration

Water coming from atmosphere may be retained in leafs from vegetation (if present) or fall in uncovered space.

The water that falls in leaf covered space builds up to leaf capacity (dependent on leaf area index) and if exceeds, the exceeding drips adds to water falling in uncovered space – potential infiltration rain.

The potential infiltrate column is the potential infiltration rain plus the water column already present.

Effective infiltration computation is an extended Richards's equation from soil to interface using head gradient with surface water head (topography plus potential infiltration column) and first soil layer water head (Equation 2).

$$Q_{infil} = \iint \left(-k_{sat}\,\vec{\nabla}(h+z)\cdot\vec{n}\right) dA_s$$

Equation 2 – Infiltration flow at the interface between runoff and porous media.

Where, Q_{infil} ($m^3.s^{-1}$) is infiltration flux, K_{sat} ($m.s^{-1}$) is saturated conductivity at the surface of porous media, h (m) in porous media is soil suction and in surface runoff is potential infiltration column height, z (m) in porous media is cell centre height and in surface runoff is topography, and A_s (m^2) is surface area available for infiltration.

Accordingly to Equation 2 if soil is saturated and infiltration occurs than it occurs at saturated conductivity but if soil is dry it will enter at higher velocity than saturated conductivity (higher head gradient).

Water that infiltrates will be routed in soil according to Richards equation (see next chapter) and the water that not infiltrates, forms the water column that can be transported in 2D runoff using St. Venant equations (see Surface Runoff chapter).

2.2.3.1.3 Porous Media Flow

Porous Media in MOHID Land is a 3D continuous domain including saturated and non-saturated zones. Porous Media flow is driven by total pressure head (H) field, which accounts for the matric potential (suction) in unsaturated areas (h_s), hydrostatic term in saturated areas (h_{hp}), and the gravity forces (Equation 3). In a saturated soil at rest, suction is zero and the hydrostatic pressure compensates the gravity producing a homogeneous H field and no flow.

$$H = h_s + z + h_{hp}$$

Equation 3 – Total Pressure Head in Porous Media.

Where, *H* (m) is total pressure head, *z* (m) is cell centre altitude (gravity term), h_s(m) is matric potential (suction head) – for unsaturated cells $h_s \leq 0$ for saturated $h_s = 0$, h_{hp}(m) is hydrostatic pressure term – for saturated cells $h_{hp} \geq 0$ for unsaturated $h_{hp} = 0$.

Combining the momentum and the mass conservation equations and using the conductivity concept we get the Richards equation for unsaturated porous media, which in the integral form is (Equation 4):

$$\frac{d}{dt}\iiint \theta \, dvol = \iint \left(-k\left(\vec{\nabla} H \cdot \vec{n}\right)\right) dA + [Sources - Sinks]$$

Equation 4 – Equation for mass conservation in water volume.

Where, θ (-) is water content (m^3 of water per m^3 soil), *k* ($m.s^{-1}$) is conductivity, *H* (m) is total pressure head.

Equation 4 shows that water accumulation inside the volume of one element is equal to fluxes through the surfaces of the element plus the sources and sinks (e.g. transpiration by plants, evaporation, groundwater flow with river, etc.). In order to solve Richards's equation we need to predict the total pressure head and conductivity distribution in soil.

From the work of Van Genuchten, 1980 the pressure head and the conductivity has a non-linear dependence from water content (Equation 5):

$$h_s(\theta) = -\left|\frac{(S_e^{\frac{-1}{m}} - 1)^{\frac{1}{n}}}{\alpha}\right|$$

Equation 5 – Matric potential (suction head) as a function of water content for unsaturated cells. Van Genuchten, 1980.

Where, h_s(m) is matric potential (suction head), α, m and n are hydraulic parameters obtained from soil p-f curves and defined as n>1 and m = 1 – 1/n, S_e(-) is relative water content.

And the conductivity in Van Genuchten, 1980 (Equation 6):

$$k(\theta) = K_s S_e^L (1 - (1 - S_e^{\frac{1}{m}})^m)^2$$

Equation 6 - Conductivity (suction head) as a function of water content. Van Genuchten, 1980

Where, k (m.s^{-1}) is conductivity, k_s (m.s^{-1}) is saturated conductivity, L and m are hydraulic parameters obtained from soil p-f curves

With the pressure head and conductivity distributions (from water content) in unsaturated soil and using the Richards equation it is possible to compute the water fluxes and determine the new water content in each cell. And thus the process is able to compute the new pressure head and conductivity distributions and continue the computation.

Solving the equations in relation to water content and then predicting suction pressure and conductivity from it assures the mass conservation of the process.

In saturated media, equations keep the same shape, suction head, h_s, is zero and instead a hydrostatic term may exist. In a saturated soil at rest the balance of all forces applied is null, and the hydrostatic pressure balances the weight. In saturated porous media, pressure is not dependent solely on water content but also on flow and cells neighbours (cell inside a saturated area has null velocity divergence) and instead of soil suction head (negative pressure), a positive pressure may occur. If there is no water movement than this effect is the hydrostatic pressure (that is integrated upwards in the saturated zone) but if movement exists, a correction is introduced in vertical pressure hydrostatic term (Equation 7):

$$\frac{\partial h_{ph}}{\partial z} = \left(1 + \frac{v_w}{K_{sat}}\right)$$ if v_w downwards (<0), only compute if $|v_w| \leq$ Ksat; if v_w upwards (>0) always compute.

Equation 7 – Hydrostatic and quasi-hydrostatic pressure term for saturated cells.

Where, h_{ph} (m) is hydrostatic pressure term, v_w(m.s^{-1}) is vertical velocity, K_{sat} (m.s^{-1}) is saturated conductivity.

Saturated areas with modulus downward velocities (negative v_w) higher then K_{sat} (e.g. interface between saturated front and unsaturated areas), will not feel the water weight above and the hydrostatic pressure term is not computed. However, if in saturated areas water movement decelerates and vertical velocities are lower than K_{sat}, the saturated area starts to feel the weight of the saturated water above. For example when the water mass is at rest, all the saturated water weight above is felt and the hydrostatic pressure term in saturated cells is the above saturated column height.

As stated in Equation 4 water mass conservation accounts for water movement in soil accordingly to pressure head distribution but also with sources and sinks and so the water balance is completed with the sinks of evapotranspiration (described in vegetation chapter) and source/sink link with river (described in chapter Porous Media and Surface Runoff Interface with river).

2.2.3.1.4 Vegetation

Water in soil can go i) back to the atmosphere by evaporation from surface or transpiration if plant root is present, ii) move in soil due to head gradients. The first component will be described hereafter. Water in leafs may also be evaporated to atmosphere. The potential water to remove from soil and leafs is computed based on climatic data (potential evapotranspiration using FAO equation[5]) adjusted for the culture and crop stage (crop evapotranspiration using K_c).

The separation process from crop evapotranspiration between the potential evaporation and potential transpiration (along plant roots) is given by Equation 9 and Equation 8 following Beer's law (Šimůnek et al. 2008).

$$PotEV = CropEVTP \times (e^{-k \times LAI})$$

Equation 8 – Computation of potential evaporation from crop evapotranspiration

$$PotTP = CropEVTP - PotEV$$

Equation 9 - Computation of potential transpiration from crop evapotranspiration.

Where, *PotTP* is potential transpiration (m.s^{-1}), *PotEV* is potential evaporation (m.s^{-1}), *CropEVTP* is crop evapotranspiration (m.s^{-1}), *k* is radiation extinction by the

[5] http://www.fao.org/docrep/x0490e/x0490e00.htm

canopy (-) as a function of sun angle, the distribution of plants, and the arrangement of leaves (between 0.5-0.75), and *LAI* is Leaf Area Index (-).

The vegetation module (refer to Figure 2) is the responsible for the transpiration and can be used as i) passive model, where the user gives the leaf area index and root depth evolutions and the model tries to transpire the potential transpiration amount being constrained by root geometry, soil available water and plant optimal heads (Feddes et al. 1978) or ii) an active model with a vegetation growth model, adapted from SWAT model version 2005 (Neitsch et al, 2005) that is by in turn adapted from EPIC model.

Vegetation module information fluxes in presented in Figure 4, where the module receives the potential transpiration from Basin module (described above) and computes actual transpiration based on vegetation stage and root definition that is sent back to Basin Module so that can be used by porous media module. The module also computes plant nutrient uptake from soil and organic matter release (plant biomass release during harvest and kill operations) and sent back to Basin module to be used by Porous Media Properties module.

Vegetation growth model (the active vegetation model) has a daily time step and in every iteration starts to check the plant stage (if it is growing, if it is dormant, etc.), then computes fluxes (nutrient uptakes from soil, biomass and leaf increase, organic matter release during harvest or kill operations, etc.) and finally updates vegetation properties (biomass, leaf area index, etc.). Effective vegetation growth is computed accounting for limitations due to environmental constraints (water and nutrient availability, temperature, radiation, humidity etc.). MOHID Land vegetation growth model managed to undergo some SWAT model limitations as for example to grow annual crops during winter months when using heat units calendar.

A more detailed description of vegetation growth model is given in Annex I.

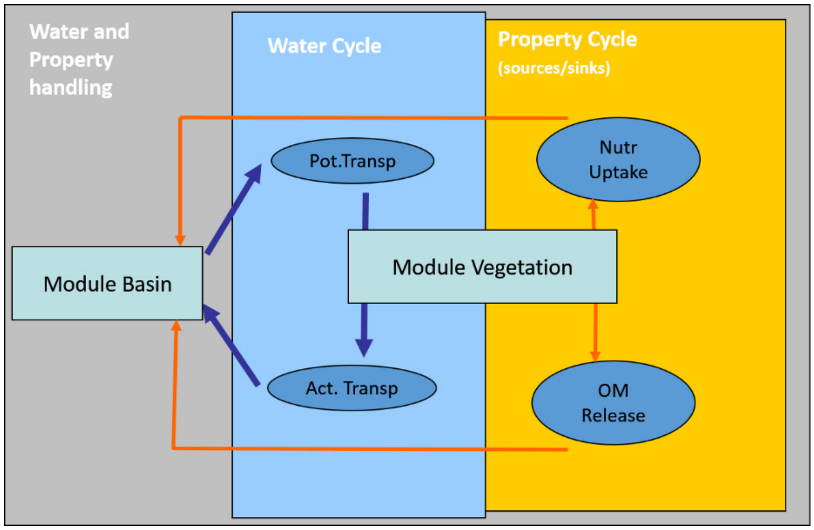

Figure 4. Vegetation Module information fluxes in water balance (blue arrows) and property balance (orange arrows).

Evaporation occurs at leaf surface and soil surface (from potential evaporation) and is limited to available water content. Moreover the user has the option to limit evaporation in soil in terms of head suction (below which evaporation ceases) or by conductivity (soil maximum evaporation velocity will be given by conductivity).

2.2.3.1.5 Surface Runoff

The water that not infiltrates (or exfiltrates from porous media) forms the water column and is able to move at the surface (2D movement).

The same principles of conservation are applied in Equation 1 with $\beta = \rho v$ (momentum) and the sources/sinks term are the pressures and shears in bottom and surface faces. Integrating momentum conservation equation in the vertical and the transversal dimensions, and neglecting surface shear because (i) it is much smaller than bottom shear and (ii) because the wind velocity is generally not aligned with the flow, the St. Venant equation for 2D is obtained (Equation 10) where Q ($m^3.s^{-1}$) is water flow, A (m^2) is the cross flow area, g ($m.\ s^{-2}$) is gravity acceleration, h (m) is water depth, S_0 (-) is the bottom slope, S_f (-) is the bottom friction slope (i.e. the slope that balances the friction force) and x_i are the flow directions (xx and yy).

$$\frac{\partial Q_i}{\partial t} + v_j \frac{\partial Q}{\partial x_i} + gA\left(\frac{\partial h}{\partial x_i}\right) - gA(S_o - S_f) = 0$$

Equation 10 – St Venant Equation for 2D.

Friction slope Sf can be defined with the Manning-Strickler empirical law (Equation 11),

$$(S_f)_i = \frac{n^2 |Q| Q_i}{A^2 R_h^{\frac{4}{3}}}$$

Equation 11 – Manning-Strickler equation for friction slope

where Rh (m) is the hydraulic radius, equal to the cross sectional area divided by the wet perimeter, and n ($s.m^{-1/3}$) is the Manning roughness coefficient.

The major forces affecting the flow are pressure, gravity and friction that together with inertia of the water determine the evolution of the flow.

MOHID Land has still an option to simulate surface flow with a simplification of St. Venant Equations that can be a faster algorithm but less generic and may be unrealistic in some situations. In areas with slow varying slope and low Froudre number the horizontal velocity gradient is small and inertia forces can be neglected (Abbot and Minns, 1998), and Equation 10 simplifies to the diffusion wave model, or zero-inertia routing (Equation 12),

$$Q_i = \frac{A\left(R_h\right)^{\frac{2}{3}} \sqrt{\frac{d(z+h)}{dx_i}}}{n}$$

Equation 12 – Diffuse wave model for 2D runoff flow.

Where *z(m),* is terrain height and $z + h$ is water level (m).

The diffuse wave formulation is a parabolic equation and is capable of representing backwater effects (Abbot and Minns, 1998).

In all formulations h is computed using the continuity equation which states that volume variation in control volume is explained by the water fluxes trough the control volume faces (Equation 13):

$$A_H \frac{\partial h}{\partial t} + \frac{\partial Q_i}{\partial x_i} = 0$$

Equation 13 – Continuity equation.

Where A_h is the cell horizontal area.

In runoff, as also described in the work of Trancoso, et al. 2009 for the river network, it is possible for the user to choose to implement: i) the kinematic wave (diffuse wave with bottom slope as S_f); ii) the diffuse wave or ii) the St. Venant formulation.

2.2.3.1.6 Porous Media and Surface Runoff Interface with river

Water exchanges between the river and the porous media is computed using the head gradient and between the river and land surface using the surface gradient. For exchanges with porous media the Richards equation is used, considering the head in the river as the free surface level and the diffusion wave equation is used to compute exchanges between the surface runoff and the river. These algorithms permit the explicit simulation of river floods and generate variable river discharge, as a function of the porous media water content and surface runoff water height along the whole catchment.

2.2.3.1.7 Surface Drainage Network

The water routed from surface runoff and groundwater flow reaches finally drainage network. Drainage Network Module handles the description of river hydrodynamics and water quality in a 1D dimension (a network of nodes and reaches). It can be run as a stand-alone-model (MOHID River Network) or integrated in MOHID Land. It solves the complete St. Venant equations (as Module Runoff) but applied to 1D and a detailed description of the Module can be found in Trancoso et al., 2009.

2.2.3.1.8 Adaptative time step

MOHD Land uses an adaptive time step that is dynamic and changes with fluxes dimension, meaning that during high surface or groundwater fluxes (as a response to precipitation events) the time step will get lower (usually in the order of seconds) but during dry season where fluxes are lower the time step can get the order of several minutes to one hour. This makes the model suitable for running not only events but also long-term simulations.

To illustrate the major functioning, time step reduction and increase can be configured by the user by setting:

- the threshold of volume variation allowed for any cell before time step is reduced:

$$Cell\ Volume\ Variation = \frac{|Vol^{t} - Vol^{t-dt}|}{Vol^{t-dt}}$$

- the time step reduction/increase in percentage of last time step.

Time step general algorithm is described in Figure 5 where for the hydrodynamics modules (Porous Media, Runoff and Drainage Network) the normal procedure is to compute heads, the corresponding fluxes, and the new volumes based on those fluxes (explicit approach). If the volume variation between one time step and the previous in any cell is higher than the defined threshold then the time step is reduced based on defined percentage and the initial volumes are resetted and the processes starts all over until the threshold has been met for all cells[6].

[6] New developments made that the condition can be chosen to be validated only in a percentage of domain cells and only test for volumes higher than a cell percentage for speed improvements.

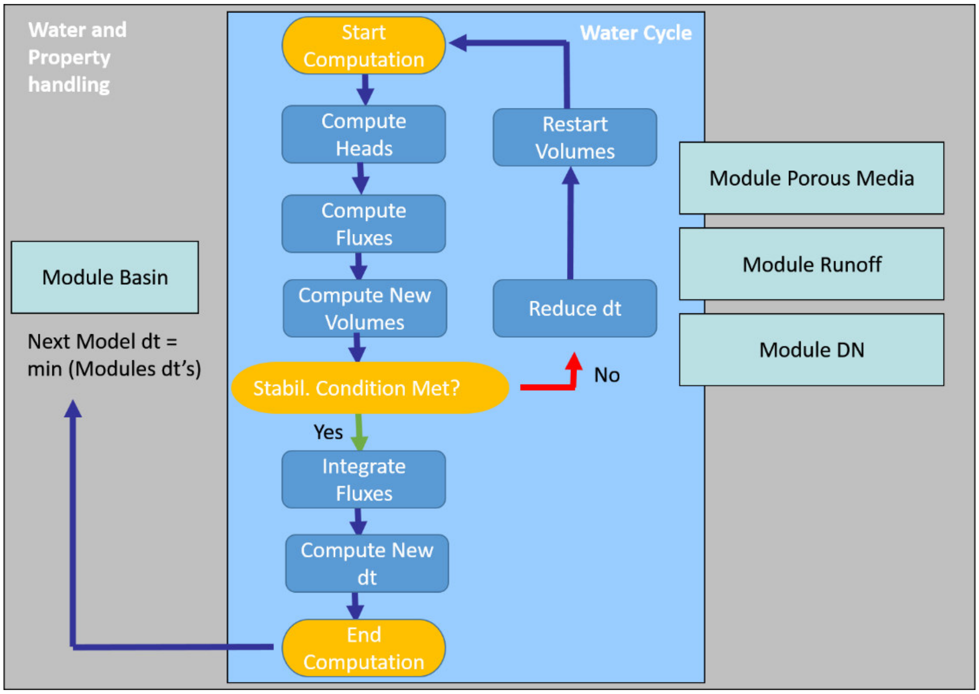

Figure 5. Time step adaptation in hydrodynamics Modules-

2.2.3.2Properties Cycle

2.2.3.2.1 Properties Transport

Property transport is derived from mass conservation equation either for porous media, runoff or drainage network transport. However, in Porous Media not all the cell is filled with water changing how volume and area for diffusion are considered. The accumulation rate in one control volume is the rate of change of property mass in one time step. The accumulation rate in the control volume is affected by the fluxes through the volume surfaces (advection and diffusion) plus the property transformation inside the volume (sources and sinks). Property concentrations (C) are defined for the centre of the faces and velocities (v) and diffusivities (γ) for the faces between adjacent cells (Figure 6).

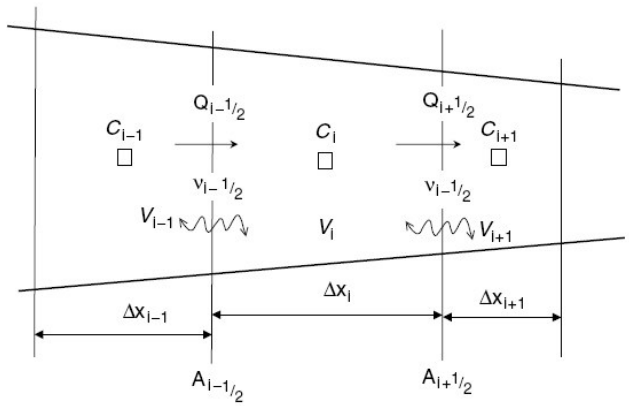

Figure 6 – Concentrations, flows, and diffusivities for control volumes. Indexes i, i-1, and i+1 for cells and indexes i-1/2 and I +1/2 for faces.

The same principles in terms of mass balance in control volume with advection-diffusion for porous media are presented in Equation 14 and for runoff or drainage network (Trancoso et al. 2009) in Equation 15, where *V (m^3)* is cell volume, θ (-) is water content (water volume per cell volume), *C* ($g.m^{-3}$) is property concentration, Q ($m^3.s^{-1}$) is flow between adjacent cells, γ ($m^2.s^{-1}$) is diffusivity, *A* (m^2) is cell area, Δx (m) is cell spatial step:

$$\frac{\left(V_i \cdot \theta_i \cdot C_i \cdot\right)^{t+\Delta t} - \left(V_i \cdot \theta_i \cdot C_i\right)^{t}}{\Delta t} = -\left(Q_{i+\frac{1}{2}} \cdot C_{i+\frac{1}{2}} - Q_{i-\frac{1}{2}} \cdot C_{i-\frac{1}{2}}\right)^{t=t*}$$
$$+\gamma_{i+\frac{1}{2}} \cdot \theta_{i+\frac{1}{2}} \cdot A_{i+\frac{1}{2}} \cdot \left(\frac{C_{i+1} - C_i}{\frac{1}{2}\left(\Delta x_i + \Delta x_{i-1}\right)}\right)^{t=t*} - \gamma_{i-\frac{1}{2}} \cdot \theta_{i-\frac{1}{2}} \cdot A_{i-\frac{1}{2}} \cdot \left(\frac{C_i - C_{i-1}}{\frac{1}{2}\left(\Delta x_i + \Delta x_{i+1}\right)}\right)^{t=t*}$$

Equation 14 – Property Transport equation for porous media. Indexes i, i-1, and i+1 for cells and indexes i-1/2 and I +1/2 for faces

$$\frac{\left(V_i \cdot C_i \cdot\right)^{t+\Delta t} - \left(V_i \cdot C_i\right)^{t}}{\Delta t} = -\left(Q_{i+\frac{1}{2}} \cdot C_{i+\frac{1}{2}} - Q_{i-\frac{1}{2}} \cdot C_{i-\frac{1}{2}}\right)^{t=t*}$$
$$+\gamma_{i+\frac{1}{2}} \cdot A_{i+\frac{1}{2}} \cdot \left(\frac{C_{i+1} - C_i}{\frac{1}{2}\left(\Delta x_i + \Delta x_{i-1}\right)}\right)^{t=t*} - \gamma_{i-\frac{1}{2}} \cdot A_{i-\frac{1}{2}} \cdot \left(\frac{C_i - C_{i-1}}{\frac{1}{2}\left(\Delta x_i + \Delta x_{i+1}\right)}\right)^{t=t*}$$

Equation 15 - Property Transport equation for runoff or drainage network. Indexes i, i-1, and i+1 for cells and indexes i-1/2 and I +1/2 for faces

In these equations t* is a time interval between t and t + Δt and $C_{i-1/2}$ the concentration in face between cell i-1 and cell i. The above equations must be described in space and time because concentrations in advection term have to be known in the face (instead of cell centre) and advective and diffusive terms can be evaluated in t (explicit) or in t + dt (implicit). Spatial and temporal discretization and advection stability methods used in porous media and runoff are inherited from MOHID framework and developed in MOHID Water. Drainage network schemes are described in Trancoso et al. 2009.

Spatial discretization in advection is chosen by the user and can be of type upwind (up to 3rd order) where face concentrations are dependent on flow direction or central differences and *leapfrog* where face concentrations are dependent on both adjacent cells independent on flow direction. For advection also a number of methods for total variation diminishing (TVD) exist to assure conservative and monotonicity for properties as *minmod*, *superbee* or *muscl* (Pietrzak, 1998).

Temporal discretization is chosen by the user and in case of explicit method the new concentration (in t + Δt) in one cell is only based on old concentration (time t) in neighbour cells, being a straightforward computation. In case of implicit method, new concentration is obtained from concentrations in t+dt evaluating the entire domain and is solved a tridiagonal system of equations using the Thomas algorithm (Thomas, 1949).

Diffusivity in porous media accounts not only for molecular diffusion (as in runoff or drainage network) but also for advective dispersion caused by erratic flow paths around soil particles and which process is not comprised in advection. Moreover molecular diffusion in soil has to account for the fact that the process effectiveness will depend on water present being represented by tortuosity. Porous media diffusivity computation is presented in Equation 16, where γ_{face} ($m^2.s^{-1}$) is diffusivity, D_{face} ($m^2.s^{-1}$) is molecular diffusion coefficient of solute in water, v_{face} ($m.s^{-}1$) is velocity in the face, λ_{face} (m) is dispersivity and ξ (-) is tortuosity (Jury et al. 1997). Tortousity was computed using the Millington-Quirk formulation in Jury et al. 1997 (Equation 17) where ϕ (-) is porosity. Water content and porosity are defined for the cell centres but diffusivity needs the computation of these properties in the faces (currently the minimum between adjacent cells is used because it will be the one limiting mass transfer).

$$\gamma_{face} = D_{face} \times \xi(\theta)_{face} + \frac{v_{face} \times \lambda_{face}}{\theta_{face}}$$

Equation 16 – Diffusivity in porous media

$$\xi(\theta)_{face} = \frac{\theta_{face}^{7/3}}{\phi_{face}^{2}}$$

Equation 17 – Tortuosity in porous media

2.2.3.2.2 Erosion/Deposition of particulate Properties

Particulated properties (associated to organic matter and cohesive sediment) are transported with water velocity (as described above), but also have a vertical flux between water column and bottom sediment (erosion and deposition). These processes are solved in Module Runoff and Module Drainage Network and are dependent on flow power or shear stress. The formulation used is the same as for MOHID Water (Franz et al. 2014, Cancino e Neves, 1999), making consistent and transversal implementation.

Erosion depends on flow power and sediment entrainment and occurs when the ambient shear stress exceeds the threshold of erosion (Partheniades, 1965). The flux of eroded matter is given by Equation 18.

$$\frac{\delta M_E}{\delta t} = \begin{cases} E\left[\frac{C}{C_S}\right]\left[\frac{\tau}{\tau_E} - 1\right], & \tau > \tau_E \\ 0, & otherwise \end{cases}$$

Equation 18: Particulated property erosion rate.

where E is the erosion constant (kg m^{-2} s^{-1}), τ is the bed shear stress (Pa),τ_E is a critical shear stress for erosion (Pa) and C and C_S are the deposited concentrations of the particulate property and sediments at the water bed interface, respectively (kg m^{-2}). The erosion constant can be defined as the soil erodibility and can be inputed as a grid based on soil or other relevant spatial information – e.g. compaction, saturation etc.)

As with erosion, deposition occurs when the ambient shear stress is lower than a specified threshold (Krone, 1962). The flux of deposited matter is given by Equation 19,

$$\frac{\delta M_D}{\delta t} = \begin{cases} CW_s\left[1 - \dfrac{\tau}{\tau_D}\right], & \tau < \tau_D \\ 0, & otherwise \end{cases}$$

Equation 19. Particulated property deposition rate

where τ_D is a critical shear stress for deposition (Pa), C is the suspended particulate property (kg m^{-3}) and w_s is the settling velocity (m s^{-1}), which can be constant value or computed from $W_s = \begin{cases} K_1\, C^m\,, & 0 \le C < CHS \\ K_1\, C_{HS}^m[1 - k_2(C - C_{HS})^{m_1}], & C \ge CHS \end{cases}$ Equation 20 (Nicholson and O'Connor (1986)).

$$W_s = \begin{cases} K_1\, C^m\,, & 0 \le C < CHS \\ K_1\, C_{HS}^m[1 - k_2(C - C_{HS})^{m_1}], & C \ge CHS \end{cases}$$

Equation 20. Settling velocity dependence on suspended

where K_1 (m^4 $kg^{-1}s^{-1}$) and K_2 (m^3 kg^{-1}) depend on sediment mineralogy and the exponents m an m_1 depend on particle size and shape.

2.2.3.2.3 Vegetation Sources/Sinks

For soil, vegetation acts as a sink of dissolved nutrients (nitrate and inorganic phosphorus) and as a source of refractory organic carbon, nitrogen and phosphorus (during grazing, at dormancy, harvest and kill operations – both root and aerial parts) and a source of labile organic nitrogen and phosphorus or mineral ammonia, nitrate and inorganic phosphorus during fertilization (depending if fertilizer used is organic or mineral).

Plant nutrient uptake is controlled by the plant nutrient equation that computes the optimal fraction of nitrogen or phosphorus in the plant biomass as a function of growth stage given optimal growing conditions. In management operations as plant kill, the root refractory material is distributed vertically in soil dependent on root distribution; plant harvest and grazing material is placed in surface; fertilization can be applied superficially or sub-superficially (on first two soil layers).

Vegetation model and these processes were described in more detail in Annex 1.

2.2.3.2.4 *Water Quality Processes in soil*

There are two main processes associated to property transformation in soil i) biologically driven, ii) chemically driven. The first processes include organic matter mineralization (ammonia, inorganic phosphorus and carbon dioxide release) and nitrification in oxic conditions and denitrification and methane production in anoxic conditions driven by bacteria activity (Sediment Quality Module). The latter processes include speciation, aqueous, mineral, gas, solid-solution, surface-complexation, and ion-exchange equilibria (PHREEQC model).

2.2.3.2.4.1 Bacterial Activity

MOHID Land includes a 0D water quality model called Sediment Quality that is a module for bacteria driven activity as mineralization, nitrification and denitrification processes in soil and was adapted from RZWQM (Ma et al., 2000). This module is used for describing mineralization, nitrification, denitrification, carbon dioxide and methane productions in soil (it computes module Porous Media Properties properties sources/sinks).

Microorganism population has autotrophic, heterotrophic aerobic, anaerobic and solubilizing bacteria population types where carbon, nitrogen and phosphorus composition are dependent on growth, death and respiration processes (Equation 21):

Equation 21. Carbon, nitrogen and phosphorus content evolution for each microorganism type.

$$\frac{dC_{micro}}{dt} = \left(K_{growth}C - K_{resp}C - K_{death}C\right) * C_{micro}$$

$$\frac{dN_{micro}}{dt} = \left(K_{growth}N - K_{resp}N - K_{death}N\right) * N_{micro}$$

$$\frac{dP_{micro}}{dt} = \left(K_{growth}P - K_{resp}P - K_{death}P\right) * P_{micro}$$

Where C_{micro}, N_{micro}, P_{micro} are carbon, nitrogen and phosphorus content of microorganisms (mg/L), respectively, and K_{growth}, K_{resp} and K_{death}, are growth, respiration and death rates (day^{-1}).

The organisms growth is obtained through inorganic nutrients mineralization, nitrification or denitrification (decay rates). The respiration is dependent on microorganisms efficiency on processing substrate and for microorganism nitrogen and phosphorus, ratios to carbon are used (microorganism need to maintain C:N and C:P ratios and excrete nitrogen or phosphors if above ratio or assimilate them if below).

The module equations were adapted from the RZWQM model to a format where maximum rates are computed (if no limitation existed) and then this maximum rate is multiplied by limiting factors (that range from zero – maximum limitation – to one – no limitation). This approach yields similar results as the original but has the advantage that is possible to know at every cell and every time step what is the limiting factor for each reaction.

More detailed information about Sediment Quality is found in Annex II.

2.2.3.2.4.2 Soil Chemistry

MOHID Land includes a 0D water quality module called PHREEQC that is imported directly from PREEQC model (Parkhurst and Appelo, 2013).

This module is able to define property speciation and equilibrium according to solution pH, ionic strength, etc., being able to process kinetically controlled reactions, solid-solution equilibria, sortion-dessortion, etc.

The Module description in more detail goes beyond this thesis focus and should be addressed in forthcoming PhD thesis.

2.2.3.2.5 Water Quality Processes in River

MOHID Land river water quality can be coupled to any of the MOHID Water available water quality 0D modules (that in Figure 2 are referenced as Water Quality Models):

- WaterQuality Module
- CE-QUAL-W2 Module
- Life Module

These modules detailed description is out of the scope of this study. Very succinctly, WaterQuality Module was adapted from U.S. EPA WASP model, and solves nitrogen, phosphorus and silica cycles, simulating bacteria, phytoplankton, zooplankton, flagellates and diatoms organisms activity (including nutrient assimilation and excretion, organic matter mineralization, denitrification, etc.). Fixed Redfield ratios are assume and a brief description and implementation to a fresh water reservoir is show in Deus et al. 2013.

CE-QUAL-W2 Module is the coupled version of the well-known trophic level water quality model (which the full original model is implemented in this thesis), and different phytoplankton species can be simulated and solves similar processes as WaterQuality Module. This model in its MOHID version (previous to CE-QUAL-W2 v3.2) does not simulate macroalgae or zooplankton influence in primary production.

Life Module is a multiparameter biogeochemical module based on ERSEM model. This module is able to simulate nutrients cycles, along with several primary producers, secondary producers and decomposers in the water column with variable N:P:C ratios and is described in more detail in Mateus, 2012.

2.2.4 Input/Output

Input and output in MOHID Land follows the same structure as MOHID framework. Model input data files use keywords to connect/disconnect processes, give path to input files (e.g. atmosphere data), choose time series location and output frequency, etc. Initial/boundary conditions (e.g. atmosphere properties, initial aquifer level or concentrations) may be of the type i) constant value; ii) time series uniform in space; iii) grid with no temporal variation; iv) grid with temporal variation. Time series and grids are in ascii format, grid with time variant values are in HDF format.

Inputs needed to implement the model in a real case watershed consist of:

- Digital Terrain Model to derive slopes, drained areas, drainage network, delineation, etc. (using pre-processor simple tools).
- Meteorology time series or HDF usually available form national monitoring networks, as precipitation, temperature, radiation, relative humidity, wind velocity, etc.
- Land use map to derive land use crops and manning coefficients (using pre-processor simple tools),
- Soil type map and van Genuchten parameters to each soil type

Model output files are in ascii format (time series) and HDF (grids with time variant values – spatial results). In the river it can be outputted water depth, velocity, flow, groundwater flow to river, surface runoff flow to river, etc.; in the basin surface, outputs may be runoff water column height, precipitation, evapotranspiration, infiltration, flows and velocities, etc., and in porous media, suction head, hydrostatic term, total head, water content, velocities, conductivities, transpiration, evaporation, etc.

Pre-processing of input files and post-processing of results until the later years was done in developed specialized tools (GIS tool, time series tool, HDF tool). A new GUI was developed in recent years to integrate all small tools (pre-processor and post-processor) in one single interface [7].

[7] http://www.actionmodulers.com/

2.2.5 Capabilities

MOHID Land as described above with a physical approach to hydrological processes, distributed and with variable time-step, alone or coupled with other physical based models, is especially suited for detailed, complex short-term processes as fast floods, inundation progression, natural-artificial drainage interactions But is also able to represent long-term processes in hydrology, soil properties transformation and vegetation dynamics.

The thesis is able to describe the multi purpose and multi scale (spatial and temporal) capacity of the MOHID Land model in contrasting applications:

- from micro scale (less than 5 km^2) for precipitation events (article describing the simulation of urban floods in Póvoa de Santa Iria)
- to small-medium-scale (less than 100km^2) for a couple of years (article describing the role of floods and first floods in nutrient export in a natural system in Enxoé watershed).
- to regional scale (Iberia Peninsula with watersheds of the order of 30-80 000 km^2 in operational way since 2010 (Brito et al., 2015).

2.2.6 Limitations

MOHID Land does not simulate reservoir operations or optimization. However it already has a reservoir module that can simulate reservoirs dynamics (volume and concentration change) given that operation rules are known (level – flow out curves, etc.). This was developed to try to represent the water retention in high artificial rivers where flow is stored in first months of hydrological cycle and differences to recorded data is evident (Brito et al. 2015).

MOHID Land may have difficulties in simulating complex aquifer systems or fractured karstic systems with different materials since it solves Richards equation based on water content that can yield discontinuities in head in the material interfaces (Celia et al., 1990).

MOHID Land does not yet include bed load transport that could be important for describing landslides.

Due to its distributed and physical approach best results are obtained with higher resolution grids and detailed topographic data (e.g. Lidar) that increases the computational effort and timing (general concern in distributed models high-resolution implementations). To minimize this limitation, in last years several technologies have been implemented (OpenMP and MPI) to increase code performance and new technologies are being studied (GPU processing) to even increase model velocity. MOHID Land is also able to use some simplifications in infiltration (use Green-Ampt and Curve Number methods instead of Richards equation in full 3D ground water model) that allows for 2D implementations with less detail in groundwater flow and produce faster simulations with no significant loss in accuracy for example for exceptional flood events.

2.3 Other Numerical Models

Besides MOHID Land models family, during the thesis development, the author, used for fresh water systems, CE-QUAL-W2 model for reservoir water quality dynamics, SWAT model for long-term hydrological and nutrient loads dynamics and SWMM model for urban drainage systems.

CE-QUAL-W2 is an open-source, bidimensional, laterally averaged, dynamic model from U.S. Corps of Engineers. The hydrodynamic component of this model uses Navier-Stokes equations for incompressible flow in the water body velocity field and turbulent diffusion coefficients calculation. In water quality component, property sources and sinks are computed considering interactions between temperature, nutrients, algae, dissolved oxygen, organic matter and sediments (Cole and Wells 2011). The model data requirements are the reservoir bathymetry, meteorology and river inflows/concentrations and reservoir outflows.

CE-QUAL-W2 model, besides this thesis, in Maretec research group was implemented in near 30 reservoirs in Portugal to assess trophic state and test nutrient reduction scenarios for INAG (national authority for Water Management) under Waste Water Treatment Plant directive. The author implemented the model in several reservoirs and conducted a team of modellers in the remainder

reservoirs. This model allowed the author to strengthen knowledge in biogeochemical processes and rapidly test sensitive analysis to retrieve key factors controlling trophic state in reservoirs.
CE-QUAL-W2 model in this thesis was used to describe the Enxoé reservoir water quality processes associated with physical (e.g. stratification, sediment deposition, etc.) and biogeochemical cycles (e.g. algae growth, organic matter mineralization, denitrification, phosphorus anoxia release from sediment, etc.).

SWAT is an open-source basin river model from U.S. Department of Agriculture and Texas A & M University, which land hydrodynamic component solves water balance, relating meteorological variables with basin features (topography, soil type and land use). In water quality component, plant growth, nitrogen and phosphorus soil cycles, sediment and pesticides transport, are simulated (Neitsch et al. 2002). The main model data requirements are land use and soil maps and meteorological and climatological data.
SWAT model, besides this thesis, in Maretec research group was implemented by the author in several small (less than 50 km^2) to large watersheds (higher then 60 000 km^2) and to above referenced reservoirs drained areas.
This model allowed the author to establish in-depth knowledge on basin hydraulics and nutrient export rates and river loads on contrasting watershed sizes and hydrological regimes and a key factor for adapting its vegetation growth model to MOHID Land.
SWAT model was applied in the thesis for Enxoé reservoir watershed. Since Enxoé watershed is around 60 km^2 where concentration time is just less than a couple hours, SWAT model was more suited for long-term simulation of nutrient loads to the reservoir.

SWMM is an open-source urban drainage system model from US Environmental Protection Agency that solves both hydrology (simple sub-watersheds volume model to estimate inputs to drainage system) and hydraulics in a complex system of pipes, channels, storage/treatment devices, pumps, and regulators. The model can solve the complete St. Venant equations for free surface and pressurized gravity driven flow (Rossman and Huber, 2016). The main data requirements are the urban drainage infrastructure system and precipitation data.

This model allowed the author to understand urban drainage hydraulics and the coupled implementation in real-time with MOHID Land made possible to develop technologies for full integration that are able to solve high variable and complex system interactions.

SWMM model was implemented in the thesis in urban drainage of Póvoa de Santa Iria coupled with MOHID Land to be able to describe the interaction between surface and urban drainage systems.

All the different models used (and tested in detail using source-code debugging) allowed the author to fully understand the wide range of model numerical approaches, their strengths, weaknesses and opportunities (usually derived from the lack of integrated approaches as described in introduction) that ultimately led to MOHID Land developments and integrated philosophy.

Another crucial aspect in modelling is the integration of field data, both for model implementation and model validation, and data used in the thesis is described next.

2.4 Field Data

Field data used in the thesis had mainly the function to implement models or to compare to model results and verify for its validity. However, it was also used to understand the natural system dynamics. The field data is describes in more detail in each of the applications but essentially ranged from:

- Static data as Digital Terrain Model from NASA SRTM 3 arc second, Land Use from CORINE Land Cover and soil data from European Soil Database to implement SWAT and MOHID Land, reservoir geometry from national water institute, Agência Portuguesa do Ambiente (APA) for CE-QUAL-W2 and urban drainage infrastructure from the managing company SIMTEJO -

Saneamento Integrado dos Municípios do Tejo e Trancão, for SWMM model.

- daily and hourly precipitation and daily air temperature, humidity, solar radiation, wind from APA national monitoring grid (SNIRH[8]) to force SWAT and MOHID Land models.
- monthly inflows to Enxoé reservoir in national monitoring grid (SNIRH) to validate watershed models SWAT and MOHID Land
- weekly river nutrient concentrations (nitrate, ammonia, inorganic phosphorus, organic nitrogen and phosphorus forms, suspended matter, etc.) recorded and analysed by Instituto Nacional de Investigação Agrária e Veterinária (INIAV) used to validate SWAT loads.
- flood rise and fall recordings via river sensor level and automatic sampler that collected samples and same properties as above were analysed by INIAV. The author was in charge of the implementation, maintenance and remote communication with automatic sampler that brought close understanding of flash floods dynamics and logistic challenges to record them.
- monthly Enxoé reservoir historic nutrient and algae concentrations at surface wall (SNIRH) and actual nutrient and algal concentrations measured at 3 points in the reservoir and monthly temperature and oxygen profiles recorded by Universidade de Évora that were used to validate CE-QUAL-W2 model results.

- every minute precipitation measured in udometer and pipe flow from 5 flow sensors (level and dopler) installed by Hidra and Contimetra in Póvoa de Santa Iria watershed to waste water management agency SIMTEJO that were used to force and validate SWMM and MOHID Land models.

[8] http://snirh.pt

- meteorological model results from IST[9] and Meteogalicia[10] to force MOHID Land model in Portugal Galiza and Iberia Peninsula MOHID Land operational models.

- daily flows and monthly water quality concentrations from SNIRH network for Portugal Galiza and Iberia Peninsula MOHID Land results validation.

Data collection and extensive data analysis for precipitation, hydrology and water quality recordings, in conjunction with modelling activities, allowed the author to understand physical and biogeochemical processes that occur both in river as reservoir systems and that are the basis for any hydrological or water quality study and for model conceptualization/development.

Finalized the description of the modelling approach and models/field data used in the applications, next is presented the applications that try to verify the thesis hypothesis about the added value of integrated modelling and incorporating the state-of-the-art knowledge acquired with that approach into MOHID Land model.

[9] http://meteo.tecnico.ulisboa.pt

[10] http://meteogaliacia.es

3 Applications

In this chapter are described the implementations that test the thesis hypothesis about the need for integration modelling to solve complex water quantity and quality problems and the creation of a modelling framework that integrates all the knowledge produced.

As described above, are presented the articles/applications objectives in a succinct way and added the journal published/submitted status:

- Chapter 3.1 where SWAT model was implemented for estimating Enxoé reservoir long-term loads (30-year annual average) to verify their magnitude. In Applied Water Science journal internal peer review process.

- Chapter 3.2 where MOHID Land model was implemented to simulate Enxoé reservoir short-term flood loads (flood duration is of the order of couple of hours) to verify their role in nutrient export. Published in May 2017 in Environmental Earth Sciences (2017) 76:377.

- Chapter 3.3 where SWAT and CE-QUAL-W2 models were coupled offline for ~10 years simulation to describe Enxoé reservoir current situation and study management responses to reduce trophic level. In review process with Environmental Earth Sciences journal (resubmitted in response to reviewers comments).

- Chapter 3.4. where MOHID Land and SWMM models were coupled online (running at the same time)) to describe Póvoa de Santa Iria urban floods current situation and possible management responses. In Environmental Modelling & Assessment journal internal peer review process.

- Chapter 3.5. where MOHID Land model that covers all Iberia Peninsula geographical area was operationalized to forecast every day for the next 4 days, flows and concentrations, that are used to feed coastal and estuary models. Published in December 2015 in Estuarine, Coastal and Shelf Science, Volume 167, p. 138-146.

The articles/applications are presented next, each with one section, where at start is reminded its objective and justification.

3.1 *Assessing water and nutrient long-term dynamics and loads to an eutrophic reservoir in the Enxoé temporary river basin, southeast Portugal.*

Previous studies in Enxoé reservoir suggested that the load from the watershed could be the driver for eutrophication. This article describes the implementation and validation of SWAT model to Enxoé watershed for long-term annual load estimation.

ASSESSING WATER AND NUTRIENT LONG-TERM DYNAMICS AND LOADS TO AN EUTROPHIC RESERVOIR IN THE ENXOÉ TEMPORARY RIVER BASIN, SOUTHEAST PORTUGAL

David Brito[1], Ramiro Neves[1], Maria A. Branco[2], Ângela Prazeres[2], Sara Rodrigues[2], Maria C. Gonçalves[2], Tiago B. Ramos[1]

[1] Maretec, Instituto Superior Técnico, Universidade de Lisboa, Av. Rovisco Pais, 1049-001 Lisboa, Portugal.

[2] Instituto Nacional de Investigação Agrária e Veterinária, Quinta do Marquês, Av. República, 2784-505 Oeiras, Portugal.

First author and corresponding author: David Brito, e-mail: odavidbrito@gmail.com, tel: 00351 962535504

Abstract

The Enxoé reservoir has been exhibiting frequent high chlorophyll-a concentrations (reaching a geometric mean 6 times the national limit for eutrophication of 10 $\mu g.L^{-1}$) since 2000, and represents the reservoir with the highest eutrophic state in Portugal. Toxic algal blooms have also been observed, which pose serious challenges to water managers as the reservoir is used for potable water production. In an effort to contribute to the reduction of the reservoir trophic state, the watershed inputs (monthly flows, and sediment, N, and P loads) were characterized with the SWAT model. Field data was collected in the ungauged watershed during 2010/2011 for model calibration/validation. Model results were then used to characterize the long-term watershed dynamics in terms of water and nutrients. SWAT estimates of the simulated flow, and sediment and nutrient loads were in good agreement with field data (R^2 between 0.42-0.78; Nash-Sutcliffe efficiencies between 0.19-0.75). The Enxoé River was characterized by a temporary flushy regime where high concentrations were transported in short time periods. As a result, nutrient loads delivered to the Enxoé reservoir were estimated to be 18 $tonN.year^{-1}$ and 0.7 $tonP.year^{-1}$ (30 years' simulation), reaching the reservoir mainly by runoff. These results were consistent with the gentle slopes, extensive agricultural activities, and low urban pressure observed in Enxoé. The magnitude of the nutrient exports suggests that the reservoir eutrophication may also be linked to the reservoir geometry (average depth of 5 m), which provides high light availability to the bottom sediments. Thus, SWAT results will be integrated into a reservoir model to depict the origin of the Enxoé trophic state and test management scenarios that may reduce it.

Keywords: Enxoé, eutrophic reservoir, nutrients, watershed modeling, SWAT model

3.1.1 Introduction

Enxoé is a temporary river located in the Alentejo region, in southeast Portugal, and is one of the tributaries of the Guadiana river. The Enxoé catchment is limited downstream by a reservoir built in 1998, which has been exhibiting the highest eutrophic state in the country ever since (CCDR Alentejo 2005; INAG 2008). Since 2000, the reservoir has had frequent chlorophyll-a concentrations higher than 50 $\mu g.L^{-1}$. The geometric average of the surface chlorophyll-a concentration measured from April to September between 1998-2009 was approximately 60 $\mu g.L^{-1}$ (INAG, 2009), whereas the national limit for eutrophication is 10 $\mu g.L^{-1}$. Moreover, toxic cyanobacteria blooms occurred (INAG 2004; Valério et al. 2005) and interrupted water distribution to the local population. This constitutes a serious problem for water management, with the constant reservoir eutrophication, particularly the presence of toxic algae in a reservoir used for water production, calling for improved management plans in the scope of the Water Framework Directive.

Cyanobacteria algae dominance is usually described by two main processes; the capability of consuming N_2 dissolved in water (Paerl et al. 2001, Havens et al. 2003, Rolff et al. 2007), and the capability of maintaining growth even under conditions of low light availability (Havens et al. 2003). The nitrogen fixation characteristics of some types of cyanobacteria allows them to be independent of the availability of inorganic forms of nitrogen (e.g., ammonia, nitrate). However, under conditions of nitrogen limitation, cyanobacteria have also the potential to generate blooms if phosphorus is available (Havens et al. 2003).

Such cyanobacterial response to phosphorus availability may have occurred in the Enxoé reservoir after 2002 when these species became dominant (INAG 2004; Coelho et al. 2008). 2000/2001 was a wet hydrologic year, and the winter floods transported adsorbed material into the reservoir. The first blooms consumed the available inorganic material while organic matter deposited. The accumulation of organic matter at the bottom of the reservoir and the corresponding increase in mineralization may have depleted the oxygen near the bottom (where mineralization is more intense). Thus, under these anoxic conditions, phosphorus may have been released from the absorbed phase to the water column and fueled blooms. These processes were noted by Coelho et al. (2008) as the probable drivers for algal bloom in Enxoé, and also for cyanobacterial dominance. Those authors further linked the cyanobacteria blooms in the reservoir to the input loads from the watershed, and considered that such blooms could be associated with phosphorus input. Usually, phosphorus is adsorbed onto fine soil particles and transported throughout the catchment associated with water erosion. Phosphorus feeding from the watershed may have fueled the process, which consists of both a fast and a delayed response in the reservoir (initial blooms arise from the consumption of input dissolved nutrients, while later blooms are attributable to sediment sources, e.g., mineralization and desorption under anoxic conditions). The same need for understanding the role of erosion and phosphorus inputs in Enxoé reservoir blooms was also stated by Ramos et al. (2015a, 2015b).

The understanding of the Enxoé trophic state must ultimately integrate the watershed and the reservoir in order to determine the impact in the reservoir of management responses in the watershed (e.g., changes in agricultural practices, erosion control). This includes coupling a watershed model and a reservoir model (integrating the available data) to determine the best-suited management strategies (in the watershed and/or reservoir) to reduce the reservoir trophic status. However, there is first the need of understanding the watershed dynamics and quantifying nutrient feeding into the Enxoé reservoir.

The SWAT model (Neitsch et al. 2002) was here used for watershed characterization of the long-term fluxes to the reservoir. This model has been widely applied to a range of watershed sizes and configurations to simulate flow and nutrient export on daily, monthly and annual scales (Gassman et al. 2007; Zhang et al. 2008). Examples of such implementation in small-sized watersheds with similar land uses as Enxoé can be found in Geza and McCray (2008), and Green and van Griensven (2008), both in the USA; Yevenes and Mannaerts (2011) application for quantifying nitrogen export in a Portuguese catchment; Dechmi et al. (2012) and Panagopoulos et al. (2011) in other semi-arid Mediterranean watersheds in Spain and Greece, respectively; and Debele et al. (2008) who also successfully linked SWAT to the reservoir model CE-QUAL-W2 for water quality management.

The objectives of this study were thus to understand the water and nutrient long-term dynamics in the Enxoé catchment using the SWAT model, and to quantify nutrient loads to the Enxoé reservoir. As Enxoé basin was ungauged, field data were first collected between 2010 and 2011 in order to calibrate/validate the model. This study is the first of a series of modeling studies aimed at improving water management plans in the Enxoé basin.

3.1.2 Material and Methods

3.1.2.1 Study area

Enxoé is a 60 km^2 catchment located in southeast Portugal, in the left margin of the Guadiana River (Figure 1). The Enxoé river has a bed length of approximately 9 km from its headwaters to the reservoir. The Enxoé reservoir (37º 59' 38.121'' N, 7º 27' 54.776'' W) limits the catchment downstream, and has a total volume of 10.4 hm^3, a surface area of approximately 2 km^2, and an average depth of 5 m.

The climate in the region is dry sub-humid to semi-arid. The precipitation regime is characterized by a highly irregular behavior, varying between relatively abundant rainfall episodes, concentrated in only a few minutes or hours, and frequent drought episodes that can last from a few months to a couple of years. The annual average precipitation is 500 mm, irregularly distributed throughout the year (80% of the annual precipitation is concentrated between October and April). As a result, the river exhibits relatively large flow in the winter as a response to rain events, reduced flow in the spring after rain ceases, and no flow/pool formation during the summer or extended drought periods (Ramos et al. 2015a).

Figure 1. Location of the Enxoé catchment and monitoring stations.

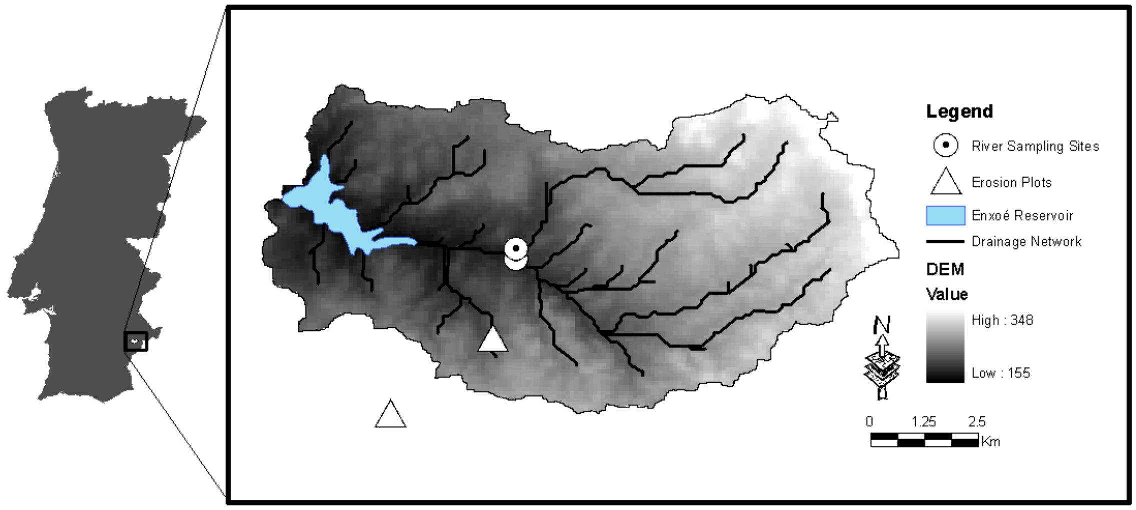

The slopes are gentle, with the river showing an average slope of approximately 2%, while the catchment has an average slope of 5-6%. These conditions promote water pooling and the occurrence of disconnected flow during dry periods. The soils in Enxoé originate mainly from granite and limestone (each with approximately 30% of the total area) and schist (with approximately 10% of the total area). The land is mainly used for growing olive trees, agro-forestry of holm-oaks ("montado"), and annual rainfed crops (wheat, oats, and sunflower), each covering approximately 30% of the total area (Figure 2; Table 1). Extensive livestock production is the most important animal-farming activity in the catchment. According to the 1999 agricultural census (INE, 2001), cow (602) and sheep (4365) production corresponds to approximately 0.1 and 0.01 livestock units (LSU), respectively. The catchment has a population of 1000 inhabitants, mainly concentrated in Vale de Vargo (Figure 2). The respective waste water treatment plant discharges outside the watershed since 2006 as a protective measure to the Enxoé reservoir. The reservoir currently supplies the villages of Mértola and Serpa (25,000 inhabitants).

Table 1 Enxoé land use (Source: Corine 2000).

Land Use	Area (km^2)	(%)
Olive trees	21	35%
Annual crops – Rotation 2	18	30%
Agro-forestry of holm-oaks (Pasture/“Montado”)	11	19%
Agro-forestry of holm oaks (Forest/ “Montado)”	7	11%
Annual crops – Rotation 1	2	3%
Water	1	2%
Urban area	<1	<1%
Total	61	100%

Figure 2. Land use distribution map (Corine 2000).

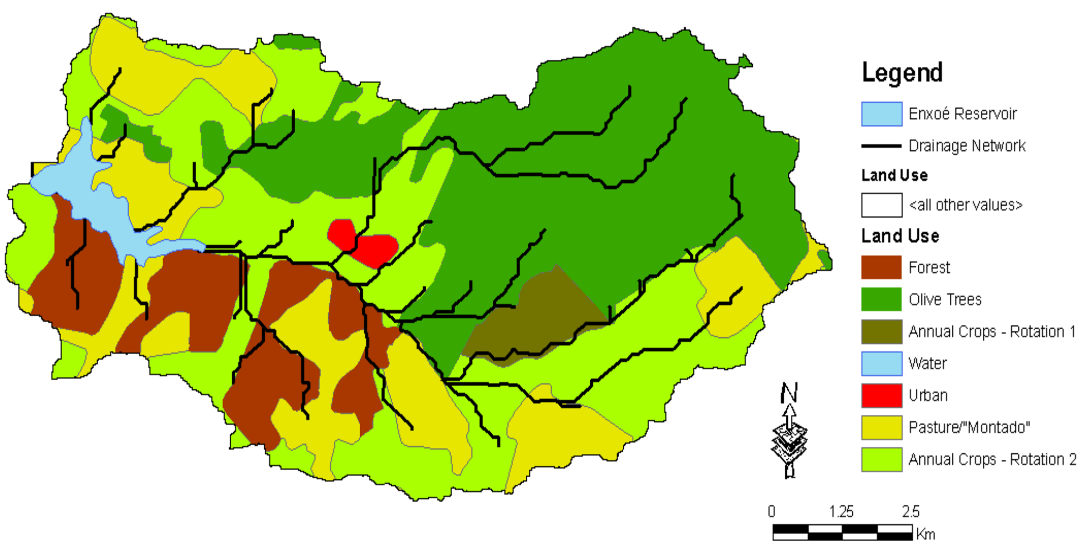

3.1.2.2SWAT model description

SWAT is a basin-scale, distributed, and continuous-time model (Neitsch et al. 2002) that includes the main hydrological and nutrient processes occurring in an extensive Mediterranean catchment like Enxoé (e.g., flow temporality, crops, agricultural practices). The SWAT model divides the watershed into sub-basins and hydrological response units (HRU) that are homogeneous in terms of soil, land use, and slope (the basic computation units). The soil domain may be divided into vertical layers.

The hydrological cycle is based on the computation of the soil water balance equation, as follows (Neitsch et al. 2002):

$$SW_t = SW_0 + \sum_{i=1}^{t}\left(R_{day} - Q_{surf} - E_a - Q_{perc} - Q_{gw}\right) \tag{1}$$

where SW_t and SW_0 are the final and initial soil water contents (mm), respectively, t is the time (days), R_{day} is the precipitation (mm), Q_{surf} is the surface runoff (mm), E_a is the actual evapotranspiration (mm), Q_{perc} is the percolation (mm), and Q_{gw} is the return flow (mm), all related to day i. The model computes evaporation from soils and plants separately as described by Ritchie (1972). Potential soil water evaporation is predicted as a function of potential evapotranspiration (PET) and leaf area index (LAI), whereas actual soil water evaporation is predicted by using exponential functions of water content and soil depth. Plant transpiration is predicted as a linear function of PET and LAI. In this study, PET was computed with the Penman-Monteith method (Jensen et al. 1990), which requires daily data on solar radiation, wind speed, air temperature, and relative humidity. Q_{perc} is estimated from the soil water content above field capacity, while Q_{gw} is computed by combining a storage routing technique and a crack-flow model (Neitsch et al. 2002). Of particular interest to this study is the estimation of surface runoff (Q_{surf}) which is computed with the modified curve number (CN) method (USDA-SCS 1972), as follows:

$$Q_{surf} = \frac{\left(R_{day} - I_a\right)^2}{\left(R_{day} - I_a + S\right)} \tag{2}$$

where I_a is the initial abstractions which includes surface storage, interception, and infiltration prior to runoff (mm), and S a retention parameter which varies with the soil type, land use, land management, slope, and soil water content. On the other hand, the subsurface flow (Q_{lat}) is simulated using a kinematic storage method dependent of the surface slope and soil water content (Neitsch et al. 2002).

Soil erosion in SWAT is computed from rainfall and surface runoff with the Modified Universal Soil Loss Equation (MUSLE) (Williams, 1975), which is a modified version of the Universal Soil Loss Equation (USLE) developed by

Wischmeier and Smith (1978). In MUSLE, the rainfall energy factor is replaced with a runoff factor, as follows:

$$\text{sed} = 11.8\left(Q_{surf}\ q_{peak}\ \text{area}_{HRU}\right)^{0.56} K_{USLE}\ C_{USLE}\ P_{USLE}\ LS_{USLE}\ CFRG \tag{3}$$

where sed is the sediment yield on a given day (ton), q_{peak} is the peak runoff rate ($m^3\ s^{-1}$), area_{HRU} is the area of the HRU (ha), K_{USLE} is the USLE soil erodibility factor, C_{USLE} is the USLE cover and management factor, P_{USLE} is the USLE support practice factor, LS_{USLE} is the USLE topographic factor, and CFRG is the coarse fragment factor. The SWAT model peak runoff rates are computed by a modified rational formula with the following form (Neitsch et al. 2002):

$$q_{peak} = \frac{\alpha_{tc} \cdot Q_{surf} \cdot \text{area}_{HRU}}{3.6 \cdot t_c} \tag{4}$$

$$\alpha_{tc} = 1 - \exp\left[2 \cdot t_c \cdot \text{Ln}(1 - \alpha_{0.5})\right] \tag{5}$$

where α_{tc} is the fraction of the daily rainfall that occurs during the time of concentration (-), t_c is the concentration time (h), and $\alpha_{0.5}$ is the fraction of the daily rain at the highest half hour intensity (-).

The nutrient component of the SWAT model includes inputs from agriculture, transport with runoff and groundwater, consumption by plants, and mineralization processes occurring in the soil (Neitsch et al. 2002). SWAT considers six different pools of phosphorus (P) in the soil. Three pools are inorganic forms of P while the other three pools are organic forms of P. Fresh organic P is associated with crop residue and microbial biomass. Active and stable organic P pools are associated with the soil humus. The organic P associated with humus is portioned into two pools to account for the variation in availability of humic substances to mineralization. Soil inorganic P is divided into solution, active, and stable pools. The solution pool is in rapid equilibrium (several days or weeks) with the active pool. The active pool is in slow equilibrium with the stable pool (Neitsch et al. 2002).

P is mainly removed from the soil by plant uptake and erosion. In the latter case, SWAT considers the amount of organic and mineral P transported with sediment to the stream with a loading function developed by McElroy et al. (1976) and later modified by Williams and Hann (1978), as follows:

$$sedP_{surf} = 0.001 conc_{sedP} \frac{sed}{area_{HRU}} \varepsilon_{P:sed} \tag{6}$$

where $sedP_{surf}$ is the amount of P transported with sediment to the main channel in surface runoff (kg ha^{-1}), $\varepsilon_{P:sed}$ is the P enrichment ratio, and $conc_{sedP}$ is the concentration of P attached to sediment in the top 10 mm (g m^{-3}), which is computed from the amount of P in the different pools, as:

$$conc_{sedP} = 100 \frac{\left(\min P_{act,surf} + \min P_{sta,surf} + orgP_{hum,surf} + orgP_{frsh,surf}\right)}{\rho_b \ depth_{surf}} \tag{7}$$

where $minP_{act,surf}$ is the amount of P in the active mineral pool (kg ha^{-1}), $minP_{sta,surf}$ is the amount of P in the stable mineral pool (kg ha^{-1}), $orgP_{hum,surf}$ is the amount of P in humic organic pool (kg ha^{-1}), $orgP_{frsh,surf}$ is the amount of P in the fresh organic pool (kg ha^{-1}), all related to top 10 mm ($depth_{surf}$), and ρ_b is the bulk density of the top soil layer (Mg m^{-3}).

Nitrogen (N) is extremely reactive and exists in a number of dynamic forms. It may be added to the soil in the form of fertilizer, manure or residue application, bacteriological fixation, and rain. In SWAT, there are five different pools of N in the soil. Two of the pools are inorganic forms of N, while the other three pools are organic forms of N. N transport occurs mainly in the nitrate and organic N forms.

Nitrate may be transported with surface runoff, lateral flow or percolation, using the following generic formula (Neitsch et al. 2002):

$$NO3 = \beta_{NO3} \ conc_{NO3,mobile} \ Q_x \tag{8}$$

where NO3 is the nitrate removed by each of the physical transport mechanisms here considered (i.e., surface runoff, lateral flow, percolation) (kg ha^{-1}), β_{NO3} is concentration of nitrate in the mobile water for the top 10 mm of soil (kg ha^{-1}) (only considered for surface runoff and subsurface lateral flow in the top layer), and Q_x is the physical transport mechanism considered (Q_{surf}, Q_{lat}, Q_{perc}). Nitrate entering the shallow aquifer from the soil profile through percolation (leaching) may remain in the aquifer, be moved with groundwater flow into the main channel, be transported out of the shallow aquifer with water moving into the soil zone in response to water deficiencies, or be moved with recharge to the deep aquifer.

On the other hand, organic N is mainly transported with sediment to the stream, similarly to P transport. The same approach developed by McElroy et al. (1976) and William and Hann (1978) is applied to separate runoff events. Estimation of the daily organic N runoff losses are based on the sediment yield, the N enrichment ratio, and the concentration of N in the topsoil layer, which is dependent of the amount of organic N in the fresh, stable, and active pools (Neitsch et al. 2002).

3.1.2.3Model setup, calibration, and validation

3.1.2.3.1 Model implementation

The SWAT model (Neitsch et al. 2002) was used to estimate the long-term water and nutrient dynamics in the Enxoé catchment, and to quantify nutrient loads to the Enxoé reservoir. Data were introduced in the model interface AVSWAT for ArcView®, and the model was run using the SWAT 2005 executable version. The model was first calibrated/validated against field data, and then results were extrapolated to the basin scale.

Table 2 describes the digital terrain model (DTM), and the land use, soil texture, and weather data used in SWAT. The land use map with SWAT classification is presented in Figure 2, where, as stated previously, olive trees (orchards), agro-forestry of holm-oaks, and annual rainfed crops each represent approximately 30% of the total area (Table 1). The land use map was obtained from Corine 2000, which was first compared with aerial pictures from 2006 and local observations for consistency.

Table 2 Data used for SWAT model implementation.

Data type	Description	Origin	Resolution	Period	Frequency
DTM	SRTM Digital Elevation	NASA	90 m	-	-
Land Use	Corine Land Cover 2000	EEA	1:100000	1999-2002	-
Soil Texture	European Soil database	JRC, EU	1:1000000	1996	-
Precipitation	Daily input	Valada and Sobral da Adiça stations, National Water Institute (www.snirh.pt/)	-	1980-2011	Daily
Other weather data	Temperature, relative humidity, solar radiation, and wind speed monthly averages for weather generator (1980-2000) and daily data (2000-2011)	Serpa station, National Meteorology Institute, and Valada, Sobral da Adiça and Monte da Torre stations, National Water Institute (www.snirh.pt/)	-	Variant for monthly averages and 2000-2011 for daily data	Monthly averages and daily data after 2000

Information about annual agricultural practices (crop rotations and fertilization) was obtained from questionnaires given to farmers. Annual rainfed crops included rotation between wheat and oats (crops rotation 2), and rotation between sunflowers, wheat, and oats (crops rotation 1) (Figure 2). The annual input fertilization loads were estimated to range from 18-80 kgN.ha^{-1}.year^{-1}, and approximately 20 kgP.ha^{-1}.year^{-1} (Table 3). The animal nutrient production was obtained from the 1999 national census data (INE, 2001) (Table 4). Animal loads were distributed homogeneously in the agro-foresty of holm-oaks (sheep and cattle) and olive trees (sheep) sites. The annual animal loads were estimated to range from 6-30 kgN.ha^{-1}.year^{-1} and 1-4 kgP.ha^{-1}.year^{-1}. Annual input fertilization and animal loads can be considered low, which is justified by the fact that agriculture and pasturing in the region are extensive.

Table 3 Enxoé agricultural practices (information collected by questioning farmers).

Agricultural Practice	Crop Wheat and Barley	Oats	Sunflower	Olive Trees
Planting	November	October	April	-
Fertilization	November (20 kgN/ha) November (18 kgP/ha) January (50 kgN/ha) February (20 kgN/ha)	March (40-80 kgN/ha)	April (22 kgP/ha)	April to July (24-60 kgN/ha)
Harvest	June	June	September	-

Table 4 Number of animals in the Enxoé watershed (INE 2001), and annual associated loads (Ministry of Agriculture 1997).

Type	Number	Annual Load Nitrogen (tonN/year)	Phosphorus (tonP/year)
cattle	602	34	5
sheep	4365	78	13

The Enxoé catchment was ungauged which partially constrained model calibration/validation due to data limitation. Thus, model predictions of the inflow to the reservoir were calibrated/validated through a reservoir balance computation using volume, discharge, precipitation, and evaporation data for the period between January 2006 and August 2009, when all the components were available. On the other hand, SWAT nutrient dynamics was calibrated/validated using data collected in the two main tributaries flowing to the Enxoé reservoir (Figure 1) between 2010 and 2011; both monitoring stations were found to have similar concentrations, trends, and values. The river data were collected on a weekly basis (with 3 samples collected each time) during autumn, winter, spring, and summer, when water existed (temporary river). The parameters evaluated in the laboratory were the electrical conductivity, pH, P, nitrate, and suspended solids.

SWAT was further calibrated/validated by qualitatively comparing model predictions with erosion data measured in plots (60-900 m^2) installed in two of the main land uses (olive trees and agro-forestry of holm-oaks) between 2010 and 2011 (Figure 1). The runoff volume and concentrations were sampled in the erosion plots in weekly to monthly basis or after strong rain events. Table 5 summarizes the data used for calibrating/validating flow and water quality in the Enxoé catchment.

Table 5 Description of the data used for SWAT model validation.

Data type	Station	Origin	Period	Frequency
Reservoir Inflow:				
Reservoir Discharges	Enxoé Reservoir (26M/01A)	National Water Institute (www.snirh.pt/)	2005-2009	Monthly
Precipitation	Herdade da Valada (26M/01C), Sobral Adiça (25N/01UG)	National Water Institute (www.snirh.pt/)	1980-2011	Daily
Evaporation	Herdade da Valada (26M/01C), Monte da Torre	National Water Institute (www.snirh.pt/)	2001-2011	Daily
Erosion:				
Erosion rates	Two plots in two main land uses. Volume and solids concentrations collected	Measured	2010-2011	Weekly to monthly
Water quality in river:				
Nutrient	Two stations in the two main tributaries	Measured	2010-2011	Weekly to monthly

3.1.2.3.2 Calibration procedure

SWAT calibration procedure involved modifying specific parameters until deviations between model predictions and observations were minimized. The SWAT model sensitivity analysis for discharge revealed that the most important parameters that impacted the results were the moisture condition II curve number (CN2), the threshold water level in shallow aquifer for base flow (Gwqmn), the soil evaporation compensation coefficient (ESCO), and the available water capacity (SOL_AWC) (Neitsch et al. 2002). However, the main differences between the hydrograph produced by using the default parameters available in the SWAT model and the real hydrographs measured in small-sized watersheds without known aquifer interactions in southern Portugal is that the SWAT model creates longer baseflows that last for months after rain events while the peaks are usually lower. These differences occur because the delay time for aquifer recharge (GW_DELAY) and the baseflow recession constant (ALPHA_BF) parameters, which control the travel timing of water between the soil and the aquifer and between the aquifer and the river, are unadjusted for small, temporary river watersheds in which travel times are small and hydrographs have a fast rise and fall correlated to rain events (Ramos et al. 2015a). Thus, in Enxoé, the calibration procedure for hydrology consisted of changing the parameters GW_DELAY and ALPHA_BF as presented in Table 4. The values chosen were the same as those obtained via other SWAT projects in the same area (Alentejo) that compared well the daily flow available, and were also of the same order as those used in studies conducted in similar temporary rivers located in arid or semi-arid areas, such as the Meca River, Spain (Galvan et al. 2009), and the Gajwel watershed, India (Perrin et al. 2012).

In terms of water quality, the river stream parameters (Table 6) were adjusted by trial and error to represent the behavior observed in the field data. Although SWAT initial results of total N and total P were satisfactory when compared to field data, the first simulations exhibited overpredictions of organic N, ammonia and inorganic P, and underpredictions of nitrate concentrations, which drove the changes in the rates for mineralization between the organic and inorganic species described in Table 6. In addition, in the first simulations, nitrate and orthophosphate concentrations appeared to be associated only with rain events, which then decreased to almost zero after an event while the respective field data concentrations remained higher throughout.

SWAT uses a QUAL-2E (Brown and Barnwell 1987) formulation for the river quality, in which P deposition is disconnected from the suspended sediment deposition, and deposition and release are not linked through a sediment state variable accounting for these fluxes. However, to maintain mass conservation, the results presented were verified so that the average annual deposition loads were higher than the release loads to assure consistency in the selected parameters.

Table 6 Calibrated parameters used in SWAT simulations.

Parameter Description	SWAT name	SWAT file	Default Value	Calibrated Value
Hydrodynamic:				
Groundwater delay (days)	GW_DELAY	.gw	31	3
Base flow recession alpha factor (days)	ALPHA_BF	.gw	0.048	1
Water Quality:				
Linear parameter for calculating the maximum amount of sediment that can be reentrained during channel sediment routing	SPCON	.bsn	0.0001	0.00005
Organic phosphorus settling rate in the reach at 20ºC [day-1]	RS5	.swq	0.05	0.35
Benthic (sediment) source rate for dissolved phosphorus in the reach at 20ºC (mg dissolved P/(m^2·day))	RS2	.swq	0.05	0.5
Benthic source rate for NH_4-N in the reach at 20ºC (mg NH_4-N/(m2·day))	RS3	.swq	0.5	10
Rate constant for hydrolysis of organic N to NH4 in the reach at 20º C (day-1)	BC3	.swq	0.21	0.25
Rate constant for biological oxidation of NH_4 to NO_2 in the reach at 20º C (day-1)	BC1	.swq	0.55	2.0
Rate constant for biological oxidation of NO_2 to NO_3 in the reach at 20º C (day-1]	BC2	.swq	1.1	3.0
Rate constant for mineralization of organic P to dissolved P in the reach at 20º C (day-1)	BC4	.swq	0.35	0.01

3.1.2.3.3 Statistical analysis

Model calibration/validation was carried out by comparing field measured data with SWAT simulated values using various qualitative and quantitative measures of the uncertainty. Graphical analyses, such as time-series plots, were used to identify the general trends, potential sources of errors, and differences between the measured and predicted values. Model performance was further evaluated using the coefficient of determination (R^2), the root mean squared error (RMSE), and the Nash–Sutcliffe model efficiency (NSE) (Nash and Sutcliffe 1970). R^2 values close to 1 indicate that the model explains well the variance of observations. RMSE values close to zero indicate small errors of estimate and good model predictions. NSE values between 0.0 and 1.0 are generally viewed as acceptable levels of performance, whereas values <0.0 indicate that the mean observed value is a better predictor than the simulated value, corresponding to unacceptable performance (Moriasi et al. 2007).

3.1.2.3.4 The long-term dynamics of the Enxoé catchment

After model calibration/validation, the SWAT model was used to extrapolate results to the long-term in order to better understand the catchment behavior in terms of water and nutrient dynamics. Hence, the water and nutrient balance was computed for a 30 year's period (1980-2010) to account for climate variability. The same data presented in Table 2 was used for the long-term study. Weather data was collected from the meteorological stations of the National Institute of Water (www.snirh.pt) located in the vicinity of the Enxoé catchment (Herdade da Valada, Sobral da Adiça, Monte da Torre stations). The same calibrated/validated parameters defined in Table 6 were naturally used in the long-term analysis.

3.1.3 Results and Discussion

3.1.3.1 Model results versus field data

The comparison between the SWAT model and the field data was made with respect to: i) water inflow to the reservoir, and ii) nutrient loads in the river.

3.1.3.1.1 Reservoir Inflow

The input flow to the reservoir has an important impact on the reservoir water volume and depth (the water quality in small depths tends to deteriorate because of the availability of light at the bottom), on the retention time (increasing the retention time increases the accumulation and time for algal assimilation of nutrients), and on the horizontal and vertical mixing of water (intense mixing may deliver bottom nutrients to the surface, where there is more light and higher temperatures). Therefore, describing the input flow from the watershed is of major importance for driving reservoir dynamics.

Figure 3 shows the comparison between monthly flows computed from the reservoir balance and SWAT predictions for 2006-2009. The respective goodness-of-fit tests are presented in Table 7. Both SWAT predictions and the estimates from the reservoir balance exhibited the same trends (higher reservoir inflows in winter as a response to precipitation and a very low or zero inflow in the summer in the absence of rain). The value of R^2 was high (0.78), showing that the model was able to explain the variability of observed data. The error of the estimate was quite small, with RMSE values reaching 0.21 $hm^3.month^{-1}$. The NSE value was also very high (0.77), thus indicating that the mean square error was much smaller than the measured data variance.

Figure 3. Comparison between measured (from the reservoir balance) and simulated (SWAT) monthly inflows to the Enxoé reservoir (top), and scatterplot of the measured versus simulated monthly inflow values (bottom) between 2006-2009.

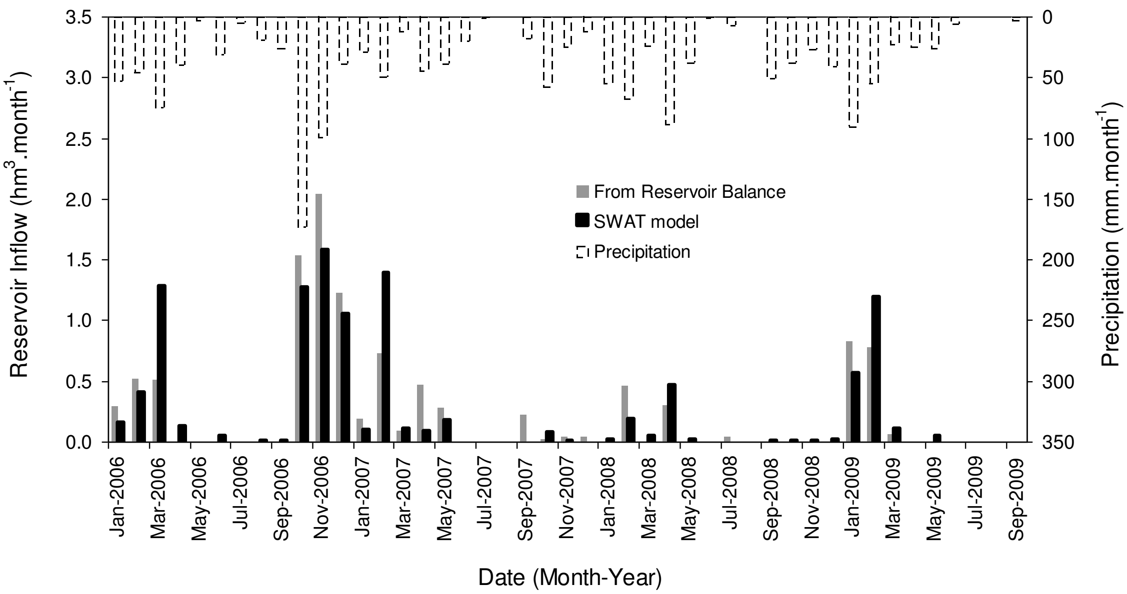

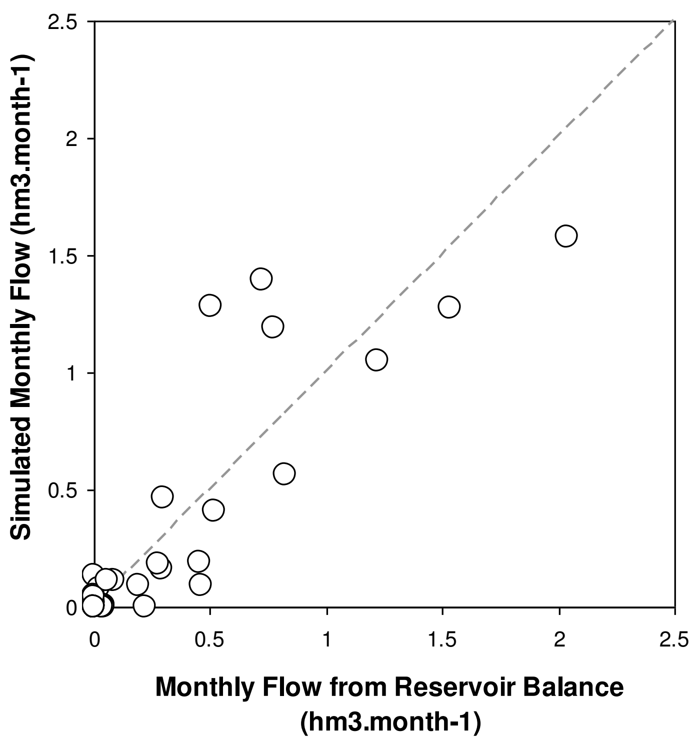

These results are comparable to those reported by Fohrer (2001) in two watersheds in Hesse, Germany (R^2 of 0.71-0.92); Geza and McCray (2008) in Turkey Creek (126 km^2), Denver, USA (R^2 of 0.62-0.74; NSE of 0.61-0.70); and Green and van Griensven (2008) in different small watersheds in Texas, USA (R^2 from 0.60-0.96; NSE from 0.59-0.95). In the Mediterranean region, Dechmi et al. (2012) obtained high R^2 and NSE values of 0.90 in the Del Reguero River watershed (20 km^2) in northern Spain, while Panagopoulos et al. (2011) found R^2 values of 0.86-092 and NSE values of 0.51-0.68 in the Arachtos catchment (2000 km^2), in western Greece. Thus, in terms of the monthly flow, the results obtained in Enxoé fall in between the results of other studies, showing that the SWAT model was able to represent the inflow to the reservoir on a monthly scale.

Table 7 Summary of the comparison of the SWAT model results to the collected data in the Enxoé watershed.

Parameter	Period	Data average	Model Average	RMSE	R^2	Nash-Sutcliffe Model Efficiency
Flow:						
Monthly Reservoir Inflow	1996-2009	0.24 hm^3.month^{-1}	0.24 hm^3.month^{-1}	0.21 hm^3.month^{-1}	0.78	0.77
Slope Erosion:						
Annual erosion rates	2010-2011	0.1 - 0.2 ton.ha^{-1}	0.35 ton.ha^{-1}	-	-	-
River Water quality:						
Monthly Total N Load	2010-2011	0.62 tonN.month^{-1}	0.50 tonN.month^{-1}	0.46 tonN.month^{-1}	0.69	0.65
Monthly Total Suspended Solids Load	2010-2011	1.86 tonTSS.month^{-1}	1.80 tonTSS.month^{-1}	2.23 tonTSS.month^{-1}	0.42	0.19
Monthly Total P Load	2010-2011	0.034 tonP.month^{-1}	0.030 tonP.month^{-1}	0.025 tonP.month^{-1}	0.63	0.62

3.1.3.1.2 River sediment and nutrient loads

Loads can give insights about the pressures that the Enxoé reservoir is subjected to, and are dependent of the catchment hydrology. Sediment and nutrient loads were estimated using SWAT daily flow predictions for the monitored period (2010-2011), using the same calibrated/validated parameters for assessing the inflows to the reservoir on a monthly scale (Table 6). During 2010-2011, the Enxoé River, as temporary, exhibited no flow or ephemeral conditions from June to October (Figure 4). The first rain events (October/November) generated flow peaks that were quickly reduced as the soil was not fully saturated and groundwater flow was greatly diminished. From December/January to March, the response to rain events still existed. Because the soil was saturated, baseflows were maintained for longer periods but still fell quickly, especially during months with less rain (January and February 2011). This temporality and flushy flow regime strongly influenced loads to the Enxoé reservoir, particularly as these conditions created long periods of low waters with increased retention times that had consequences for the river water quality and promoted in-stream processes, as observed in a similar-sized catchment by Lillebø et al. (2007).

Figure 4. SWAT estimate of the Enxoé river flow during 2010-2011, when water quality data were collected.

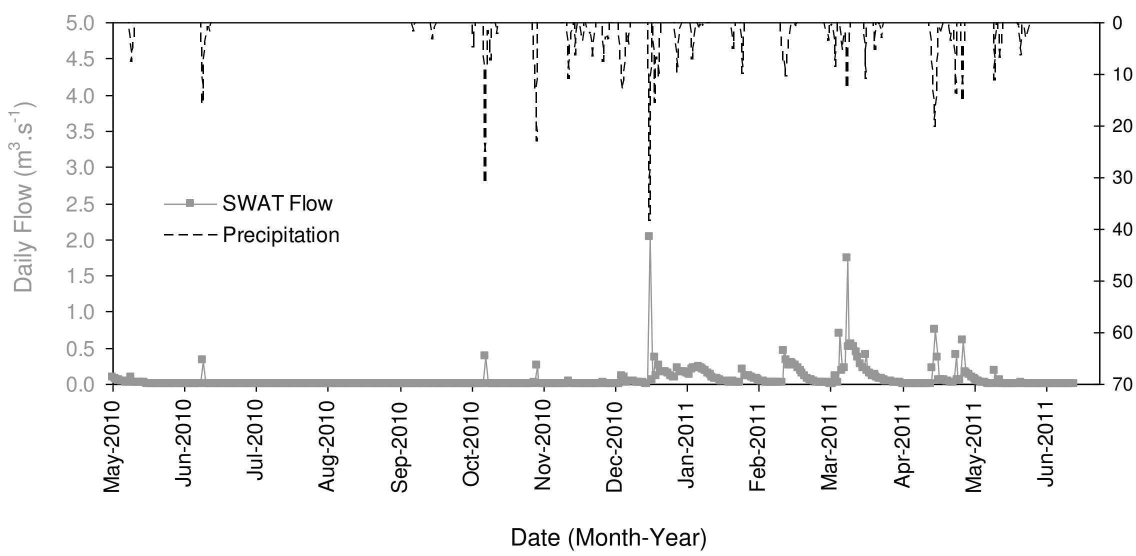

Sediment load

The model fit to the measured total suspended sediment (TSS) loads resulted in lower R^2 (0.42) and NSE (0.19) values than for flow, P, and N (Table 7). However, these results were highly dependent on the value observed in December

2010, when approximately 8 $tonTSS.month^{-1}$ were predicted by the model while only 1 $tonTSS.month^{-1}$ was observed in the field data (Figure 5). Without it, the R^2 and NSE values would have reached 0.78 and 0.71, respectively, which would be more in accordance with the results obtained for the N and P.

Figure 5. Comparison between the measured and simulated (SWAT) total suspended solids (TSS) loads (top), and scatterplot of the measured versus simulated TSS loads (bottom) during 2010-2011 (dots denote averages while the segment represents the maximum and minimum monthly load).

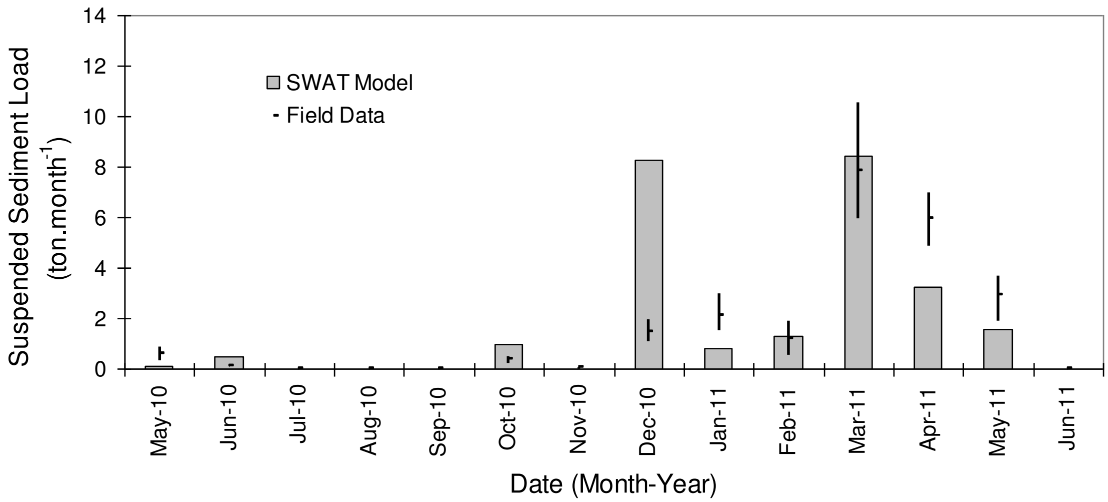

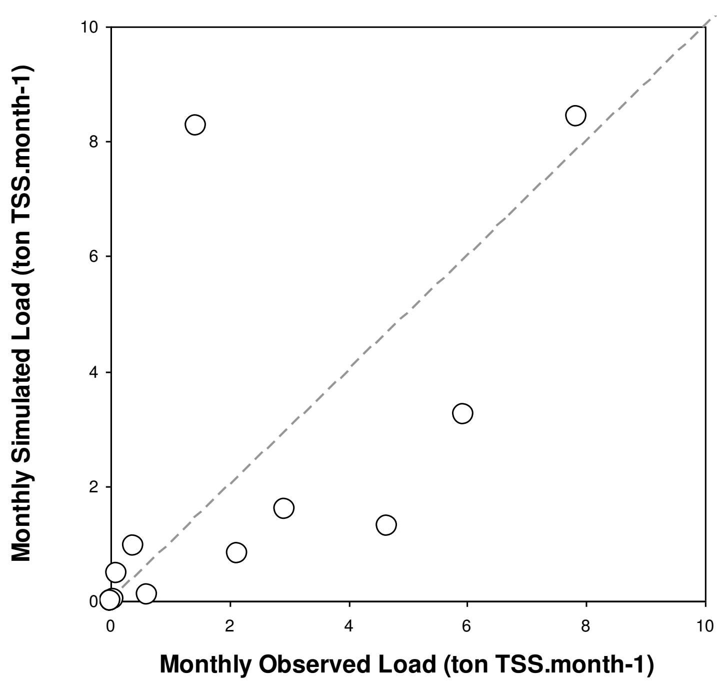

That difference may be attributable to the quality of field data during that period. In fact, several rain events occurred in December 2010 that produced large flow peaks. The rain event of 19/12/2010 (38 mm) even generated the highest flow peak (Figure 4). Therefore, it was expected that the December 2010 large flow peak would produce a high sediment load as estimated by SWAT. That same trend was observed in March 2011, with SWAT generating high loads consistent with the observed data when heavy rains and high flow peaks also occurred. However, due to the fact that the field data were collected three weeks before the event of 19/12/2010, and after that only in February, the sampled SST concentrations in December 2010 may not be characteristic of that month, meaning that some degree of uncertainty associated to data needs to be taken into account here.

On the other hand, the mismatch between model predictions and field observations in December 2010 may also be attributable to model structure errors. On 19/12/2010, a single rain event carried out 7 of a total of 8 tons of TSS transported during that month. The estimation of this high sediment load on a single day resulted from the high peak runoff rates that the MUSLE equation (Eq. 4) generated. For reduced t_c (higher slopes in the watershed) and high $\alpha_{0.5}$ values, q_{peak} may be several times higher than Q_{surf}, yielding artificial erosion rates.

Similar weaker fits to sediment loads data have been reported in the literature. Dechmi et al. (2012) with respect to daily loads (R^2 of 0.18) and Panagopoulos (2011) with respect to monthly loads (NSE of 0.34-0.38) linked it to field data extrapolations. Chu et al. (2004) with respect to monthly loads (R^2 of 0.19; NSE of 0.11) associated it to possible miss predictions of flow in Warner Creek, Maryland, USA. Aside from the value registered in December 2010, the R^2 (0.78) and NSE (0.71) values obtained are of the same order of magnitude as those of Dechmi et al. (2012) for monthly loads (NSE of 0.52-0.72), and Gikas et al. (2005) in the Vistonis lagoon, Greece (R^2 generally higher than 0.70 and up to 0.98 in 9 stations). The better fit is also consistent with the fact that the average erosion rates predicted by SWAT in Enxoé in 2010-2011 were similar to the ones measured in the field erosion plots during that period (0.1 to 0.4 $ton.ha^{-1}.year^{-1}$; Table 7). The erosion plot results are only used for indicative comparison though because data only exist for one year.

Nutrient loads

The simulated nutrient loads showed a good fit to the measured field data during 2010-2011. The values of R^2 were relatively high for both N (0.69) and P (0.63), while the NSE values were quite satisfactory (0.65 and 0.62 for N and P, respectively). The RMSE values were also relatively low. These results are in line with reports from other applications using the SWAT model. For example, for the total P monthly load, Dechmi et al. (2012) obtained an R^2 of 0.70-0.71 and an NSE of 0.63-0.66, whereas Green and van Griensven (2008) obtained higher values for organic P and soluble P (R^2 of 0.72-0.78; NSE of 0.5-0.78), and for nitrate and organic N (R^2 of 0.7-0.8; NSE of 0.68).

The monthly total N (Figure 6) and P (Figure. 7) loads showed, as expected, that these were low or nil during the summer months (July to September 2010) when flow was reduced or absent. In the beginning of winter or spring (rainy months) higher loads occurred, with SWAT representing well this trend. However, the model clearly showed an under prediction of the nutrients loads between January and March 2011, reaching differences of 1 $tonN.month^{-1}$ and 0.05 $tonP.month^{-1}$ when compared to field data. Considering that measured concentrations during these months were fairly stable, the precipitation registered during those months was low (Figure 4) and as consequence the river flow peaks produced as a direct surface water response were also low, and visible base flow was still observable because the soil was saturated from the previous months. In this circunstances, model under predictions of field data during the period between January and March 2011 can only have three possible explanations.

Figure 6. Comparison between the measured and simulated (SWAT) nitrogen loads (top), and scatterplot of the measured versus simulated nitrogen loads (bottom) during 2010-2011 (dots denote averages while the segment represents the maximum and minimum monthly load).

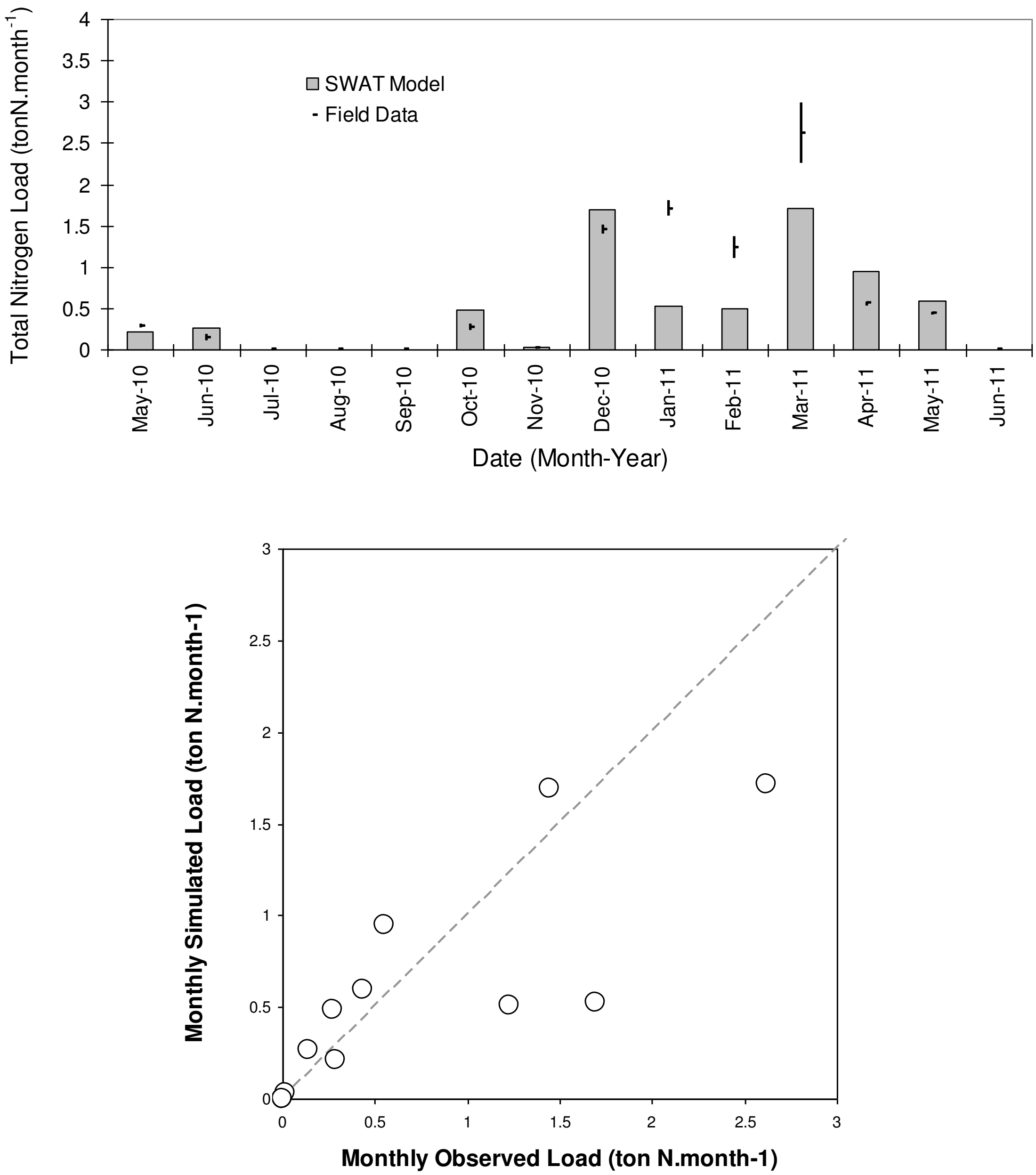

Figure 7. Comparison between the measured and simulated (SWAT) phosphorus loads (top), and scatterplot of the measured versus simulated phosphorus loads (bottom) during 2010-2011 (dots denote averages while the segment represents the maximum and minimum monthly load).

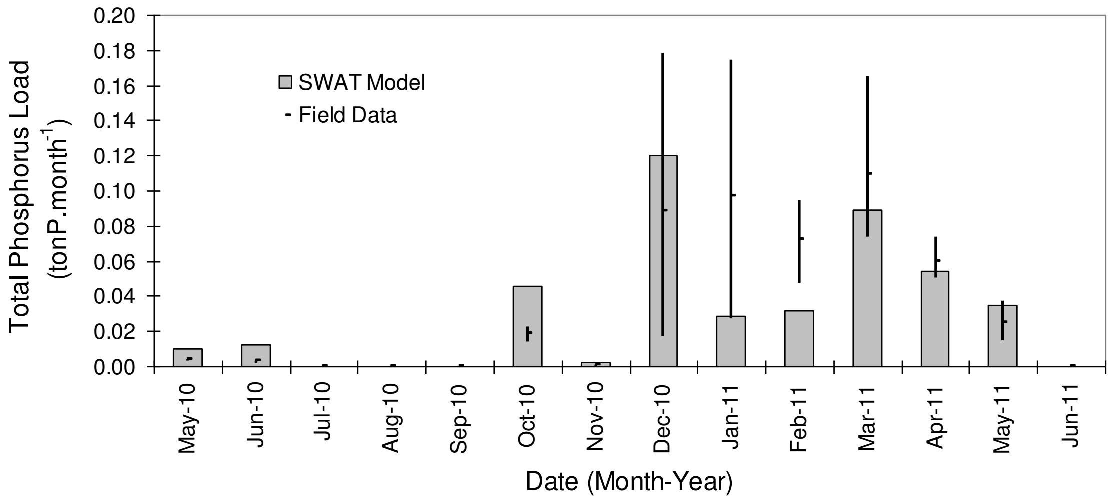

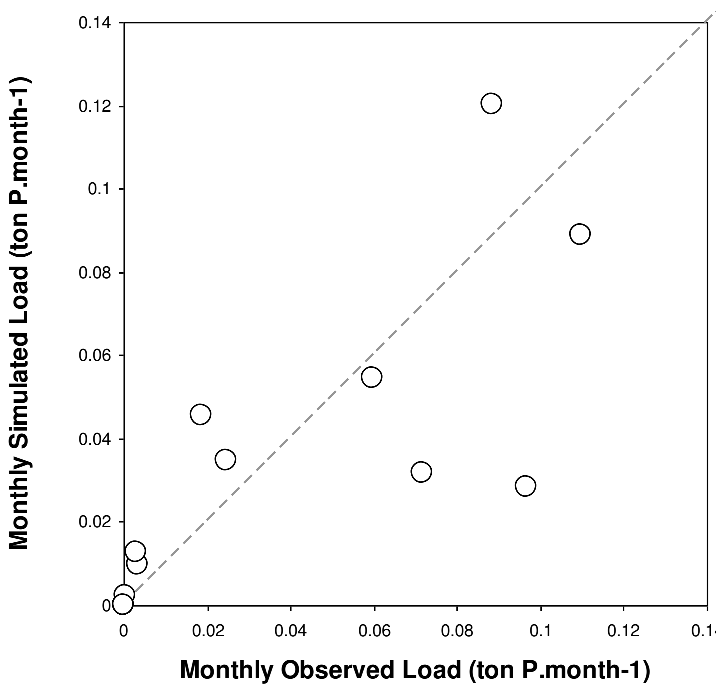

Since the surface water flow between January and March 2011 was reduced but base flow was still present, one could consider that in these months, loads under predictions could be explained by the lack of groundwater feeding and fertilization. However, this would only affect nitrate transport (P is retained in the surface and is hardly transported through soil or from groundwater to the river). Nevertheless, the SWAT model was tested for the amount of fertilization that would achieve the order of magnitude of the N loads registered in the field data between January and February 2011. Only by considering an unrealistic high value of 500 kg mineralN.ha^{-1} would be possible to match those values as rain, infiltration, percolation, and groundwater flow were not enhanced during these months since, as seen, rain was limited, Also, vegetation was able to uptake the most part when fertilization amounts were smaller.

A second explanation could be a lack on load being delivered by the surface water. However, the surface water was reduced in these months as a result of lower precipitation and flow peaks (Figure. 4). Also, TSS loads (transported by surface water) did not exhibit the same under predictive trend as seen for N and P loads. Nonetheless, the type of fertilization (mineral and organic forms) was also tested in SWAT, but the effect was almost unobservable during January and February 2011 due to the low surface water flows; only in the following months that effect was observed, increasing the estimated load and exceeding the field data.

If the explanation for the SWAT under prediction behavior between January and March 2011 was not in the surface or groundwater flow, the alternative answer should be the river itself. In SWAT, the in-stream processes are important for defining the order of magnitude of nutrient concentrations in low waters, but cannot be used as an infinite source of nutrients. Additionally, the source needed to fit model load predictions to field data in those months would generate abnormal loads in the remaining months. Therefore, the process generating an additional source of nutrients should be mostly present in these months (January to March).

A possible explanation could be related to animal access to the river resulting in a consequent direct nutrient source. However, animals were present in the catchment throughout the year. Moreover, storm events would typically be followed by concentration peaks, specifically of ammonia, that were not verified in field data (ammonia was low, while the concentrations of other N species were stable throughout the seasons).

A more likely explanation should be the development of river beds in the Enxoé river and the biochemical processes that occur at the sediment/water column interface. In Enxoé, the reed bed developed intensively (high density) inside the river sections upstream and downstream of the sampling point where water was retained in pools or shallow aquifers during the spring. These reed beds dried out during the summer and were dragged downstream by high flows in the winter. The remaining roots inside the river bed may have been the organic matter source that promoted in-stream processes mainly after the first winter months, particularly in months with lower flows like January and February 2011, during which the residence time increased (because of the occurrence of disconnected flow and pools). Thus, the reed bed density needed to fit SWAT loads to field data in those months was quantified. It was assumed percentages of the root fraction of 10-50%, and contents of N of 5-50% and P of 1-10% in those roots (producing a wide range of model results for different crops). A density of 5 to 10 $ton.ha^{-1}$ in the river bed upstream of the sampling point was determined to be sufficient, which corresponded to 0.5 to 1 kg $biomass.m^{-2}$. These amounts are quite reasonable for the Enxoé river because in some areas it is not possible to see the river bed, while in other areas, the occurrence is sparser. In the case of P, the amount needed to develop the reed bed plants (i.e., the amount that may be mineralized in roots and generate the field data loads) was less than the annual deposition load, whereas N could be available from deposition and soil and groundwater nitrate pools. There is little information in the literature about this subject (reed beds are used mostly considered for water treatment) and on the modeling of such in-stream processes. The contributions of these processes do not significantly impact the annual loads (they represent 10 to 20% of the annual load), but because this is an open research subject, these in-stream processes should be studied in more detail in the future, using modeling tools with more advanced stream water quality approaches.

3.1.3.2 Enxoé watershed long-term budget

After model calibration/validation, SWAT was used to understand the catchment dynamics in terms of water and nutrient balance. The computed water, sediment, and nutrient budgets for the 30 years' period (1980-2010) are presented in Figure 8. Approximately 80-85% of precipitation (annual average is 500 mm) was evapotranspirated, while the remaining was transported to the river by groundwater and lateral flow (10-15%) or by runoff (5%).

Figure 8. The Enxoé watershed annual average water and nutrient balance and export to the river: water and nitrogen annual averages (top), and sediment and phosphorus annual averages (bottom).

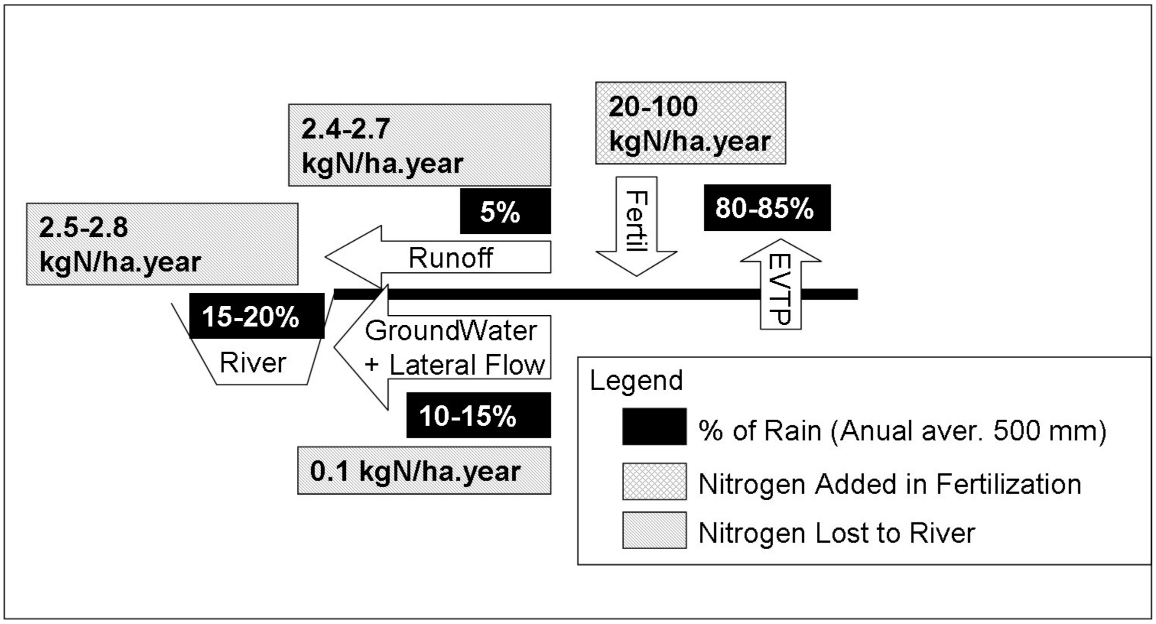

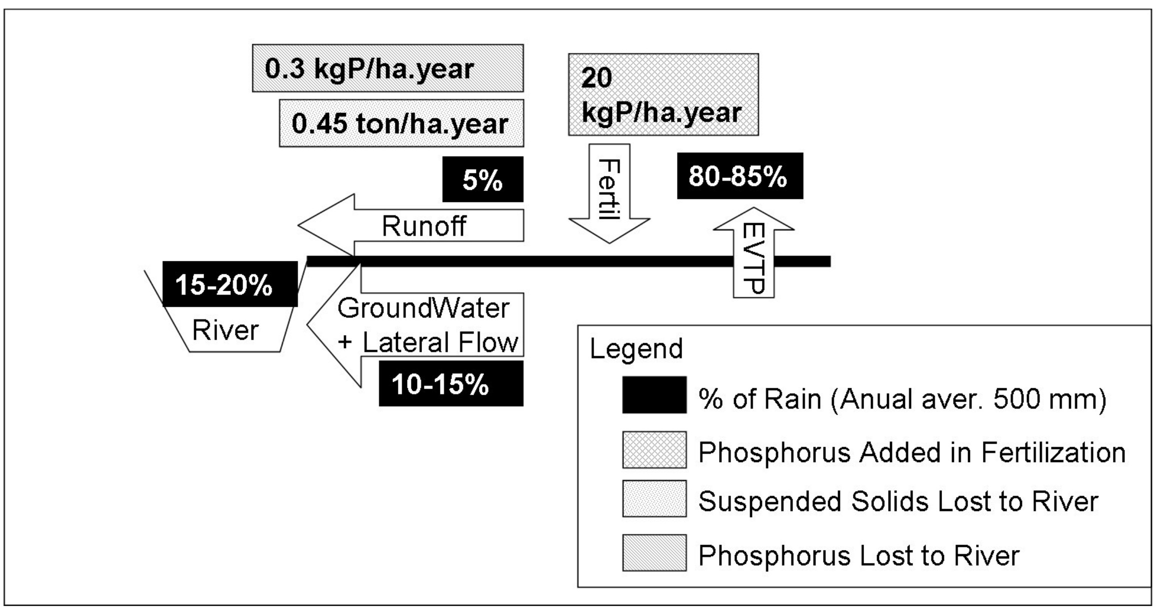

The annual erosion rate averaged 0.45 $ton.ha^{-1}.year^{-1}$ (Figure 8) with some sub-basins producing values of up to 1-2 $ton.ha^{-1}.year^{-1}$. Kosmas et al. (1997) investigated the land use effect on the measured erosion rates in several

Mediterranean watersheds and found similar erosion rates in areas cultivated with wheat or olive groves (0.01-0.2 $ton.ha^{-1}.year^{-1}$). Roxo and Casimiro (1997) measured values up to 2.5 $ton.ha^{-1}.year^{-1}$ in erosion plots located in Vale Formoso, Alentejo. Bakker et al. (2008) estimated erosion rates of 2-5 $ton.ha^{-1}.year^{-1}$ in Amendoeira, a similar sized catchment located in Alentejo, using a soil erosion model. As Enxoé has relatively gentle slopes (2% slope along the river and 5% average slope in the sub-basins) and agriculture is extensive, the simulated/measured erosion rates can be considered similar to those conducted for sites with similar land uses, slopes, and climate conditions. However, Enxoé erosion rates were considerably low when compared to studies conducted in similar land uses but with higher average slopes. For example, Vanwalleghem (2011) reported erosion rates between 29 and 47 $ton.ha^{-1}.year^{-1}$ in three olive groves located in Spain, with average slopes of 25%.

Because of the flushy regime, runoff exports to the river carried 20 times more N (2.4-2.7 $kgN.ha^{-1}.year^{-1}$) than groundwater (0.1 $kg.ha^{-1}.year^{-1}$) (Figure 8). Also, P was mainly transported by runoff because its inorganic forms are normally retained at the soil surface and transported in the particulate form, attached to fine soil particles (erosion). The P export rate was estimated to be 0.3 $kg.ha^{-1}.year^{-1}$ (Figure 8). The nutrient export values in Enxoé were of the same order of magnitude as those obtained by Green and van Griensven (2008), who reported values of 1-3 $kgN.ha^{-1}.year^{-1}$ and 0.1-0.3 $kgP.ha^{-1}.year^{-1}$ in small sub-basins with corn and wheat in the USA (annual precipitation was less than 890 mm). Alvarez-Cobelas et al. (2010) also reported values of 0.05-7 $kgN.ha^{-1}.year^{-1}$ and 0.0004-1.6 $kgP.ha^{-1}.year^{-1}$ in three semi-arid sub-catchments with vineyards and forest in Spain (annual precipitation was 400 mm). These authors further concluded that high N exports occurred in areas where agriculture was more nutrient intensive and the annual precipitation was higher, promoting nitrate leaching. For example, Salvia-Castellví et al. (2005) found nitrate exports of 27-33 $kgN.ha^{-1}.year^{-1}$ in agricultural watersheds with annual precipitation ranging from 700-1200 mm. On the other end, P exports tend to be higher in areas with high erosion and can reach hundreds of kgP.ha^{-1} in a single event, as described in Ramos and Martínez-Casasnovas (2004, 2006) for a vineyard in northeast Spain.

Based on SWAT simulations (30 years), the nutrient loads delivered to the Enxoé reservoir were estimated to be 18 tonN.$year^{-1}$ and 0.7 tonP.$year^{-1}$, which can be considered within the same range as those obtained in other extensive agricultural areas with gentle slopes (low erosion) and reduced human presence. SWAT simulations further showed that 90% of the annual N and P loads was delivered, on average, to the reservoir over 15 days, while 90% of the sediment load was delivered over 8 days (Table 8). This behavior, where high concentrations are transported in short time periods, is an important feature in temporary flushy regimes and may have a significant impact on the reservoir (e.g., González-Hidalgo et al. 2007). Thus, future work will involve the application of a reservoir model that will be fed by the loads estimated in this study in order to test different management strategies to reduce the trophic state of the Enxoé reservoir.

Table 8 Number of days to achieve 90% of the annual load transported to the Enxoé reservoir (SWAT average predictions for the period 1980-2010).

	Nº of days to transport 90% of annual load		
	Total N	Total P	TSS
Average	12	14	8
Maximum	28	27	23
Minimum	1	1	1

3.1.4 Conclusions

This study aimed at understanding the water and nutrient long-term dynamics in the Enxoé catchment, and quantifying nutrient loads to the Enxoé reservoir. SWAT model predictions of the monthly flow, and sediment, P, and N loads were compared to the field data, producing R^2 values between 0.42-0.78, and NSE value between 0.19-0.77. The SWAT model was thus able to capture the main long-term trends and processes that generate, transport and transform nutrients in the Enxoé watershed.

Model simulations showed that the Enxoé River is characterized by a temporary flushy regime where high concentrations are transported in short time periods. N (2.5-2.8 $kg.ha^{-1}.year^{-1}$), suspended solids (0.45 $ton.ha^{-1}.year^{-1}$), and P (0.3 $kg.ha^{-1}.year^{-1}$) exports reach the reservoir mainly by runoff and over a very short number of days (8-15 days). As a result, nutrient loads delivered to the Enxoé reservoir were estimated to be 18 $tonN.year^{-1}$ and 0.7 $tonP.year^{-1}$ (30 year simulation). These results can be considered within the same range as those obtained in other extensive agricultural areas with gentle slopes (low erosion) and reduced human presence.

The average to low nutrient inputs from the watershed suggest that the high eutrophic status of the reservoir may not be due only to the input loads. The reservoir geometry (average depth of 5 m) may also promote high light availability at the bottom where nutrient and organic matter accumulate from watershed floods, deposition, and diagenesis. Nutrient release to the water column may then support the phytoplankton communities. This hypothesis will be tested by integrating SWAT results into a reservoir model to depict the origin of the Enxoé trophic status and test management scenarios that may reduce it.

Because Enxoé is a small temporary watershed with a tendency toward a flushy regime, and in-stream processes may have an important role on describing the nutrient concentrations in low waters, two parallel research topics are suggested for future investigation: i) the role of floods on watershed dynamics and on annual loads; and ii) the analysis of in-stream and pool water quality processes occurring in low waters and discontinued flow.

Acknowledgments

The present work was supported within the framework of the EU Interreg SUDOE IVB program (SOE1/P2/F146 AguaFlash project), the Project Mirage (EU-FP7), and the Project EUTROPHOS (PTDC/AGR-AAM/098100/2008) of the Fundação para a Ciência e a Tecnologia (FCT). T. B. Ramos was supported by the FCT grant SFRH/BPD/110655/2015.

References

Alvarez-Cobelas M, Sánchez-Andrés R, Sánchez-Carrillo S, Angeler DG (2010) Nutrient contents and export from streams in semiarid catchments of central Spain. J Arid Environ 74(8):933–945

Bakker MM, Govers G, van Doorn A, Quetier F, Chouvardas D, Rounsevell M (2008) The response of soil erosion and sediment export to land-use change in four areas of Europe: The importance of landscape pattern. Geomorphology 98(3–4):213-226, doi:10.1016/j.geomorph.2006.12.027

Brown LC, Barnwell Jr TO (1987) The enhanced water quality models QUAL2E and QUAL2E-UNCAS documentation and user manual. EPA document EPA/600/3-87/007. USEPA, Athens, GA

CCDR Alentejo (2005) Anuário de recursos hídricos do Alentejo. Ano Hidrológico 2003/2004. MAOTDR, Évora, Portugal

Chu TW, Shirmohammadi A, Montas H, Sadeghi A (2004) Evaluation of the SWAT model's and nutrient components in the piedmont physiographic region of Maryland. Trans ASAE 47(5):1523–1538

Coelho H, Silva A, Chambel-Leitão P, Obermann M (2008) On the origin of cyanobacteria blooms in the Enxoé reservoir. 13th World Water Congress, International Water Resources Association, Montpellier, France

Debele B, Srinivasan R, Parlange J-Y (2008) Coupling upland watershed and downstream waterbody hydrodynamic and water quality models (SWAT and CE-QUAL-W2) for better water resources management in complex river basins. Environ Model Assess 13: 135-153, doi:10.1007/s10666-006-9075-1

Dechmi F, Burguete J, Skhiri A (2012) SWAT application in intensive irrigation systems: Model modification, calibration and validation. J Hydrol 470–471:227-238, doi:10.1016/j.jhydrol.2012.08.055

Fohrer N, Eckhardt K, Haverkamp S, Frede HG (2001) Applying the SWAT Model as a Decision Support Tool for Land Use Concepts in Peripheral Regions in Germany. In Stott DE, Mohtar RH, Steinhardt GC (eds) Sustaining the Global Farm, pp 994-999. Selected papers from the 10th International Soil Conservation Organization Meeting, Purdue, USA

Galván L, Olías M, Fernandez de Villarán R, Domingo Santos JM, Nieto JM, Sarmiento AM, Cánovas CR (2009) Application of the SWAT model to an AMD-affected river (Meca River, SW Spain). Estimation of transported pollutant load. J Hydrol 377(3–4):445-454, doi:10.1016/j.jhydrol.2009.09.002

Gassman PW, Reyes MR, Green CH, Arnold JG (2007) The Soil and Water Assessment Tool: Historical development, applications, and future research directions. Trans ASABE 50(4):1211–1250, doi:10.13031/2013.23637

Geza M, McCray JE (2008) Effects of soil data resolution on SWAT model stream flow and water quality predictions. J Environ Manage 88(3):393-406, doi:10.1016/j.jenvman.2007.03.016

Gikas GD, Yiannakopoulou T, Tsihrintzis VA (2005) Modeling of nonpoint-source pollution in a Mediterranean drainage basin. Environ. Model. Assess. 11(3):219–233

González-Hidalgo JC, Peña-Monné JL, de Luis M (2007) A review of daily soil erosion in Western Mediterranean areas. Catena 71(2):193-199

Green CH, van Griensven A (2008) Autocalibration in hydrologic modeling: Using SWAT2005 in small-scale watersheds. Environ Model & Soft 23:422-434

Havens KE, James RT, East TL, Smith VH (2003) N:P ratios, light limitation, and cyanobacterial dominance in a subtropical lake impacted by non-point source nutrient pollution. Environ Poll 122:379-390

INAG (2004) Plano de Ordenamento da Albufeira do Enxoé, estudos de caracterização e pré-proposta de ordenamento. Instituto da Água, MAOTDR, Lisboa

INAG (2008) Poluição provocada por nitratos de origem agrícola. Directiva 91/676/CEE, de 12 de Dezembro de 1991. Relatório (2004-2007). Publicação conjunta do MAOTDR e MADRP, Lisboa, Portugal

INAG (2009) Management of the Trophic Status in Portuguese Reservoirs Volume I Criteria and assessment of the Trophic Status. Study in the scope of WWTP diretive and sensitive area plans. December 2009.

INE (2001) Recenseamento Geral Agrícola. Instituto Nacional de Estatística, Lisboa

Jensen ME, Burman RD, Allen RG (1990) Evapotranspiration and irrigation water requirements. ASCE Manuals and Reports on Engineering Practice No. 70, ASCE, NY, 332 pp

Kosmas C, Danalatos N, Cammeraat LH, Chabart M, Diamantopoulos J, Farand R, Gutierrez L, Jacob A, Marques H, Martinez-Fernandez J, Mizara A, Moustakas N, Nicolau JM, Oliveros C, Pinna G, Puddu R, Puigdefabregas J, Roxo M, Simao A, Stamou G, Tomasi N, Usai D Vacca A (1997) The effect of land use on runoff and soil erosion rates under Mediterranean conditions. Catena 29(1):45-59, doi:10.1016/S0341-8162(96)00062-8

Lillebø AI, Morais M, Guilherme P, Fonseca R, Serafim A, Neves R (2007) Nutrient dynamics in Mediterranean temporary streams: A case study in Pardiela catchment (Degebe River, Portugal). Limnologica 37(4):337-348.

McElroy AD, Chiu SY, Nebgen JW, Aleti A, Bennet FW (1976) Loading functions for assessment of water pollution from nonpoint sources. Environ Prot Tech Serv, EPA 600/2-76-151

Ministry of Agriculture (1997) Código das Boas Práticas Agrícolas para a protecção da água contra a poluição de nitratos de origem agrícola. MADRP, Lisboa

Moriasi DN, Arnold JG, Van Liew MW, Bingner RL, Harmel RD, Veith TL (2007) Model evaluation guidelines for systematic quantification of accuracy in watershed simulations. Trans ASABE 50(3):885–900

Nash JE, Sutcliffe JV (1970) River flow forecasting through conceptual models: Part 1. A discussion of principles. J Hydrol 10(3):282-290

Neitsch SL, Arnold JG, Kiniry JR, Srinivasan R, Williams JR (2002) Soil and Water Assessment Tool. User's Manual. Version 2005. GSWRL Report 02-02, BRC Report 2-06, Temple, Texas, USA

Paerl HW, Fulton RS, Moisander PH, Dyble J (2001) Harmful freshwater algal blooms: with an emphasis on cyanobacteria. The Scientific World J 1:76-113

Panagopoulos Y, Makropoulos C, Mimikou M (2011) Reducing surface water pollution through the assessment of the cost-effectiveness of BMPs at different spatial scales. J Environ Manage 92(10):2823–2835

Perrin J, Ferrant S, Massuel S, Dewandel B, Maréchal JC, Aulong S, Ahmed S (2012) Assessing water availability in a semi-arid watershed of southern India using a semi-distributed model. J Hydrol 460–461:143-155, doi:10.1016/j.jhydrol.2012.07.002

Ramos MC, Martínez-Casasnovas JA (2004) Nutrient losses from a vineyard soil in Northeastern Spain caused by an extraordinary rainfall event. Catena 55(1):79–90

Ramos MC, Martínez-Casasnovas JA (2006) Nutrient losses by runoff in vineyards of the Mediterranean Alt Penedès region (NE Spain). Agric Ecosys & Environ 113(1–4):356–363

Ramos TB, Gonçalves MC, Branco MA, Brito D, Rodrigues S, Sánchez-Pérez JM, Suavage S, Prazeres A, Martins JC, Fernandes ML, Pires FP (2015a) Sediment and nutrient dynamics during storm events in the Enxoé temporary river, southern Portugal. Catena 127:177-190, doi:10.1016/j.catena.2015.01.001

Ramos TB, Rodrigues S, Branco MA, Prazeres A, Brito D, Gonçalves MC, Martins JC, Fernandes ML, Pires FP (2015b) Temporal variability of soil organic carbon transport in the Enxoé agricultural watershed. Environ Earth Sci 73:6663-6676, doi:10.1007/s12665-014-3888-z

Ritchie JT (1972) Model for predicting evaporation from a row crop with incomplete cover. Water Resour Res 8:1204-1213

Rolff C, Almesjo L, Elmgren R (2007) Nitrogen fixation and abundance of the diazotrophic cyanobacterium Aphanizomenon sp. in the Baltic Proper. Marine Eco Prog Series 332:107-118

Roxo MJ, Casimiro PC (1997) Long term monitoring of soil erosion by water, Vale Formoso Erosion Centre – Portugal. Soil Conservation and Protection for Europe Project. http://eusoils.jrc.ec.europa.eu/projects/scape/uploads/97/Roxo_Casimiro.pdf (last accessed: August 2016)

Salvia-Castellví M, Iffly JF, Borght PV, Hoffmann L (2005) Dissolved and particulate nutrient export from rural catchments: A case study from Luxembourg. Sci Total Environ 344(1–3):51–65

USDA-SCS, 1972. Section 4: Hydrology. In National Engineering Handbook. Natural Resources Conservation Service, USA

Valério E, Pereira P, Saker ML, Franca S, Tenreiro R (2005) Molecular characterization of Cylindrospermopsis raciborskii strains isolated from Portuguese freshwaters. Harmful Algae 4(6):1044-1052, doi:10.1016/j.hal.2005.03.002

Vanwalleghem T, Amate JI, de Molina MG, Fernández DS, Gómez JA (2011) Quantifying the effect of historical soil management on soil erosion rates in Mediterranean olive orchards. Agric Ecosyst & Environ 142(3–4):341-351, doi:10.1016/j.agee.2011.06.003

Williams JR (1995) The EPIC model. In Singh VP (ed). Computer models of watershed hydrology, pp 909-1000. Water Resources Publications

Williams JR, Hann RW (1978) Optimal operation of large agricultural watersheds with water quality constraints. Texas Water Resources Institute, Texas A&M Univ Tech Rept No 96

Wischmeier WH, Smith DD (1978) Predicting rainfall erosion losses: a guide to conservation planning. Agriculture Handbook 282, USDA-ARS

Yevenes MA, Mannaerts CM (2011) Seasonal and land use impacts on the nitrate budget and export of a mesoscale catchment in Southern Portugal. Agric Water Manage 102: 54-65, doi:10.1016/j.agwat.2011.10.006

Zhang X, Srinivasan R, Van Liew M (2008) Multi-Site Calibration of the SWAT Model for Hydrologic Modeling. Trans ASABE 51(6):2039-2049

3.2 *Modeling flood dynamics in a temporary river basin draining to an eutrophic reservoir in southeast Portugal.*

The previous article/application in Section 3.1 showed that annual loads entering Enxoé reservoir from the watershed are low and representative of extensive agriculture, gentle slopes and low human occupation. However the majority of the annual loads strike the reservoir in less then two weeks per year (flushy regime). As so this article describes the implementation of MOHID Land model (physically based and with variable time step) to the watershed, especially suited for reduced time of concentration to depict the flood role on loads to the reservoir.

Environ Earth Sci (2017) 76:377
DOI 10.1007/s12665-017-6713-7

ORIGINAL ARTICLE

Modeling flood dynamics in a temporary river draining to an eutrophic reservoir in southeast Portugal

David Brito[1] · **Ramiro Neves**[1] · **Maria A. Branco**[2] · **Maria C. Gonçalves**[2] · **Tiago B. Ramos**[1]

Received: 11 November 2016 / Accepted: 17 May 2017 / Published online: 23 May 2017

Abstract Enxoé is a small temporary river with a flushy regime, which flash floods carry significant loads to the reservoir. As a result, the reservoir, which supplies 25,000 inhabitants, exhibits a high trophic state and cyanobacteria blooms since its construction in 1998, with water abstractions requiring extensive treatment. This study aimed to understand the contribution of flash floods to the Enxoé's reservoir high trophic state using a modeling approach. This was the first time the river was monitored and that a modeling study was carried out. The MOHID-Land model was implemented to assess the water path in the catchment, and was integrated with field data to compute river loads. Results confirmed the importance of flash events. During flash floods, water properties were determined by soil surface and river bottom wash out, and depended mostly on the flush sequence and intensity. Model simulations showed that soil surface permeability reduction was an important factor regulating surface runoff while soil moisture was low. The first flood after the dry period contributed to 2% of the yearly discharge, 3% of yearly N load, and 7% of the yearly P loads. Winter floods contribution differed, producing 10% of both yearly discharge and loads. However, concentration of particulate matter and organic compounds in the first flood were one order of magnitude higher than in winter floods. This was due to river bottom resuspension and erosion of riparian areas, representative dynamics of a flushy regime. During subsequent winter floods, nutrient concentrations tended to remain constant as the watershed surface and respective soils were washed. Further work should link a watershed model to a reservoir model to depict the flood impact in the reservoir, and test management strategies to reduce the reservoir trophic state.

Keywords Enxoé · Flash floods · Nutrient loads · Watershed modeling · MOHID-Land

✉ David Brito
odavidbrito@gmail.com

1 MARETEC, Instituto Superior Técnico, Universidade de Lisboa, Av. Rovisco Pais, 1049-001 Lisbon, Portugal

2 Instituto Nacional de Investigação Agrária e Veterinária, Av. da República, Quinta do Marquês, 2780-157 Oeiras, Portugal

Introduction

Enxoé is a temporary river located in the Alentejo region, southeast Portugal. The precipitation regime is characterized by a highly irregular behavior, varying between relatively abundant rainfall episodes, concentrated in only a few minutes or hours, and frequent dry episodes that can last from a few months to a couple of years. As a result, the Enxoé River exhibits relatively large flow in the winter as a response to rain events, reduced flow in the spring as rain ceases, and no flow/pool formation during the summer or extended dry periods. During the wetter seasons, soil moisture allows for the development of luxuriant vegetation along the river bed producing organic detritus directly through the decay of plants biomass, but also indirectly through animal feces released during grazing. Detritus biomass and nutrients accumulated in the river bed sediments are then flushed out, especially during the first autumn flash flood, promoting the eutrophication of the water reservoir located downstream.

Before reservoir construction, loads carried during floods were transported downstream into the Guadiana River, with no impact on the Enxoé River biogeochemical status. The construction of the reservoir in 1998 changed the global water and nutrient dynamics by trapping loads. Since then, the Enxoé reservoir has been exhibiting the highest eutrophic state in Portugal, often registering chlorophyll-a geometric average concentrations above 50 μg L^{-1}. Cyanobacteria blooms have also frequently occurred during the spring and summer seasons (INAG 2004). The eutrophic condition of the reservoir and the occurrence of cyanobacteria blooms are problematic in that the reservoir is the water supply for two communities (Mértola and Serpa with 25,000 inhabitants in total) and extensive water treatment is needed.

Brito et al. (2017) pointed out nutrient loads generated in the catchment and the remobilization of nutrients from the reservoir bed as the main probable causes for the reservoir eutrophic conditions. These hypotheses are supported by the dominance of cyanobacteria during reservoir blooms, and by the occurrence of *N* limitation conditions in the photic zone (INAG 2004). As a result, the species that are able to consume N_2 dissolved in the water or grow under low-light conditions close to the nutricline often bloom when mineral N becomes suddenly available (e.g., after flood events or vertical mixing events driven by strong winds).

The quantification of loads carried out during flash floods is thus important to establish the reservoir nutrients' budget, but also to forecast cyanobacteria blooms driven by the sudden discharge of fresh nutrients. Flash floods in arid and semiarid regions are mostly generated by surface runoff or by subsurface water that arrives faster to the river bed than groundwater flow. The time to reach the discharge peak depends on the watershed characteristics (size, topography, soil properties, land cover, soil crusting, soil sealing), rain distribution, and soil moisture content (James and Roulet 2009; Li et al. 2012). In Enxoé, first floods occur usually in autumn when soil moisture is reduced and water retention capacity is high. Consequently, the fraction of rainwater discharged is much smaller than in winter floods when soil capacity for retaining water is lower. However, first floods are responsible for carrying most of the debris and mineralized nutrients accumulated at the soil surface and on river bed during the dry periods, and thus have an important role in the biochemical processes occurring downstream (Obermann et al. 2009). Continuous monitoring is thus essential to quantify loads transported during those early flash flood events.

As monitoring data are usually scarce, especially when collection frequency needs to be high as in the case of floods with peak rises occurring within a few minutes to a few hours and because automatic monitoring schemes are costly, different modeling tools have been developed to better describe flash flood events, fill data gaps, and understand the effects of such events on basic functions of ecosystems, namely on soil retention, and water and nutrient regulation. The first feature needed to simulate a flood is that the model must have a time step that can represent the flood fast rise and fall; in flash floods that may represent hourly or sub-hourly time steps (Boughton and Droop 2003). The second feature is that the model should be able to simulate soil infiltration conditions, runoff generation, routing, and storm drainage systems (Hsu et al. 2000).

Traditionally, watershed models put their efforts on describing long-term dynamics. The time steps used are of the order of one day to one hour to enhance computation time, as are the cases of the SWAT (Neitsch et al. 2002) and HSPF models (Bicknell et al. 1993), respectively, making them unsuited for the analysis of flash floods in small watersheds as Enxoé (concentration times of a couple of hours). However, other models exist that have lower time steps and are more suited for modeling floods, as the KINEROS (Woolhiser et al. 1990), MIKE 11 (Havnø et al. 1995), and HEC-RAS (Brunner 2010) models.

MOHID-Land (Trancoso et al. 2009; Neves 2013) is a distributed model based on primitive equations for surface runoff and flow in the vadose zone and in the aquifer. The surface runoff is simulated solving the full St. Venant equations allowing for backwater movement, flooding, and the drying process of the riparian zones (Bernard-Jannin et al. 2016). The surface runoff interacts with the ground compartment through infiltration and exfiltration. The vadose and the saturated zones are solved simultaneously without an explicit interface. The catchment is described using a 3D grid for porous media. Flow in the porous media is based on the Richards equation, while infiltration can be simulated using Darcy's equation and surface pressure due to surface runoff water column or using empirical algorithms (e.g., Green and Ampt). A river network is used to simulate surface runoff where the river width is smaller than the horizontal grid step. The time step is variable to increase accuracy during events when soil moisture or surface water volumes changing rate is high. Examples of diverse MOHID-Land applications can be found in Neves (2013).

This study aims to evaluate the contribution of flood events to the Enxoé reservoir total loads using MOHID-Land. The model was used to simulate peak discharge flows and fluxes during flood events. As Enxoé basin was ungauged, field data were first collected between 2010 and 2011 to calibrate/validate the model. This study is the second of a series of modeling studies aimed at improving water management plans in the Enxoé basin.

Material and methods

Study area

Enxoé is a 60 km^2 catchment located in southeast Portugal, in the left margin of the Guadiana River. The Enxoé River has a bed length of approximately 9 km from its headwaters to the reservoir. The Enxoé reservoir (37°59′ 38.121″N, 7°27′ 54.776″W) limits the catchment downstream and has a total volume of 10.4 hm^3, a surface area of approximately 2 km^2, and an average depth of 5 m. The climate in the region is dry sub-humid to semiarid, with an average air temperature of 15 °C, reaching maximums of 40 °C during some days in the summer, and minimums below zero in the winter. The annual average precipitation is 500 mm, irregularly distributed throughout the year (80% of the annual precipitation is concentrated between October and April). The average watershed slope is below 6%, while the average river slope is 2% promoting water pooling and the occurrence of disconnected reaches during dry periods.

The land is mainly used for growing olive trees, agroforestry of holm-oaks ("montado"), and annual rainfed crops (wheat, oats, and sunflower), each covering approximately 30% of the total area (Fig. 1; Table 1). The main soils are Luvisols (covering 47% of the area), Cambisols (31%), Calcisols (14%), and Vertisols (6%) (FAO 2006). Soil textures vary between loamy and silty loamy classes. Extensive livestock production is the most important animal-farming activity in the catchment. According to the 1999 agricultural census (INE 2001), cow (602) and sheep (4365) production corresponds to approximately 0.1 and 0.01 livestock units (LSU), respectively.

The catchment has a population of 1000 inhabitants, mainly concentrated in Vale de Vargo. The respective wastewater treatment plant discharges outside the watershed since 2006 as a protective measure to the Enxoé reservoir.

Field monitoring data

The Enxoé River water was monitored at the sampling station located upstream the reservoir during one hydrological year (September, 2010 to August, 2011). A multiparametric YSI 6920 measuring probe (YSI Incorporated, Ohio, USA) was used to monitor the water stream level, turbidity (by nephelometry), the water temperature, the electrical conductivity, and dissolved oxygen continuously. Readings were taken every 15 min during flood events and daily during non-flood events. An automatic water sampler (EcoTech Umwelt-Meβsysteme GmbH. Bonn, Germany) with 8 bottles, 2 L each, was used for monitoring water quality during floods. The monitoring station was positioned near the bank of the river, where the movement of water was considered representative of river flow. The pump inlet of the automatic water sampler was placed next to the measuring probe pipe. The probe was programmed to activate the automatic water sampler when the water level varied more than 10 cm on both rising and falling stages of flood events. As a result, automatic sampling varied from 3 min during flash events to 15 h during low flow. Manual sampling was also carried out at weekly intervals using 2-L bottles collected near the probe location. Automatic and manual water sampling was monitored for salinity, pH, suspended solids, nitrate, nitrite, ammonia, phosphate, total N, and total P. Further details can be found in Ramos et al. (2015).

The MOHID-Land model

Model description

MOHID-Land is an integrated model with four compartments or mediums (atmosphere, porous media, soil surface,

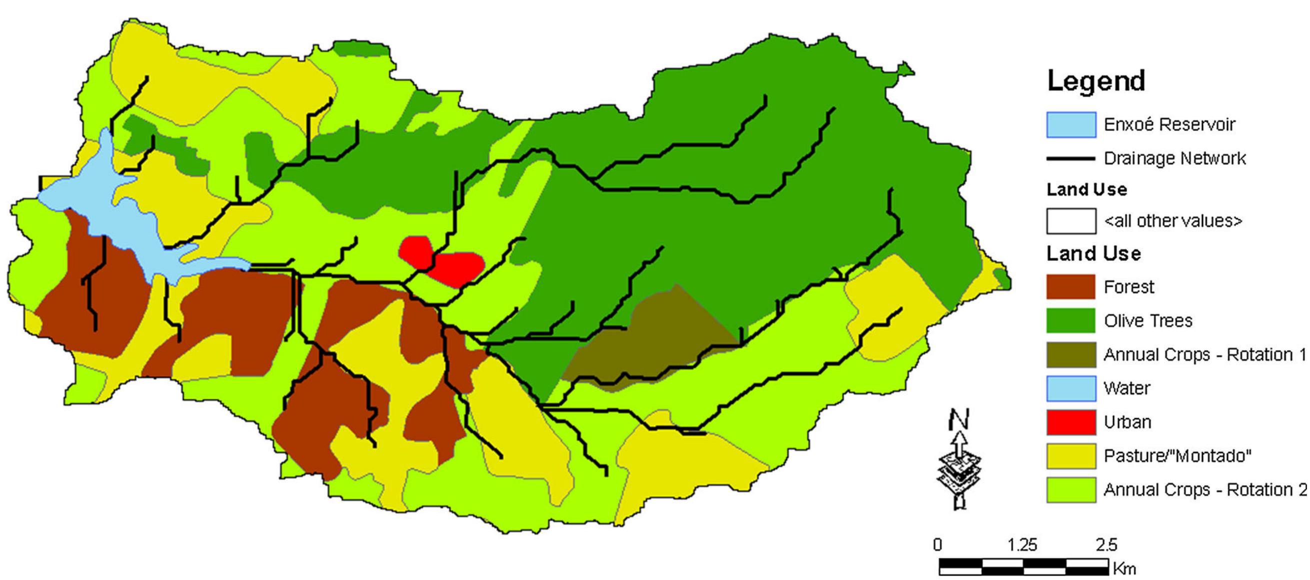

Fig. 1 Enxoé land use. *Source* Corine 2000

Table 1 Enxoé land use. *Source* Corine 2000

Land use	Area (km^2)	Percentage of total area (%)
Olive trees	21	35
Annual crops	20	33
Agro-forestry of holm-oaks (Pasture/"montado")	11	19
Agro-forestry of holm-oaks ("montado" forest)	7	11
Water	1	2
Urban area	<1	<1
Total	61	100

and river network). Water moves through the mediums based on mass and momentum conservation equations. The atmosphere is not explicitly simulated but provides data necessary for imposing surface boundary conditions to the model (precipitation, solar radiation, wind, etc.) that may be space and time variant. The model is based on finite volumes organized into a structured grid, rectangular in the horizontal plane, and cartesian type in the vertical plane. Surface land is described by a 2D horizontal grid, and the porous media is a 3D domain which includes the same horizontal grid as the surface complemented with a vertical grid with variable layer thickness. The river network is a 1D domain defined from the digital terrain model (DTM), with reaches linking surface cell centers. Fluxes are computed over the faces of the finite volumes, and state variables are computed at the center to assure conservation of transported properties. The model uses an explicit algorithm with a variable time step, that is maximum during dry season when fluxes are reduced and minimum when fluxes increase (e.g., during rain events).

Porous media The spatial distribution of transient soil water contents and volumetric fluxes are obtained using the Richards equation:

$$\frac{\partial \theta}{\partial t} = \frac{\partial}{\partial x_i}\left(K(\theta)\left(\frac{\partial h}{\partial x_i} + \frac{\partial z}{\partial x_i}\right)\right) - S \qquad (1)$$

where θ is volumetric water content ($m^3\ m^{-3}$), h is the soil pressure head (m), t is time (s), z is the vertical space coordinate (m), x_i are the xzy directions (−), K is the hydraulic conductivity ($m\ s^{-1}$), and S is the sink term accounting for water uptake by plant roots ($m^3\ m^{-3}\ s^{-1}$). The unsaturated soil hydraulic properties can be described using different functional relationships (e.g., van Genuchten 1980).

Evapotranspiration MOHID-Land uses a modified version of the EPIC model (Neitsch et al. 2002) for computing vegetation growth. SWAT model crop databases (Neitsch et al. 2002) are used in MOHID-Land for defining plant potential growth curves. Actual growth is then computed accounting for limitations due to environmental constraints (water availability, temperature, nutrients, etc.).

Reference evapotranspiration (ET_0) may be given by the user or computed using the FAO Penman–Monteith method (Allen et al. 1998). Crop evapotranspiration (ET_c) is then obtained by combining ET_0 with a crop coefficient (K_c, adimensional):

$$ET_c = K_c * ET_0 \qquad (2)$$

The partition of ET_c into potential crop transpiration (PotTransp) and potential soil evaporation (PotEvap) is computed as a function of Leaf Area Index (LAI, $m^2\ m^{-2}$) (Ritchie 1972):

$$\text{PotTransp} = ET_c * (1 - \exp(-0.463 * \text{LAI})) \qquad (3)$$

$$\text{PotEvap} = ET_c - \text{PotTransp} \qquad (4)$$

Actual crop transpiration is computed from potential transpiration as a function of root distribution and soil water availability (Feddes et al. 1978). Actual soil evaporation may be limited from PotEvap by defining a head threshold or through the soil hydraulic conductivity function since evaporation lowers with drying (ASCE 1996).

Infiltration Infiltration velocity is computed using the Darcy's law:

$$\Phi_z = -K_{sat} A_{inf}\left(\frac{\partial h}{\partial z} + 1\right) \qquad (5)$$

where Φ_z is the infiltration flux ($m^3\ s^{-1}$), K_{sat} is saturated soil hydraulic conductivity ($m\ s^{-1}$), and A_{inf} is the effective infiltration area (m^2). Infiltration velocity can then be lowered due to soil compaction (or soil sealing in urban watersheds) where the area for infiltration is reduced.

Surface water The forces acting in surface water (runoff and river flow) are pressures represented by surface level gradients, gravity and bottom friction. Applying Newton's second law to the result of these forces, the St. Venant equation is obtained:

$$\frac{\partial Q_i}{\partial t} + v_j \frac{\partial Q_i}{\partial x_j} + g A_v\left(\frac{\partial w}{\partial x_i} - (S_0)_i + (S_f)_i\right) = 0 \qquad (6)$$

where Q_i is the water flow ($m^3\ s^{-1}$), A_v is the cross-sectional flow area (m^2), g is the gravity acceleration ($m\ s^{-2}$),

w is water depth (m),

$$(S_0)_i = -\partial z / \partial x_i$$

(−) is the bottom slope, S_{fi} is the bottom friction slope (i.e., the slope that balances the friction force), and subscript i and j denote the flow directions (one in river and two in runoff). S_{fi} is computed with the Manning–Strickler equation:

$$(S_f)_i = \frac{n^2|Q|Q_i}{A_v^2 R_h^{\frac{4}{3}}} \quad (7)$$

where n is manning rugosity (s m$^{-1/3}$) and R_h is hydraulic radius (m).

The water level in each cell (runoff or river) is obtained from the continuity equation:

$$\frac{\partial A_v}{\partial t} + \frac{\partial Q_i}{\partial x_i} = 0 \quad (8)$$

The MOHID-Land river equations and processes are described in detail in Trancoso et al. (2009). Runoff flow is a 2D implementation of the same general equations being both derived from Newton's second law and continuity equation. Water fluxes between the river and the porous media are computed using the head gradient and the Richards equation, as for surface infiltration and exfiltration. Surface water exchange between the river and riparian zones is computed based on the kinematic approach, neglecting bottom friction and using an implicit algorithm to avoid instabilities. These algorithms permit the simulation of river floods based on the primitive equations along the whole catchment.

Model implementation, calibration, and validation

The Enxoé catchment was ungauged before this study, limiting long-term model evaluation. Thus, MOHID-Land predictions of monthly inflows to the reservoir were first evaluated against those computed from the reservoir budget (2006–2009). The reservoir budget was estimated using the reservoir storage rate of change, reservoir discharge, precipitation, and evaporation data (Table 2). Model evaluation was further carried out at the sampling location by comparing MOHID-Land predictions of the river water level with measured values collected between 2010 and 2011.

Table 3 presents the data used for implementing MOHID-Land in the Enxoé watershed. The DTM was obtained from NASA with a 70–90-m resolution, and using a square horizontal grid with 43 × 64 cells, each with 200 m × 200 m. The porous media was discretized into 8 vertical layers (with varying thickness from 10 cm at the surface to 1 m at the impermeable bottom). Soil information (soil types and soil texture) was extracted from the European soil geographical database at scale 1:1000000. The soil hydraulic parameters of the van Genuchten–Mualem model (van Genuchten 1980) were estimated from soil texture data using Saxton et al. (1986) pedotransfer functions. The CORINE 2000 (100 m resolution) land use map (Fig. 1) was used for defining the vegetation type and surface rugosity. The main agricultural practices (crop rotations and fertilization) were obtained from questionnaires given to farmers (Table 4). Weather data were obtained from local meteorological stations (Table 2). The river network was derived from the DTM using the highest slope in 8 directions, while the section shape was computed with an automatic interpolation tool based on field observations. Special care was taken to define the section where levels were measured to allow for a direct comparison between model predictions and field measurements. This section had a permanent pool and was chosen to assure that the probe was permanently immersed (Fig. 2). Sections were thus configured in the model to represent the pool and the narrowing of the downstream section that was not represented in the altimetry information (90 m resolution).

Model calibration involved optimizing parameters presented in Table 5 by trial and error until deviations between MOHID-Land predictions and, first, the reservoir budget monthly inflows (2006–2009), and then, measured water levels (2010–2011) were minimized. Various quantitative measures of the uncertainty were used, such as the coefficient of determination (R^2), the root mean squared error (RMSE), and the Nash–Sutcliffe model efficiency (NSE) (Nash and Sutcliffe 1970). R^2 values close to 1 indicate that the model explains well the variance of observations. RMSE values close to zero indicate small errors of estimate and good model predictions. NSE values between 0.0 and 1.0 are generally viewed as acceptable levels of performance, whereas values <0.0 indicate that the mean observed value is a better predictor than the simulated value, corresponding to unacceptable performance.

Normalized cumulative loads (NCL) were also calculated to visualize and characterize the transport of material during events, as follows:

$$\mathrm{NCL} = \frac{\int_{t0}^{t} \beta(t) \cdot Q(t)\mathrm{d}t}{\int_{t0}^{tf} \beta(t) \cdot Q(t)\mathrm{d}t} \quad (10)$$

where $Q(t)$ is the instantaneous flow rate, $\beta(t)$ is the instantaneous property concentration, and t_0 and t_f are the temporal limits of the event. Cumulative flow is computing using $\beta(t) = 1$.

Table 2 Description of data for MOHID-Land model evaluation

Data type	Station	Origin	Period	Frequency
Monthly reservoir inflow				
Reservoir discharges	Enxoé reservoir (26 M/01A)	SNIRH, National Water Institute	2005–2009	Monthly
Precipitation	Herdade da Valada (26M/01C), Sobral Adiça (25 N/01UG)	SNIRH, National Water Institute	1980–2011	Daily
Evaporation	Herdade da Valada (26 M/01C), Monte da Torre	SNIRH, National Water Institute	2001–2011	Daily
Flood level				
Water depth	Probe measurements	Project	2010–2011	15 min

Table 3 Description of data for MOHID-Land model implementation

Data type	Description	Origin	Resolution	Period	Frequency
DTM	SRTM digital elevation	NASA (earthexplorer.usgs.gov/)	90 m	–	–
Land use	Corine land cover 2000	EEA (http://www.eea.europa.eu)	1:100000	1999–2002	–
Soil texture	European soil database	JRC, EU (http://www.eusoils.jrc.ec.europa.eu/	1:1000000	1996	–
Meteorological data	Meteorological stations	SNIRH, National Water Institute (http://www.snirh.pt/)	–	1980–2011	Hourly

Table 4 Enxoé agricultural practices

Agricultural practice	Crop			
	Wheat and barley	Oats	Sunflower	Olive trees
Planting	November	October	April	–
Fertilization	November 20 kgN/ha	March 40–80 kgN/ha	April 22 kgP/ha	April to July (24–60 kgN/ha)
	November 18 kgP/ha			
	January 50 kgN/ha			
	February 20 kgN/ha			
Harvest	June	June	September	–

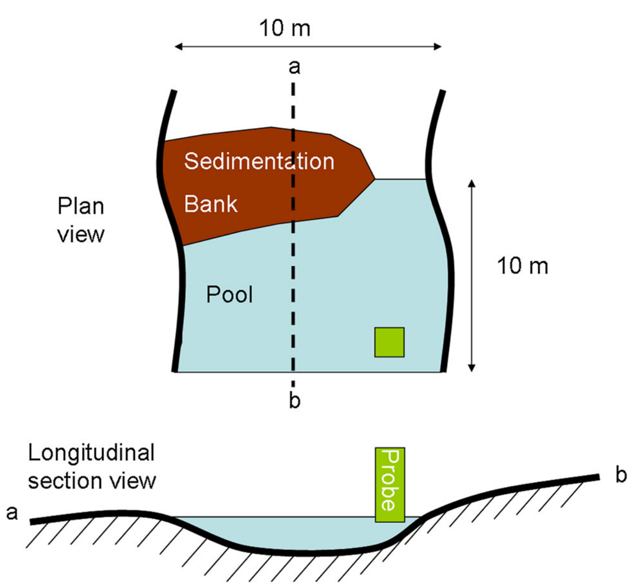

Fig. 2 Cross section definition of the location of the automatic sampling

Results and discussion

Model performance

Monthly inflows to the reservoir

River flow to the reservoir has an important role in the reservoir water volume and depth (water quality in small depth reservoirs tends to deteriorate due to the availability of light to the bottom); in the retention time (increased retention time promotes nutrient accumulation and algal assimilation); and in the horizontal and vertical mixing of water (intense mixing may deliver bottom nutrients to shallower depths where light availability and temperatures are higher). As so, describing input flows from the watershed is of major importance for driving reservoir dynamics and understanding the main reasons for the eutrophic status in the Enxoé reservoir.

Figure 3 presents model predictions of monthly inflows to the Enxoé reservoir and compares these values with the

Table 5 Parameter calibrated during model evaluation

Parameter description	Selection criteria	Values	References
Manning–Strickler's roughness coefficient	From land use map and river bed material	0.01–0.3	Panday and Huyakorn (2004)
Impermeable area (%)	From land use Map; calibration parameter for floods	5–50%	Estimated
Evapotranspiration coefficient—Kc (–)	Constant	0.7	Allen et al. (1998)
Feddes vegetation stress heads (m)	From land use map	–0.01 to –30	Feddes et al. (1978)
Soil van Genuchten hydraulic parameters	From soil map (textures) using pedotransfer functions	–	Saxton et al. (1986)

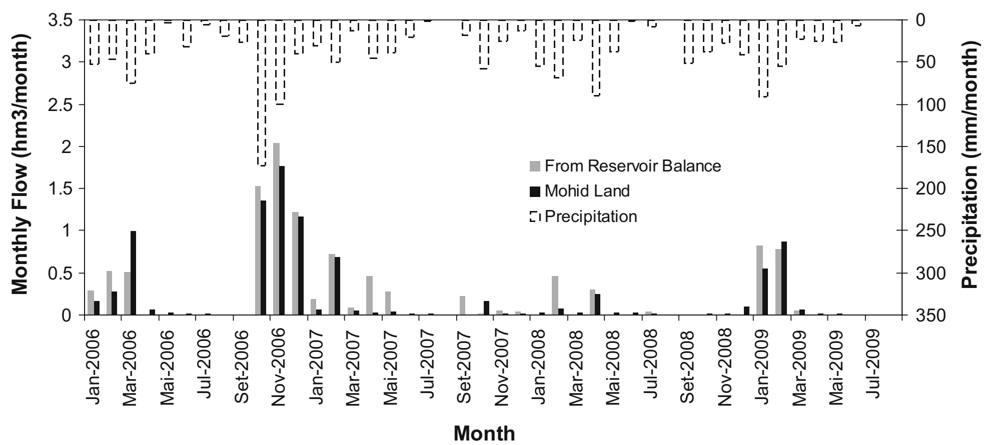

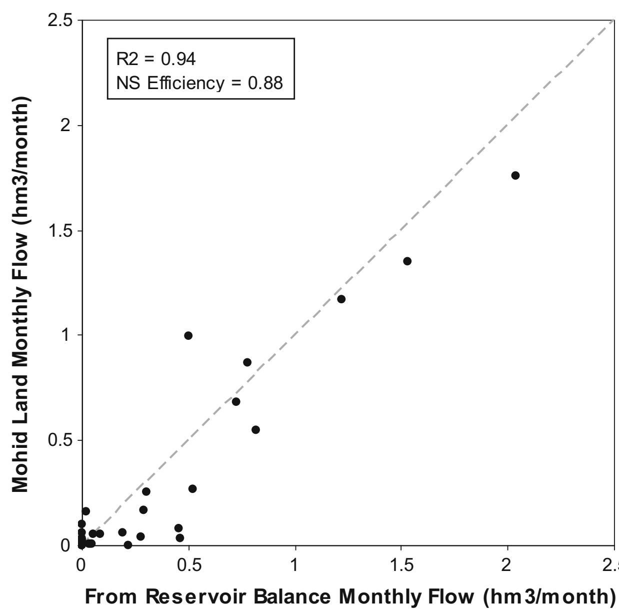

Fig. 3 Monthly inflow to the Enxoé reservoir: time series of estimated flows from the reservoir balance versus MOHID-Land predictions (*top*); scatterplot of estimated versus predicted flows (*bottom*)

values computed from the reservoir budget (2006–2009). MOHID-Land showed the same trend as the values obtained from the reservoir budget, producing higher reservoir inflows in the winter as a response to precipitation, and very low or zero inflows in the summer with the absence of rain. The value of R^2 was high (0.94), showing that the model was able to explain the variability of observed data (Table 6). The error of the estimate was quite small, with RMSE values reaching 0.15 hm^3 -month^{-1}. The NSE value was also very high (0.88), thus indicating that the mean square error was much smaller than the measured data variance.

Deviations between model predictions and reservoir budget values were comparable with results available in the literature for similar watersheds using the SWAT model (Table 7). Results obtained here should be especially

Table 6 Goodness-of-fit indicators between measured values and MOHID-Land predictions

Parameter	Period	Data average	Model average	RMSE	R^2	Nash–Sutcliffe efficiency
Monthly flow						
Monthly Reservoir inflow	1996–2009	0.20 hm^3 $month^{-1}$	0.24 hm^3 $month^{-1}$	0.15 hm^3 $month^{-1}$	0.94	0.88
Hourly flood water depth						
October 2010 flood	28 Oct–31 Oct	0.50 m	0. 59 m	0.22 m	0.27	0.63
February 2011 flood	13 Feb–18 Feb	0.86 m	0.79 m	0.17 m	0.70	0.62

Table 7 Bibliography statistical parameters for monthly flows using SWAT model

Study	Location	R^2	Nash–Sutcliffe efficiency
Fohrer et al. (2001)	Hesse, Germany	0.71; 0.92	
Geza and McCray (2008)	Turkey Creek and Denver, USA	0.62; 0.74	0.61; 0.70
Green and van Griensven (2008)	Texas, USA	0.60–0.96	0.59–0.95
Dechmi et al. (2012)	Del Reguero River, Spain	0.90	0.90
Panagopoulos et al. (2011)	Arachtos, Greece	0.86–0.92	0.51–0.68
Brito et al. (2017)	Enxoé, Portugal	0.78	0.77

compared with those from Brito et al. (2017), who obtained slightly worse indicators ($R^2 = 0.78$; NSE = 0.77) when comparing SWAT inflow predictions with the same monthly flow estimates used in this study. MOHID-Land predictions of monthly inflows can thus be considered as satisfactory to good (Moriasi et al. 2007), representing well water long-term dynamics in the Enxoé watershed.

Flood events

Floods in Enxoé are representative of a flushy regime, with implications on the transported material to the reservoir and on the reservoir response. Nine floods were registered during the 2010–2011 hydrological year (Ramos et al. 2015). Two of those events were selected for simplification: (1) the first flood event of the year (October 2010); and (2) one event representing winter floods (February, 2011).

Figure 4 shows the measured water level during the first flood event (October 2010). Measured water levels reacted fast to the rain event (7 mm h^{-1}), with two discharge peaks reaching the monitoring probe in 2–5 h, while recession lasted 12 h. This fast rise and fall behavior is common in Mediterranean small-sized watersheds. Obermann et al. (2007, 2009) observed the arrival of discharge peaks 1.30 h after the beginning of rain events in a 67 km^2 catchment in Vene, France. Also, Rozaris et al. (2010) registered flow peaks arriving at the outlet of the Merhavia watershed (27 km^2) in less than 3 h.

The MOHID-Land model could not reproduce October 2010 first flash flood without considering some degree of soil crusting/compaction in the modeling approach (Fig. 4). As described above, MOHID-Land controls infiltration fluxes based on the surface pressure gradient and surface soil hydraulic conductivity, which can then be lowered due to the effect of soil crusting/compaction (or soil sealing in urban watersheds). Permeability reduction was implemented in the model by reducing the available infiltration area in each cell. The rate of reduction was a function of the drained area, increasing as cells were closer to river valleys (where deposition, cattle grazing, and machinery activity are more intense). The best fit to flood data was obtained considering a loss of infiltration area ranging from 5% in headwaters up to 50% at the river sections (Table 5). The resulting effect is presented in Fig. 4, with MOHID-Land simulations being now able to reproduce October 2010 discharge peaks. The agreement between measured and simulated water levels produced relatively low R^2 (0.27) but satisfactory NSE (0.63) values, showing that the model was able to represent the main trends and magnitude of measured data (Table 6). The lower fit was explained by inconsistent measured precipitation as measured water levels further increased on October 30, 2010 (immediately after the first peak, indicative of successive rain events), while no additional precipitation was recorded (records with 0 mm).

Figure 5 presents the measured and simulated water depths for February 2011 flood event. The same flushy behavior was observed, with rainfall producing multiple discharge peaks with fast rising stages. Recession lasted longer (almost a day), probably due to higher groundwater flow as a response to aquifer level increase. Again, MOHID-Land could not reproduce the multiple discharge peaks without including some degree of soil

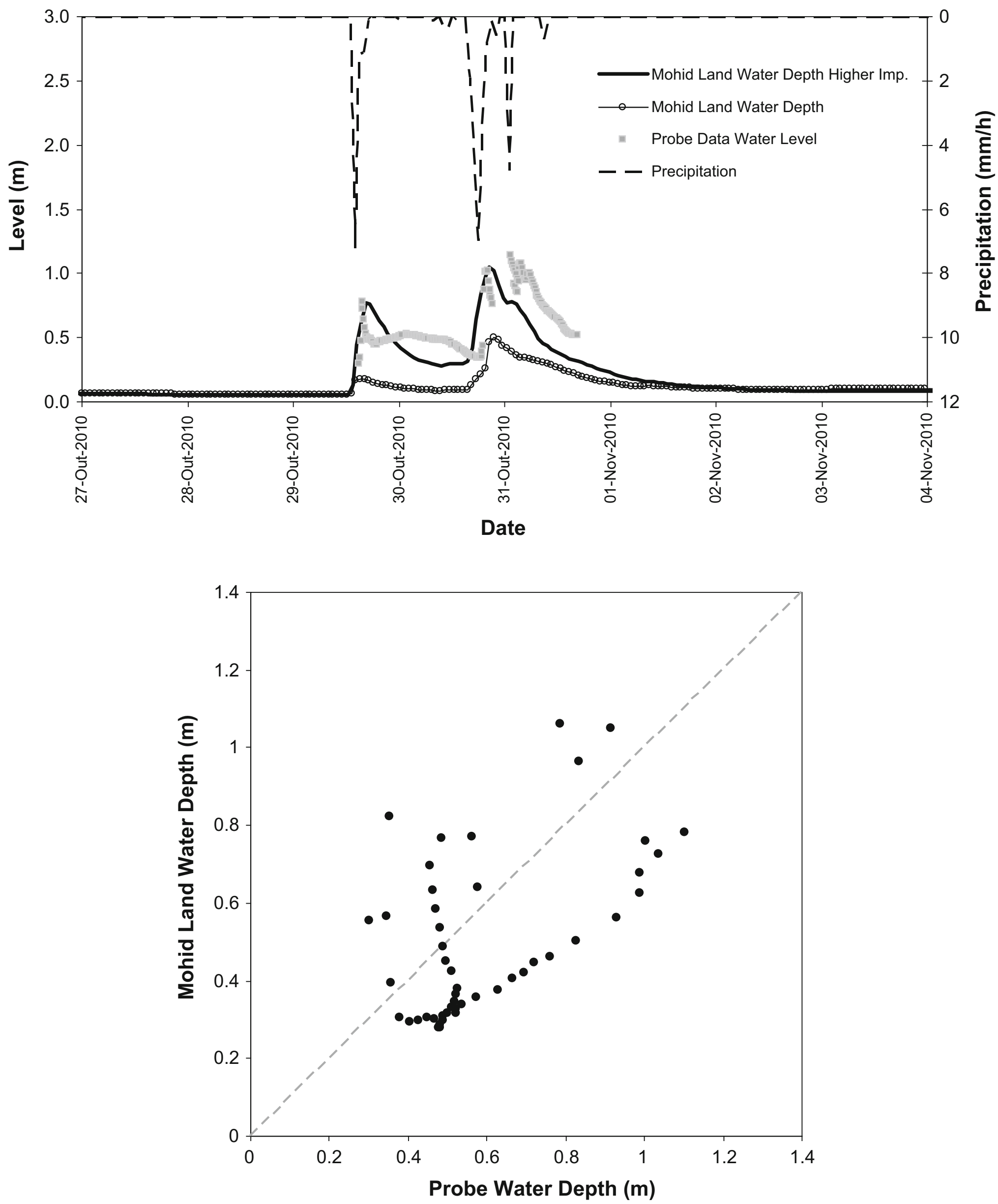

Fig. 4 Enxoé River water depth during October 2010 flood event: time series of measured water levels versus MOHID-Land predictions (*top*); scatterplot of measured versus predicted water levels (*bottom*)

crusting/compaction in the modeling approach (Table 5). Only the third discharge peak was well represented using the different approaches (with and without permeability reduction) since soils were already saturated, infiltration was almost absent, and practically all rainfall was being converted to runoff and river flow. When soil gets saturated the suction gradient is null and infiltration velocity is the saturated conductivity (Eq. 5). If the whole soil column gets saturated, pressure in the soil increases and the infiltration flux vanishes. This is why the reduction of the effective infiltration area makes a difference only after a dry period and is also why surface runoff is mostly expected only when soil is nearly saturated or heavy rains occur (James and Roulet 2009; Li et al. 2012). When considering permeability reductions, the goodness-of-fit indicators for February 2011 flood event resulted in R^2 and NSE values of 0.70 and 0.62, respectively, showing once again that the model was able to accurately reproduce the trends and the values of measured data.

The permeability reduction did not affect significantly the monthly results (Fig. 3) since at this time scale the most important process for river flow was the balance between precipitation and evapotranspiration. Loss of permeability would mostly affect the water path. However, soil

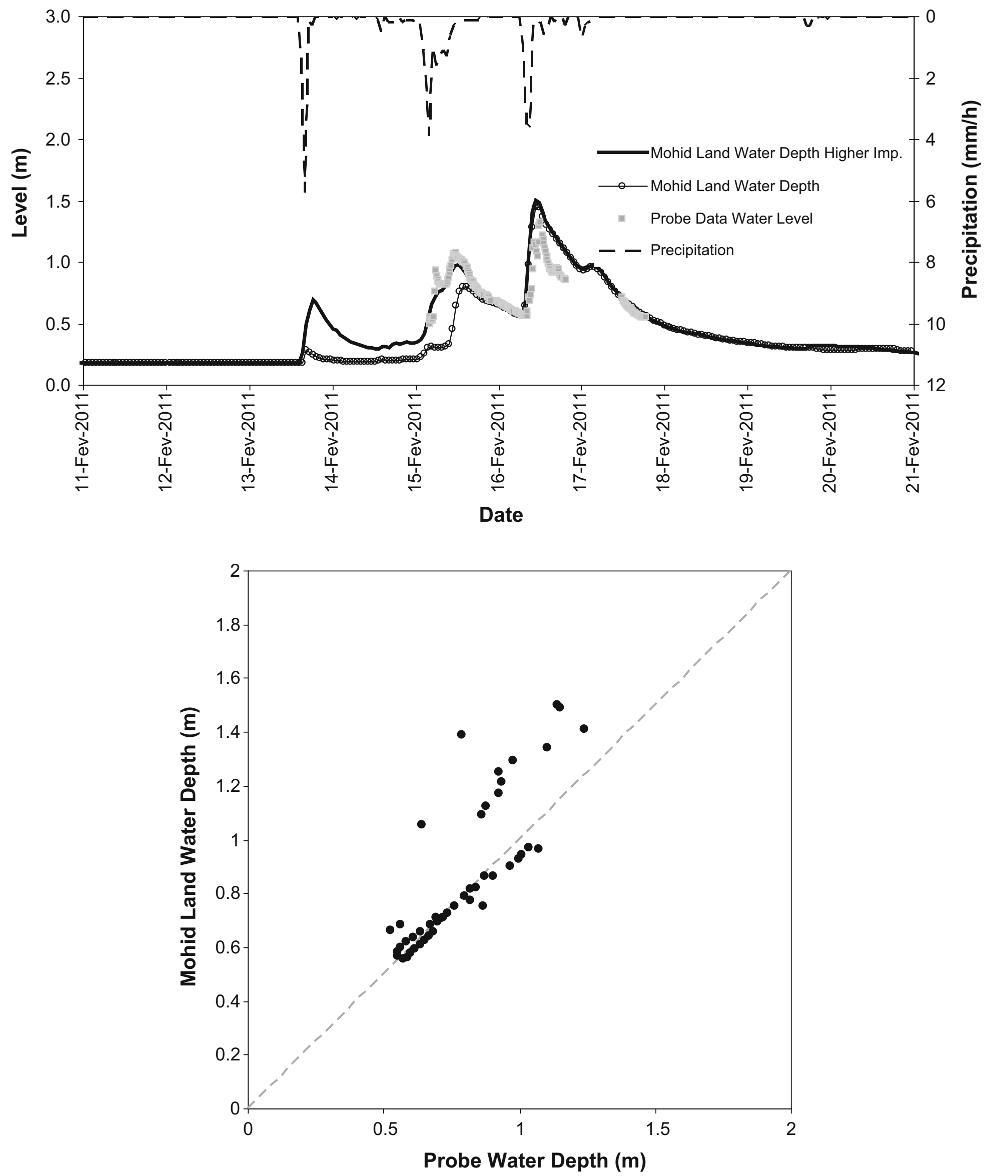

Fig. 5 Enxoé River water depth during February 2011 flood event: time series of measured water levels versus MOHID-Land predictions (*top*); scatterplot of measured versus predicted water levels (*bottom*)

permeability (e.g., soil crusting, soil compaction) assumed an important role when modeling short-term water dynamics (flood events) in Enxoé as observed above. The loss of soil permeability may be a result of overgrazing, tillage practices, fires, biological activity, and rain (Assouline 2004). Rain destroys soil aggregates and releases materials that may fill soil pores locally (soil crusting) or downstream if transported by runoff (deposition) (Assouline and Ben-Hur 2006). In arid and semiarid zones, soil susceptibility to crusting is also highly correlated with silt and low organic matter contents of soils (Singer and Le Bissonnais 1998; Ramos et al. 2000). Moreover, pores in tilled soils may lose vertical continuity direction (Panini et al. 1997) as wheel compaction associated with machinery activity has higher impact on soil surface degradation than rainfall (Li et al. 2009). All these processes are increasingly important along gentle slope regions (located mostly along the river valleys) because these are preferential depositional areas where cattle grazing and machinery activity may be more intense. However, since none of these processes can be described explicitly by the model, the loss of soil permeability in MOHID-Land had to be implicitly modeled as described above.

Various studies have noted the difficulty in describing the spatial and temporal variability of runoff production in arid or semiarid areas (Michaud and Sorooshian 1994; Chahinian et al. 2005; Al-Qurashi et al. 2008). The main difficulties have been associated with the initial conditions, precipitation distribution, soil type, land use, and soil crusting. Nonetheless, MOHID-Land results are comparable to those obtained using diverse models. For example, Chahinian et al. (2005) used four models (based on Green–

Table 8 Flood contributions to annual yields

Flood	Duration days*	Volume (hm^3)	% of Annual discharge	% Annual TSS load	% of Annual total N load	% of Annual total P Load
29–31 Oct 2010	3	0.05	2	8	3	7
13–18 Feb 2011	6	0.2	9	23	9	12

* Including rise and recession stages

TSS total suspended sediments

Ampt, Richards equation, Horton model, and Soil Conservation Service (SCS) equation) to describe 28 flood events in a 1200 m^2 watershed in southern France (NSE values >0.7 in only 8 events). Donnelly-Makowecki and Moore (1999) simulated 50 flood events in a 60 ha watersheds in Canada using TOPMODEL (NSE values varied from 0.89 to 0.93). Rozalis et al. (2010) used the SCS equation for infiltration and diffuse wave for routing in a 27 km^2 watershed in Israel; the maximum R^2 and NSE values found were 0.9 and 0.83.

In the Enxoé watershed, about 10% of the soils have silty–loam texture; 30% of the area has olive trees and annual crops, with tillage practices affecting soil structure; and 30% includes agro-forestry of holm-oaks which are extensively pastured, where large herds contribute to soil compaction. As a result, Enxoé quick response to rain events (even for the first flood) and the local pedology, agriculture practices, and pasturing suggested the loss of soil permeability as an important process for surface water generation. Precipitation rates were considered acceptable since when soil was widely saturated the model predicted well consecutive floods (Fig. 5). Also, monthly flow analysis generated good results, suggesting that calculation of evapotranspiration was also accurate enough.

Estimates of nutrient loads to the Enxoé reservoir

After model validation, model discharges were combined with measured sediment and nutrient concentrations to estimate river loads during 2010–2011. The results were used to quantify the contribution of floods (and particularly the first flood) to the annual water and nutrient budgets, and to qualitatively describe flood dynamics using NCL (Eq. 10). Table 8 shows the contribution of the two flood events considered above to the annual budgets, in terms of water yields and sediment and nutrient loads. October 2010 flood contributed to 2% of the total water yield, 8% of the total suspended solids (TSS), 3% of total N, and 7% of total P received by the reservoir. February 2011 flood contributed to 9% of total discharge, 23% of TSS, 9% of total N, and 12% of total P. The results showed that N loads varied proportionally to water yields, while P loads were proportionally much more important in the first flood.

Although October 2010 first flood generated less volume (dryer soil and higher infiltration) and less load (less than 3% of annual volume and less than 7% of annual nutrient load) than February flood event (which produced 10% of the annual volume and nutrient loads), biologic systems respond to the increase of concentration and thus these flash loads may significantly change downstream water body concentrations. Figure 6 shows the total N and total P concentrations measured during October 2010 and February 2011 flood events. To ease the interpretation of data, the water level is also shown. In October 2010, measured total N and total P concentrations were, respectively, 5 and 50 times higher in the flood than in low waters. On the other hand, in February 2011 total N and total P concentrations measured in the flood and in low waters were very similar. This was explained by the accumulation of organic matter in land and river bed during the dry season that were then transported downstream with the first flood creating high concentration peaks (Lillebø et al. 2007; Obermann et al. 2009). During subsequent winter floods, the soil surface was washed and only the dissolved material lost by soil leaching contributed to homogenize concentrations in the river and in groundwater.

One curious feature also present in Fig. 6 is the high total N concentrations measured in October 2010, just after the two discharge peaks. These concentrations correspond almost completely to nitrate and represent the arrival of the groundwater to the river (as a response to precipitation and rising aquifer level). Similar patterns of nitrate (displaying anticlockwise hysteresis) were found in other watersheds with diverse sizes and climatic conditions (House and Warwick 1998; Oeurng et al. 2010; Chen et al. 2012) and can be a consequence of fertilization of winter crops or mineralization of organic matter during the first rain events.

Figure 7 shows the relations between NCL and normalized cumulative discharge (NCD) for TSS, total N, total P, nitrate (in N), and orthophosphate (in P) collected with automatic sampler during the flood events considered

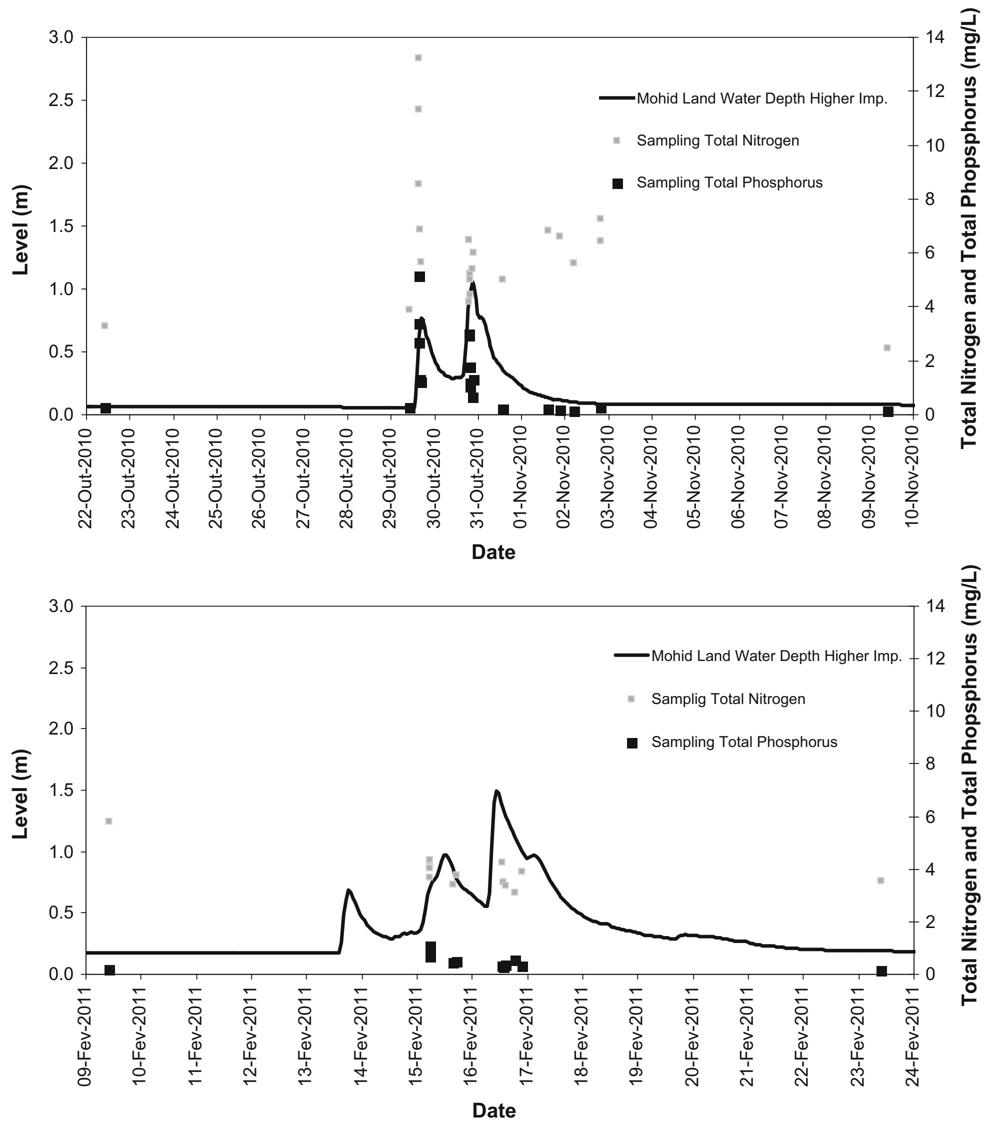

Fig. 6 Measured total nitrogen and total phosphorus concentrations in the Enxoé River: October 2010 flood event (*top*); February 2011 flood event (*bottom*)

above. MOHID-Land model discharges were integrated using a 5-min time step, and concentrations were interpolated. During October 2010 flood, TSS, total N, and total P showed a quick increase in NCL during early values of NCD when compared to dissolved properties, meaning that the first flood rising stage contributed stronger for particulate loads increase than for dissolved loads that arrived later. The TSS slope curve (Fig. 7) was higher during the flood's rising stage, summing 60% of the total load in just 20% of the flood volume. Total P (in which the adsorbed components are associated with suspended solids) summed 40% of the load, being transported by 30% of the flood volume. On the other hand, nitrate arrived later than TSS and organic compounds since they are more prone to travel through subsurface flow.

Results for February 2011 flood were identical for dissolved and particulate properties, showing that concentrations were more constant along the flood event as a result of soil surface wash out (Fig. 7).

The flushing behavior mechanics of October 2010 first flood is in line with descriptions published in the literature. Wanielista and Yousef (1993) reported that 50% of TSS were transported by the first 25% of the water discharge during a flash flood event. Bertrand-Krajewski et al. (1998) referred that at least 80% of TSS load were transported by 30% of the water discharge, also during a flash flood event. Obermann et al. (2009) found FF_{25} (load fractions in 25% of flood volume) of 0.39–0.72 for TSS (in Enxoé, this value corresponded to 0.69 for the first flood event registered in October 2010), 0.38–0.61 for total P (0.35 in Enxoé), and 0.29–0.36 for total N (0.31 in Enxoé) in Vene river, France.

Figure 8 shows the relative TSS concentration (measured values) and flow (modeled) for 2010 first flood (October). The figure shows a sudden increase of TSS, with the

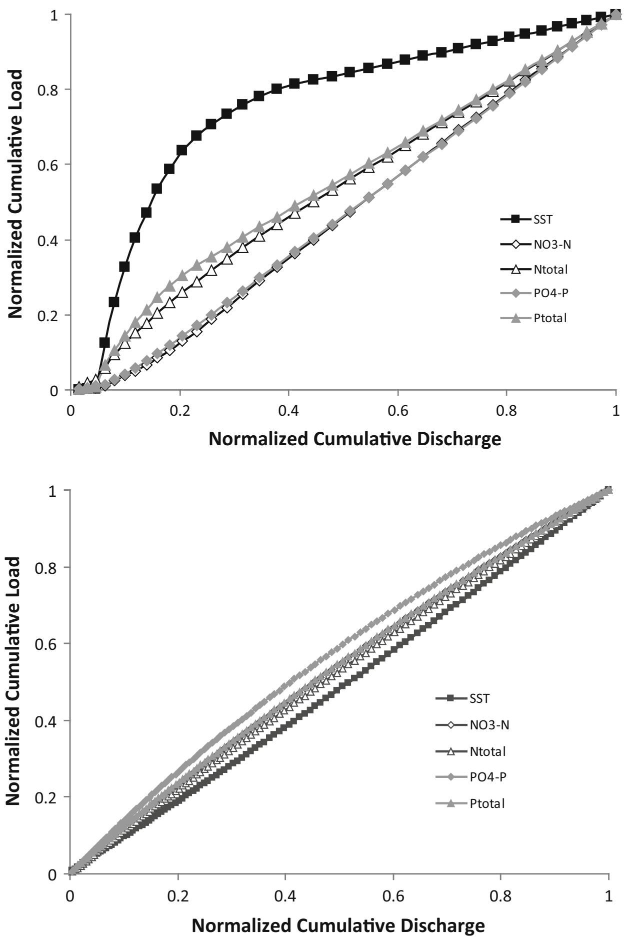

Fig. 7 Normalized cumulative loads of total suspended solids (TSS), total nitrogen (Ntotal), nitrate (NO_3–N), total phosphorus (Ptotal) and orthophosphate (PO_4–P) versus normalized cumulative discharge for October 2010 flood (*top figure*) and for February 2011 flood (*bottom figure*)

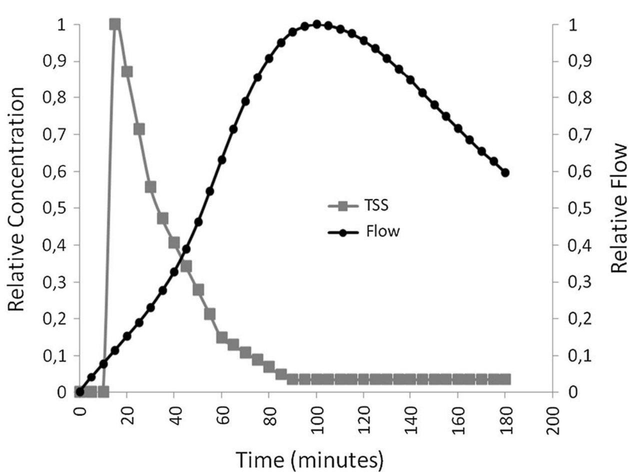

Fig. 8 Total suspended solids (TSS) relative concentration and relative flow (1 for maximum and 0 for minimum during event) for first peak discharge in October 2010 flood

maximum concentration being measured 10 min after the beginning of the flood when discharge was only 10% of its maximum. From then onwards concentration started to decrease and reached a stable value 1 h 30 after the beginning of the flood, when discharge was at maximum. The fast evolution of TSS concentration (and other organic concentrations) during the first flood required a small integration time to compute loads accurately. This argument can be used to justify the need for distributed models like MOHID-Land with short time steps to simulate floods. After integrating fluxes over one year, it was found that Enxoé catchment exports were 3.7 kgN ha^{-1} $year^{-1}$ (13 tonN $year^{-1}$) and 0.3 kgP ha^{-1} $year^{-1}$ (1 tonP $year^{-1}$), in line with estimates of 2.8 and 0.3 kgN ha^{-1} $year^{-1}$ made also for Enxoé with the SWAT model (Brito et al. 2017). Nutrient exports to the Enxoé reservoir were further in range with similar watersheds with extensive agriculture areas, gentle slopes (low erosion), and reduced human presence (Alvarez-Cobelas et al. 2010).

Conclusions

This study contributes for understanding the causes of the high trophic state registered in the Enxoé reservoir since its construction in 1998. The MOHID-Land model was used to simulate the catchment hydrology, and an intense monitoring program was implemented, including continuous measurements obtained using automatic high-frequency sampling during flood events and regular monitoring during non-flood events. The quality of MOHID-Land results was assessed by computing deviations between predictions and measurements. R^2 values of 0.94 and NSE values of 0.88 were obtained for monthly flow integrations. For water level hourly values, R^2 values reached up to 0.70 and NSE values were higher than 0.60.

Infiltration reduction due to soil compaction (e.g., soil crusting) was shown to be a major factor influencing the formation of floods in Enxoé when the soil was dry. As soil moisture increased and soil storage capacity decreased that process lost importance. As a consequence, model simulations were not able to fully reproduce catchment hydrology while considering infiltration as a continuous process along the catchment surface area, except when the soil was saturated. Only when considering a reduction of the infiltration surface area (up to 50% of the effective area) the MOHID-Land model was able to satisfactory simulate complete flood events, including rising and recession stages, and multiple peak discharges.

Furthermore, while first flood events in Enxoé had lower weight in terms of load (lower flow because of infiltration), suspended solids and organic matter were high (5 to 50 times the low water), potentially influencing reservoir primary production and oxygen consumption. Flushy regimes where flood rise peaks may occur within one hour or less and concentrations may rise and fall in a question of minutes call for the use of models with short time steps (minutes or seconds) to accurately predict loads. Distributed models able to simulate high-frequency events determining phosphorous and suspended particulate matter dynamics are thus essential to simulate the hydrological processes in Mediterranean areas like in Enxoé.

The eutrophic condition of the reservoir and the occurrence of cyanobacteria blooms is problematic in that the reservoir is the water supply for two communities (Mértola and Serpa with 25,000 inhabitants in total), and extensive water treatment is needed. Thus, further developments involve adopting a modeling integration strategy to couple a watershed and a reservoir model to depict the reservoir eutrophication origin and test management scenarios to reduce the trophic state.

Acknowledgements The present work was supported within the framework of the EU Interreg SUDOE IVB program (SOE1/P2/F146 AguaFlash project), the Mirage Project (EU-FP7), and the EUTROPHOS Project (PTDC/AGR-AAM/098100/2008) of the Fundação para a Ciência e a Tecnologia (FCT). MARETEC acknowledges the ERDF Funds of the Competitiveness Factors Operational Programme—COMPETE, and National Funds from the FCT (Project UID/EEA/50009/2013). T. B. Ramos was supported by the FCT Grant SFRH/BPD/110655/2015.

References

Allen RG, Pereira LS, Raes D, Smith M (1998) Crop evapotranspiration—guidelines for computing crop water requirements. Irrig drain paper 56. FAO, Rome

Al-Qurashi A, McIntyre M, Wheater H, Unkrich C (2008) Application of the Kineros2 rainfall–runoff model to an arid catchment in Oman. J Hydrol 355:91–105

Alvarez-Cobelas M, Sánchez-Andrés R, Sánchez-Carrillo S, Angeler DG (2010) Nutrient contents and export from streams in semiarid catchments of central Spain. J Arid Environ 74(8):933–945

ASCE (1996) Hydrology handbook. American Society of Civil Engineers, Task Committee on Hydrology Handbook, II Series. GB 661.2.H93.1996.96-41049

Assouline S (2004) Rainfall-induced soil surface sealing: a critical review of observations, conceptual models, and solutions. Vadose Zone J 3:570–591

Assouline S, Ben-Hur M (2006) Effects of rainfall intensity and slope gradient on the dynamics of interrill erosion during soil surface sealing. Catena 66:211–220

Bernard-Jannin L, Brito D, Sun X, Jauch E, Neves R, Sauvage S, Sánchez-Pérez JM (2016) Spatially distributed modelling of surface water-groundwater exchanges during overbank flood events—a case study at the Garonne River. Adv Water Res 94:146–159

Bertrand-Krajewski J-L, Chebbo G, Saget A (1998) Distribution of pollutant mass vs volume in stormwater discharges and the first flush phenomenon. Water Res 32(8):2341–2356

Bicknell BR, Imhoff JC, Kittle JL, Donigian AS, Johanson RC (1993) Hydrological simulation program—FORTRAN (HSPF): users manual for release 10. EPA-600/R-93/174, U.S. EPA, Athens, GA, 30605

Boughton W, Droop O (2003) Continuous simulation for design flood estimation—a review. Environ Model Soft 18:309–318

Brito D, Neves R, Branco MA, Prazeres Â, Rodrigues S, Gonçalves MC, Ramos TB (2017) Assessing water and nutrient long-term dynamics and loads to an eutrophic reservoir in the Enxoé temporary river basin, southeast Portugal. Appl Water Sci (**under review**)

Brunner GW (2010) HEC-RAS river analysis system user's manual. ver. 4.1

Chahinian N, Moussa R, Andrieux P, Voltz M (2005) Comparison of infiltration models to simulate flood events at the field scale. J Hydrol 306:191–214

Chen N, Wu J, Hong H (2012) Effect of storm events on riverine nitrogen dynamics in a subtropical watershed, southeastern China. Sci Total Environ 431:357–365

Dechmi F, Burguete J, Skhiri A (2012) SWAT application in intensive irrigation systems: model modification, calibration and validation. J Hydrol 470–471:227–238

Donnelly-Makowecki LM, Moore RD (1999) Hierarchical testing of three rainfall-runoff models in small forested catchments. J Hydrol 219:136–152

FAO (2006) World reference base for soil resources. A framework for international classification, correlation and communication. World Soil Resource Report 103. Food and Agriculture Organization of the United Nations, Rome

Feddes RA, Kowalik PJ, Zaradny H (1978) Simulation of field water use and crop yield. Simulation Monographs Pudoc, Wageningen

Fohrer N, Eckhardt K, Haverkamp S, Frede HG (2001) Applying the SWAT model as a decision support tool for land use concepts in peripheral regions in Germany. Sustaining Global Farm. In: Papers from the 10th international soil conservation organization meeting, pp 994–999

Geza M, McCray JE (2008) Effects of soil data resolution on SWAT model stream flow and water quality predictions. J Environ Manag 88:393–406

Green CH, van Griensven A (2008) Autocalibration in hydrologic modeling: using SWAT2005 in small-scale watersheds. Environ Model Soft 23:422–434

Havnø K, Madsen MN, Dørge J (1995) MIKE 11—A generalized river modelling package. In: Singh VP (ed) Computer models of watershed hydrology. Water Resources Publications, Colorado, pp 809–846

House WA, Warwick MS (1998) Hysteresis of the solute concentration/discharge relationship in rivers during storms. Water Res 32:2279–2290

Hsu MH, Chen SH, Chang TJ (2000) Inundation simulation for urban drainage basin with storm sewer system. J Hydrol 234:21–37

INAG (2004) Plano de Ordenamento da Albufeira do Enxoé, estudos de caracterização e pré-proposta de ordenamento. Instituto Nacional da Água, Lisboa

INE (2001) Recenseamento Geral Agrícola. Instituto Nacional de Estatística, Lisboa

James AL, Roulet NT (2009) Antecedent moisture conditions and catchment morphology as controls on spatial patterns of runoff generation in small forest catchments. J Hydrol 377:351–366

Li YX, Tullberg JN, Freebairn DM, Li HW (2009) Functional relationships between soil water infiltration and wheeling and rainfall energy. Soil Tillage Res 104:156–163

Li H, Sivapalan M, Tian F (2012) Comparative diagnostic analysis of runoff generation processes in Oklahoma DMIP2 basins: the Blue River and the Illinois River. J Hydrol 418–419:90–109

Lillebø AI, Morais M, Guilherme P, Fonseca R, Serafim A, Neves R (2007) Nutrient dynamics in Mediterranean temporary streams: a case study in Pardiela catchment (Degebe River, Portugal). Limnologica 37(4):337–348

Michaud J, Sorooshian S (1994) Comparison of simple versus complex distributed runoff models on a midsized semiarid watershed. Water Resour Res 30:593–605

Moriasi DN, Arnold JG, Van Liew MW, Bingner RL, Harmel RD, Veith TL (2007) Model evaluation guidelines for systematic quantification of accuracy in watershed simulations. Trans ASABE 50(3):885–900

Nash JE, Sutcliffe JV (1970) River flow forecasting through conceptual models: part 1. A discussion of principles. J Hydrol 10(3):282–290

Neitsch SL, Arnold JG, Kiniry JR, Srinivasan R, Williams JR (2002) Soil and water assessment tool. Users manual. Version 2005. GSWRL Report 02-02, BRC Report 2-06, Temple, Texas, USA

Neves R (2013) The MOHID concept. In: Mateus M, Neves R (eds) Ocean modelling for coastal management e case studies with MOHID. IST Press, Lisbon, pp 1–11

Obermann M, Froebrich J, Perrin J-L, Tournoud M-J (2007) Impact of significant floods on the annual load in an agricultural catchment in the Mediterranean. J Hydrol 334:99–108

Obermann M, Rosenwinkel KH, Tournoud MG (2009) Investigation of first flushes in a medium-sized Mediterranean catchment. J Hydrol 373:405–415

Oeurng C, Sauvage S, Sánchez-Pérez JM (2010) Temporal variability of nitrate transport through hydrological response during flood events within a large agricultural catchment in south–west France. Sci Total Environ 409:140–149

Panagopoulos Y, Makropoulos C, Mimikou M (2011) Reducing surface water pollution through the assessment of the cost-effectiveness of BMPs at different spatial scales. J Environ Manag 92:2823–2835

Panday S, Huyakorn P (2004) A fully-coupled physically-based spatially distributed model for evaluating surface/subsurface flow. Adv Water Resour 27:361–382

Panini T, Torri D, Pellegrini S, Pagliai M, Salvador-Sanchis MP (1997) A theoretical approach to soil porosity and sealing development using simulated rainstorms. CATENA 31:199–218

Ramos MC, Nacci S, Pla I (2000) Soil sealing and its influence on erosion rates for some soils in the Mediterranean area. Soil Sci 165:398–403

Ramos TB, Gonçalves MC, Branco MA, Brito D, Rodrigues S, Sánchez-Pérez JM, Suavage S, Prazeres A, Martins JC, Fernandes ML, Pires FP (2015) Sediment and nutrient dynamics during storm events in the Enxoé temporary river, southern Portugal. CATENA 127:177–190

Ritchie JT (1972) Model for predicting evaporation from a row crop with incomplete cover. Water Resour Res 8(5):1204–1213

Rozalis S, Morin E, Yair Y, Price C (2010) Flash flood prediction using an uncalibrated hydrological model and radar rainfall data in a Mediterranean watershed under changing hydrological conditions. J Hydrol 394:245–255

Saxton KE, Rawls WJ, Romberger JS, Papendick RI (1986) Estimating generalized soil–water characteristics from texture. Soil Sci Soc Am J 50(4):1031–1036

Singer MJ, Le Bissonnais Y (1998) Importance of surface sealing in the erosion of some soils from a mediterranean climate. Geomorphology 24(1998):79–85

Trancoso AR, Braunschweig F, Chambel-Leitão P, Obermann M, Neves R (2009) An advanced modeling tool for simulating complex river systems. Sci Total Environ 407:3004–3016

van Genuchten MTh (1980) A closed form equation for predicting the hydraulic conductivity of unsaturated soils. Soil Sci Soc Am J 44:892–898

Wanielista MP, Yousef YA (1993) Stormwater management. Wiley, Hoboken

Woolhiser DA, Smith RE, Goodrich DC (1990) KINEROS, a kinematic runoff and erosion model: documentation and user manual. USDA research service, ARS-77, p 130

3.3 Integrated modelling for water quality management in an eutrophic reservoir in southeast Portugal

This article/application integrates the inputs and knowledge acquired from the two previous implementations producing an integrated watershed-reservoir modelling (offline) approach in order to depict the trophic level origin and test management scenarios for its reduction.

Integrated modelling for water quality management in an eutrophic reservoir in southeast Portugal

David Brito[1], Tiago B. Ramos[1], Ramiro Neves[1], Maria C. Gonçalves[2], Manuela Morais[3]

[1] MARETEC, Instituto Superior Técnico, Universidade de Lisboa, Av. Rovisco Pais, 1049-001 Lisboa, Portugal.

[2] Instituto Nacional de Investigação Agrária e Veterinária, Quinta do Marquês, Av. República, 2784-505 Oeiras, Portugal.

[3] Laboratório da Água, Universidade de Évora, Rua da Barbarrala, 1, Parque Industrial e Tecnológico, 7000 Évora, Portugal.

First author and corresponding author: David Brito, e-mail: odavidbrito@gmail.com, phone: 00351 962535504

Abstract

The Enxoé reservoir was built in 1998. Since 2000, it has been exhibiting frequent high chlorophyll-a concentrations - reaching a geometric mean 3 times higher than the national limit for eutrophication - representing the reservoir with the highest eutrophic state in Portugal. Toxic algal blooms have also been often observed, which pose serious challenges to water managers as the reservoir is used for potable water production (25000 inhabitants). The objective of this study was to implement a reservoir model (CE-QUAL-W2) with inputs from a watershed model (SWAT) in order to represent the actual reservoir state, and test management measures to reduce its trophic level and algal blooms concentration peaks. The integrated model was used to depict the trophic status origin. Simulations were also compared with measured data at the reservoir surface (water level, nitrate, orthophosphate, suspended solids, and oxygen) and in water profiles (temperature, oxygen). The model was able to represent stratification and thermocline depths, as well as the actual chlorophyll-a and dissolved oxygen concentrations. Model results showed that internal phosphorus load from deposited sediments was an important factor for fuelling reservoir high blooms. This process occurs mainly in summer when stratification takes place and reaeration is reduced, promoting anoxia conditions near the bottom. Since the reservoir is relatively shallow (average 5 m), released phosphorus can then easily reach the photic zone in most part of the reservoir and be consumed. Different management scenarios were tested, suggesting that a mesotrophic level can hardly be reached and maintained by reducing loads (both external and internal). It is suggested that only a reservoir dam height increase can lead to a mesotrophic level, by blocking anoxia phosphorus release from sediments to the photic zone. Future work should focus on cost benefit analysis to test the feasibility of each proposed scenarios.

Keywords: Eutrophic reservoir; integrated modelling; CE-QUAL-W2; SWAT; phosphorus.

3.3.1 Introduction

Enxoé is a temporary river watershed limited downstream by a reservoir built in 1998. The reservoir has been exhibiting the highest eutrophic state in Portugal since 2000, registering frequent chlorophyll-a concentrations higher than 50 $\mu g.L^{-1}$, with maximums of 200 $\mu g.L^{-1}$, over the years. The geometric average of surface chlorophyll-a concentration also reached 33 $\mu g.L^{-1}$ during 2001-2011, whereas the national limit for eutrophication is 10 $\mu g.L^{-1}$ [11]. Moreover, toxic cyanobacteria blooms occurred (INAG 2004; Valerio et al. 2005) and interrupted water distribution to the local population. This constitutes a serious problem for water management, with the constant reservoir eutrophication, particularly the presence of toxic algae in a reservoir used for water production, calling for improved management plans in the scope of the Water Framework Directive.

Cyanobacteria algae dominance is usually controlled by two main processes: some species are able to consume N_2 dissolved in the water (Paerl et al. 2001; Havens et al. 2003; Rolff et al. 2007), while others are further able to maintain growth even under conditions of low light availability (Havens et al. 2003). The nitrogen fixation characteristics of some types of cyanobacteria further allows them to be independent of the availability of inorganic forms of nitrogen (e.g., ammonia, nitrate). Under conditions of nitrogen limitation, these species have then the potential to generate blooms if phosphorus is available (Havens 2003).

Such cyanobacterial response to phosphorus availability may have occurred in the Enxoé reservoir after 2002, with identified species in 2003 and 2005 (Valério 2008). Previous studies linked cyanobacteria blooms in the Enxoé reservoir to nutrient input loads from the watershed, and hypothesized that such blooms could be associated to phosphorus inputs (Ramos et al. 2015a, 2015b; Brito el al. 2017a, 2017b). Those authors considered that phosphorus feeding from the watershed may have fuelled the process, which consisted of both a fast and a delayed response in the reservoir, where initial blooms arised from the consumption of input

[11] Portuguese trophic level classification was chosen adapted from OCDE and the geometric average is used to reduce the weight of extreme values.

dissolved nutrients, while later blooms were attributable to sediment sources, e.g., mineralization and desorption under anoxic conditions (Coelho et al. 2008).

However, a more comprehensive approach was required to fully understand the main physical and biochemical processes related to the eutrophication of the Enxoé reservoir. One viable option was by integrating the watershed and the reservoir in order to determine the impact of management practices in the reservoir. Examples of such integration were given by Liu et al. (2015) who linked the SWAT (Neitsch et al. 2002) and CE-QUAL-W2 (Cole and Wells 2011) models to estimate nitrogen retention in the Shanmei Reservoir, in China. Mateus et al. (2014) used those same models to determine management measures that could reduce the trophic level of the Tâmega reservoir, Portugal. Debele et al. (2008) also implemented SWAT and CE-QUAL-W2 for determining their feasibility in representing hydrodynamic and water quality observations in the Cedar Creek Reservoir, in USA. Xu et al (2007) did the same with the HSPF and CE-QUAL-W2 models in the Occoquan watershed, USA. These integrated approaches proved useful to represent the actual water body status and test the impact on the reservoir of management changes.

The SWAT model has been widely applied to a large range of watershed sizes and configurations to simulate flow and nutrient export on daily, monthly and annual scales (Gassman et al. 2007; Zhang et al. 2008). Examples of SWAT implementation in watersheds with similar size and land uses as Enxoé include the work of Geza and McCray (2008) and Green and van Griensven (2008) both in USA, Yevenes and Mannaerts (2011) in Portugal, and Dechmi et al. (2012) and Panagopoulos et al. (2011) in Spain and Greece, respectively. CE-QUAL-W2 model is widely applied for describing hydrodynamics and water quality in reservoirs, estuaries, and rivers (Martin et al. 2013; Lung and Bai 2003; Kurup et al. 2000, Makinia et al. 2005).

The current paper applies a state-of-the-art modelling integration tool, combining the best knowledge in the watershed and in the reservoir for improving water quality management. The objective was to couple a watershed model (SWAT) and a reservoir model (CE_QUAL-W2) by integrating the available field data in order to determine the origin of the Enxoé reservoir eutrophication and test the best-suited management strategies (in the watershed and reservoir) to reduce the reservoir trophic status. This study complements a series of modeling studies aimed at improving water management plans in the Enxoé basin.

3.3.2 Material and methods

3.3.2.1 Study site

Enxoé is a 60 km^2 catchment located in southeast Portugal, in the left margin of the Guadiana River (Figure 1). The Enxoé River has a bed length of approximately 9 km from its headwaters to the dam. The reservoir (37º 59' 38.121'' N, 7º 27' 54.776'' W) has a total volume of 10.4 hm^3, a surface area of approximately 2 km^2, an average depth of 5 m (max depth of 17 m near the dam), and an average residence time of 2 years. The reservoir level fluctuates 1-2 m from the maximum in wet years, and 4-6 m in dry years (e.g., 2006 and 2008). The reservoir also exhibits high algae and suspended solids content for the most part of the year, with Secchi disk depths around 1-3 m, creating thermal stratification during spring that lasts up to winter when higher flows and wind occur. Chlorophyll concentrations usually peak in the autumn (when flow and nutrient inputs from the watershed start while reservoir water temperatures are still relatively high) and in the summer (usually higher, due to high temperature and low turbidity).

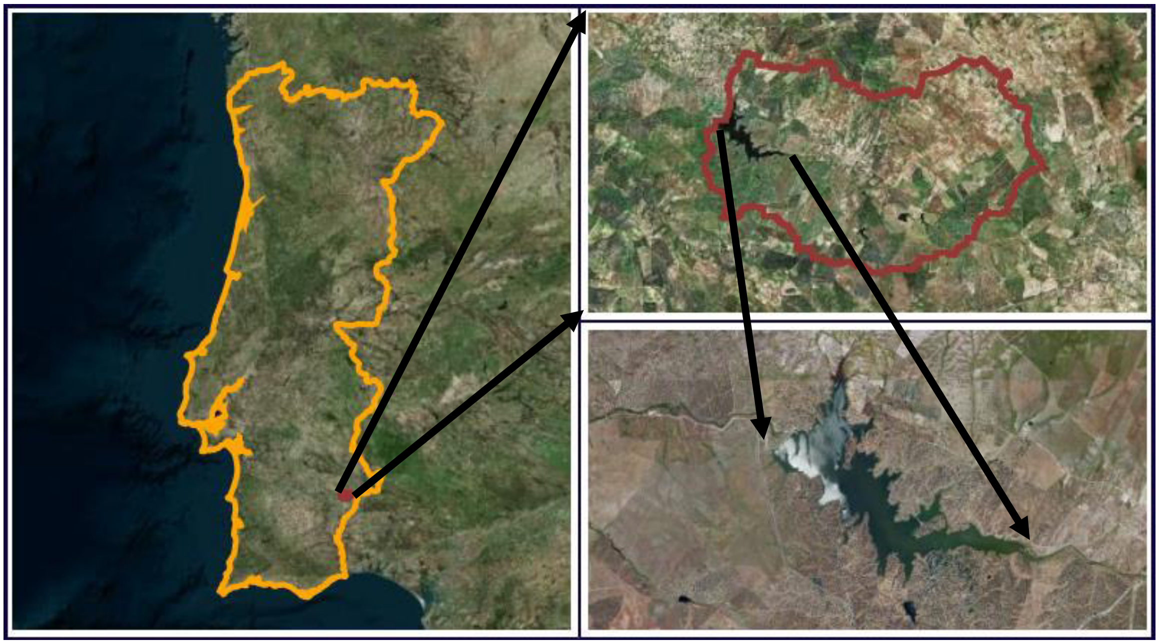

Figure 1. Location of the Enxoé watershed in Portugal (left) and Enxoé reservoir in the watershed (right).

The climate in the region is dry sub-humid to semi-arid, with temperatures averaging 16 ºC and ranging from -5 ºC in winter to near 40 ºC in summer. The precipitation regime is characterized by a highly irregular behaviour, varying between relatively abundant rainfall episodes, concentrated in only a few minutes or hours, and frequent drought episodes that can last from a few months to a couple of years. The annual average precipitation is 500 mm, irregularly distributed throughout the year (80% of the annual precipitation is concentrated between October and April). As a result, the river exhibits relatively large flow in the winter as a response to rain events (up to 2 $hm^3.month^{-1}$), reduced flow in the spring after rain ceases, and no flow with pool formation during the summer or extended drought periods (Ramos et al. 2015a). The slopes are gentle, with an average river slope of approximately 2%, while the watershed shows an average slope of 5-6%. The gentle slopes promote water pooling and the occurrence of disconnected flow. The average maximum hourly wind is 2 $m.s^{-1}$, reaching maximums of 20 $m.s^{-1}$.

The soils in Enxoé originate mainly from granite and limestone (each with approximately 30% of the total area) and schist (with approximately 10% of the total area). The land is mainly used for growing olive trees, agro-forestry of holm-oaks (“montado”), and annual rainfed crops (wheat, oats, and sunflower), each covering approximately 30% of the total area. Extensive livestock production is the most important animal-farming activity in the catchment. According to the 1999 agricultural census (INE, 2001), cow (602) and sheep (4365) production corresponds each to approximately 0.1 livestock units (LSU) per ha of agricultural surface. The catchment has a population of 1000 inhabitants, mainly concentrated in Vale de Vargo. The respective waste water treatment plant discharges outside the watershed since 2006 as a protective measure to the Enxoé reservoir. The reservoir currently supplies the villages of Mértola and Serpa for drinking water (25,000 inhabitants).

3.3.2.2 Modelling approach

3.3.2.2.1 Study background

The Enxoé watershed is small (60 km^2), and the river exhibits a flushy regime that was never studied in detail before. There was the need for assessing both the long-term (annual nutrient and suspended sediment loads) and short-term (flash flood loads) inputs to the reservoir in order to understand the watershed dynamics and its effect on the reservoir trophic level.

Two approaches were considered: (i) long term loads were estimated with the SWAT model (Neitsch et al. 2002) by comparing model predictions of flows and loads with recorded reservoirs inflows and discrete sampling measurements (Brito et al. 2017a), respectively; and (ii) short term loads were assessed by applying the MOHID-Land model (Neves 2013) for predicting continuous probe measurements obtained during flash flood events (Brito et al. 2017b).

The two models have different structures that are especially suitable for those purposes. SWAT is a semi-empirical model with highly developed crop and management modules that use sub-basins for reservoir balance and daily time steps, making it adequate to run for large periods (e.g., years, decades) but failing in the detailed description of flash floods and related processes that in Enxoé occur in just a couple of hours. On the other hand, MOHID-Land is a physically based and distributed model with variable time step (in the order of seconds or less during intense fluxes as floods), being thus able to describe flash flood formation and propagation.

SWAT estimates of Enxoé nitrogen long-term loads reached 2.5-2.8 $kgN.ha^{-1}.year^{-1}$ (28 $tonN.year^{-1}$), total suspended solids (TSS) loads were 0.45 $ton.ha^{-1}.year^{-1}$, and phosphorus loads were 0.3 $kg.ha^{-1}.year^{-1}$ (0.6 $tonP.year^{-1}$). These estimates were comparable with those found in similar extensive agricultural areas with gentle slopes (low erosion) and reduced human presence (Brito et al. 2017a).

MOHID-Land results, validated with field data taken in low waters and flood events during two years, showed that by considering floods dynamics the effective annual phosphorus transport to the reservoir could be up to 3 times the average annual phosphorus loads estimated by SWAT; in an average year that would be 1.8 $tonP.year^{-1}$. Also, MOHID-Land and SWAT estimates of phosphorus loads reaching the drainage network were very similar (1.8 $tonP.year^{-1}$). However, SWAT then considered that only 0.6 $tonP.year^{-1}$ would reach the reservoir, with the remainder being deposited in the river bed. On the other hand, MOHID-Land results showed that the deposited material would later be ressuspended during floods and would also reach the reservoir (Brito et al. 2017b). Despite that, SWAT model estimates were used in this study to feed the reservoir since MOHID-Land simulated only hydrodynamics. The extra phosphorus load that reached the reservoir, and that was not described by SWAT, was used to proxy the actual situation of internal phosphorus load (see section 2.2.3.).

3.3.2.2.2 Models description

The SWAT model

SWAT (Neitsch et al. 2002) implementation in the Enxoé catchment was already described in detail in Brito et al. (2017a). Thus, only a brief description of model setup will be given here. SWAT is a basin river model developed at Texas A&M University, where the land hydrodynamics component solves the water balance, relating meteorological variables with basin features (topography, soil type, and land use). For water quality assessment, the model further simulates plant growth, nitrogen and phosphorus soil cycles, and sediment and pesticides transport (Neitsch et al. 2002). The river outputs that served as inputs to CE-QUAL-W2 were the nitrogen and phosphorus pools (dissolved forms as nitrate, ammonia, orthophosphate), organic matter, suspended solids, and oxygen.

In Enxoé, SWAT implementation was defined with 65 sub-watersheds and 161 Hydrological Response Units (HRU's) in order to describe the land use and soil distribution of the base data maps. These included NASA SRTM with 3 arc seconds for the digital terrain model, CORINE land Cover for land use, the European soil geographical database at scale 1:1000000 for soil texture, and the meteorological stations of the Portuguese Environmental Agency's (APA) network for weather data. The agricultural practices (crop rotations, fertilization) were obtained from farmers' questionnaires, and consisted of rotations between wheat and oats, and between sunflower, wheat and oats. Annual fertilization loads ranged from 40-90 $kgN.ha^{-1}.year^{-1}$ and 20 $kgP.ha^{-1}.year^{-1}$ (Ramos et al. 2015a; Brito et al. 2017a). Animal nutrient production was obtained from the National Institute of Statistics (INE, 2001). The annual animal loads were distributed homogeneously along the sites with agro-forestry of holm-oaks and pasture (sheep and cattle) and olive trees (sheep) and throughout the year following the extensive regime of animal production in Enxoé.

SWAT model implementation used the default boundary and initial conditions, including ground water losses to deep aquifer, drainage network outflow, and meteorological input data from recorded meteorological stations. Model calibration consisted of adjusting the hydraulic parameters that control the travel timing of water between the soil and the aquifer, and the aquifer and the river since these showed to be relevant when modelling small temporary river watersheds with small travel times and fast rise and fall hydrographs. In terms of water quality, in-stream rates were changed to represent in pool processes that occur in Enxoé after rain events cease, river water disconnections due to temporary pool formations, and high retention times. Further details can be found in Brito et al. (2017a).

The CE-QUAL-W2 model

The CE-QUAL-W2 model (Cole and Wells 2011) version 3.7 was used for simulating the water quality in the Enxoé reservoir. CE-QUAL-W2, developed at US Corps of Engineers, is a bidimensional, laterally averaged, dynamic model. The hydrodynamics component uses Navier-Stokes equations for incompressible flow in the water body velocity field and turbulent diffusion coefficients calculation. The water quality component computes property sources and sinks considering interactions between temperature, nutrients, algae, dissolved oxygen, organic matter, and sediments (Cole and Wells 2011).

Figure 2 presents the geometry used to describe the main Enxoé reservoir areas and orientations at full capacity, consisting of 12 segments with lengths of 150-350 m and widths of 300-1000 m at surface. A minimum of 4 vertical layers at upstream and a maximum of 17 layers near the dam, all with 1 m height, were further considered. The depth information was defined based on available reservoir and wall geometry data provided by APA.

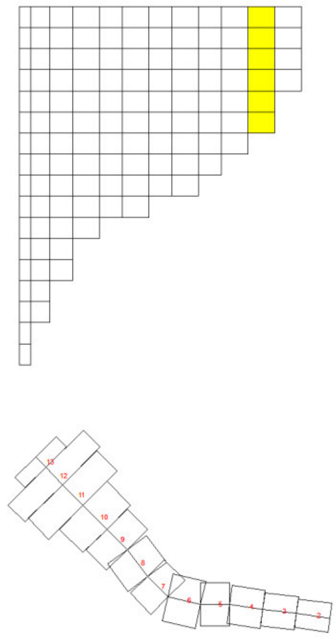

Figure 2. CE-QUAL-W2 grid definition for Enxoé in plan view (bottom) and profile view along the axis (top).

Model boundary conditions included: river daily inputs of nitrate, ammonia, orthophosphate, organic matter, total suspended solids, and oxygen computed with SWAT (Brito et al. 2017a); weather daily data (air temperature, humidity, wind velocity and direction, and cloud cover) from the nearest meteorological station (Herdade da Valada, located 4 km from the reservoir); the reservoir outflow computed from the reservoir balance between inflows, evaporation, and storage (Brito et al. 2017a); and the bottom internal load from sediments in anoxic conditions (mainly phosphorus).

Model simulations started in 2001 and ended in 2011. Initial conditions (reservoir level and concentrations) were obtained from measured data. Initial concentrations were assumed to be homogeneous in depth (simulations started in winter), in consistency with measured data.

Daily weather data was used in model simulations since hourly records showed frequent gaps. However, since wind gusts with high intensity during long periods can have a strong effect on stratification destruction, daily averages of maximum hourly wind velocities were also used in CE-QUAL-W2 (sensitivity analysis showed then better comparison between temperature predictions and field data than when using average hourly wind values). Dew point temperature was computed as in Lawrence (2005):

$$T_d = T - (100 - RH) / 5 \tag{1}$$

where T_d is the dew point temperature (ºC), T is the air temperature (ºC), and RH is the relative humidity (-). Reservoir first results showed consistent underestimation of winter minimum temperatures. Dew point values were limited to a minimum of 10ºC or would very often drop to negative temperatures during winter that in turn would result in high evaporation and temperature losses from the reservoir. In fact, a vertical air temperature gradient may form above the surface water, increasing temperatures at night (in comparison to meteorological station 4km away) and reduces evaporation losses (Condie and Webster 1997). Thus, this phenomenon ended up being accounted for in CE-QUAL-W2 by imposing a limit to the dew point values, which is the variable directly used in the model for simulating evaporation.

3.3.2.2.3 CE-QUAL-W2 model calibration/evaluation

The CE-QUAL-W2 model was calibrated/validated for the period 2001-2011 (current situation). After that, different management scenarios with reduced nutrient loads and reservoir geometry changes were tested to assess the reservoir trophic level response.

The field data used for calibration/validation of the CE-QUAL-W2 model were: (i) hourly reservoir levels provided by APA for the period 2001-2011; (ii) monthly reservoir surface concentrations (nitrate, ammonia, orthophosphate, chlorophyll-a, oxygen, suspended solids) provided by APA for the period 2001-2011 (APA, 2017); and (iii) measured seasonal profiles of temperature, oxygen, turbidity, and pH, as well as Secchi disk measurements, collected under the scope of this study, for the period August 2009 - March 2012.

Both qualitative and quantitative measures of uncertainty were used to compare observed data with predicted values. Graphical analyses, such as time-series plots, were used to identify general trends, potential sources of error, and differences between measured and predicted values. CE-QUAL-W2 model performance was further depicted by mean values, standard deviations, correlations, and the root mean squared error (RMSE), given by:

$$RMSE = \frac{\sum_{i=i}^{n}(O_i - S_i)^2}{n} \quad (2)$$

where O_i is the observed data, S_i is the simulated data, and n is the total number of data records. RMSE values close to zero indicate small errors of estimate and good model predictions. The Taylor diagrams were also used for graphical representation of model performance (Taylor, 2001).

Model evaluation included the comparison of model predictions with respective measurements of daily reservoir water levels and monthly concentrations of nitrate, total suspended solids, orthophosphate, chlorophyll-a, and dissolved oxygen. Model calibration procedures involved modifying a set of parameters listed in Table 1 and mapped in Figure 3 until deviations between model predictions and observations were minimized. These included changing algal growth rates and optimum temperatures for the different species, reducing extinction coefficients that control light availability at lower depths, and reducing suspended sediment sink rates. The calibrated parameters were thus modified to best fit measures of i) suspended sediment by reducing sink rates (justified by measured high suspended sediment concentration representative of very fine material, in consistency with wind driven resuspension in low depth reservoirs as Enxoé); ii) algal blooms and oxygen depletion by adapting algal rates and phosphorus internal loads; and iii) temperature profiles by adjusting extinction coefficients.

Table 1 CE-QUAL-W2 parameters for the Enxoé reservoir.

#	Parameter	Description	Default value	Calibrated Value
1	AG #1	Algal growth rate for diatoms (day^{-1})	0.3-3.0	1
2	AG #2	Algal growth rate for clorophicae (day^{-1})	0.7-9.0	3
3	AG #3	Algal growth rate for cyanobacteria (day^{-1})	0.5-11	2.5
4	AT1 #1	Algal minimum temperature for diatoms (ºC)	5	5
5	AT1 #2	Algal minimum temperature for chlorophicae (ºC)	5	12
6	AT1 #3	Algal minimum temperature for cyanobacteria (ºC)	5	15
7	AT2 #1	Algal first optimum temperature for diatoms (ºC)	25	10
8	AT2 #2	Algal first optimum temperature for chlorophicae (ºC)	25	15
9	AT2 #3	Algal first optimum temperature for cyanobacteria (ºC)	25	23
10	AT3 #1	Algal last optimum temperature for diatoms (ºC)	35	22
11	AT3 #2	Algal last optimum temperature for chlorophicae (ºC)	35	26
12	AT3 #3	Algal last optimum temperature for cyanobacteria (ºC)	35	26
13	AT4 #1	Algal maximum temperature for diatoms (ºC)	40	24
14	AT4 #2	Algal first maximum temperature for chlorophicae (ºC)	40	29
15	AT4 #3	Algal first maximum temperature for cyanobacteria (ºC)	40	29
16	AR #1	Maximum dark algal respiration rate for diatoms (day^{-1})	0.04/0.01-0.59	0.03
17	AR #2	Maximum dark algal respiration rate for chlorophicae (day^{-1})	0.04/0.01-0.59	0.03
18	AR #3	Maximum dark algal respiration rate for cyanobacteria (day^{-1})	0.04/0.01-0.59	0.03
19	AE #1	Maximum excretion rate for diatoms (day^{-1})	0.04/0.014-0.044	0.03

20	AE #2	Maximum excretion rate for chlorophicae (day^{-1})	0.04/0.014-0.044	0.03
21	AE #3	Maximum excretion rate for cyanobacteria (day^{-1})	0.04/0.014-0.044	0.02
22	AM #1	Maximum mortality rate for diatoms (day^{-1})	0.1	0.05
23	AM #2	Maximum mortality rate for chlorophicae (day^{-1})	0.1	0.02
24	AM #3	Maximum mortality rate for cyanobacteria (day^{-1})	0.1	0.02
25	AS #1	Settling velocity for diatoms ($m.day^{-1}$)	0.1/0.2	0.1
26	AS #2	Settling velocity for chlorophicae m.(day^{-1})	0.1/0.1	0.1
27	AS #3	Settling velocity for cyanobacteria ($m.day^{-1}$)	0.1/<0-0.05	-0.1
28	EX SS	Extinction Coefficient for suspended solids (m^{-1})	0.1	0.01
29	EX OM	Extinction Coefficient for organic matter (m^{-1})	0.1	0.01
30	EX ZOO	Extinction Coefficient for zooplâncton (m-1)	0.1	0.01
31	BETA	Fraction of incident solar radiation absorbed at the water surface (%)	0.45	0.45
32	SSS	Suspended solids settling rate (m day-1)	1	0.01
33	POMS	POM settling rate (m/day)	0.001-20	0.25
34	LDOMDK	Labile DOM decay rate (day^{-1})	0.1/0.01-0.64	0.12
35	RDOMDK	Refractory DOM decay rate (day^{-1})	0.001/0.0001-0.0064	0.002
36	LPOMDK	Labile POM decay rate (day^{-1})	0.08/0.001-0.1	0.08
37	RPOMDK	Refractory POM decay rate (day^{-1})	0.001/0.001-0.1	0.02
38	DO1	Dissolved Oxygen concentration limitation curve first point (mg L-1)	-	1E-5
39	DO2	Dissolved Oxygen concentration limitation curve second point (mg L-1)	-	5.0
40	DOK1	Dissolved Oxygen limitation fraction first point	-	0.1
41	DOK2	Dissolved Oxygen limitation fraction second point	-	0.99
42	ZG	Zooplankton maximum growth rate (day^{-1})	1.5	0.19

43	ZR	Zooplankton maximum respiration rate (day^{-1})	0.1	0.1
44	ZM	Zooplankton maximum mortality rate (day^{-1})	0.01	0.01
45	PO4R,	Anoxia ortophosphate release fraction of SOD (-)	0.001/0.03-0.15	0.05
46	NH4R	Anoxia ammonia release fraction of SOD (-)	0.001/0.05-0.15	0.037
47	SOD	Sediment Oxygen Demand ($gO2.m^{-2}$ day^{-1})	0.1-1.0	0.1
48	AERATION	Rearation Method	LAKE 6	LAKE 6
49	NH4DK	Ammonium decay rate (day^{-1})	0.001-0.95	0.15
50	NO3DK	Nitrate decay rate (day^{-1})	0.03/0.05-0.15	0.7

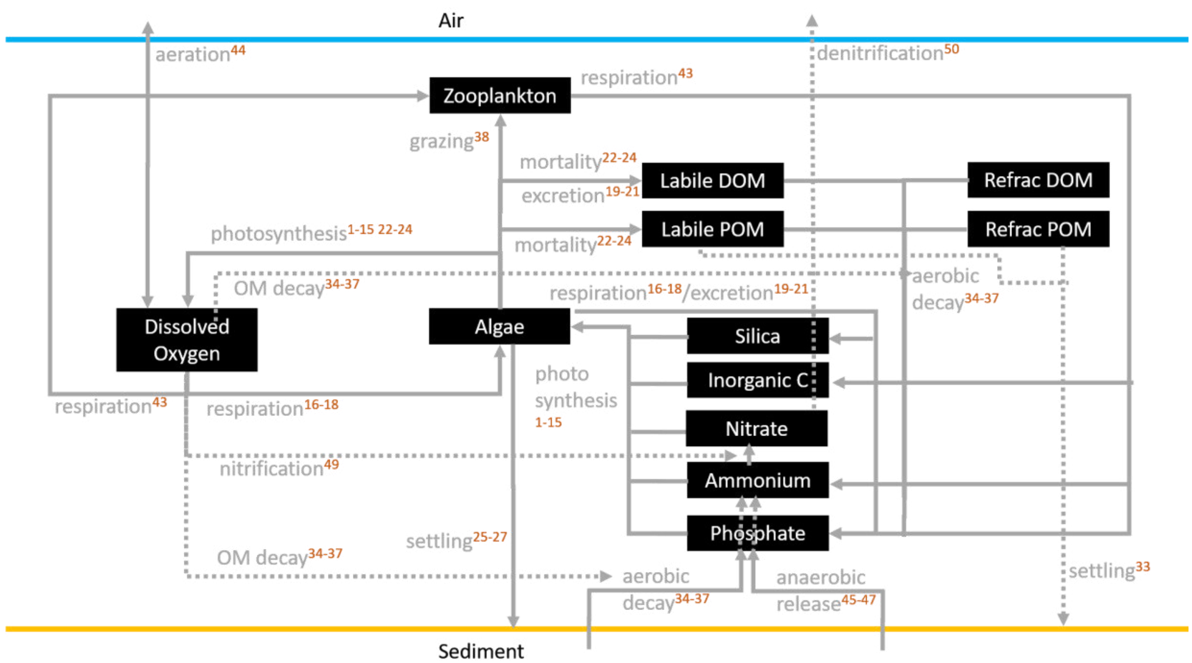

Figure 3. CE-QUAI-W2 main water quality state variables (black boxes) and processes (arrows) with the definition of parameters numbers (orange) associated to each process (see Table 1).

CE-QUAL-W2 simulates the internal sediment phosphorus load in anoxia conditions (desortion) with a zero order reaction based on Sediment Oxygen

Demand (SOD; $mgO_2.m^{-2}$) and bottom oxygen availability. The model also simulates oxic sediment organic matter mineralization with a first order reaction where organic matter input to the sediment is accounted. To parameterize the zero order anoxic release of phosphorus in the current situation, the order of magnitude of the internal phosphorus load was estimated based on MOHID-Land results (Brito et al. 2017b). As explained earlier, this represents a value three times higher than the annual estimated SWAT load (flood loads carrying phosphorus adsorbed to sediments would contribute with an extra of 1.2 $tonP.year^{-1}$ to the reservoir). The reservoir balance showed that half of the suspended solids inputs from the watershed (that transport the adsorbed phosphorus) deposited while the remainder exited the reservoir. As so, the estimate of annual internal phosphorus load (deposited phosphorus from flood loads) was considered to be 0.6 $tonP.year^{-1}$ (half of the flood load contribution), being similar to the phosphorus load entering from the river (0.6 $tonP.year^{-1}$ estimated by the SWAT model). CE-QUAL-W2 SOD phosphorus fraction (Table 1) were adjusted accordingly and only with this order of internal phosphorus load the model was able to represent field data magnitude in the current situation, suggesting that the internal load computed is realistic. One should remind that CE-QUAL-W2 dynamically computes the effective phosphorus release based on SOD and effective bottom oxygen concentration. Thus, for case scenarios where the reservoir is able to recover the trophic state and oxygen near the bottom increases, phosphorus internal load would be reduced accordingly and the model should be able to reproduce those effects.

Some inconsistencies were found in CE-QUAL-W2 when modelling oxygen reaction limitations, resulting in oxygen profiles that tended fast to zero below the thermocline. The code was then modified to overcome these inconsistencies. CE-QUAL-W2 nitrification dependence on oxygen follows a Monod type relationship, described as:

$$DOfNit = \frac{O_2}{O_2 + KDO} \quad (3)$$

where DOfNit (-) is the dissolved oxygen fraction to be multiplied by the nitrification rates, KDO ($mg\ L^{-1}$) is the half-saturation dissolved oxygen concentration and O_2 the water dissolved oxygen ($mg.\ L^{-1}$). However, for organic matter decay and algal respiration this relationship is replaced by an ON/OFF switch that only when oxygen concentrations is near zero the mineralization rates are switched off (oxygen factor is zero). Above zero oxygen concentrations mineralization is not dependent or limited by oxygen (factor is always one):

$$DOfMinEx = \begin{cases} 1 \; if \; DO \geq 1E-10 \\ 0 \; if \; DO < 1E-10 \end{cases} \tag{4}$$

where DOfMinEx (-) is the dissolved oxygen fraction to be multiplied by mineralization and algal excretion rates, and DO is the dissolved oxygen concentration (mg L^{-1}). However, this formulation is not used generally in water quality models as the example of WASP model (EPA, 2009) or ERSEM model (Butenschön et al. 2016) where Monod type oxygen limitations are used. The original formulation in CE-QUAL-W2 made that Enxoé modelled dissolved oxygen profiles in summer tended fast to zero just after thermocline (no surface exchange) despite all efforts to reduce it (see section 3). On the other end, dissolved oxygen field data profiles were asymptotic to bottom minimum oxygen concentrations, which ranged from 1 to 3 mgO_2. L^{-1}. Therefore, CEQUAL-W2 model v3.7 code was changed so that all oxygen limitations could be defined by two points (each with an oxygen concentration and a fraction between zero and one), similarly to CE-QUAL-W2 temperature rate multipliers:

$$DOAux = DOK1 * EXP\left[\frac{LOG\left(\frac{DOK2*(1.0-DOK1)}{DOK1*(1.0-DOK2)}\right)}{(DO2-DO1)*(DO-DO1)}\right] \tag{5}$$

$$DOf = \frac{DOAux}{1+DOAux-DOK1} \tag{6}$$

where DOf (-) is the dissolved oxygen fraction to be multiplied by rates, DO (mg L^{-1}) is the dissolved oxygen concentration, DO1 (mg L^{-1}) and DO2 (mg L^{-1}) are the two dissolved oxygen concentrations points, and DOK1 (-) and DOK2 (-) are the respective limitation fractions. The latter formulation uniformed the oxygen limitation for all processes (mineralization, nitrification, and algal respiration), and combined with the parameters defined in Table 1, allowed for the modelled oxygen profiles in summer to "detach" from zero below thermocline, producing a similar asymptotic behaviour as field data. Both the original and modified formulations are presented below.

3.3.2.3 Management scenarios

Five scenarios were considered to further investigate the response of the Enxoé trophic level to different management options:

- MS1 - No change scenario. This was the “control” scenario with the same forcing as the current situation;
- MS2 - Nutrient load reduction scenario, with no watershed loads. This was an hypothetical scenario to depict the evolution of the reservoir while considering only the internal sediment phosphorus load and verify whether it could be enough to fuel the algal blooms;
- MS3 - Nutrient load reduction scenario, with 50% reduction in watershed loads (nutrients, organic matter) and 50% reduction in phosphorus SOD fraction. This represented a 50% load reduction from the watershed, both during low waters and flood events;
- MS4 - Nutrient load reduction scenario, with 50% reduction in watershed loads (nutrients, organic matter) and no sediment phosphorus load. This was similar to the previous one, but required, for instance, bottom aeration to avoid anoxia formation and phosphorus internal load even though its existence in the bottom sediment;
- MS5 - Reservoir dam height increase by 10 m without any reduction in loads. This scenario tried to test the geometry effect on the trophic level.

The scenarios were run continuously from the end of the current situation simulation (for 10 years onward) to depict how the reservoir would evolve and how fast. It was used the same forcing as the current situation (e.g. same meteorology) except for the scenario specific definitions. For the last scenario, it was necessary to run the current situation again since the vertical geometry changed to include the dam height increase. As there is no reservoir volume-elevation curve for the new elevations and to maintain the surface area and surface fluxes, 10 layers (1m each) with the same surface dimensions as the original ones were added to the original reservoir geometry for simplification. To have a sense of the different reservoir extent that the new configuration would produce, the original surface area and the scenario surface area are presented in Figure 4, based on rough topography (NASA SRTM 3 arc second elevation). The scenario extent makes that the reservoir at full capacity would submerge a couple of roads, a waste water treatment plant (WWTP), private land, and a street in the urban area of Vale de Vargo.

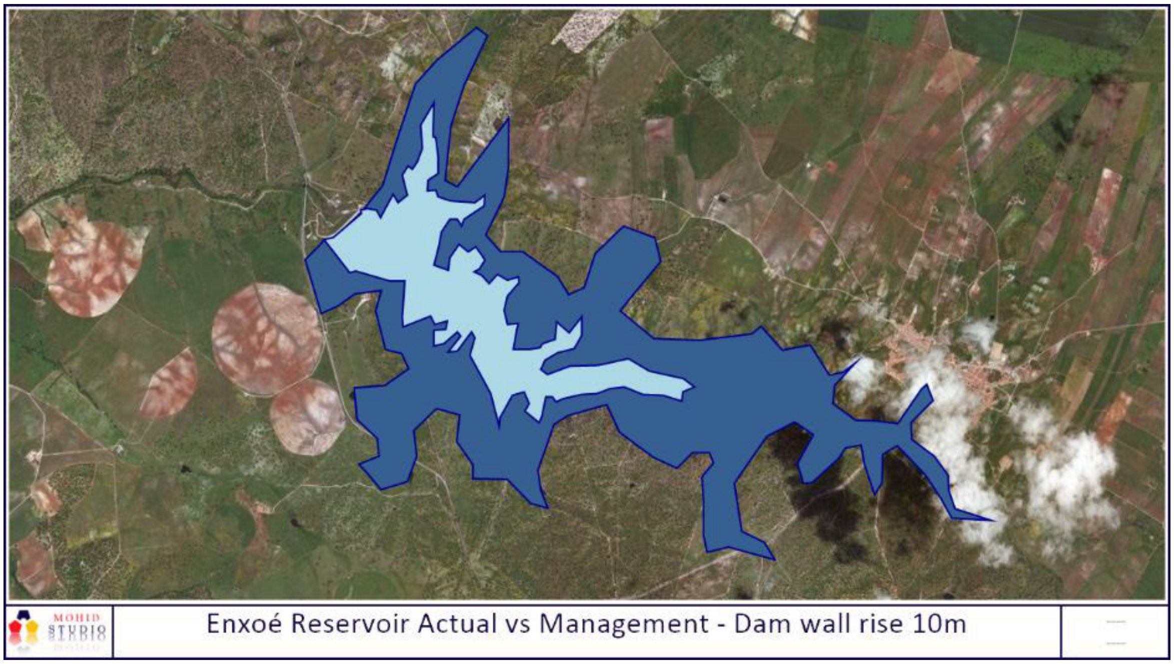

Figure 4. Map with elevation at dam top in current situation (light blue) and in scenario of 10m higher (dark blue). Based on NASA SRTM 3 arc second Elevation data.

3.3.3 Results and Discussion

3.3.3.1 Reference situation

Figure 5 compares model predictions of water temperature with measured profiles near the Enxoé reservoir dam (17 m deep at full storage) during selected time periods. In summer months (June to August), a thermal stratification was clearly observed, with differences between surface and bottom temperatures reaching 10ºC (e.g. 24-Aug-2009, 23-Jun-2010, and 18-July-2011). The thermocline usually occurred around 4-8 m depth. During winter months, stratification disappeared due to lower air temperatures and stronger winds. Homogeneous temperature profiles with lower water temperatures were then observed (e.g. 01-Feb-2010, 29-Out-2011, and 25-Nov-2011).

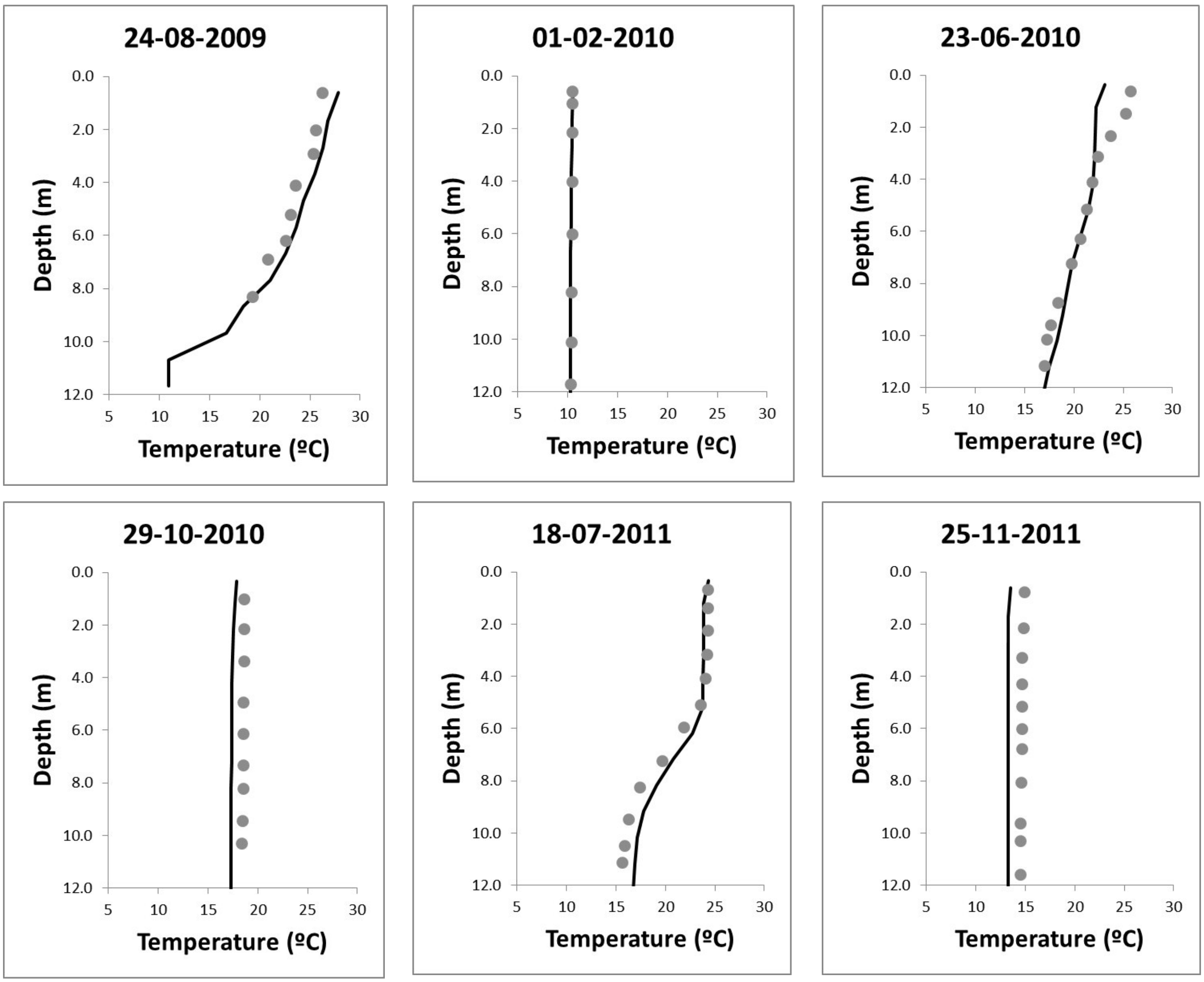

Figure 5. Temperature profiles at Enxoé wall for different dates (model results in continuous black line and field data in grey circles).

Figure 5 further shows that model results were able to describe both winter homogeneous profiles and summer stratification, including the thermocline location. This means that CE-QUAL-W2 was able to represent the main temperature processes occurring in the reservoir, i.e., one main driver for water circulation in the reservoir.

Figure 6 shows the comparison between model predictions (for original and modified version of CE-QUAL-W2) of dissolved oxygen profiles and field measurements taken near the Enxoé dam. Dissolved oxygen main seasonal patterns were similar to temperature. In summer months (June to August), a stratification was observed, with the maximum difference between surface and bottom concentrations reaching 5-10 mg L^{-1} (e.g. 24-Aug-209, 23-Jun-2010, and 18-July-2011). Oxygen changes were very pronounced in the thermocline at 4 m due to existence of bottom sink processes (mineralization, nitrification), which occurred as the capacity to oxygenate was reduced with depth. In winter months, stratification disappeared due to lower air temperatures and stronger winds. Homogeneous profiles were then observed, showing higher dissolved oxygen concentrations (e.g. 01-Feb-2010, 29-Oct-2011, and 25-Nov-2011).

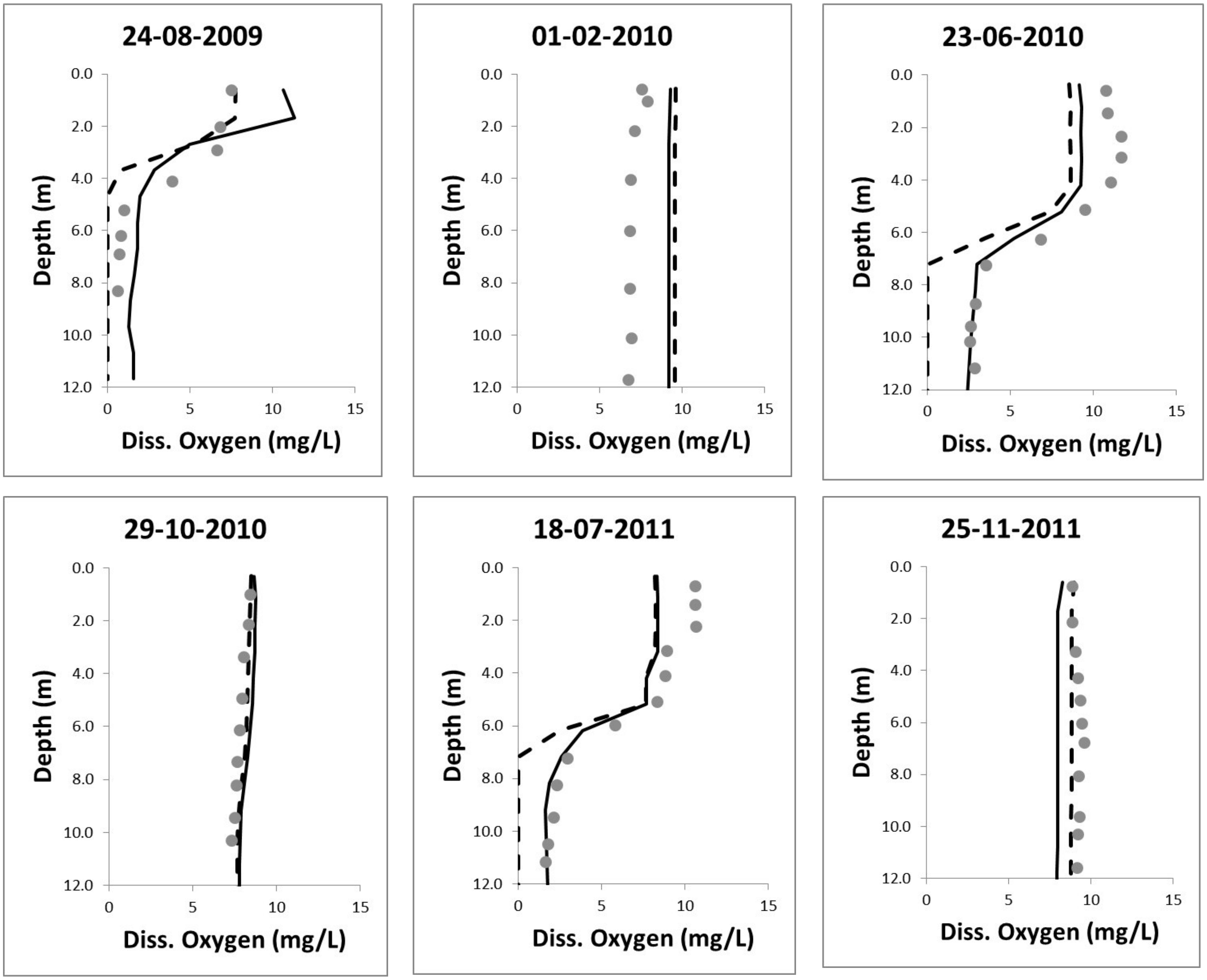

Figure 6. Dissolved oxygen profiles at Enxoé wall for different dates (model results in continuous black line for modified CE-QUAL-W2 version and dashed line for original CE-QUAL-W2 version and field data in grey circles).

Figure 6 further shows that model results were able to represent winter homogeneous profiles and summer stratified profiles. However, the model in the original formulation tended to underestimate dissolved oxygen near the bottom during summer months. The first hypotheses was that it could be due to high decay processes occurring near the bottom (mineralization, nitrification), lack of algal production (depths were relative shallow), and increased deposition of surface oxygen during winter instead of being lost or consumed.

Sensibility tests were made to test each of those hypotheses. The reduction of the decay processes (reduction of mineralization and nitrification rates in the water column) improved the fitting of oxygen levels near the bottom but decreased the availability of nutrients and surface chlorophyll-a content, i.e., made the model underestimate organic matter in the reservoir.

Reducing extinction coefficients or increasing sediment deposition (by reducing light attenuation) resulted in higher oxygen concentrations near the bottom (algae had more light available to start producing more oxygen) but the model started to deviate from measured surface suspended solids or measured temperature profiles. The suspended solids registered very high concentrations in the reservoir (Figure 7), and measured values were consistent with measured Secchi disks that showed minimum values of 1 m and maximum of 3 m. The Secchi disk data revealed that the photic zone was usually above/around the thermocline depth, and that algae production was very limited below that depth, not being a reasonable explanation for model underestimation of oxygen in that zone.

Lastly, a parallel study carried out using a lagrangian vertical geometry and the MOHID-Water model (Neves 2013) including the coupling with CE-QUAL-W2 water quality model, showed reduced numerical diffusion but did not improve oxygen profile description either until oxygen limitation was changed (unpublished work).

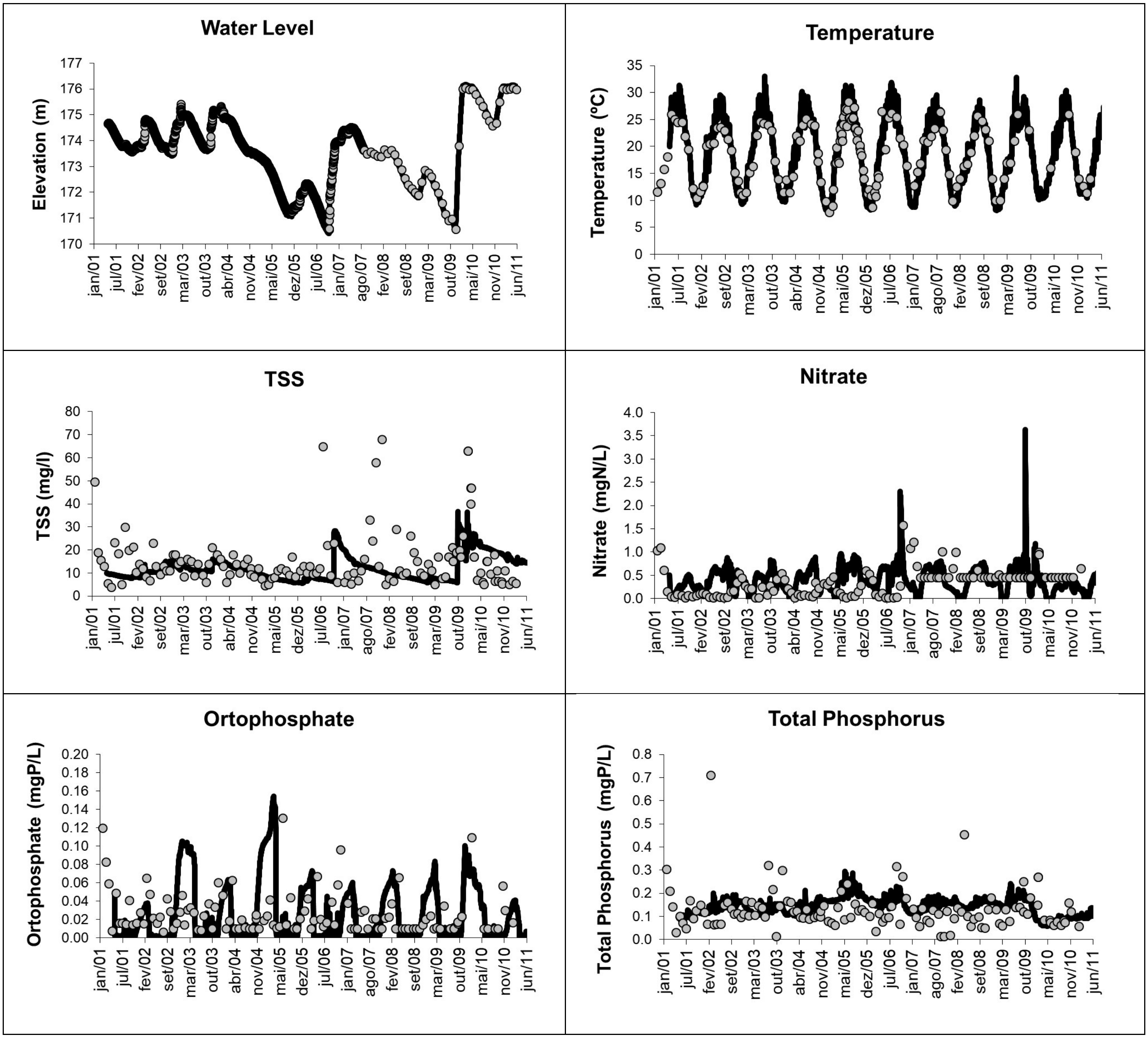
Water Level
Elevation (m)
177
176
175
174
173
172
171
170
jan/01 jul/01 fev/02 set/02 mar/03 out/03 abr/04 nov/04 mai/05 dez/05 jul/06 jan/07 ago/07 fev/08 set/08 mar/09 out/09 mai/10 nov/10 jun/11
Temperature
Temperature (ºC)
35
30
25
20
15
10
5
0
jan/01 jul/01 fev/02 set/02 mar/03 out/03 abr/04 nov/04 mai/05 dez/05 jul/06 jan/07 ago/07 fev/08 set/08 mar/09 out/09 mai/10 nov/10 jun/11
TSS
TSS (mg/l)
80
70
60
50
40
30
20
10
0
jan/01 jul/01 fev/02 set/02 mar/03 out/03 abr/04 nov/04 mai/05 dez/05 jul/06 jan/07 ago/07 fev/08 set/08 mar/09 out/09 mai/10 nov/10 jun/11
Nitrate
Nitrate (mgN/L)
4.0
3.5
3.0
2.5
2.0
1.5
1.0
0.5
0.0
jan/01 jul/01 fev/02 set/02 mar/03 out/03 abr/04 nov/04 mai/05 dez/05 jul/06 jan/07 ago/07 fev/08 set/08 mar/09 out/09 mai/10 nov/10 jun/11
Ortophosphate
Ortophosphate (mgP/L)
0.20
0.18
0.16
0.14
0.12
0.10
0.08
0.06
0.04
0.02
0.00
jan/01 jul/01 fev/02 set/02 mar/03 out/03 abr/04 nov/04 mai/05 dez/05 jul/06 jan/07 ago/07 fev/08 set/08 mar/09 out/09 mai/10 nov/10 jun/11
Total Phosphorus
Total Phosphorus (mgP/L)
0.8
0.7
0.6
0.5
0.4
0.3
0.2
0.1
0.0
jan/01 jul/01 fev/02 set/02 mar/03 out/03 abr/04 nov/04 mai/05 dez/05 jul/06 jan/07 ago/07 fev/08 set/08 mar/09 out/09 mai/10 nov/10 jun/11

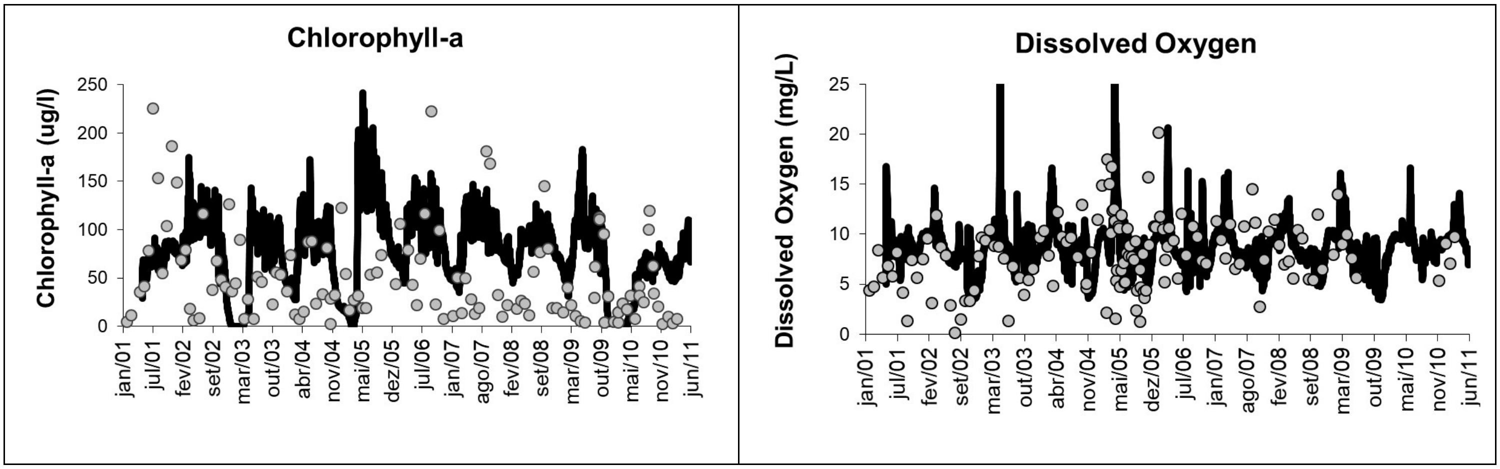

Figure 7. Time series of surface properties (water level, temperature, total suspended sediment – TSS, nitrate, orthophosphate, total phosphorus, chlorophyll-a, dissolved oxygen) at Enxoé wall for different dates (model results in continuous black line and field data in grey circles).

Only by considering the changes implemented in the CE-QUAL-W2 code (modified version) it was possible to “detach” from zero the bottom dissolved oxygen concentrations below the summer thermocline, increasing oxygen availability, and reproducing better the field data.

Figure 7 presents field measurements of water level, water temperature, total suspended solids (TSS), nitrate, orthophosphate, chlorophyll-a, and dissolved oxygen contents at the surface near the reservoir dam and compares those with the respective CE-QUAL-W2 model predictions (modified version) for the entire simulation period (2001-2011).

Measured and simulated water levels were very similar, which was expected since outflows were computed based on the reservoir balance. In the first years, the yearly level variation was only 1-2 m, but during 2004-2006 and 2008-2009 the reservoir level reduced to its minimum observed level (elevation around 170 m – 10 m depth near the dam) due to the extended droughts registered.

Measured surface water temperature ranged from 10 ºC in winter to 25-30 ºC in the summer. Model results were able to reproduce the minimum values but overestimated maximum temperature peaks at times. This overestimation was higher in years when the reservoir had higher water levels, and can be related to evaporation water cooling effect, which increased with the surface area. However, that overestimation did not significantly influence results since both field data values and overestimated modelled values were in the optimal temperature range for simulating algal growth.

Measured surface TSS concentrations showed base values of 10 mg.L^{-1} and peak values up to 60-70 mg.L^{-1}. Model estimations were able to represent base values but underestimated maximum peaks (values went up to 30-40 mg.L^{-1}) during high flow events. This can be related to the watershed flood transport process that occurs in just a few hours and is therefore difficult to describe with a daily time step watershed model such as SWAT (Brito et al., 2017b). However, as explained before, the missing input material end up being implicitly included in the internal phosphorus load computation.

Measured surface nitrate concentrations were very low, ranging between 1 mg.L^{-1} and the detection limit (0.5 mg.L^{-1}). Model results were able to represent the range of variation of field data, as well as the two higher peaks. These were coincident with the watershed inflows after drought years, which transported the deposited material accumulated in the watershed.

Measured surface ortophosphate concentrations ranged between 0.02 and 0.1 mg.L^{-1}. Model results showed a similar trend as field data, being able to reproduce both minimum and maximum orders.

Total phosphorus is a good measure of not only the inorganic but also the organic material present in the reservoir. Measured values averaged 0.1 mg.L^{-1} and the model was able to get the order of magnitude of the field data, suggesting that the predicted organic load was also correct.

Measured surface chlorophyll-a concentration registered minimum values on the order of units of ug.L^{-1}, but were frequently above 50 ug.L^{-1}, reaching maximum values above 200 ug.L^{-1}. Modelled results were able to reproduce the maximum values and most of the minimum values, having the tendency to overestimate these though (generally in winter). Three hypotheses were advanced: i) autumn/winter algal growth was not limited enough; ii) the algal maximum rates for mortality, excretion, and respiration were underestimated; or iii) zooplankton grazing was underestimated. Each of these hypotheses was tested. In terms of temperature limitation, increasing minimum algal temperatures affected algal growth globally (and not only during measured minimums); the calibrated temperatures for cyanobacteria were already adjusted to higher spring/summer temperatures; and light limitation was not likely to be the problem since modelled temperature profiles showed a good agreement with the measured ones (also in the surface), independently of the season, suggesting correct light extinction estimation. After performing sensibility tests on maximum algae mortality, excretion, and respiration, model results showed that these processes affected globally the algal concentrations and not only its minimum values. Finally, zooplankton growth effectively controlled algal decay and specifically its minimums, but testing higher growth rates produced long periods of very low algae concentrations (near zero) that were inconsistent with field data. Thus, the current algae results represented the best possible results, with the model being able to reproduce the maximum values and main trends. This was essential for scenario testing, considering a water management perspective.

Modelled surface dissolved oxygen concentrations were well represented, including the oversaturation and intense production (reaching up to 20 mg L^{-1}) observed in the field data during algal blooms. The lower values (lower than 5 mg L^{-1}) were also simulated in response to the oxidization of organic matter. Minimum concentrations were lower in field data than in the model during the first years. This was related to the differences found in algae (and organic matter) content between field data and model estimates. Algal decayed and consumed more oxygen in reality than in model estimates explaining the differences found in the minimum values. However, the model was able to reproduce most of the dissolved oxygen trends, and its minimums and maximums in the remaining years, showing that all key aspects for simulating this parameter were accounted for.

Overall, CE-QUAL-W2 was able to represent the main trend values of the properties that influence water circulation (water level and temperature). The model was further able to satisfactory describe nutrient, algae, and dissolved oxygen trends, as well as the minimum and maximum values.

Table 2 and Figure 8 present the statistical indicators obtained by comparing model predictions with field measured data. Model estimates were in the same order of magnitude as field data (similar average and median). The water level showed the best performance (high correlation value of 0.99; low RMSE value of 0.04 m; and similar deviation as data) since outflows were computed to define the reservoir volume data. Temperature was also well predicted, with a high correlation value of 0.97 and small errors (less than 2 ºC). Water quality results for nutrients, algae, and oxygen showed the worst statistical indicators, with RMSE values reaching 100% of the average values, and results deviating from the observed values in the Taylor's diagram (Figure 8). This is a common behaviour in water quality simulations: while water temperature shows a typical seasonal variation mainly due to solar radiation that is straightforward simulated, organic matter, nutrient, oxygen, and algae are a complex system that is often simplified in model formulations. Also, algal populations and individuals are usually lumped to functional groups to describe the general main processes and behaviours. As so, while the orders of magnitude of values, minimum and maximums could be reproduced, the exact timings were difficult to tackle and a sync between field data and simulated values was hard to reach.

Table 2 Statistics analysis of field measured data and model estimates for the entire field data period 2001-2011.

Property	N	Data average	Data Median	Data St Dev	Model average	Model Median	Model St Dev	RMSE
Water Level (m)	2349	173.6	173.8	1.2	173.5	173.7	1.2	0.04
Temperature (ºC)	135	18.9	19.75	5.4	19.2	19.5	6.5	1.8
Dissolved Oxygen (mg L^{-1})	141	8.2	8.0	3.4	12.1	10.6	5.6	7.6
Ammonia (mgN L^{-1})	114	0.3	0.17	0.38	0.23	0.2	0.15	0.4
Nitrate (mgN L^{-1})	117	0.34	0.41	0.28	0.39	0.34	04.27	0.4
Orthophosphate (mgP L^{-1})	116	0.32	0.15	0.39	0.02	0.003	0.03	0.48
Suspended Solids (mg L^{-1})	126	14.7	11.5	11.4	18.9	19.3	6.34	13.65
Chlorophyll-a (µg L^{-1})	124	51.7	33.9	48.1	76.9	81.6	41.2	62.9

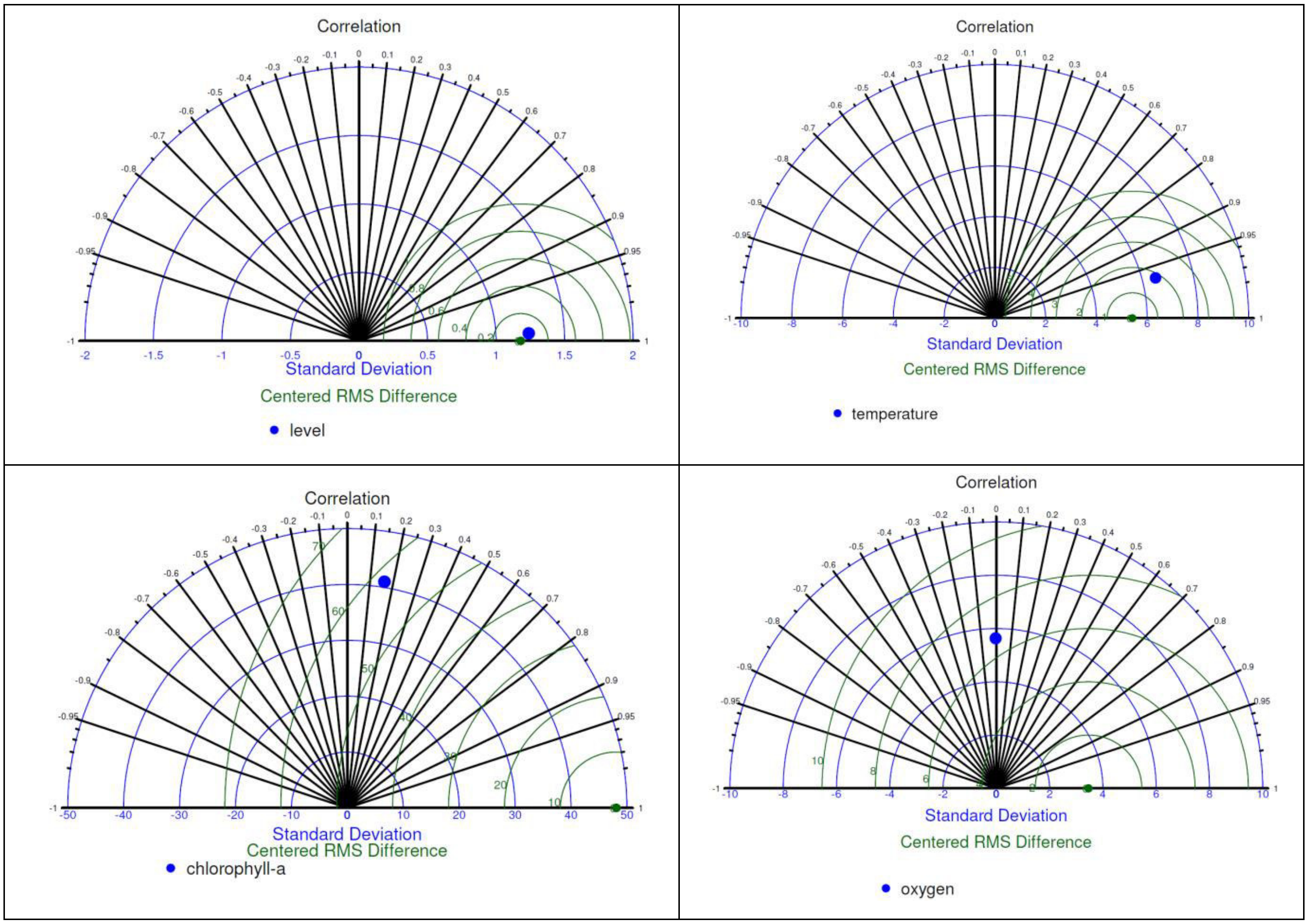

Figure 8 – Taylor diagrams for model fit for water level (top left), water temperature (top right), chlorophyll-a (bottom left) and dissolved oxygen (bottom right). Observed point (perfect fit) is represented by a green dot and actual model result by a blue dot.

The CE-QUAL-W2 model simulations were obtained after integrating results from SWAT, and were for a small reservoir with 10.4 hm^3. Nonetheless, results were comparable with those reported after implementing CE-QUAL-W2 in large reservoirs, such as the 45000 hm^3 Tucurui reservoir in Brazil (Deus et al. 2013) or the 5900 hm^3 Karkheh Reservoir in Iran (Noori et al. 2015), and in medium sized reservoirs, such as two reservoirs in Taiwan with 183 and 659 hm^3 (Kuo et al. 2006) or the 1400 hm^3 Shanmei Reservoir in China (Liu et al. 2015), where the ratio of RMSE to average values were below 0.6.

The measured trophic state (geometric average of chlorophyll-a) for the period 2001-2011 was 33 $\mu g.L^{-1}$ while the estimated value given by the model was 53 $\mu g.L^{-1}$ (both corresponding to eutrophic since they are higher than the 10 $\mu g.L^{-1}$ defined as the national limit for eutrophication). The difference between measured and predicted trophic state values returned around 60% of the measured value, but the difference between measured and predicted averages of annual maximum chlorophyll-a values was less than 1% of the measured value. This is obviously important from a management standing point since algal blooms and maximum values are essential for water abstraction and treatment planning.

The CE-QUAL-W2 model results for the current situation were further compared to estimates using the Vollenweider model (Vollenweider and Kerekes 1980) and reservoir phosphorus concentration expected in Table 3. This model considered the physical characteristics of the reservoir (reservoir surface area, total volume, and average depth), the average inflows and outflows, and the total load (1.8 $tonP.year^{-1}$ including external and internal sources). Results showed that the expected phosphorus concentration in the reservoir was 0.1 $mgP.L^{-1}$, corresponding to the same order of measured and modelled maximum orthophosphate and average total phosphorus concentrations. Results of the Vollenweider model were thus consistent with Enxoé's eutrophic state and CE-QUAL-W2 predictions.

Table 3 – Vollernweider model for Enxóe in the current situation.

Parameter	Units	Computation	Value
Lake area (A)	m^2	-	2050000
Lake volume (V)	m^3	-	10400000
Lake discharge (Q)	$m^3.yr^{-1}$	-	5045760
Hydraulic Residence Time (T)	yr	V/Q	2.06
Mean depth (Z mean)	m	-	5
Flushing rate	yr^{-1}	1/T	0.49
Total Annual Loading (Pload)	$kg.yr^{-1}$	-	1800
Water inflow (Wi)	m^3	-	6622560
Surface overflow rate (qs)	$m.yr^{-1}$	Zmean/T	2.43
Total areal P loading (Lp)	$g.m^{-2}yr^{-1}$	Pload*1E3/A	0.878
Vollenweider in-lake P concentration	$mg.L^{-1}$ or $g.m^{-3}$		0.149

The present integrated model was considered as able to represent the main aspects of reservoir stratification (that influences hydrodynamics) and long-term surface data. As so, the model was used to extrapolate results and predict the most effective management actions that could reduce the Enxoé reservoir trophic level

3.3.3.2 Reservoir nutrient budgets

After model calibration and satisfactory simulation of measured field data (surface and profiles), CE-QUAL-W2 was used to represent the Enxoé reservoir budgets and understand the main processes responsible for feeding its high trophic level.

Figure 9 shows the estimated nitrogen and phosphorus average annual fluxes in each component (river inflow, reservoir outflow, denitrification, algal assimilation/respiration plus zooplankton respiration, sediment release in anoxic conditions, and organic matter decay or mineralization) for the period 2001-2011. For nitrogen, 60% of the input was routed outside the reservoir with outflow; a high nitrogen recycle existed due to algae nitrogen assimilation/death and consequent organic matter decay, including denitrification while in anoxic conditions (most part of summer). For phosphorus, 140% of the input was routed outside the reservoir with outflow; almost 100% of the input (around 0.6 $tonP.year^{-1}$) was generated in sediment bottom release; the internal phosphorus recycling processes (algae assimilation, organic matter decay or mineralization) removed 55% of the phosphorus input.

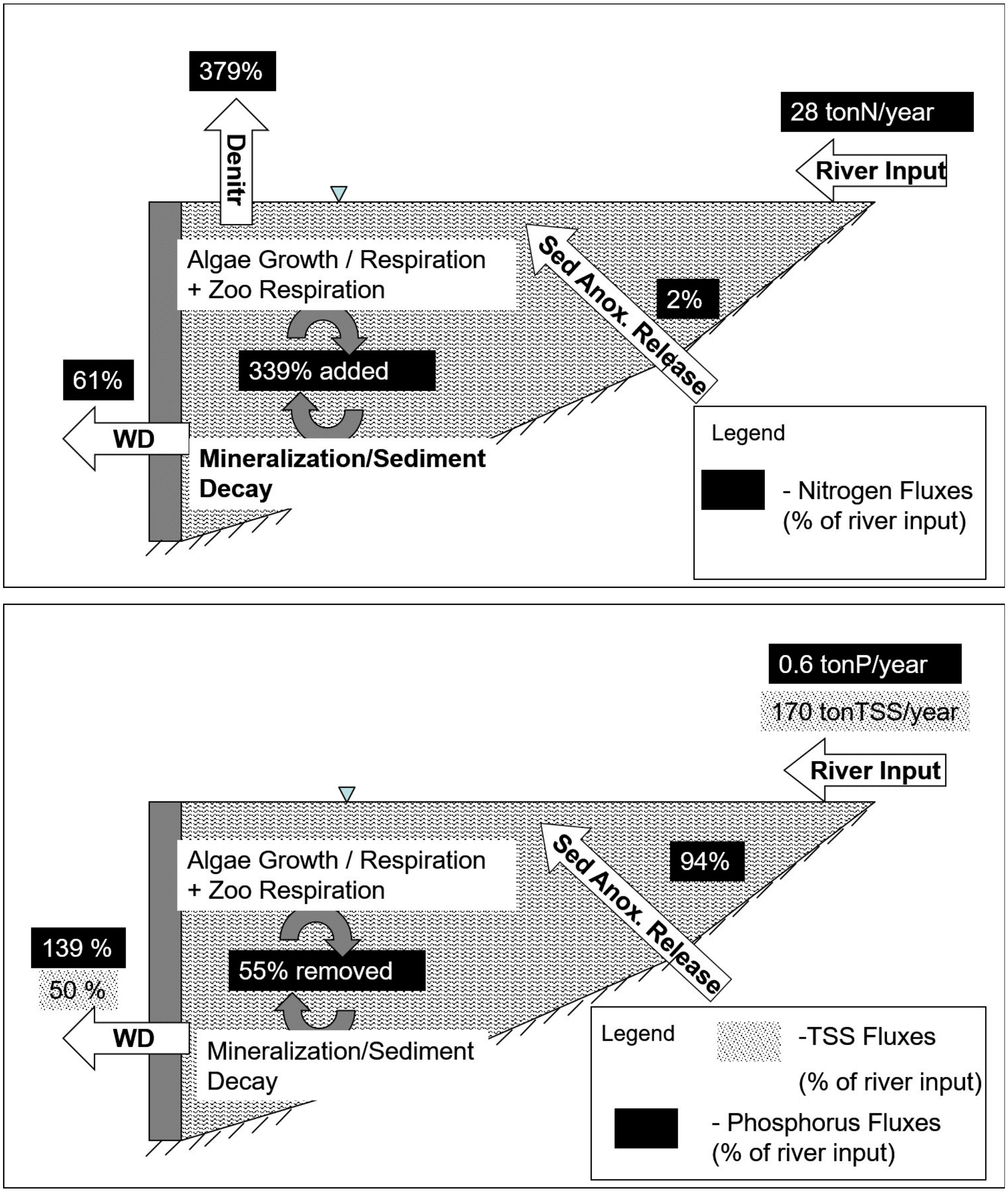

Figure 9. Enxoé reservoir nutrient budget: nitrogen (top) and phosphorus (bottom) fluxes. Values in percentages are the ratios between each flux and the reservoir input from the river (WD - water discharge; TSS - total suspended sediments).

The Enxoé reservoir acted as a nutrient recycler between algal cycles, with reduced dependency on watershed inputs because of cyanobacteria dominance, which were able to assimilate atmospheric N_2, being sustained by internal sediment phosphorus loads (of the same order of the watershed input). Søndergaard et al. (1992) also reported a relatively high sediment phosphorus release rate in Lake Arresø (Denmark) during resuspension because of the low Fe:P ratio and the type of sediment. The importance of internal phosphorus loading for reservoirs' water quality was further discussed by Søndergaard et al. (2003), who referred that internal phosphorus release contribution to a reservoir's high trophic level can extend for several decades even when external loading has been reduced.

3.3.3.3 Reservoir response to management scenarios

Table 4 presents the average and mean annual maximum chlorophyll-a concentrations of all the management scenarios considered, while Figure 10 and Figure 11 present the dam surface chlorophyll-a and oxygen time series concentrations, respectively.

The MS1 scenario, which corresponded to a continuation of current conditions (used the same forcing as in the original current simulation), resulted in similar patterns and higher average and maximum concentrations as compared to the current situation. This constituted a base scenario for comparison of the remaining simulations. Nonetheless, results show that in case of similar forcing conditions, not changing managment can have a negative impact on the reservoir, increasing even more chlorophyll-a concentrations.

Table 4 Enxoé Management scenarios maximum and average chlorophyll-a concentrations and respective reductions.

Scenario	Maximum*	Reduction in Maximum**	Average*	Reduction in Average**
Measured Data – Current Situation	158 ug L^{-1}	-	55 ug.L^{-1}	
Model CS – Current Situation	159 ug L^{-1}	-	79 ug.L^{-1}	
Model MS1 – Management Scenario – No change to current situation	203(120) ug.L^{-1}	-	99(66) ug.L^{-1}	
Model MS2– Management Scenario – Removal of load in river in relation to current situation	176 (83) ug.L^{-1}	13 (31) %	86 (46) ug.L^{-1}	13 (30) %
Model MS3 – Management Scenario - Reduction of 50% P load (river input + bottom sediment SOD P fraction) in relation to current situation	97(54) ug L^{-}	52 (55) %	52(35) ug.L^{-1}	47 (47) %
Model MS4 – Management Scenario - Reduction of 50% P load in river + Removal of sediment P load, in relation to current situation	44(31) ug L^{-1}	78 (74) %	25(21) ug.L^{-1}	75 (68)
Model MS5 – Management Scenario – Increase dam wall of 10m (average depth 15m instead of 5m)	18.4(16.6) ug L^{-1-}	91 (86) %	5.8(8.3) ug L^{-1}	94 (87) %

* values computed for 2002 – 2010 period for current situation and hypothetic 8 following years for scenarios. Maximum values are the average of annual maximums and last two years values are presented in brackets. ** Reduction in percentage for scenarios in comparison to MS1.

The MS2 scenario, which tested the dependence on internal load, showed reductions of 13% for average and maximum chlorophyll-a concentrations during the entire simulation period in relation to MS1 (Table 4). These reductions were hardly noticeable over the years (Figure 10), meaning that internal phosphorus loads were able to fuel algal blooms during the time period considered.

The MS3 scenario, with 50% phosphorus load reduction (from river input and bottom sediment SOD fraction), led to a reduction of chlorophyll-a maximum and average concentrations between 47-52% when compared with MS1.

The MS4 scenario, similar as MS3 with 50% reduction from river input but with the removal of the internal phosphorus load (e.g. by maintaining dissolved oxygen levels high in the bottom), resulted in 75-78% reduction in the average and maximum chlorophyll-a concentrations when compared to MS1. Applying this reduction to the current situation field data average (55 μg L^{-1}), the resulting average chlorophyll-a concentrations values yielded 12-14 μg.L^{-1} (or geometric averages of 7-8 μg.L^{-1} as used in the national trophic status definition). Yet, the achieved trophic level was still 30-40% above or below (considering average or geometric average values) the national level for eutrophication (10 μg.L^{-1}), being difficult to sustain it as safe. Decreasing loads to these levels would require i) to reduce the suspended material inflow to the reservoir (that is loaded with phosphorus), especially during flood events; and ii) to remove anoxia in the bottom. The first management option could be accomplished by placing retention barriers upstream to retain sediment, by preserving riparian vegetation which would partially use some of the nutrients exported to the river before they reached the reservoir, or by promoting conservation tillage practices in the watershed (Hashemi et al. 2016). The second measurement option could be achieved by using oxygen aeration in the bottom. These results follow Marsdsen (1989), who pointed out that improvements in the condition of highly eutrophic lakes require very large reductions in external phosphorus loading.

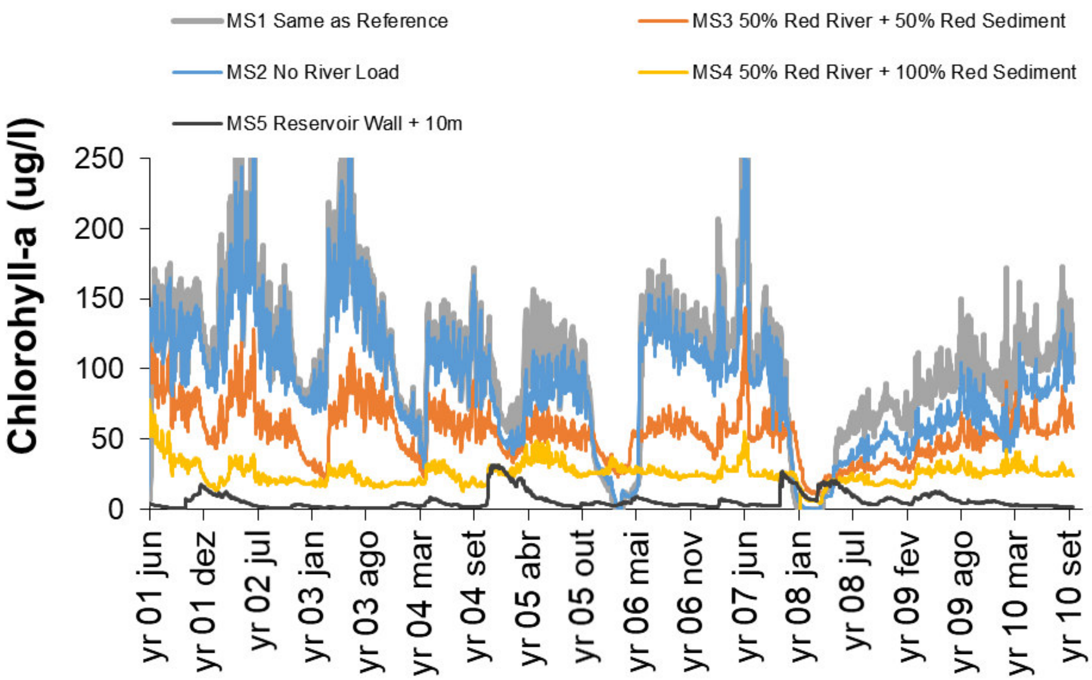

Figure 10. Enxoé future scenarios for chlorophyll-a concentration.

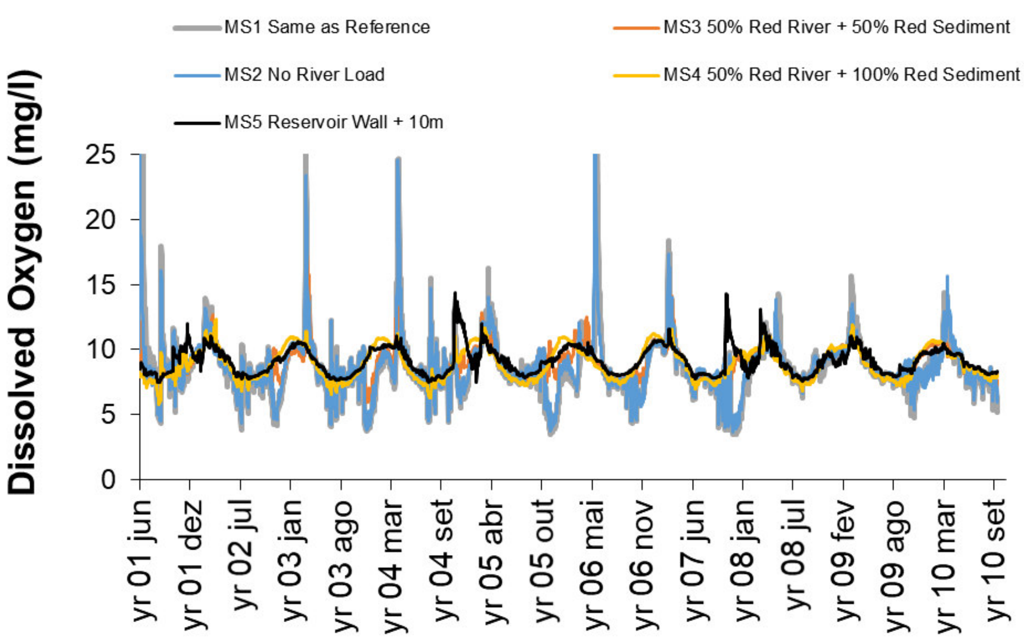

Figure 11. Enxoé future scenarios for dissolved oxygen.

The difficulty in reaching a safe trophic state in the Enxoé reservoir and the expected high investments needed for implementing the latter scenarios highlighted the need for an additional scenario to depict the trophic state relation to the reservoir geometry (Enxoé reservoir has 5 m average depth). The Vollernweider model was applied for a dam wall increase of 10 m (average depth then increased to 15 m). The expected phosphorus concentration output without considering any load reduction reached 0.05 $\mu g.L^{-1}$ (Table 5), representing a mesotrophic state (Vollenweider and Kerekes 1980). These results agreed with those from IST (2009) and Mateus et al. (2004), who studied the trophic levels of 30 reservoirs in Portugal under the scope of the WWTP directive. They showed that reservoirs with mean depths lower than 10 m were in eutrophic state even with low urban or diffuse loads. On the other hand, higher mean depths limited the summer phosphorus internal load from reaching the photic/algal production zone in most of the reservoirs, blocking the predominant mechanism for algal blooms in the absence of river inputs (low/absent inflows in summer). The same was found with the current study. As a result of a depth increase of 10 m in MS5, chlorophyll-a concentrations were reduced 91-94% in relation to MS1. Applying this reduction to the current situation field data average (55 µg L-1), the resulting average values yielded an average chlorophyll-a concentration of 3-5 $\mu g.L^{-1}$ (or a geometric average of 2-3 $\mu g.L^{-1}$), representing also a mesotrophic level and 2-3 times lower than national eutrophication level.

Table 5 – Vollernweider model for Enxóe management scenario of 10m increase in dam.

Parameter	Units	Computation	Value
Lake area (A)	m^2	-	2050000
Lake volume (V)	m^3	-	10400000
Lake discharge (Q)	$m^3.yr^{-1}$	-	5045760
Hydraulic Residence Time (T)	yr	V/Q	2.06
Mean depth (Z mean)	m	-	15
Flushing rate	yr^{-1}	1/T	0.49
Total Annual Loading (Pload)	$kg.yr^{-1}$	-	1800
Water inflow (Wi)	m^3	-	6622560
Surface overflow rate (qs)	$m.yr^{-1}$	Zmean/T	7.28
Total areal P loading (Lp)	g.m-2yr-1	Pload*1E3/A	0.878
Vollenweider in-lake P concentration	mg.L-1 or g.m-3		0.05

The scenarios reductions were forced instantaneously (no smooth transition) and the trophic state reduction was linear with load reduction in a 10 year period when phosphorus internal load was changed. On the other hand, the change in chlorophyll-a and dissolved oxygen concentrations was slow and almost not noticeable when only river external load was acted upon, even in the MS2 total removal scenario (Figure 10 and Figure 11).

Future studies should focus on: i) integrating a full water quality watershed model with adsorbed phosphorus component and a reservoir model with sediment diagenesis to further detail the phosphorus pathways; and ii) cost-benefit analyses to determine the best management approaches based on the current/further work proposed.

The management scenarios were intentionally set for testing extreme conditions. The best approach can likely be a mix of several management options. Since geometry changes will be limited, approaches should test also how to reduce phosphorus load to the reservoir, particularly during flood events (e.g. managing erosion with agricultural practices or trapping sediment in ditches, etc.), and the feasibility of removing internal load from sediment.

3.3.4 Conclusions

This work presented a novel integrated modelling approach that coupled a watershed (SWAT) and a reservoir model (CE-QUAL-W2) to depict the origin of the Enxoé reservoir trophic state; the highest in Portugal.

The previous modelling studies estimated nutrient loads from the watershed to the reservoir of 28 $tonN.year^{-1}$ and 0.6 $tonP.year^{-1}$ for the period 2001-2011. Although these values can be considered relatively low, corresponding to similar values reported in the literature for extensive agricultural areas with gentle slopes (low erosion) and reduced human presence, short term floods were found to be able to transport up to 3 times the average annual phosphorus load..

The integrated model results were compared with collected profile information during 2 years (temperature, oxygen) and surface properties measured during the entire reservoir lifetime (chlorophyll-a, nitrate, orthophosphate, suspended sediment, oxygen). The model was able to represent stratification formation with spring-summer high temperatures, reduced inflows and wind, as well as its destruction with winter increased flow and wind velocity. The model was further able to represent the thermocline depth (at around 4m) and changes in depth. The model was also satisfactorily fitted to the water surface data, in respect to nutrient, suspended sediment, oxygen and chlorophyll-a concentrations.

The reservoir budget showed that phosphorus load from bottom sediment and nitrogen load from the atmosphere can fuel blooms when nutrient inputs from the watershed are low. Also, internal recycle (algal and organic matter decay, and nutrient assimilation and decay) can sustain high algal concentrations for months. Since atmosphere nitrogen input is not controllable, the most effective options to control the reservoir trophic level is by controlling internal phosphorus load or its geometry. The management scenarios showed that the internal sediment phosphorus load is vital for regulating the trophic state. Reducing phosphorus load by 75% (externally from watershed sources and internally from bottom sediment source) could reduce the reservoir trophic level close to eutrophication limit, but only with a reservoir wall increase of 10 m (by limiting the phosphorus internal load to reach the photic zone in most of the reservoir) could sustain a mesotrophic state level.

Future studies should address phosphorus pathways in more detail (from a model development perspective) and produce cost-benefit analyses to compare the scenarios proposed to depict the best approach for trophic state and algal blooms reduction (from a management perspective).

Acknowledgments

The present work was supported within the framework of the EU Interreg SUDOE IVB program (SOE1/P2/F146 AguaFlash project), the Project Mirage (EU-FP7), and the Project EUTROPHOS (PTDC/AGR-AAM/098100/2008) of the Fundação para a Ciência e a Tecnologia (FCT). MARETEC acknowledges the national funds from the FCT (Project UID/EEA/50009/2013). T. B. Ramos was supported by the FCT grant SFRH/BPD/110655/2015.

References

APA (2017) Analytical techniques for water quality parameters, ARH-Alentejo laboratories. 2017. From http://apambiente.pt/_zdata/LRA/Parametros_Metodos_ARHALT_Site_2017.pdf accessed in august 2017. In Portuguese.

Brito D, Neves R, Branco MA, Prazeres Â, Rodrigues S, Gonçalves MC, Ramos TB (2017a) Assessing water and nutrient long-term dynamics and loads to an eutrophic reservoir in the Enxoé temporary river basin, southeast Portugal. Applied Water Science (under review)

Brito D, Neves R, Branco MA, Gonçalves MC, Ramos TB (2017b) Modeling flood dynamics in a temporary river basin draining to an eutrophic reservoir in southeast Portugal. Environ Earth Sciences. 2017; 76:377.

Butenschön, M., Clark, J., Aldridge, J. N., Allen, J. I., Artioli, Y., Blackford, J., Bruggeman, J., Cazenave, P., Ciavatta, S., Kay, S., Lessin, G., van

Leeuwen, S., van der Molen, J., de Mora, L., Polimene, L., Sailley, S., Stephens, N., and Torres, R.: ERSEM 15.06: a generic model for marine biogeochemistry and the ecosystem dynamics of the lower trophic levels, Geosci. Model Dev., 9, 1293-1339,

Cole TM, Wells SA (2011) CE-QUAL-W2: A Two-Dimensional, Laterally Averaged, Hydrodynamic and Water Quality Model, Version 3.71. User manual. U.S. Army Corps of Engineers, Washington, DC, 20314-1000.

Coelho H, Silva A, Chambel-Leitão P, Obermann M (2008) On the origin of cyanobacteria blooms in the Enxoé reservoir. 13th World Water Congress, International Water Resources Association, Montpellier, France

Condie, SA., and Webster IT (1997) The influence of wind stress, temperature, and humidity gradients on evaporation from reservoirs, Water Resour. Res., 33(12), 2813–2822

Debele B, Srinivasan R, Parlange J-Y (2008) Coupling upland watershed and downstream waterbody hydrodynamic and water quality models (SWAT and CE-QUAL-W2) for better water resources management in complex river basins. Environ Model Assess 13: 135-153, doi:10.1007/s10666-006-9075-1

Dechmi F, Burguete J, Skhiri A (2012) SWAT application in intensive irrigation systems: Model modification, calibration and validation. J Hydrol 470–471:227-238, doi:10.1016/j.jhydrol.2012.08.055

Deus R, Brito D, Mateus M, Isabella K, Fornaro A, Neves R, Alves CN (2013) Impact evaluation of a pisciculture in the Tucuruí reservoir (Pará, Brazil) using a two-dimensional water quality model. J Hydrol 487:1-12

EPA (2009) WASP7 Stream Transport Model Theory and User's Guide Supplement to Water Quality Analysis Simulation Program (WASP) User Documentation

Gassman PW, Reyes MR, Green CH, Arnold JG (2007) The Soil and Water Assessment Tool: Historical development, applications, and future research directions. Trans ASABE 50(4):1211–1250, doi:10.13031/2013.23637

Geza M, McCray JE (2008) Effects of soil data resolution on SWAT model stream flow and water quality predictions. J Environ Manage 88(3):393-406, doi:10.1016/j.jenvman.2007.03.016

Green CH, van Griensven A (2008) Autocalibration in hydrologic modeling: Using SWAT2005 in small-scale watersheds. Environ Model & Soft 23:422-434

Havens KE, James RT, East TL, Smith VH (2003) N:P ratios, light limitation, and cyanobacterial dominance in a subtropical lake impacted by non-point source nutrient pollution. Environ Poll 122:379-390

INAG (2004) Plano de Ordenamento da Albufeira do Enxoé, estudos de caracterização e pré-proposta de ordenamento. Instituto da Água, MAOTDR, Lisboa

IST (2009) Management of the Trophic Status in Portuguese Reservoirs. Report on classification and trophic state reduction in the scope of WWTP Directive. Instituto da Água. Lisboa.

INE (2001) Recenseamento Geral Agrícola. Instituto Nacional de Estatística, Lisboa

Jiang X, Jin X, Yao Y, Li L, Wu F (2006) Effects of oxygen on the release and distribution of phosphorus in the sediments under the light condition. Environ Pollut 141(3):482-487

Kurup RG, Hamilton DP, Phillips RL (2000) Comparison of two 2-dimensional, laterally averaged hydrodynamic model applications to the Swan River Estuary. Math Comp Simulation 51(6):627-638

Kuo JT, Lung WS, Yang CP, Liu WC, Yang MD, Tang TS (2006) Eutrophication modelling of reservoirs in Taiwan. Environ Model Soft 21(6):829-844

Lawrence MG (2005) The relationship between relative humidity and the dew point temperature in moist air: A simple conversion and applications. Bull Am Meteo Soc 86: 225–233

Liu M, Chen X, Yao H, Chen Y (2015) A coupled modeling approach to evaluate nitrogen retention within the Shanmei Reservoir watershed, China. Estuarine, Coastal Shelf Sci 166:189-198

Lung WS, Bai S (2003) A water quality for the Patuxent Estuary: Current conditions and predictions under changing land-use scenarios. Estuaries 26:267–279

Makinia, J., Wells, S., and Zima, P. (2005) "Temperature Modeling in Activated Sludge Systems: A Case Study", Water Environment Research, Vol 77, No. 5, Sept-Oct 2005

Martin N, McEachern P, Yu T, Zhu DZ (2013) Model development for prediction and mitigation of dissolved oxygen sags in the Athabasca River, Canada. Sci Total Environ 443: 403-412

Mateus M, Almeida C, Brito D, Neves R (2014) From Eutrophic to Mesotrophic: Modelling Watershed Management Scenarios to Change the Trophic Status of a Reservoir. Int J Environ Res Public Health 11(3):3015–3031

Neitsch SL, Arnold JG, Kiniry JR, Srinivasan R, Williams JR (2002) Soil and Water Assessment Tool. User's Manual. Version 2005. GSWRL Report 02-02, BRC Report 2-06, Temple, Texas, USA

Neves R (2013) The MOHID concept. In: Mateus M, Neves R (Eds) Ocean Modelling for Coastal Management e Case Studies with MOHID. IST Press, Lisbon, pp. 1-11

Noori R, Yeh HD, Ashrafi K, Rezazadeh N, Bateni SM, Karbassi A, Kachoosangi FT, Moazami S (2015) A reduced-order based CE-QUAL-W2 model for simulation of nitrate concentration in dam reservoirs. J Hydrol 530:645-656

Paerl HW, Fulton RS, Moisander PH, Dyble J (2001) Harmful freshwater algal blooms: with an emphasis on cyanobacteria. The Scientific World journal 1:76-113

Panagopoulos Y, Makropoulos C, Mimikou M (2011) Reducing surface water pollution through the assessment of the cost-effectiveness of BMPs at different spatial scales. J Environ Manage 92(10):2823–2835

Ramos TB, Gonçalves MC, Branco MA, Brito D, Rodrigues S, Sánchez-Pérez JM, Suavage S, Prazeres A, Martins JC, Fernandes ML, Pires FP (2015a) Sediment and nutrient dynamics during storm events in the Enxoé temporary river, southern Portugal. Catena 127:177-190, doi:10.1016/j.catena.2015.01.001

Ramos TB, Rodrigues S, Branco MA, Prazeres A, Brito D, Gonçalves MC, Martins JC, Fernandes ML, Pires FP (2015b) Temporal variability of soil organic carbon transport in the Enxoé agricultural watershed. Environ Earth Sci 73:6663-6676, doi:10.1007/s12665-014-3888-z

Rolff C, Almesjo L, Elmgren R (2007) Nitrogen fixation and abundance of the diazotrophic cyanobacterium Aphanizomenon sp. in the Baltic Proper. Marine Eco Prog Series 332:107-118

Taylor, K.E. (2001) Summarizing multiple aspects of model performance in a single diagram. J. Geophys. Res. 106: 7183–7192.

Valério E, Pereira P, Saker ML, Franca S, Tenreiro R (2005) Molecular characterization of Cylindrospermopsis raciborskii strains isolated from Portuguese freshwaters. Harmful Algae 4:1044-1052

Valério E (2008) Molecular Approaches in Cyanobacteria: from Detection and Diversity to DNA-Based Bionsensors. Ph.D Thesis, Faculdade de Ciências, University of Lisbon.

Vollenweider RA, Kerekes JJ (1980) Background and Summary Results of the OECD Cooperative Program on Eutrophication." In: Proceedings of an International Symposium on Inland Waters and Lake Restoration. U.S. Environmental Protection Agency. EPA 440/5-81-010. pp. 26-36.

Xu Z, Godrej NA, Grizzard TJ (2007) The hydrological calibration and validation of a complexly-linkerd watershed-reservoir model for the Occoquan watershed, Virginia. J Hydrol 3-4:167-183

Yevenes MA, Mannaerts CM (2011) Seasonal and land use impacts on the nitrate budget and export of a mesoscale catchment in Southern Portugal. Agric Water Manage 102:54-65

Zhang X, Srinivasan R, Van Liew M (2008) Multi-Site Calibration of the SWAT Model for Hydrologic Modeling. Trans ASABE 51(6):2039-2049

3.4 Integrated modelling framework for urban flood management. Study case in Póvoa de Santa Iria, Portugal.

This article/application integrates MOHID Land for surface water (rivers, streams and runoff) and SWMM for drainage systems (domestic and pluvial) in a online fashion (running simultaneously) to depict the cause of urban floods and test management scenarios to reduce them.

INTEGRATED MODELLING FRAMEWORK FOR URBAN FLOOD MANAGEMENT. STUDY CASE IN PÓVOA DE SANTA IRIA, PORTUGAL.

David Brito[1], Frank Braunschweig[1], Afonso Sebastião[2], Joana Cardoso[2], Filipa Ferreira[2], José Saldanha Matos[2], Miguel Santos[3], Sara Proença[3].

[1]Action Modulers, Estrada Principal 29, 2640 Mafra, Portugal

[2]Hidra, Hidráulica e Ambiente, Av. Defensores de Chaves, nº 31, 1º Esq. 1000-111 Lisboa, Portugal

[3]Águas de Lisboa e Vale do Tejo - Sub-Sistema de saneamento do Tejo e Trancão, Etar de Alcantara Av. de Ceuta, 1300-254 Lisboa, Portugal

Abstract

With increasing soil impermeabilization and “permeable” urban planning, urban floods tend to be faster, with higher intensity what in turn usually originates higher damage to infrastructures, services or persons.

To answer to the complexity of the system (natural system linked with urban drainage, domestic and storm water in non-separated systems, obstructions, diameter reduction, siltation, tide influence) it was developed an integrated modelling approach using MOHID Land to compute hydrologic processes (precipitation – runoff) up to urban drainage system and hydraulic process associated to surface water routing and SWMM model to compute flow in urban domestic and storm water systems. The linkage of the two models needed to be done in run-time (since inflows/outflows of the drainage system are computed based on both models hydraulic heads that feedback on each other) and it was done using OpenMI standard.

This work proposes a novel approach by coupling open-source models for urban flood management (surface water and urban drainage) that were forced and validated with high frequency data (every minute precipitation and measured flows and levels for 3 winter months).

The integrated model was implemented in a small urban watershed where high frequency field data was recorded (precipitation, level and flow for 3 winter months in 2014/2015 with 1 minute frequency). The objective was to verify model fit to data and to depict key aspects that control flooding to produce management scenarios that could alleviate flooding effects.

Model results and field data pointed out critical areas with reduced diameters and that suffer from siltation (tide influence). The model results show that cross section reduction towards a railway line makes that the pipe capacity is rapidly filled what originates overflow and flooding in strong rain events.

Actual situation and management scenario simulations with infrastructural changes (doubled the diameter in critical points) showed that flooded volume could be reduced around 30% during a 10 year return period event.

This study was able to get good model fit to data in the time scale of minutes (not even hourly lumping) that shows the great potential of this integrated tool to simulate fast intense urban floods.

It was develop a straightforward new set of linkage between state-of-the-art surface water and drainage system models that could be used to aid in solving flood management problems at urban scale.

Keywords: integrated modelling, MOHID Land, SWMM, urban flood

3.4.1 Introduction

With population increase and concentration in urban areas in last centuries, tipically with weak urban planning and low control on impermeable area density, increased flood probability (reduced water retention upstream) and increased flood impact as more population and services started to occupy near stream areas, leading to higher flood risk. Unplanned urban growth also led existing urban drainage systems to start to be short on capacity and fruifull in inproper connections between storm water and domestic drainage systems, that reduced system capacity and increase flood impact. When the urban agglomerates are located near a coastal or river, "external" water level rises may even block drainage system outflows and increase the problem.

The urban flood system is a pool of complexity since it mixes

- the natural drainage system (natural water cycle, precipitation, soil infiltration, runoff generation and routing to the natural drainage network and possible over bank flow)
- the urban drainage system (managed water cycle, precipitation, entrance in drainage system in building and road gutters, routing in pipes, possible overflow in manholes)
- the mix between the two where streams enter urban drainage and/or urban drainage discharges in streams
- the receiving medium that based on levels can block outflow or enter the system.

The existence of a single model that describes all these processes in detail is usually not found, even in component-based models as MOHID Land that has a modular structure to add new processes in a staighforward way (Buahin, 2015). This happens because model scope and detail focus, usually follow the developers team's field of study (e.g. computational fluid dynamics, agronomy, ecology, groundwater, etc). Big additions to a model in terms of different geometries, processes, discretization, etc., need big code changes and graphical interface changes that can have ripple side effects (Voinov and Shugart (2013), and can only be feasible in a interdisciplinary framework). Thus, the detail description of these processes asks for an integration procedure (strongly present in Water Framework Directive) so that the best detail in each area (surface flooding, urban drainage) is achieved.

The first implementation on flood modelling go as far as the 60's (Preissmann, 1961) for 1D finite diferences of St. Venant equation, and in 70's through 90's the approaches tended to be 1D since that was the format of the data available (river profiles). In the 90's with computer processor development and GIS processing, 2D implementations gained strenght, usually with simplifications of the St. Venant equations by ignoring inertia (Hunter et al. 2005). The "boom" of 2D models arose with more computer power and the widespread availability of 2D data from satellite (e.g. Synthetic Aperture Radar) or Lidar in 00's (Bates, 2012).

On one hand, some examples of widely used, distributed, open-sources flood models are LISFLOOD-FP (from Bristol University, described in Bates and De Roo, 2000) that is an 1D kinematic wave model for river and 2D diffusive wave for surface runoff (simplifications of the St. Venant equations) or the HEC River Analysis System (HEC-RAS, from US Army Corps of Enginners, described in Brunner, 2010) that solves the full 1D Saint-Venant equations for an unsteady open channel flow and results between sections are interpolated to 2D. MIKE Flood is a commercial package using existing Danish Hidraulic Institute (DHI) 1D river MIKE Hydro River and 2D overland flow MIKE 21 where also Full St. Venant equations are solved, using finite differences (DHI, 2007). MOHID Land model solves the full 2D and 1D Saint Venant equations in surface runoff and river network using finite volumes (assuring mass conservation) being a state of the art in surface flood models.

On the other hand, one of the most widely used, open-source urban drainage system model is SWMM (Storm Water Management Model from US Environmentl Protection Agency described in Rossman 2016) that solves both hydrology (simple sub-watersheds volume model to estimate inputs to drainage system) and hydraulics in a complex system of pipes, channels, storage/treatment devices, pumps, and regulators. The model can solve the complete St. Venant equations for free surface and pressurized gravity driven flow. MIKE Urban is a commercial package using existing DHI MOUSE and MIKE 1D where also complete St Venant equations are used.

In the last years some approaches have successfully linked different open source models for urban modelling as the couple of SWAT and SWMM models with a sediment transport model (Shrestha et al., 2014) by using OpenMI standard. OpenMI has been also used to couple InfoWorks-CS and InfoWorks-RS for studying sewer-river linking (Smolders et al., 2008) and the three-dimensional surface water hydrodynamic model, Environmental Fluid Dynamics Code (EFDC) and InfoWorks-CS, to study river, drainage system interaction (Zhu et al. 2016).

However, few are the works done up to now to integrate full distributed surface water model with urban drainage model as Kidmose, 2015 that used MIKE She and Mouse to evaluate forced infiltration fluxes. And it lacks integrated real-time models implementations with open-source models with high frequency data for validation.

This work proposes a novel approach by coupling open-source models (MOHID Land and SWMM) for urban flood management (surface water and urban drainage) that were forced and validated with high frequency data (every minute precipitation and measured flows and levels for 3 winter months).

The objective was to develop a straightforward new set of linkage between state-of-the-art surface water and drainage system models that could be used to aid in solving flood management problems at urban scale.

3.4.2 Material and methods

In this section it is shown the site, the modelling methodology and the field data used to validate model results.

3.4.2.1 Study Site

The study site where the integrated model was applied is located 15km N-NE from Lisbon, at Póvoa de Santa Iria location, near Tagus river (Figure 1Figure). The watershed dimension (composed primarily by two small streams of similar size) is around 2km x 1km and is essentially an urban area (mid density) with industrial compounds in the downstream part (railway separates uphill steeper and urban area from flatter and industrial use near the river). The two main streams that flow SE, enter the urban system in the downstream part. (Figure 2Figure).

Figure 1. Póvoa de Santa Iria study site location.

Figure 2. Digital Terrain Model and natural and storm water drainage network. Source DTM: SIMTejo.

The drainage system is in theory separate sewer system (storm water drainage system and domestic system completely separated) but it is known to have some improper connections (the 2 systems are parallel in big part of the site) so it is categorized as pseudo-separate sewer system.

The storm water system follows the two main streams and diameters are around 1000 mm before the railway crossing, where it reaches to depths of around 10cm (due to silting in pipes that suffer from tide influence) - Figure 3Figure .

The domestic system also follows a similar pattern and the diameters are around 200 mm. The domestic flows are routed to a pumping station where are then routed to a WWTP.

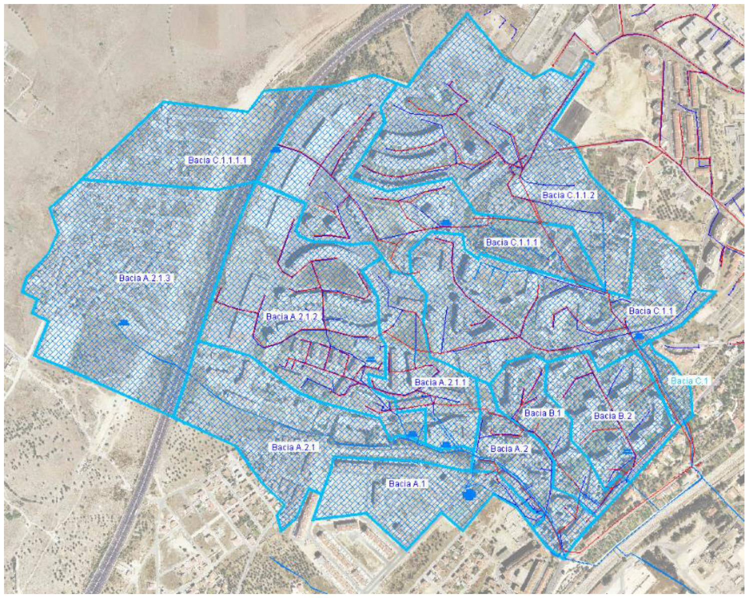

Figure 3. Storm water drainage network in Póvoa de Santa Iria system.

The site had in the past years some events of floods in the downstream part and this study was a first approach to understand the problematic areas and suggest improvements that could reduce flooding.

3.4.2.2Modelling Methodology

As shown before, the detailed description of the surface and urban drainage flows and their integration calls for two detailed models be used for each domain. Moreover, the link of the two models needs to be done online (running at the same time) since the outflows of the urban system may return as inflows after surface routing, or inflows to urban system can return to surface if pipe capacity is exceeded. There are several examples of model integration interfaces as the Earth System Modeling Framework (ESMF) (Hill et al., 2004), Model Coupling Toolkit (MCT) (Warner et al., 2008), Community Surface Dynamics Modeling System (CSDMS) (Peckham et al., 2013), Object Modeling System (OMS) (David et al., 2002), and the Open Modeling Interface (OpenMI) standard (Moore and Tindall, 2005; Gregersen et al., 2005, 2007). Even that all may have their advantages, OpenMI was chosen since it is a generic interface (can deal with different kind of models and geometries), open-source project with more than a decade work, and developed within a modern and flexible programming language (C#).

The two models used were MOHID Land for surface water, developed at IST, university of Lisbon where the first author is a major developer and SWMM for urban systems, developed at EPA (US Environmental Protection Agency). The standard followed for model integration was OpenMI[12].

Both models were set and run in MOHID Studio, a GUI developed by Action Modulers to prepare, run and explore model results.

The two models and OpenMI description and implementations are described next.

3.4.2.2.1 OpenMI

In this implementation MOHID Land model is used to simulate all processes associated with surface water in the watershed (precipitation, infiltration and surface flow routing) and SWMM model to simulate urban drainage flow behaviour. MOHID Land feeds SWMM with stream inflows and gutter potential inflow and SWMM returns the effective gutter inflow (it may occur that the effective gutter inflow is lower than the potential due to limited pipe capacity) and outflow through manholes (Figure 4). All water exchanges between models are computed based on hydraulic gradients.

[12] https://sites.google.com/a/openmi.org

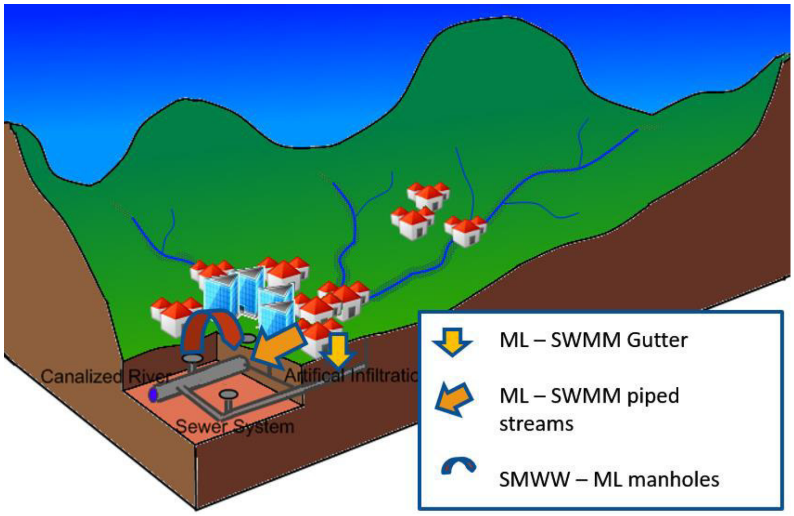

Figure 4. Conceptual fluxes integration between MOHID Land and SWMM models.

The complexity of the processes involved in natural and urban drainage (natural streams that enter storm flow drainage, urban drainage inflow and overflow that interact with surface water) make that MOHID Land and SWMM need to run simultaneously since one solution influences the other.

The standard interface used for the two models to exchange data was OpenMI that was developed in a European project called HarmonIT[13]. OpenMI is a software component interface definition that means that it sets standards and methods for model exchange (e.g. standardizes that models need to expose time and data in exchange points and provides methods for automatic spatial and temporal interpolation). The user needs to assure that models are OpenMI compliant and needs to set the exchange (define which state variables from each model and at which points and code the exchange).

MOHID Land and SWMM models were not OpenMI compliant and since they are open-source models, development was made in Action Modulers so that they were OpenMI compliant and the links between them were built consistently.

[13] http://www.openmi.org/archives/harmonit

SWMM model was modified to compute at each time step:

- the inflows from steet gutter, with a potential value imposed from MOHID Land, as lateral flow;
- water surface level, computed by MOHID Land.;
- overflow water in manholes during flood.

MOHID Land model was changed to compute at each time step::

- potential water outlow through street gutter;
- water inflow from manholes (computed from SWMM).

This required the development at different levels (Figure 5Figure):

- Inside models to expose timing and exchange fluxes through public methods
- Creating dll and .net access so that the the public methods are translated from the model original language to C# (one of the OpenMI available languages).
- Creating a model wrapper where OpenMI standards (quantities, spatial elements, links, accessor methods between models are defined) are configured.

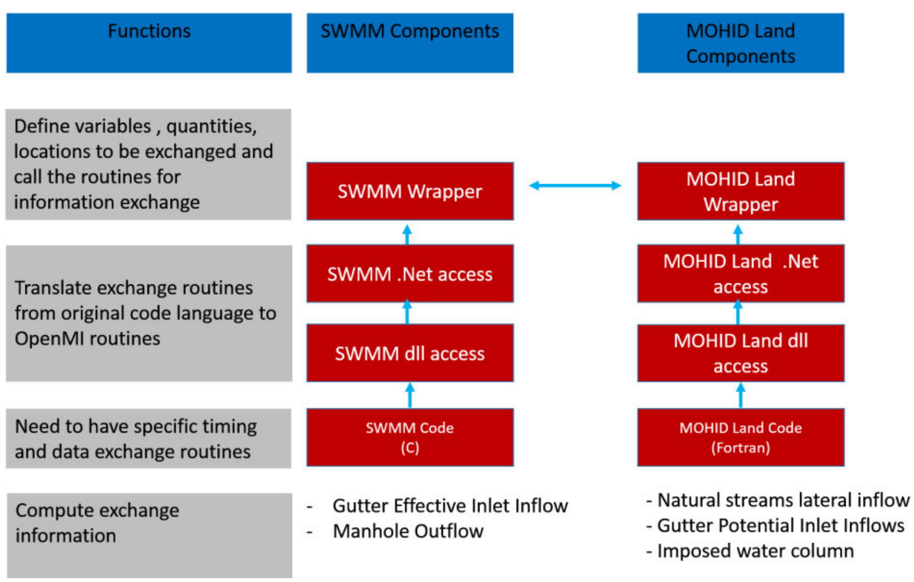

Figure 5. OpenMI developments in SWMM, MOHID Land models and in interface.

Also a new development was made in MOHID Land and in the OpenMI interface especially suited for the study site (since sewer is pseudo separated), that allowed to define that MOHIDLand potential gutter inflow would be directed to specific SWMM nodes (storm water nodes only).

3.4.2.2.2 MOHID Land model

Processes

The surface water model used is MOHID Land a distributed, continuous, variable time step watershed model that includes processes in atmosphere (model forcing), interception and evaporation in leafs, infiltration and evapotranspiration in soil, and routing of water and properties trough surface runoff, porous media or river network using a finite volume approach based on mass and momentum balance equations (Trancoso et al. 2009).

MOHID Land is an integrated model grouping 4 compartments or mediums (atmosphere, porous media, soil surface and river network) and water moves through the mediums based on mass and momentum balances. The atmosphere is not explicitly simulated but provides data necessary for imposing surface boundary conditions to the model (precipitation, solar radiation, wind, etc.) that is space and time variant. Surface land is described by a 2D horizontal grid that can use variable spatial step. The surface elevation is specified in the centre of each grid cell using a digital terrain model (DTM). The porous media is a 3D domain with the same horizontal grid as surface, and vertical grid, also allowing variable layer thickness. The river network is a 1D domain defined from DTM by reaches linking surface cell centres (Figure 6Figure).

MOHID Land model uses a finite volume approach (control volume) for computing state variables and fluxes. Each grid cell is a control volume, being the state variables computed in their centres and the fluxes (and related variables) on the faces.

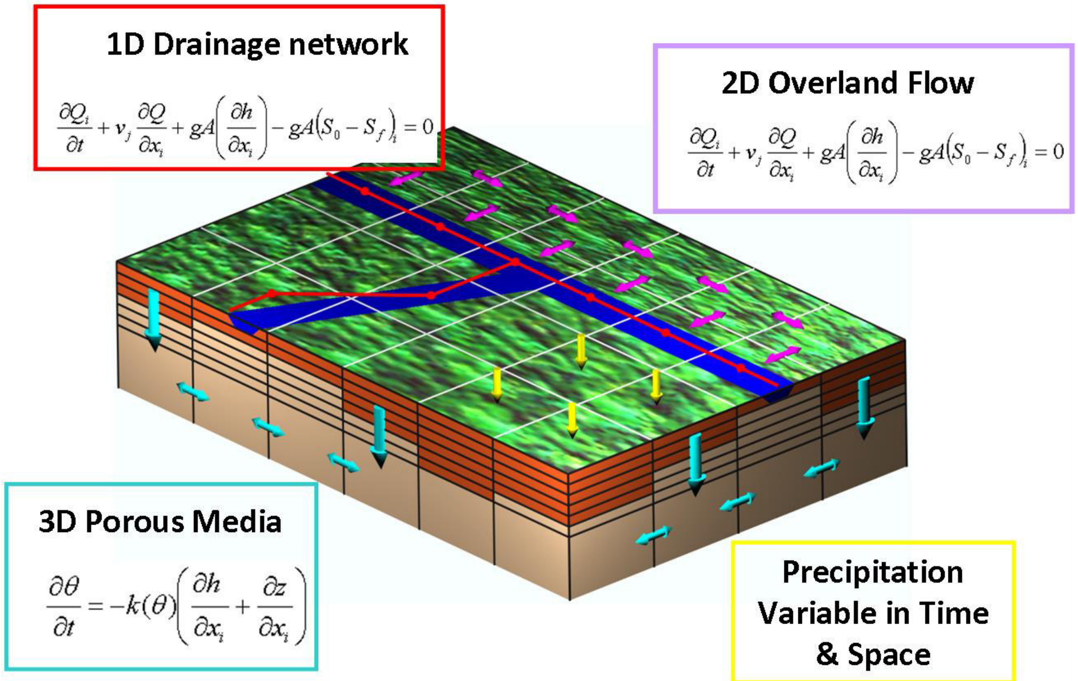

Figure 6. MOHID Land Geometry and equations.

In the context of this implementation it was used only the 2D and 1D surface components (surface runoff and river) and a simplified infiltration based on Green Ampt. In the integrated modelling approach, MOHID Land computed lateral inflow to SWMM (input from natural streams), gutter input to SWMM (from surface water) and manhole output from SWMM (to surface water).

For 2D and 1D surface components is used the St. Venant equation (Equation 10) where Q ($m^3.s^{-1}$) is water flow, A (m^2) is the cross flow area, g ($m.\ s^{-2}$) is gravity acceleration, H (m) is water elevation, S_0 (-) is the bottom slope, S_f (-) is the bottom friction slope (i.e. the slope that balances the friction force) and x_i are the flow directions (xx and yy).

$$\frac{\partial Q_i}{\partial t}+v_j\frac{\partial Q_i}{\partial x_j}+gA\left(\frac{\partial H}{\partial x_i}\right)-gA(S_o-S_f)=0$$

Equation 22 – St Venant Equation for 2D.

Friction slope Sf can be defined with the Manning-Strickler empirical law (Equation 11),

$$(S_f)_i = \frac{n^2|Q|Q_i}{A^2 R_h^{\frac{4}{3}}}$$

Equation 23 – Manning-Strickler equation for friction slope

where Rh (m) is the hydraulic radius, equal to the cross sectional area divided by the wet perimeter, and n ($s.m^{-1/3}$) is the Manning roughness coefficient.

The St Venant equations are the most complete set of equations for depth integrated flow where the major forces affecting the flow are pressure, gravity and friction that together with inertia determine the evolution of the flow.

For infiltration it was used Green Ampt model

$$i(t) = K_s \left[\frac{h_{wetfront} \Delta\Theta}{I(t)} + 1 \right]$$

Equation 24 – Green Ampt Infiltration

Where i(t) is infiltration rate at instant t (mm/h), K_s is saturated conductivity (mm/h), $h_{wetfront}$ is soil suction head at wetting front (m), Δθ is soil initial deficit in water content (m^3/m^3), I(t) is accumulated infiltration up to time t (m).

Green Ampt equation represents the loss of soil capacity to infiltrate as infiltration progresses, lowering infiltration rates with time (as accumulated infiltration increases). The Green Ampt parameters are dependent on soil types and soil moisture before events.

Geometry

The model was implemented in the 2D surface runoff component with 600x440 cells with cells around 4m x 4m to have a compromise between number of cells and surface definition so that in the area most the main streets had at least two cells to describe them. In the natural river system 1D model (before entrance in urban drainage system) was implemented with 3202 nodes that are placed at 2D cell centres (Figure 6Figure).

Base Data

Data from digital terrain model were provided by SIMTEJO (1m resolution contour lines) and interpolated to the computational mesh. The natural drainage network was obtained directly from topography based on the direction of flow was interrupted in the connection to the SWMM network (Figure) corresponding to the entry of streams in the urban network.

Soil permeability in the study area was estimated from the information provided by SIMTEJO in terms of buildings, and complemented with streets and sealed floors obtained from TeleAtlas and Google satellite images (Figure 7Figure).

Figure 7. Soil impermeabilization considered in study area and urban drainage network.

It was also considered the buildings geometry for surface water interaction (data from SIMTEJO) in the downstream area where the two models coexist. After first results it was verified that the surface model was not accounting two main obstacles perpendicular to upstream – downstream direction, namely the railway line and the wall in Rua da República. These constraints were added with the railway as 0.5m above terrain and the street as 1.5m above terrain, as shown in Figure 8Figure .

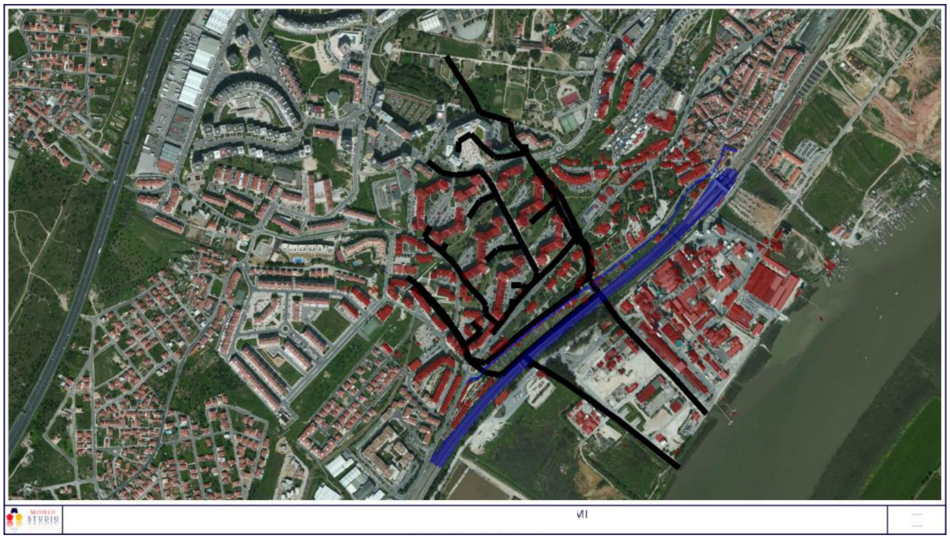

Figure 8. Buildings in red (source SIMTEJO), urban drainage network in black and obstacles considered for surface modelling in blue.

Boundary and Initial Conditions

MOHID Land model implementation has 2 boundary conditions:

- In atmosphere where precipitation was inputted as a time series (homogeneous in space) from measured data (see next chapters)
- In downstream river interaction with SWMM model, all the river flow computed downstream is removed from river (to be inputted in SWMM as a lateral inflow)

As initial conditions for each event analysed the surface has no water columns as it occurs in reality where the small streams have very low drainage areas and only flow when it rains.

Parametrization

Since MOHID Land surface water routing is physically based, the only parameters in the implementation were manning resistance and Green-Ampt infiltration parameters.

The manning resistance used for surface water was 0.035 (s.m$^{1/3}$) that according to bibliography (e.g. Chow, 1959 e van der Sande et al., 2003) are typical values for areas with natural systems and rivers (urban area has in between buildings gardens and bushes) and streams are only artificialized when entering the storm water system.

In what respects the Green-Ampt infiltration model, it was performed a sensibility analysis to the different parameter of the equation, using parameters from typical soil types (Maidment, 1993), It was verified that generated flow is inversely proportional to the soil infiltration capacity (as expected) and the parameters that yielded best results in adjusting to watershed behaviour was the associated to “sandy clay” soil (Maidment, 1993 and **Error! Reference source not found.**). These oil parameters are in the range of the normally used by Action Modulers in flood studies and are one of the parameter classes of the suggested for SWMM model implementation (following Maidment soil classes and parameters).

Table1. Used Green-Ampt parameters for the MOHID Land implementation.

Wet front Suction Head (m)	Saturated Conductivity (mm/h)	Initial water content deficit (m^3water/m^3soil)
0.239	1.20	0.091

3.4.2.2.3 SWMM model

Processes

SWMM model is a dynamic rainfall-runoff simulation model used for single event or long-term (continuous) simulation of runoff quantity and quality from primarily urban areas. The runoff component of SWMM operates on a collection of sub catchment areas that receive precipitation and generate runoff and pollutant loads. The routing portion of SWMM transports this runoff through a system of pipes, channels, storage/treatment devices, pumps, and regulators. SWMM tracks the quantity and quality of runoff generated within each sub catchment, and the flow rate, flow depth, and quality of water in each pipe and channel during a simulation period comprised of multiple time steps (Rossman and Huber, 2016)

SWMM model is a distributed model that solves manning equation for surface runoff flow (where sub-basins are treated as non-linear reservoirs) and may solve the complete St Venant equations for pipe flow in a variable time step fashion.

For the integrated implementation only the SWMM pipe flow is used (complete St. Venant equations presented in MOHID Land model description) since MOHID Land provides SWMM the inflow from the upstream areas.

Base Data

For the construction of the SWMM project it was used as base data the infrastructure registration present in the remodelling of the system (ENHÍDRICA, 1997), topographic surveys (source SIMTEJO) and railway company ("Infraestruturas de Portugal") data (in the railway storm water crossing).

It was necessary to impose localized pressure losses in critical considered sections, associated with section reductions ("bottlenecks") and in transition points in the storm water drainage system, from open air to pressurized flow. Pressure losses were also considered in areas where obstructions were identified. This information was carried out based on the Hidra field campaigns and vast experience in SWMM modelling.

Geometry

In Figure 9Figure is presented the SWMM geometry with storm water and domestic systems, including the pumping station. The network is comprised by 186 nodes, in which 119 are domestic and 57 from storm water system. The pipe lengths ranges from a few meters to around 100m and pipe height is around 200 mm in domestic and around 1000 mm in storm water before the railway crossing. During railway crossing the storm water pipe depth lowers to up 100-200 mm due to silting (tide influence). This situation was registered in field campaigns and implemented in SWMM project by defining a lower section pipe.

The pipe discretization (lengths up to 100m) and density is similar to the used in similar studies with model coupling (e.g. Shrestha et al. 2014 that coupled SWAT and SWMM models).

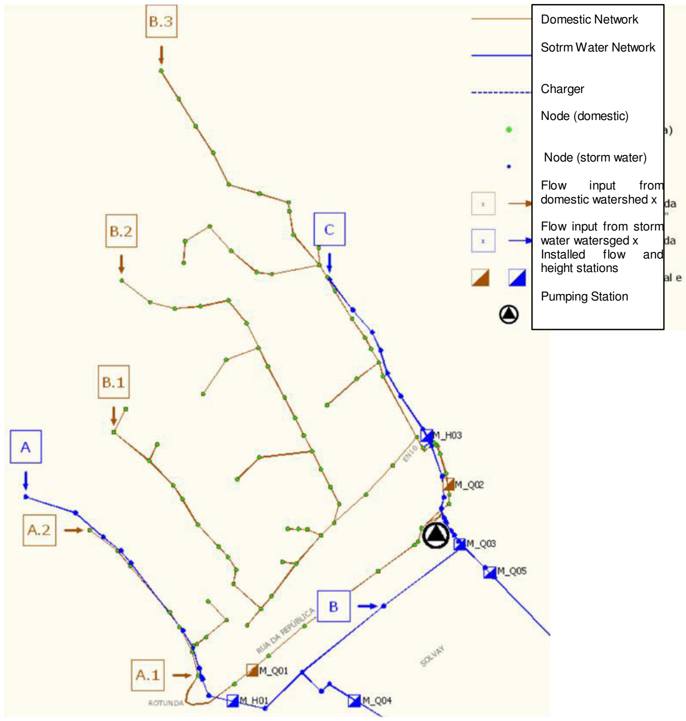

Figure 9. SWMM network representation – in Brown the domestic system and in blue the storm water system.

Boundary and Initial Conditions

SWMM model implementation has 5 boundary conditions:

- Domestic input
- stream input is inserted in nodes as a lateral inflow (from MOHID Land)
- surface water hydraulic head is imposed in nodes (from MOHID Land surface water column)
- gutter inflow is inserted in nodes as an inlet inflow (from MOHID Land)
- manhole outflow is removed from the nodes (to MOHID Land)
- tide imposed in river Tagus (data from Nation Hidrographic Institute)

SWMM initial condition is no flow and no water in pipes. Since the system is very small (branches with wider distance is 1km) and the model is run for a period before event longer than water retention time in the system, this initialization has no impact in results since correct conditions are met quite fast.

Parametrization

The domestic input into the system was computed based on water use patterns (variable during the day and different from week days to weekend).

Since throughout the system was verified to exist improper connections between storm water and domestic system, it was considered a percentage of pluvial water to be connected to domestic. This percentage was tested by running integrated model and comparing results in domestic system with field data. This percentage was around 10-20%, depending on system branches.

3.4.2.2.4 Simulations

It was performed a current situation simulations where from measured precipitation input the integrated modelling approach was compared to measured flow and levels in different points of the urban drainage system.

After model validation and since the recorded events did not produce floods, it was simulated a 10 year return period synthetic event and with the information gathered of the critical elements, it was produced a simulation with improvements in the urban drainage network to check the feasibility to reduce flooding.

3.4.2.2.5 Goodness-of-fit statistics for the evaluation of the model performance

To quantify the accuracy of the model results, two statistical indicators were used: the R^2 (squared pearson correlation coefficient) that represents the linearity of modelled and measured data (value of 1 is when both series are one the same segment) and the NSE or Nash-Sutcliffe Efficiency (Nash and Sutcliffe, 1970).

Model results with high R^2 show that model and measured data have same linear tendencies. However the source of error can be high (relative differences to the average are similar but absolute differences may vary). Squared Pearson Correlation coefficient is presented in Equation 25.

Equation 25. Squared Pearson Correlation Coeffiient

$$R^2 = \frac{\sum_{i=n}^{N}\left(X_{sim}^{i} - \bar{X}_{obs}^{i}\right)^2}{\sum_{i=n}^{N}\left(X_{obs}^{i} - \bar{X}_{obs}^{i}\right)^2}$$

where X_{sim} is the simulated value, X_{obs} is the observed value, $\sim X_{obs}$; is the mean of the observations, and N is the total number of observations.

As so, the NSE was used that both evaluates tendency and error. The expression is similar to that of R^2 (sum of quadratic differences) but the NSE "oblies" that the linear regression curve is the diagonal so the deviations computed are effective absolute errors. NSE is one of the most widely used. The values of NSE vary from –infinity to 1, whereby an NSE value of 1 corresponds to a perfect model. The equation is presented Equation 26.

Equation 26. Nash-Sutcliffe Efficiency.

$$NS = 1 - \frac{\sum_{i=n}^{N}\left(X_{sim}^{i} - X_{obs}^{i}\right)^2}{\sum_{i=n}^{N}\left(X_{obs}^{i} - \bar{X}_{obs}^{i}\right)^2}$$

where X_{sim} is the simulated value, X_{obs} is the observed value, $\sim X_{obs}$; is the mean of the observations, and N is the total number of observations.

3.4.2.3Field Data

In order to accurately describe the drainage system several field campaigns were carried out to get infrastructure information where registration was lacking.
Moreover, it were installed automatic sensors in several points in domestic and storm water system, recording from 6 December 2014 to 8 February 2015, recording data every minute:

- 5 flow stations with ultrasonic, press ion and velocity sensors.
- 3 level stations with pressure sensor.
- 1 rain gauge.

The distribution of the sensors was done so that both the domestic and storm water main branches was monitored. In Figure 10Figure it is shown the drainage system and the locations of the measured stations.

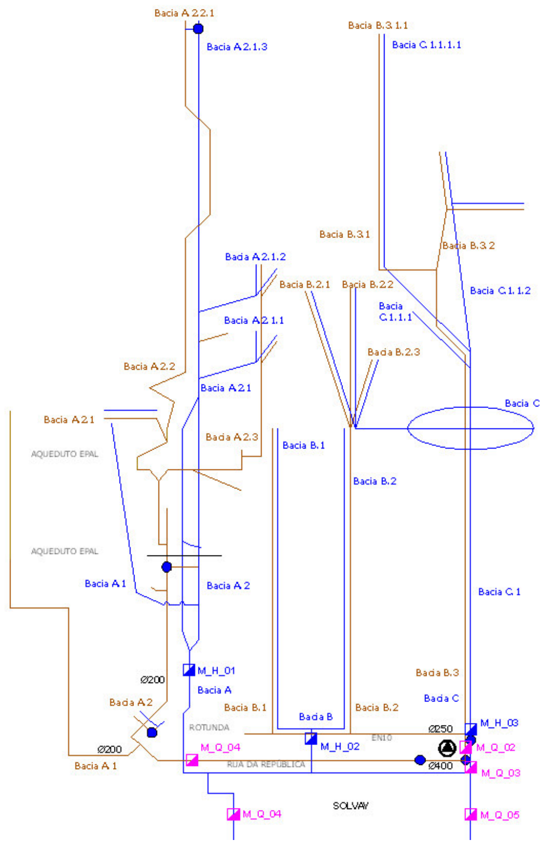

Figure 10. Schematic representation of the domestic and storm water system, identifying the sensor locations for flow measurement in pink (code M_Q_XX) and level measurements in blue (code M_H_XX).

During the recording period, the events with higher precipitation were:

- 13th December 2014, events E6 to E9
- 15th to 18th January 2015, events E21, E35, E37 and E39

In Table 2 it is shown the precipitation events for this periods, where it can be seen the event E9 where 5.1mm/h were recorded during around 1h or E35 with similar precipitation rate but during 7h.

These were the events simulated and the results with the integrated model were compared with the measured level and flows for the same periods.

Table 2. Events registered in 13th Decemebr 2014, 15th to 18th January 2015 and 6th Febriary 2016 with precipitation higher than 0.1m and events separated by at least 30 minutes.

Events	Days	Duration	Total Precipitation (mm)	Average Intensity (mm/h)	Maximum Intensity (mm/h)
E6	13th December 2014	5:00	16.0	3.2	66.0
E7		1:34	1.5	1.0	6.0
E9		1:17	6.6	5.1	60.0
E10		0:30	0.3	0.6	6.0
E11		0:50	0.7	0.8	6.0
E18		0:08	0.4	3.0	6.0
E21	15 to 18thJanuary 2015	4:27	11.9	2.7	12.0
E24		0:10	0.4	2.4	6.0
E25		0:27	0.7	1.6	6.0
E28		0:04	0.4	6.0	6.0
E30		0:15	0.3	1.2	6.0
E31		0:36	1.1	1.8	12.0
E32		0:24	1.1	2.8	18.0
E33		0:04	0.5	7.5	12.0
E35		7:53	33.2	4.2	60.0
E36		0:23	0.8	2.1	6.0
E37		1:31	2.5	1.6	12.0
E39		0:44	1.5	2.0	12.0

3.4.3 Results and Discussion

The results are presented first for the reference situation where measured flow and level was compared to model results.

After model comparison, it was studied flood events with a return period of 10 years so that flooding would occur and it was tested a scenario with suggested improvements in the storm water infrastructure to depict the impact in flooding situation.

3.4.3.1 Reference Situation

3.4.3.1.1 Comparison to Field Data

In the Figure 11Figure and Figure 12Figure is presented the comparison between observed and simulated flow and water depth for several points in the urban drainage infrastructure (see chapter about field data) for the events of December 2014 and January 2015.

Domestic system

On top on the two figures are presented stations M_Q_01 and M_Q_02 both from domestic system (one at each branch) where observed base values are around 30L/s, maximum flows are reached around 200 L/s and time to peak is around 1h, in both periods. It can be seen clearly the effect of improper storm water connections since the flows almost increase one order of magnitude during precipitation events. The integrated model is able to represent both the base values and the maximum values, with the interaction associated with improper connections to domestic system. The model is also able to represent flow increase and recession periods timings and curve slopes, showing that is propagating correctly the flood wave.

In terms of statistical fit, the model capacity to represent the same trends and order of values as observed data in the two monitoring points in domestic system is shown by R^2 around 0.7-0.8 and NashSutfcliffe efficiencies higher than 0.5. In January 2015 event the M_Q_02 point got a lower fit (NS of 0.25) because the overprediction in the period before the higher peak.Only looking at model estimation, the behaviour in this station is similar to other stations (where flows in the overprediction sub-period are slight higher than first events) so the estimated model results seem to be consistent throughout the stations, while observed data don not. The origin of the difference may be related to measurement issues.

Storm water system

On the middle of the two figures, are presented the water depth in M_H_01 (west branch) and flow in M_Q_03 (east branch), that are two stations before the railway crossing, and one at each branch. During the two events the flow reached up to 1 and 2 m3/s and around 0.2m and 0.6m (respectively in flow station and level station).

Before flood events the water level is just a few centimetres and flow below 200 L/s. The integrated model is able to represent both the maximum flows and depths and base values. The model is also able to represent event peak rise and fall with correct timings.

The statistical fit of the model to observed data is quite satisfactory with R^2 ranging from 0.8-0.9 and NS from 0.7-0.8, showing that in the storm water system, where no assumption needs to be made about lateral inputs (as occurs in domestic), the results are closer to observed data where the order of values between model and data is very similar in the majority of the simulation. In December 2014 in station M_Q_03 the NS value was lower 0.3 due to an overprediction in the second event. However this situation is similar to the one described above where model results are consistent throughout the stations (where good results exist for this sub-period) but field data not, what suggests that the difference is related to measurement issues.

The last portion of the two figures (bottom) is represented flow in station M_Q_04 (east branch) that is located after railway crossing, after the diameter bottleneck. It is not shown here but the two branches have similar flows since they have similar drained areas and in station M_H_01 the flows (only recorded level) are very similar to station M_Q_03. So from upstream to downstream of the railway crossing the flows get reduced by almost half. This situation is due to the diameter reduction and the model results could only represent this behaviour after reducing the pipe diameter to describe the observed silting effect.

In this events it did not occurred flooding since the water that was unable to pass under the railway network, was diverted to an open air ditch that is located parallel to the railway line. In stronger rain events this ditch may not have enough capacity (the ditch has 1.2m deep and 1.4m wide and is estimated a maximum capacity of 3 to 5 m3/s) and flooding occur.

The integrated model is able to represent the flow order of values and trend in observed values in station M_Q_04 in a quite satisfactory way with R^2 ranging from 0.6 to 0.9 and NS around 0.7-0.8.

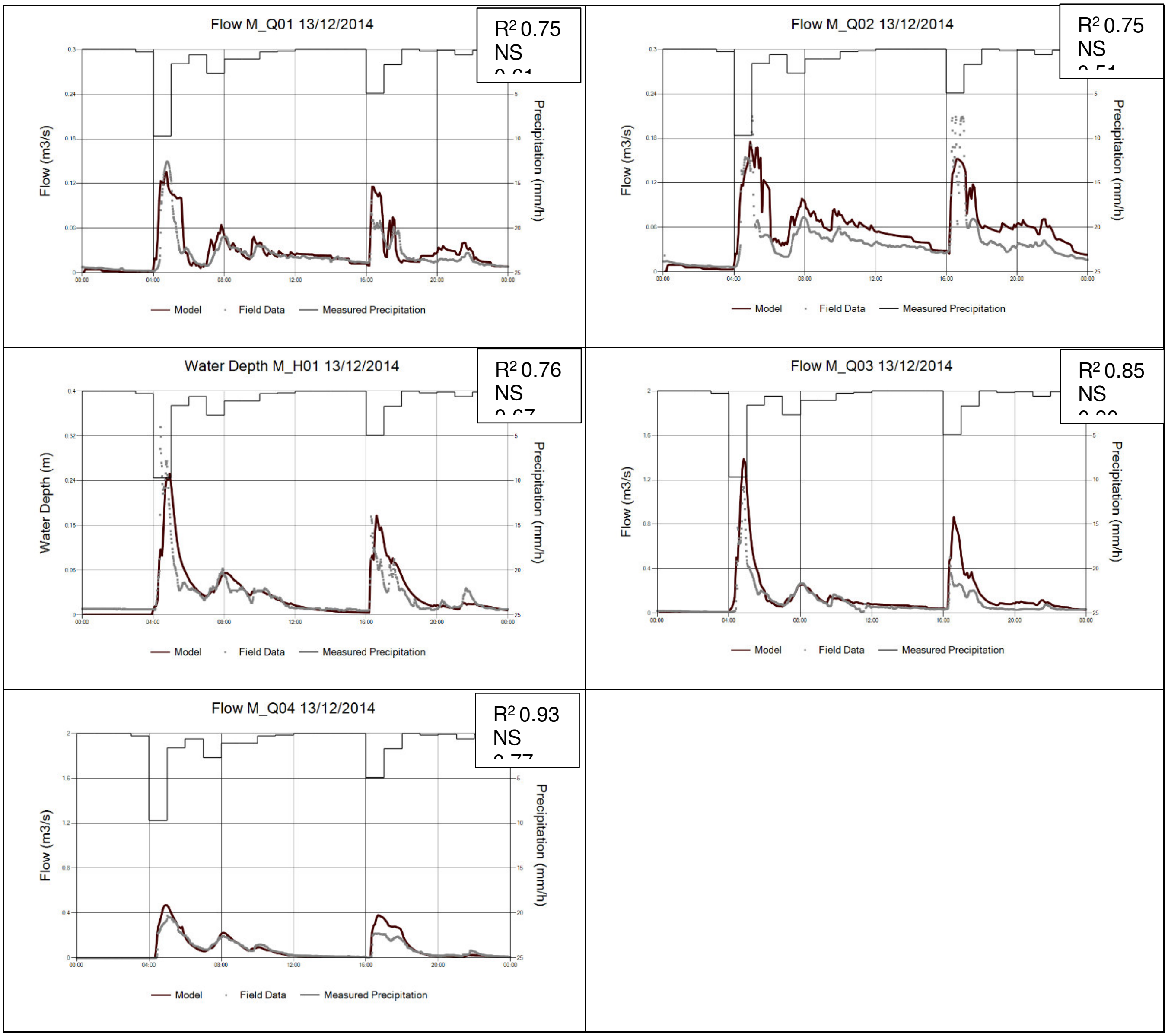

Figure 11. Comparison between modelled (black) and observed (grey) flows and level height in December 2014 event. Hourly precipitation is shown in inverse vertical axis. In each graph R^2 and NS (Nash Sutcliffe coefficient is presented)

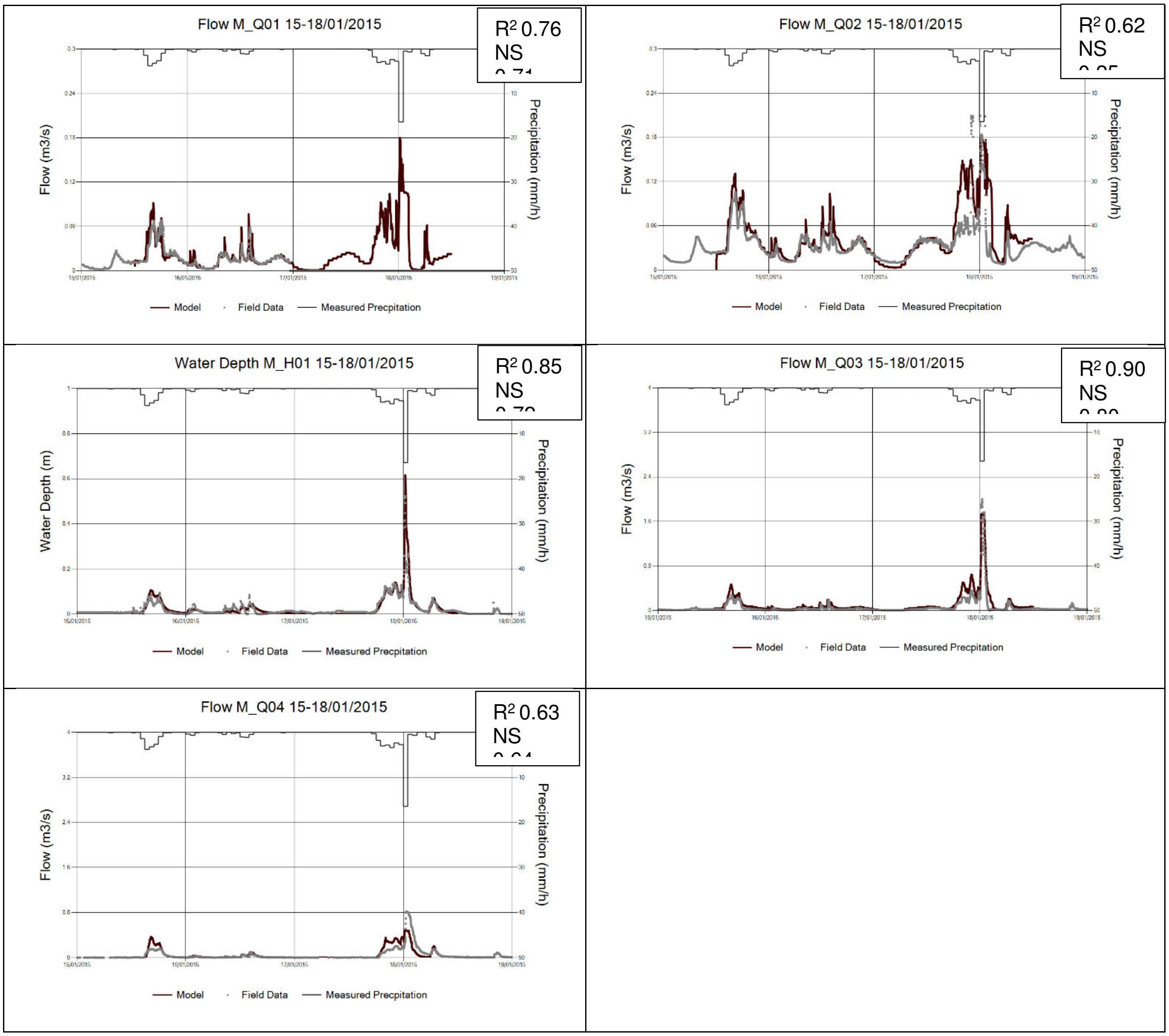

Figure 12. Comparison between modelled (black) and observed (grey) flows and level height in January 2015 events. Hourly precipitation is shown in inverse vertical axis.

The integrated model results show that the model was able to represent the observed flow and levels with a degree of detail that is suited for flood assessment. This results are in line with othes presented in bibliography for integrated models as Shrestha, 2014 that integrated SWAT model for watershed and SMM model (forcing with hourly rain) and obtained NS efficiencies from 0.6 to 0.8 in simulated daily flow in channels. Kidmose et al. (using MIKE SHE for surface and MOUSE model for storm water with every minute recorded rain during events) show the tendency to overestimate flows even in daily and monthly scales.

It is important to refer that this study was able to get good fit to data in the time scale of minutes (not even hourly lumping) that shows the great potential of this integrated tool to simulate fast intense urban floods.

Since the observed events did not create flooding in the study site, to test the flood behaviour in reference situation and test scenarios, the model implementation was tested with a 10 year return period.

3.4.3.1.2 10 year return period event

It was defined a synthetic precipitation event with a return period of 10 years, obtained from IDF curves published for Portugal by Matos e Silva, 1986. The total event duration was set to 4h and the precipitation distributed according to Matos, 1987 with a centred peak during 20 minutes and the precipitation volume of the period before maximum is 1.5 times the period after the maximum (Figure 13Figure).

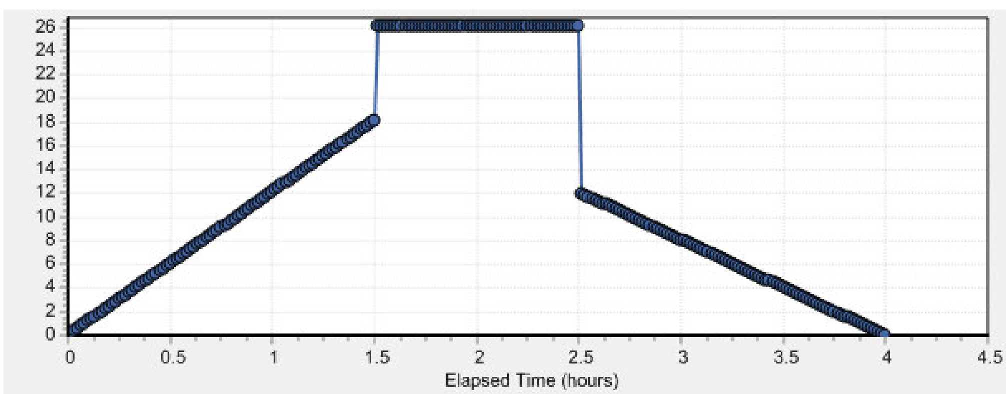

Figure 13. Precipitation event (mm/h) for 10 year return period.

The imposed precipitation results in input flows to the drainage system around 7-9 m^3/s in the peak of the event for the two main streams that enter in the two main storm water branches (Figure 14Figure). Remind that the flows in the observed events had a maximum flow of around 2 m^3/s and no flood occurred.

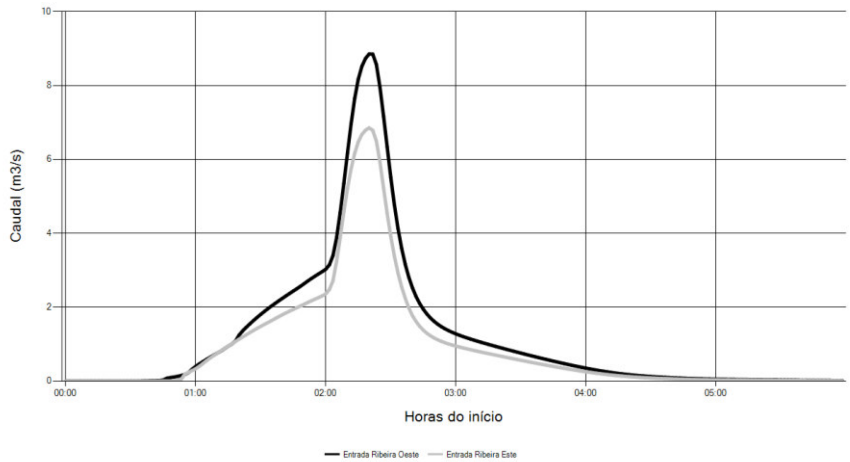

Figure 14. Estimated flow at the entrance of the SWMM network in each branch (East grey and West black) for the event with return period of 10 years.

In Figure 15Figure is presented for the peak flow instant the pipe percentage full and water columns generated at surface. It can be seen that the domestic system in the downstream part gets at full capacity (upstream parallel network to railway line) as also the storm water system before and after the railway crossing where the open air ditch (downstream parallel network to railway line) tries to divert the excess water that is unable to pass under the railway system.

As a consequence of the high flow compared to the capacity of the system, water column is formed at surface in the main streets and accumulates near the railway elevation, the “Rua da Republica” wall and in the downstream depressions.

It should be noted that the origin of the overflow is not only in the railway passage but generally around the network since the input stream flow is higher then the system capacity. However upstream of the tunnel it is shown that the network gets constantly at full capacity and promoting surface flooding.

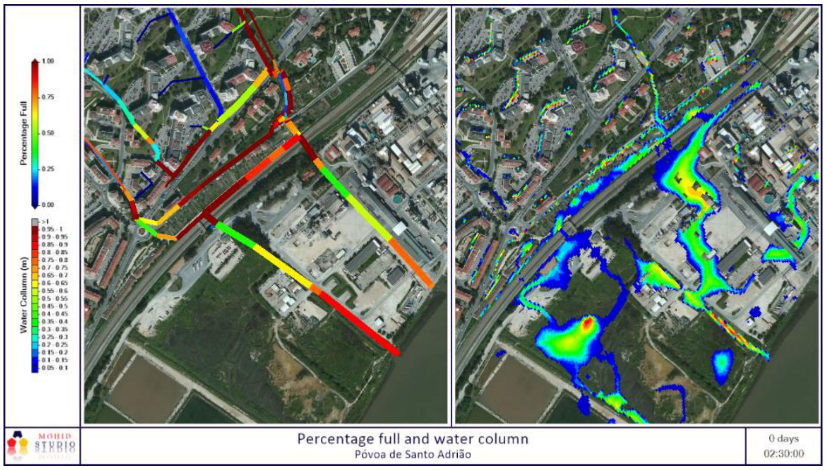

Figure 15. Pipes percent full (left) and water column (right) for the instant with higher flows during the 10 year return period event for current situation.

3.4.3.2Management Scenario

The modelling study integrating the field campaigns surveys showed that exist a couple of bottlenecks that tend to reduce the drainage system flow capacity:

- In the two storm water branches (East and West) during the railway crossing the section is greatly reduced from around 1m deep to up 0.5m or less that associated to low slopes difficult the flow progression.
- In the West branch it was observed during field campaigns the occurrence of silting that even reduce more the system capacity. In the East branch it was not observed but the observed flows (in the same order as the ones in West branch), suggest that the same is occurring.

It was created a management scenario, where infrastructural changes were performed in the identified bottlenecks to check the impact on the volume of water that exits the sewer system and flood extension.

The scenario created duplicated the width of the pipes in the railway crossing and removed any obstacles related to silting that were added to represent the actual situation.

3.4.3.2.1 10 year return period event

The scenario with the infrastructural changes was run with the same forcing as actual situation for comparison.

In Figure 16 is presented the pipe percentage full for the instant 1 hour before the maximum flow and in Figure 17Figure the same but for the maximum flow snapshot. It can be seen that for the maximum flow instant (lateral flows into the urban system around 7-9 m^3/s) the actual situation and management scenario results in terms of pipe utilization is very similar, being both at full capacity in most part of the downstream network around the railway crossing. This happens because the inflows to the storm water system, at the maximum flow instant, are so high that even with infrastructural changes, the system gets to full capacity.

However, for the instant 1h before max flow, inflows are on the order of 2 m^3/s (that the storm water system can tackle) and the infrastructural measures reduce the bottleneck factor that the railway crossing produces by releasing more flow downstream and so the upstream pipes are far from full capacity, while in the actual situation, even with 2 m^3/s they would be almost full.

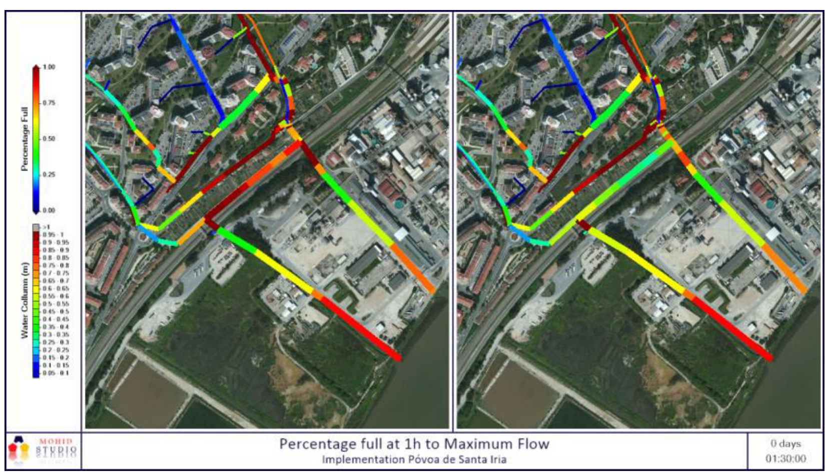

Figure 16. Pipes percent full in actual situation (left) and in management scenario (right) for the instant 1h before higher flows during the 10 year return period event.

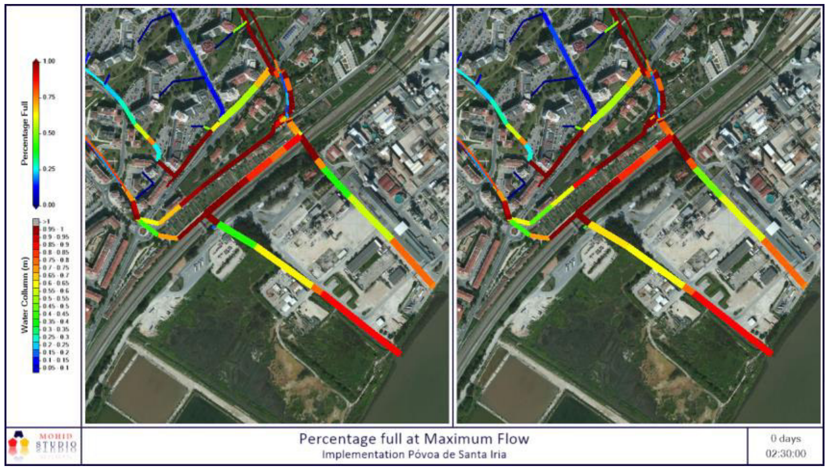

Figure 17. Pipes percent full in actual situation (left) and in management scenario (right) for the instant with higher flows during the 10 year return period event.

In terms of flooding extension differences it is presented in Figure 18Figure on top the water columns at the maximum flow instant and on bottom a zoom to the “Rua da Republica” that is a critical area that usually floods. The water columns are higher in accumulation zones as the railway line, the “Rua da Républica” wall and downstream flat areas where columns range from 5 to 20 cm (blue colours) to around 30 to 50 (green colours). The water column reduction due to infrastructure changes is around 5 cm (15% reduction) in the “Rua da Republica”.

The integrated model water balance shows that the total volume that SWMM overflowed to MOHID Land in actual situation with 10 year return period event was around 17 000 m3 (around 35% of total stream inflow) and with infrastructure changes it reduced to around 12 000 m3 (around 30% reduction). This is consistent with the 5cm reduction verified in “Rua da República” since the flooded area is in the order of 100 000 m2.

It should be noted that the 10 year return period event creates inflows to the drainage system that start overflowing almost in the entire system generating surface runoff throughout and making the infrastructure changes to have less impact in flooded area extension (the origin of the flooding is generalized throughout the system). Also the fact that the downstream areas are very flat makes that changes in volume are less visible.

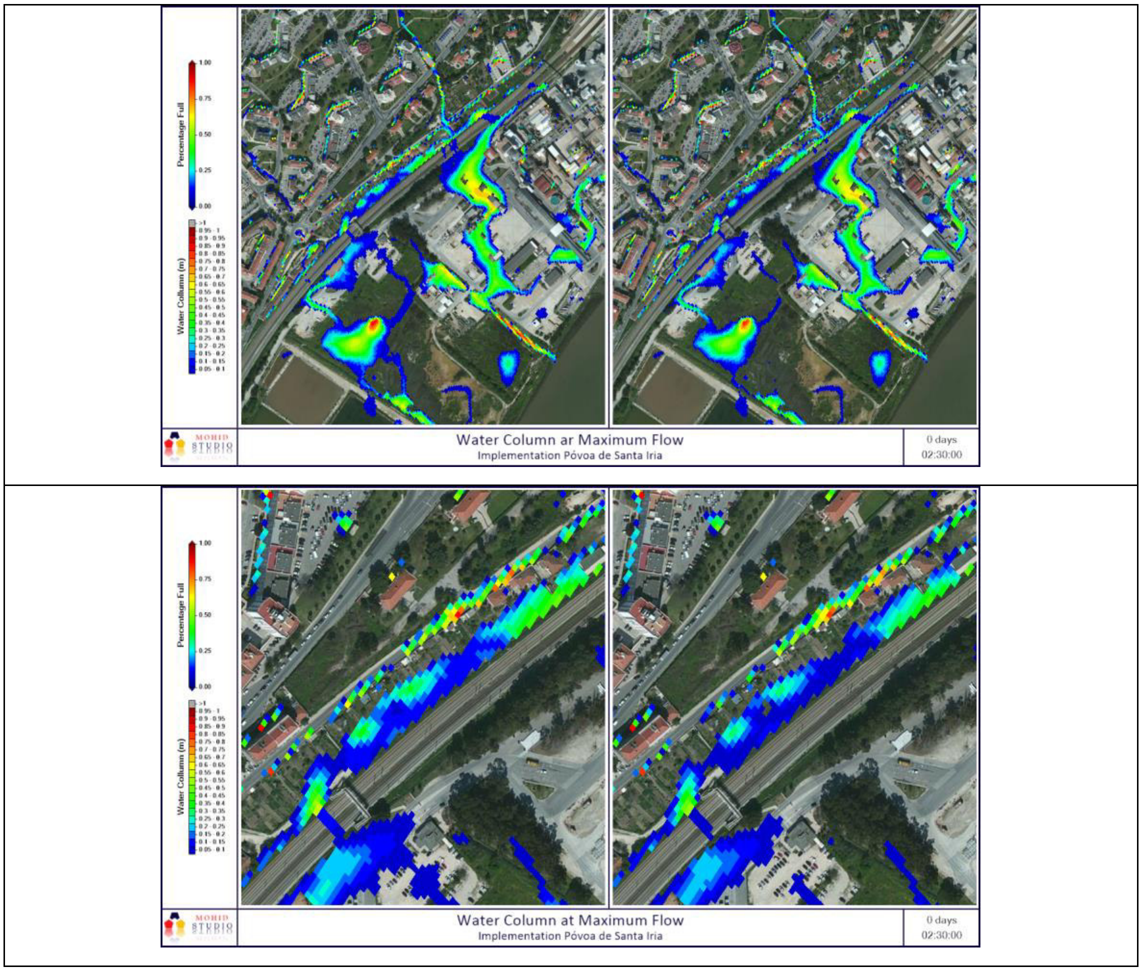

Figure 18. Water column in actual situation (left) and in management scenario (right) for the instant with higher flows during the 10 year return period event. Bottom – detail over Rua da República.

3.4.4 Conclusions

It was implemented an integrated model for surface water – urban drainage using MOHID Land and SWMM, run in parallel to describe the actual situation and determine flooding key aspects and to test management scenarios that could reduce flooding.

It was carried out field work using pressure and velocity sensors to measure levels and flows and to compare to field data. The comparison shows that the integrated model was able to represent both the same trends and order of values as observed data (R^2 from 0.7 to 0.9 and NS from 0.6 to 0.8), being suited for estimating the system behaviour under flood conditions.

Model results and field data showed that there is a big constraint in pipe dimension as one approaches railway line and during its crossing where storm water pipe dimensions go from 1m depth to less than 0.5m and around 0.1-0.2 m in areas that suffer from siltation (tide influence). The model results show that cross section reduction makes that the pipe capacity is rapidly completed upstream of the line crossing what originates overflow and flooding.

The integrated model was run for a synthetic 10 year return period event for actual situation and for a scenario where cross sections near railway line were increased (in some areas doubled and removed siltation obstructions) and the overflow volume was reduced by 30% what reduced around 5cm in water column in one critical area when floods occur ("Rua da República").

The observed data events had return periods below 2 years and there was no signficant overflow (stream inflows up to a maximum of 2 m^3/s). The 10 year return period event resulted in stream inflows around 7-9 m^3/s that surpassed the system capacity not only in railway crossing but generally in all system, making that flooding extension reduction due to infraesructural changes only near railway crossing not so significant. However, the present work suggests that for return periods between the 2 years and 10 years, where the majority of the system has capacity to tackle stream inflows and the bottleneck will exist mostly on railway line crossing, the infrastructural changes may be more effective in reduction flood extension. It should be investigated further the system behaviour under this events and the possibility of infrastructure measures in a broader area or other types (e.g. taking advantage of upstream system network with available volume, reservoir construction for flood dampening, etc).

Acknowledgments

The present work was done in the scope of the project “Póvoa de Santa Iria pumping station design and urban storm water system behaviour” from SIMTEJO and delivered by Engidro, Hidra and Action Modulers.

References

Bach, P.M., Rauch, W., Mikkelsen, P.S., McCarthy, D.T., Deletic, A. (2014) A critical review of integrated urban water modelling – Urban drainage and beyond, Environmental Modelling & Software, Volume 54, April 2014, Pages 88-107, ISSN 1364-8152, http://dx.doi.org/10.1016/j.envsoft.2013.12.018.

Bates, P. D. (2012), Integrating remote sensing data with flood inundation models: how far have we got?. Hydrol. Process., 26: 2515–2521. doi: 10.1002/hyp.9374

Bates, P.D., De Roo, A.P.J. (2000) - A simple raster-based model for flood inundation simulation.J Hydrol, 236 (2000), pp. 54–77

Buahin C. A., Horsburgh, J.S (2015) - Evaluating the simulation times and mass balance errors of component-based models: An application of OpenMI 2.0 to an urban stormwater system, Environmental Modelling & Software, Volume 72, October 2015, Pages 92-109, ISSN 1364-8152, http://dx.doi.org/10.1016/j.envsoft.2015.07.003.

Bulatewicz, T., Yang, X., Peterson, J. M., Staggenborg, S., Welch, M., Steward, D.R. (2010) - Accessible integration of agriculture, groundwater, and economic models using the Open Modeling Interface (OpenMI): methodology and initial results. Hydrol. Earth Syst. Sci., 14, 521–534, 2010.

Chen, A.S., Evans, B., Djordjević, S., Savić, D.A. (2012) Multi-layered coarse grid modelling in 2D urban flood simulations, Journal of Hydrology, Volumes 470–471, 12 November 2012, Pages 1-11, ISSN 0022-1694, http://dx.doi.org/10.1016/j.jhydrol.2012.06.022.

Gallegos, H.A., Schubert, J.E., Sanders, B.F. (2009) - Two-dimensional, high-resolution modeling of urban dam-break flooding: A case study of Baldwin Hills, California, Advances in Water Resources, Volume 32, Issue 8, August 2009, Pages 1323-1335, ISSN 0309-1708, http://dx.doi.org/10.1016/j.advwatres.2009.05.008.

ENGIDRO (2012) - Projeto de remodelação do troço final do coletor doméstico na Rua da República – Póvoa de Santa Iria.

ENHÍDRICA (1997) - Remodelação da Rede de Saneamento de Póvoa de Santa Iria – Cadastro do Sistema.

Guinot, V. (2011) - Multiple porosity shallow water models for macroscopic modelling of urban floods, Advances in Water Resources, Volume 37, March 2012, Pages 40-72, ISSN 0309-1708, http://dx.doi.org/10.1016/j.advwatres.2011.11.002.

HIDRA / ENGIDRO (2014) - Projeto da Execução da EE da Póvoa de Santa Iria e Estudo de Comportamento Hidráulico do Sistema de Drenagem Urbana – Fase A.

Hunter, N. M., Horritt, M.S., Bates, P.D., Wilson, M.D., Werner, M.G.F (2005) - An adaptive time step solution for raster-based storage cell modelling of floodplain inundation, Advances in Water Resources, Volume 28, Issue 9, September 2005, Pages 975-991, ISSN 0309-1708, http://dx.doi.org/10.1016/j.advwatres.2005.03.007.

Hsu, M.H., Chen, S.H., Chang, T.J. (2000) -Inundation simulation for urban drainage basin with storm sewer system J. Hydrol., 234 (1–2) (2000), pp. 21–37

Hurford, A.P., Maksimovic, C., Leitao J.P. (2010) - Urban pluvial flooding in Jakarta: applying state-of-the-art technology in a data scarce environment. Water Sci. Technol., 62 (10) (2010), pp. 2246–2255

Kidmose, J., Troldborg, L., Christian Refsgaard, J. (2015) - Nils Bischoff, Coupling of a distributed hydrological model with an urban storm water model for impact analysis of forced infiltration, Journal of Hydrology, Volume 525, June 2015, Pages 506-520, ISSN 0022-1694, http://dx.doi.org/10.1016/j.jhydrol.2015.04.007.

MAIDMENT D.R. (1993) - Handbook of Hydrology, Editor in Chief, McGrawHill, Inc., 1993, pp 5.1-5.39

MATOS, M. R. S. (1987) - Métodos de Análise e de Cálculo de Caudais Pluviais em Sistemas de Drenagem Urbana - Estudo Referenciado em Dados Experimentais de Bacias Urbanas Portuguesas. Tese para Especialista do LNEC, Lisboa. Portugal.

Merkuryeva, G., Merkuryev, Y., Sokolov, B. V., Potryasaev, S., Zelentsov, V.A., Lektauers, A. (2015) - Advanced river flood monitoring, modelling and forecasting, Journal of Computational Science, Volume 10, September 2015, Pages 77-85, ISSN 1877-7503, http://dx.doi.org/10.1016/j.jocs.2014.10.004.

Preissmann A. (1961) - Propagation des intumescences dans les canaux et rivières. In: Proceedings of the First Congress of the French Association for Computation, Grenoble, France, 1961, p. 433–42.

Salvadore, E., Bronders, J. Batelaan, O. (2015) -Hydrological modelling of urbanized catchments: A review and future directions, Journal of Hydrology, Volume 529, Part 1, October 2015, Pages 62-81, ISSN 0022-1694, http://dx.doi.org/10.1016/j.jhydrol.2015.06.028.

Shrestha, N.K. , Leta, O.T., De Fraine, B. (2013) - OpenMI-based integrated sediment transport modelling of the river Zenne, Belgium. Environmental Modelling & Software 47 (2013) 193e206

SIMTEJO (2012) - Projeto de Reabilitação do Sistema Elevatório de Póvoa de Santa Iria – Estudo Prévio.

Zhu, Z., Oberg, N., Morales, V. M, Quijano, J.C., Landry, B.C., Garcia, M.H. (2016 Integrated urban hydrologic and hydraulic modelling in Chicago, Illinois, Environmental Modelling & Software, Volume 77, March 2016, Pages 63-70, ISSN 1364-8152, http://dx.doi.org/10.1016/j.envsoft.2015.11.014.

3.5 Integrating operational watershed and coastal models for the Iberian Coast: watershed model implementation.

This article describes the MOHID Land operationalisation for Iberian Peninsula and Western Iberia, with not only hydrology but also water quality processes in soil and river and property transport in all mediums what represents the full model capabilities (partially developed during this thesis). With the objective to integrate the water cycle both in land and in coastal areas, providing the best available forecast from inland and solve the river boundary condition problem for coastal models.

Estuarine, Coastal and Shelf Science 167 (2015) 138–146

Contents lists available at ScienceDirect

Estuarine, Coastal and Shelf Science

journal homepage: www.elsevier.com/locate/ecss

Integrating operational watershed and coastal models for the Iberian Coast: Watershed model implementation – A first approach

David Brito, F.J. Campuzano*, J. Sobrinho, R. Fernandes, R. Neves

Maretec – Instituto Superior Técnico, Universidade de Lisboa, Av. Rovisco Pais, 1049-001 Lisbon, Portugal

A R T I C L E I N F O

Article history:
Received 6 October 2014
Received in revised form
20 October 2015
Accepted 27 October 2015
Available online 31 October 2015

Keywords:
Western Iberia
Numerical modelling
Mohid land
Catchment
Nutrient budget
Iberian Peninsula

A B S T R A C T

River discharges and loads are essential inputs to coastal seas, and thus for coastal seas modelling, and their properties are the result of all activities and policies carried inland. For these reasons main rivers were object of intense monitoring programs having been generated some important amount of historical data. Due to the decline in the Portuguese hydrometric network and in order to quantify and forecast surface water streamflow and nutrients to coastal areas, the MOHID Land model was applied to the Western Iberia Region with a 2 km horizontal resolution and to the Iberian Peninsula with 10 km horizontal resolution. The domains were populated with land use and soil properties and forced with existing meteorological models. This approach also permits to understand how the flows and loads are generated and to forecast their values which are of utmost importance to perform coastal ocean and estuarine forecasts. The final purpose of the implementation is to obtain fresh water quantity and quality that could be used to support management decisions in the watershed, reservoirs and also to estuaries and coastal areas.

A process oriented model as MOHID Land is essential to perform this type of simulations, as the model is independent of the number of river catchments. In this work, the Mohid Land model equations and parameterisations were described and an innovative methodology for watershed modelling is presented and validated for a large international river, the Tagus River, and the largest national river of Portugal, the Mondego River. Precipitation, streamflow and nutrients modelling results for these two rivers were compared with observations near their coastal outlet in order to evaluate the model capacity to represent the main watershed trends. Finally, an annual budget of fresh water and nutrient transported by the main twenty five rivers discharging in the Portuguese coast is presented.

1. Introduction

In recent decades, the population increase in urban areas led to a spatial concentration of water demand for production and irrigation. This demand was generally compensated by using surface water, which in the Iberian Peninsula present a high inter-annual variation, constraining water management decisions. In addition, population concentration in alluvial plain areas increased the need of appropriate flood risk policies and action plans in order to prevent and mitigate flooding episodes.

In order to obtain the appropriate information for water resources planning and management, river monitoring networks were designed and implemented. The hydrometric network in Portugal was observing streamflow and precipitation until the 90's or 00's while water quality monitoring started in the 00's. Due to economic constraints, the amount of active stations and the data reliability from the Portuguese hydro-meteorological network has been declining as a result of the maintenance interruption of the automatic monitoring stations since the beginning of the 2010's and field data collection in Portugal is nowadays quite sparse. The Portuguese case is part of a more general trend in hydrometric networks decline observed in many countries around the world (Mishra and Coulibaly, 2009).

A way to reduce the uncertainty of the quality and quantity of the fresh water resources is through mathematical models. Numerical models, once validated, could fill data gaps and link sources of pressure to the observed state in the catchment and allow scenario testing. Watershed models first appeared in the 50's – 60′s making the focus on water - the called rainfall-runoff modelling – (Donigian and Imhoff, 2002), and not until the 70′s did water

* Corresponding author.
E-mail address: campuzanofj.maretec@tecnico.ulisboa.pt (F.J. Campuzano).

http://dx.doi.org/10.1016/j.ecss.2015.10.022
0272-7714/

quality begin to gain notice, with models focusing in the soil loss and nutrient and pesticide export to rivers (Horn et al., 2004).

In the next decades the need for management-oriented process integration led to the development of watershed models with detailed land management such as the SWAT model (Neitsch et al., 2005) which is a semi-distributed watershed model with a strong semi-empirical component that reduces running time over large basins, but strongly increases the need for field data prior to model implementation.

In last decade, distributed physically-based models developed with the increasing computation capacity reducing the number of model empirical parameters and thus increasing model applicability in systems lacking data. Two examples are the MIKE SHE model (Refsgaard and Storm, 1995) and the SHETRAN model (Ewen et al., 2000) which were both originated from the SHE model (*Système Hydrologique Européen*) and are a reference in the generation of physically-based, integrated, distributed watershed models. Conceptually, these models and MOHID (Neves, 2013) are very close; nevertheless the former use finite-differences as the numerical method while MOHID Land uses finite-elements and the equations are solved for volumes ensuring, by default, mass conservation.

In this work, we present the tools, methodologies and a preliminary validation as the base to obtain accurate forecasts of fresh water quantity and quality that could be used to support modellers and managers targeting large regions at different scales, such as watersheds, reservoirs, estuaries, and coastal areas.

2. Study area

The study area covers the entire Iberian Peninsula with a surface area around 580 000 km^2 and more specifically to the rivers discharging in the Portuguese coastal area. Iberia presents several largest rivers including the Douro River (area ca. 100 000 km^2), the Tagus and the Ebro rivers (area ca. 80 000 km^2), the Guadiana River (area ca. 70 000 km^2) and the Guadalquivir River (area ca. 60 000 km^2) that, with the exception of the Ebro River, have international character sharing their catchment between continental Spain and Portugal and discharging on the Atlantic Ocean draining on its way almost two thirds of the territory. For the scope of the validation of the presented methodology study, we will focus mainly on the Tagus River with a total length ca. 1000 km, the longest river of the Iberian Peninsula, and the Mondego River, the longest river located exclusively in Portuguese territory (Length 230 km, area 6.600 km^2).

The determination of the rainfall is of the utmost importance, as it is a primary variable in most hydrological models. The precipitation in the Iberian Peninsula is characterized by high spatial and temporal variability because of a complex orography and diverse atmospheric regimes. Mean annual precipitation varies between more than 2000 mm in the northwest coast and less than 200 mm in the south-eastern coast (AEMET and IM, 2011).

In Iberia most of the precipitation falls between October and May and is produced by large-scale atmospheric perturbations that originate in the Atlantic sector and move eastwards (Serrano et al., 1999; Santos et al., 2005). During winter, western Iberia is affected by westerly winds, influenced by the position of the Icelandic low, that carry moist air and produce rainfall events mainly in northern Portugal. The precipitation is intensified by the passage of cold fronts associated with families of transient depressions and more efficient when the Icelandic low is very deep and shifter southwards (Trigo et al., 2004). In addition to the seasonal character, the Iberian Peninsula is also characterized by a strong inter-annual precipitation variability presenting very wet and dry years occur with some frequency affecting the hydrological cycle and by consequence the river flow and water resources (Trigo et al., 2004; Paredes et al., 2006).

3. Materials and methods

3.1. Modelling grids

Two domains covering the Iberian Peninsula (IP domain) and the Western Iberia (WI domain), with 10 km and 2 km horizontal resolution respectively (Fig. 1), were populated using the NASA SRTM three arc-second digital terrain elevation, that in the studied area has a horizontal resolution of 70–90 m (Farr et al., 2007). The IP domain, with 80 $\times$ 130 cells in horizontal and 8 vertical layers, allows the reproduction of large trans-boundary rivers discharging in Western Iberia as the Tagus, Douro and Guadiana rivers at their natural state. The WI domain, 250 $\times$ 160 cells in horizontal and 8 vertical layers, provides high resolution results for Portugal and the Galicia region (Northwest Spain), encompassing watersheds up to 10 000 km^2.

Along with the topographic data, the model was provided with land use and soil properties. In order to have a common source for both modelling domains, the Corine Land Cover 2006 – CLC2006 (EEA, 2007) with a resolution of 100 m was used to derive crop types for the vegetation growth model, surface impermeabilisation and Manning resistance following Van der Sande et al. (2003) and Chow (1959) suggested correspondences.

The soil hydraulic permeability and retention capacity control the infiltration and groundwater movement and surface water quantity. Soil map distribution and hydraulic characteristics, necessary to specify the van Genuchten model parameters, were obtained from the Joint Research Centre database (http://eusoils.jrc.ec.europa.eu/) for both domains with a 900 m resolution.

In the absence of detailed information on agricultural practices in a wide area as the Iberia Peninsula, it was used the auto-fertilization concept from SWAT model. In practical terms, this means that agricultural practices are assumed to be optimal since the fertilization occurs according to the plant needs. Maximum values of 50 kg/ha.day and 200 kg/ha.year of fertilizer where considered based on the good agricultural practices guide for Portugal (DGADR, 1997).

The objective of this model implementation was to represent the large scale hydrological and water quality processes, including evapotranspiration and river discharges, and not the local processes associated for example with land use changes smaller than the cell size. More detailed approaches can however be implemented in areas of interest having the boundary conditions given by the Iberia Peninsula or Western Iberia model applications.

The atmospheric boundary conditions for the WI domain were obtained from the MM5 model (Grell et al., 1994) with a horizontal resolution of 9 km implemented by the IST meteorological group (http://meteo.ist.utl.pt). For the IP domain, results from a WRF model (Skamarock et al., 2005) application with 12 km resolution computed by Meteogalicia (http://www.meteogalicia.es) were used as atmospheric forcing. Both meteorological models results were interpolated to the MOHID Land grids.

3.2. MOHID land model

The MOHID Land model is the catchment component of the MOHID Modelling System (Neves, 2013; http://www.mohid.com). The MOHID land model is a 3D distributed, continuous, physically based, variable time step model using a finite-volume approach based on mass and momentum balance equations. The simulated processes include interception and evaporation in leafs, infiltration and evapotranspiration in soil/vegetation, vegetation growth,

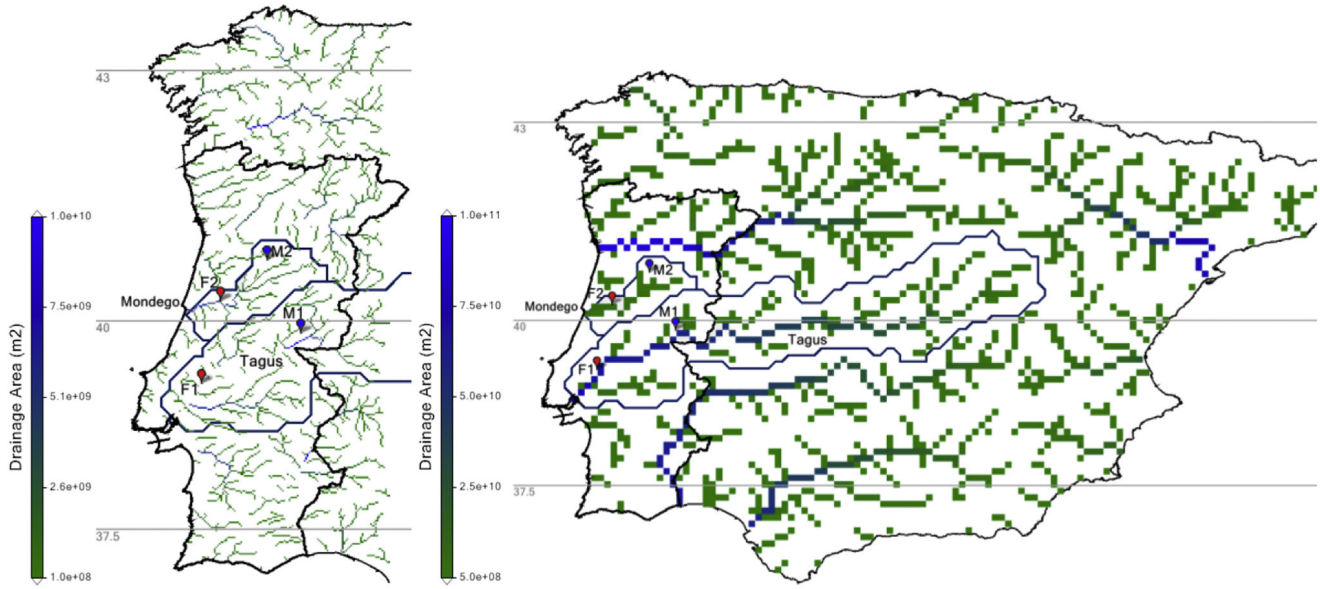

Fig. 1. Main water lines in the Western Iberian Peninsula (WI domain, left) and in the complete Iberian Peninsula (IP domain, right) indicating the drainage area obtained with the MOHID Land for the 2 and 10 km resolutions respectively and the location of the hydrological (F1 and F2) and meteorological (M1 and M2) stations used for the model validation. The drained area by the Mondego River and the Tagus River appears enclosed by continuous lines in both domains.

routing of water trough surface runoff, porous media or river network and water quality processes, i.e. mineralization, nitrification, denitrification in porous media and rivers, including primary production (Trancoso et al., 2009). Sediment transport and erosion/deposition are also computed for surface waters. The main innovation for this application was the simultaneous simulation of all watersheds without the need of identifying catchment limits and outlets, as is common practice on most watershed models.

MOHID Land is an integrated model grouping four compartments or mediums - atmosphere, porous media, soil surface and river network – moving water through the mediums based on mass and momentum balances. Atmosphere forcing provides the necessary data for imposing surface boundary conditions i.e. precipitation, solar radiation, wind, air temperature and moisture. Surface land is described by the 2D horizontal grid used by the porous media module. The surface elevation is specified in each grid cell centre using a digital terrain model (DTM). Porous media is computed as a 3D domain with the same horizontal grid as the surface runoff layer, and a vertical grid, allowing variable layer thickness. The river system is defined as a 1D network extracted from the DTM and formed by reaches linking surface cell centres.

MOHID model uses a finite-volume approach for computing state variables and fluxes. Each grid cell is a control volume, being the state variables computed in their centres and the fluxes and associated variables on the cell faces. Surface runoff over the ground and river network is solved using the full St. Venant (Equation (1)) and mass conservation equations (Equation (2)).

St. Venant equation

$$\frac{\partial Q_i}{\partial t}+\frac{\partial u_j Q_i}{\partial x_j}+gA\left(\frac{\partial h}{\partial x_i}\right)-gA\left(S_0-S_f\right)_i=0 \tag{1}$$

Mass conservation equation

$$\frac{\partial Vol}{\partial t}+\int\limits_{S_{Vol}}(u_j n_j)dS_{Vol}=0 \tag{2}$$

where Q is water flow (m^3 s^{-1}), u is the water velocity, A is the cross flow area (m^2), g is gravity acceleration (ms^{-2}), h is water depth (m), S_0 is the bottom slope, S_f is the bottom friction slope, the slope that balances the friction force, and x is the space coordinate, S_{Vol} is the surface that encompasses the finite-volume.

The porous media in MOHID Land is a 3D domain including saturated and non-saturated zones. The flow is driven by the total pressure head (H) which accounts for gravity, the matric potential in unsaturated areas and hydrostatic pressure in saturated areas. Per unit of area the flux is given by Equation (3):

Water flux in the ground.

$$\Phi_i=-k(\theta)\frac{\partial H}{\partial x_i} \tag{3}$$

where $k(\theta)$ is the hydraulic conductivity a function of the soil moisture in the unsaturated zone and a constant, the saturated conductivity, in the saturated zone. The rate of accumulation of water per unit of volume in the ground – the rate of change of soil moisture – is the integral of this flux along the surface of the finite-volume (Equation (4)):

Ground water conservation equation

$$\frac{\partial\theta\cdot Vol}{\partial t}+\int\limits_{S_{Vol}}(\Phi_i n_i)dS_{Vol}=0 \tag{4}$$

where θ is cell soil moisture content (m^3 water·m^{-3} soil). If this volume converges to one point, the Richards equation (Richards, 1931) for unsaturated soil is obtained. When the soil is saturated, there is no water accumulation and the integral of the fluxes is zero.

Vegetation growth was computed using the SWAT model vegetation module, based on the heat units concept that drive the plant activity and using crop database for plant potential growth curves (Neitsch et al., 2005). Growth is computed taking into account the limitations due to environmental constraints (i.e. water and nutrients availability, temperature, solar radiation). Potential evapotranspiration is computed using the FAO Penman-Monteith equation (Allen et al., 1998) being effective evapotranspiration computed as a function of root distribution and soil water availability.

Model's compartments are linked dynamically through fluxes computed at the interfaces. The computation of these fluxes requires some hypotheses since the equations solved in each compartment are different, even between the saturated and the non-saturated zones of the porous media. Water flux between the river and the porous media is computed using the head gradient and saturated conductivity. Fluxes between the river and land surface are computed using the free surface gradient and assuming critical flow in case of land flooding. These algorithms permit the explicit simulation of river floods and generate variable river discharge, as a function of the water content and flow along the whole catchment. At the interface between saturated and not saturated zone, there is no real physical interface but equations to compute the pressure and the conductivity change. In order to simplify the convergence procedure cells are considered as being saturated when the soil moisture is between 98% and 100%. In practice this is equivalent to assume a storage capacity as used is models for saturated soils, e.g. MODFLOW, Hoffmann et al. (2003).

Dissolved properties transport in the soil, at surface by runoff and in the river is described by the advection diffusion equation (Equation (5)) where β is any property concentration (mgl^{-1}), ϑ is diffusivity (m^2 s^{-1}) and (S_o−S_i) is difference between the sources and the sinks of β integrated inside the finite-volume.

Advection−Diffusion Equation

$$\frac{\partial\theta\cdot\beta\cdot Vol}{\partial t}+\int_{S_{Vol}}\beta(\Phi_i n_i)dS_{Vol}=\int_{S_{Vol}}\left(\vartheta\frac{\partial\beta}{\partial x_i}\right)n_i dS_{Vol}+(S_o-S_i) \qquad (5)$$

In order to simulate carbon, nitrogen and phosphorus cycling in soil, the Root Zone Water Quality Model (Ahuja et al., 2000) was coupled to MOHID Land thus being able to represent soil bacteria activity that drives mineralization, nitrification and denitrification processes. The decays rates are dependent on temperature, salinity, nutrient availability, substrate and carbon in the case of heterotrophs.

MOHID Land computes algae activity, nutrient assimilation, mineralization, nitrification/denitrification processes taking place in rivers using an algorithm initially based on the WASP model (Wool et al., 2001) that has been updated to simulate extra processes (Mateus et al., 2012), including macroalgae (Trancoso et al., 2005) and the competition between these and benthic herbs (Ascione−Kenov et al., 2013).

Regarding particulate material transport in river and surface runoff, the erosion/deposition processes are calculated based on Partheniades (1965) depending on surface shear, sediment strength and deposition velocity. Erosion occurs when the ambient shear stress exceeds a limiting threshold and deposition occurs when the ambient shear stress is lower than that specified threshold (Trancoso et al., 2009; Franz et al., 2014). Table 1 summarizes the model main parameters, their typical values and references.

MOHID Land has been applied from plot to watershed scales. At a watershed scale the model was used in the FP7 ‘MyWater’ research project focused on obtaining reliable information on water quantity, quality and usage for appropriate water management. The model was applied to Tâmega River in the Douro watershed, Portugal, to quantify water input to the reservoir and model results were compared to available data (http://mywater-fp7.eu/). Furthermore, MOHID Land model was applied in an integrated approach with the reservoir model MOHID Water and SWAT in Enxoé, Portugal to depict the origin of this eutrophicated reservoir and its results compared to field data (Eutrophos https://eutrophosproject.wordpress.com/, Mirage http://www.mirage-project.eu/and Aguaflash http://www.aguaflash-sudoe.eu/research projects). The model was also applied to natural wetlands, Ebro and Bidasoa in Spain, Garonne (France) and Tagus (Portugal), to determine natural depuration potential and its results compared to piezometer data in the context of Attenagua project (http://www.attenagua-sudoe.eu/).

An example of a plot scale implementation is the Nitrosal project, created to determine salinity effect on crop production and where the model was applied to a 1D soil column in Alvalade (Portugal). Other examples include Aquapath-Soil (www.agro-evapo.eu) and Figaro (www.figaro-irrigation.net/). European research projects, which aimed at crop optimization and end-user support.

3.3. Operational modelling

The pre-processing of meteorology, model preparation and execution and model post-processing are handled by the operational Automatic Running Tool (ART), a software for model simulations automation developed at Instituto Superior Técnico. The ART tool pre-processes inputs from different sources needed to run the model; executes the Mohid Land using the configured files and store, graphs and distributes the model results via OPeNDAP, smartphone and Webpages (Fig. 2). The simulated period started in January 2010 and is currently running and producing forecasts for both domains that can be accessed at http://forecast.maretec.org/.

4. Results and discussion

In order to validate the methodology, modelling results were compared with river monitoring data from the Portuguese National Institute for Water (INAG) published in their portal SNIRH (http://www.snirh.pt). Due to the monitoring network constraints regarding availability and quality of the observed data for the current decade, the meteorological data was obtained from the internet database tutiempo.net (http://www.tutiempo.net).

Monthly averaged meteorological and hydrological data, including nutrient concentrations were compared with model results to evaluate the model ability a) to represent the main trends in observed data and b) to forecast river loads to coastal areas, which is one of the main objectives of the models implementation. Several monitoring stations near the each river mouth were selected to evaluate the meteorological, river flow and water quality properties

Table 1
MOHID Land model parameter description.

Parameter description	Variability	Values	Reference(s)
Manning-Strickler's roughness coefficient	From land use map	0.01 to 0.3	Van der Sande et al., 2003, Chow 1959
Impermeable Area (%)	From land use map	0.5−1 in urban, artificial areas and 0 in forest and agricultural areas	–
Feddes vegetation stress heads (m)	From land use map	−0.01 to −30	Feddes et al., 2001
Soil van Genuchten hydraulic parameters	From soil map database	–	–

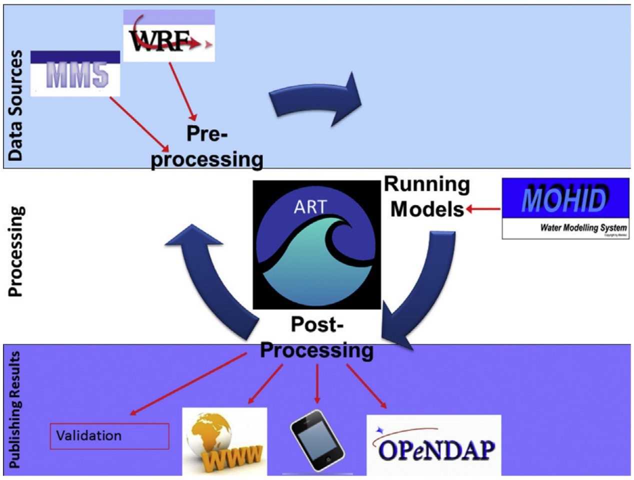

Fig. 2. General scheme of the Automatic Running Tool (ART) where it can be distinguished the pre-processing, modelling and post-processing cycle of operations including only elements used for the WI and IP Mohid Land applications.

as no single stations collect all these properties.

The IP domain modelling results were evaluated by comparing the modelling results for the Tagus River, the longest estuary of the Iberian Peninsula, with atmospheric and hydrometric observations. Precipitation results obtained from the WRF model application were compared with the Castelo Branco station (M1 in Fig. 1, 39.83N and 7.48W) in the Tagus catchment. The modelled river flow was compared with the streamflow measured at Almourol station (F1 in Fig. 1, 39.22N, 8.67W), located 70 km off the head of the estuary. The Ómnias station data, located some 30 km downstream from the Almourol station was used to validate water properties.

The largest Portuguese non-transboundary river, the Mondego River, was used for evaluating the WI domain modelling results. The Açude de Coimbra station located in the city of Coimbra (F2 in Fig 1, 40.22N, 8.44E) located around 40 km afar from the coast, was used to perform flow and water properties validation and the Viseu station (M2 in Fig 1, 40.71N, 7.88E); was used to assess the MM5 precipitation results.

4.1. Meteorology and hydrology for the Tagus and Mondego rivers

Monthly averaged observations and modelling results – precipitation and flow - for the Tagus and Mondego rivers are shown in Fig. 3 for the period between January 2011 and December 2013. Table 2 shows the statistical parameters for the comparison of meteorological and watershed modelling results and field data observations. Precipitation computed by MM5 (9 km grid) and WRF (12 km grid) display a similar agreement with the data being both able to match most of the rain events. They are able to represent the main trends of the automatic monitoring stations and display peaks with identical magnitude both achieving coefficients of determination (R^2) around 0.9 as a consequence it can be concluded that both MM5 and WRF models for the WI and IP domains respectively reproduce significantly the precipitation patterns observed in the data collected by tutiempo.net (Fig. 3a and b) and are adequate to force the hydrological models. Both stations present a similar distribution of rain for the studied periods as rainfall is associated to the same originating mechanism though peaks are more intense in the Mondego watershed and presenting on average a larger abundance of precipitation following the typical North to South pattern present in the Portuguese territory.

Modelled streamflow shown in Fig. 3(c and d) follows a pattern consistent with the rainfall (Fig. 3a and b). We should take into consideration that the modelling results are reproducing the watersheds without any human intervention apart from nutrient input due to agricultural practices and thus water removed from their courses for irrigation, human consumption or accumulated in water reservoirs and dams are not considered in this first version of the model.

During the dry season flows are low and thus measured and simulated values are almost identical. The model predicts an increase in flow values as soon as the raining season in autumn starts, however measured values remain low. In winter and spring the agreement increases again. The difference of behaviour between measured and simulated discharges is attributed to the fact that after the summertime reservoirs storage is at its minimum and consequently they accumulate most of the inflowing water. In winter, reservoirs are close to their maximum capacity so they collect a lower portion of the rainwater and thus the river flow is similar to its natural flow.

In Fig. 4, river modelled flows from the WI and IP domains are compared with observations for the Tagus River station (F1 in Fig. 1). The WI river flow would correspond to the rain water collected mainly in the Portuguese territory (Fig. 1), assuming that no water is flowing from Spain, while the IP river flow would correspond to the complete watershed. In this figure, it can be observed that both curves coincide during the dry periods, while the observed values are closer to the WI flows after the beginning of the rain periods, indicating that most of the water is retained upstream, and as the rainy season progresses the observed values approaches the IP curve indicating that the reservoirs are close to reach their full capacity and the river discharge is similar to the natural flow. It can be concluded that discharges computed in autumn without considering the reservoir storage would be overestimated. This effect would increase along with the catchment size. If the Tagus River is regarded considering only its Portuguese part of the catchment, the forecasts improve, except during rainy winters. This means that the impact of the Portuguese reservoirs on the discharge is much lower than the impact of the Spanish reservoirs, as 70% of the catchment is located in Spanish territory.

In any case, the modelled flow for the whole Tagus and Mondego catchments, without considering reservoirs storage, obtained satisfactory R^2 values around 0.6 (Table 2). This range of values are similar to the ones obtained in similar case studies as Yang et al. (2014) obtained for 3 watersheds from 30 to 300 km^2 in USA. However, in natural watersheds values of R^2 values usually range from 0.6 to 0.9 as the works of Fohrer et al. (2001) in two watersheds in Hesse, Germany (R^2 of 0.71 and 0.92), Geza and McCray (2008) in a 126 km^2 watershed in Denver, USA (R^2 of 0.62 and 0.74) or Green and van Griensven (2008) in small watersheds in Texas, USA (R^2 0.60 to 0.96). The modelling results could be improved by including the effect of the reservoirs in the simulations. For that reason, the modelling results would tend to be closer to the observed values as the degree of human intervention is lower.

Fig. 5 shows the Mondego river flow, observed and modelled, and the water level in the Aguieira Reservoir (40.34N, 8.20W), the main reservoir in the catchment. This reservoir is used for power generation, flood control, water supply and irrigation. The figure shows that when the model computes excess flow the level in the reservoir increases. This result explains the origin of the differences between measured and computed flow and indicates the importance of the inclusion of reservoirs in future versions of the hydrographic model. The scenario without reservoirs had the advantage of illustrating their impact in the system. Additionally, in Fig. 5 can be observed how the reservoir volume decreases during

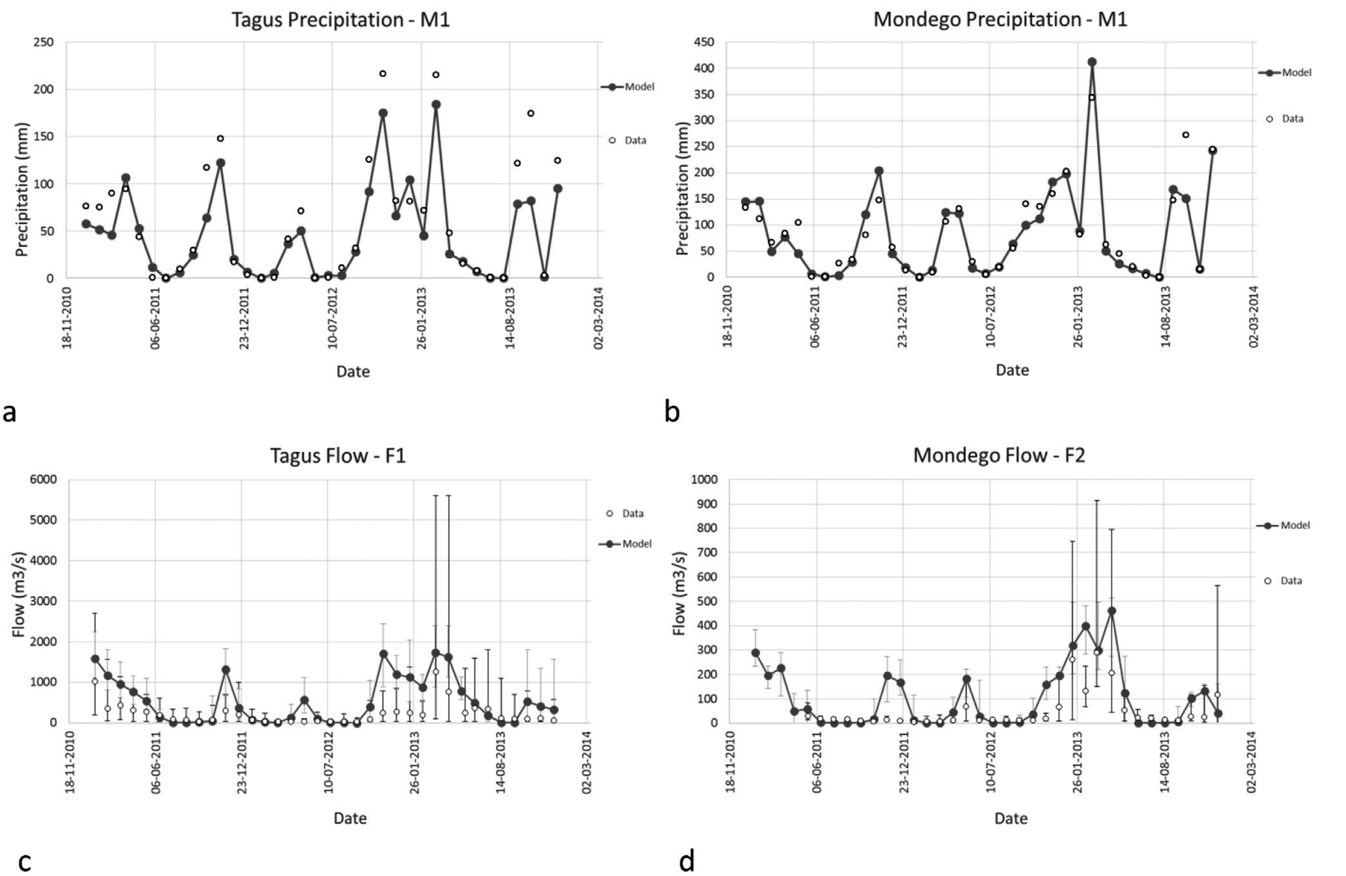

Fig. 3. Monthly averaged modelling results (solid line) and observations (white circles) for the Tagus River (left side) and for the Mondego River (right side) for precipitation (top) and river flow (bottom) for the period 2011–2013. The graphs include error bars for flow observations (black bars) and for the flow modelling results (grey bars). Error bars for model precipitation are not visible, as the standard deviation values are too small.

Table 2
Statistical parameters for the meteorological and hydrometric monthly averages corresponding to the Tagus and Mondego Rivers watersheds in the period 2011–2013 (n = 36).

Station	Watershed	Type	Obs. average	Model. average	R^2	RMSE
Viseu	Mondego	Meteo	86.00 mm	84.08 mm	0.88	30.91 mm
Castelo Branco	Tagus	Meteo	59.77 mm	55.19 mm	0.90	19.83 mm
Açude de Coimbra	Mondego	Flow	48.76 $m^3 s^{-1}$	93.59 $m^3 s^{-1}$	0.60	93.77 $m^3 s^{-1}$
Almourol	Tagus	Flow	228.59 $m^3 s^{-1}$	533.71 $m^3 s^{-1}$	0.59	495.98 $m^3 s^{-1}$

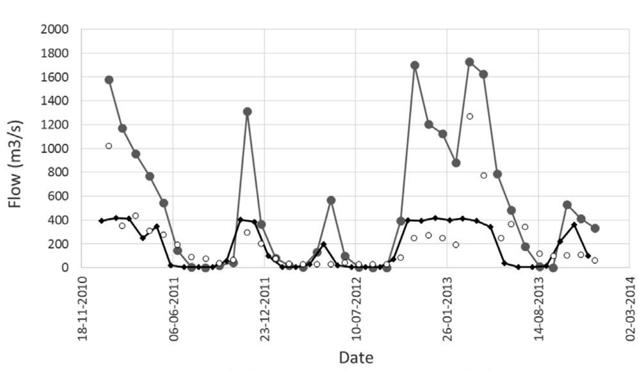

Fig. 4. Monthly averaged modelling results for the Iberian Peninsula domain (solid grey line) and for the Western Iberia domain (solid black line) and observations (white circles) for the Almourol station in the Tagus River (F1 in Fig. 1) for the period 2011–2013.

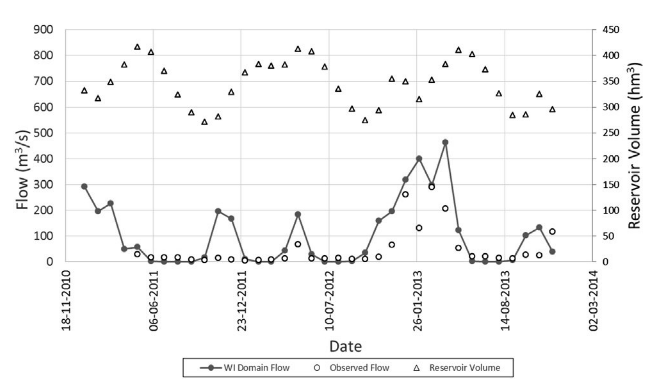

Fig. 5. Monthly averaged modelling results for the Mondego River (solid line), observations (white circles) and volume accumulated in the Aguieira reservoir (white triangles) for the period 2011–2013.

the summer period due to human consumption as that volume has no impact in the observed river flow.

4.2. Water properties for the Tagus and Mondego rivers

Regarding the water properties of the water running in these two rivers, the modelling results for temperature and dissolved nutrient concentrations, nitrate and orthophosphate, were compared with observed values. It should be noted that the number of water quality observations and the limit of detection of the measured are poor to evaluate the water quality on those watersheds. We should also bear in mind the different horizontal model resolution of the modelling domains.

In Fig. 6 are represented monthly averaged measured and computed variables describing water quality for both catchments and in Table 3 describes some statistical indicators. Visual analysis of the figures show that temperature is better described in the Mondego than in the Tagus, nitrate is well described in both catchments apart from two abnormal peaks in both catchments and phosphate is poorly described in the Tagus River water quality station. The temperature and orthophosphate measured values in this Tagus station are usually above the computed, being both abnormally high values for the study area. Both nutrients in the Mondego model present peaks simultaneously during low discharge conditions that were preceded by high flow conditions (Fig. 6 d and f). These concentrations are the result of the mineralisation of the particulate organic matter previously transported by the high run-off. As the water column is low, a small mass of

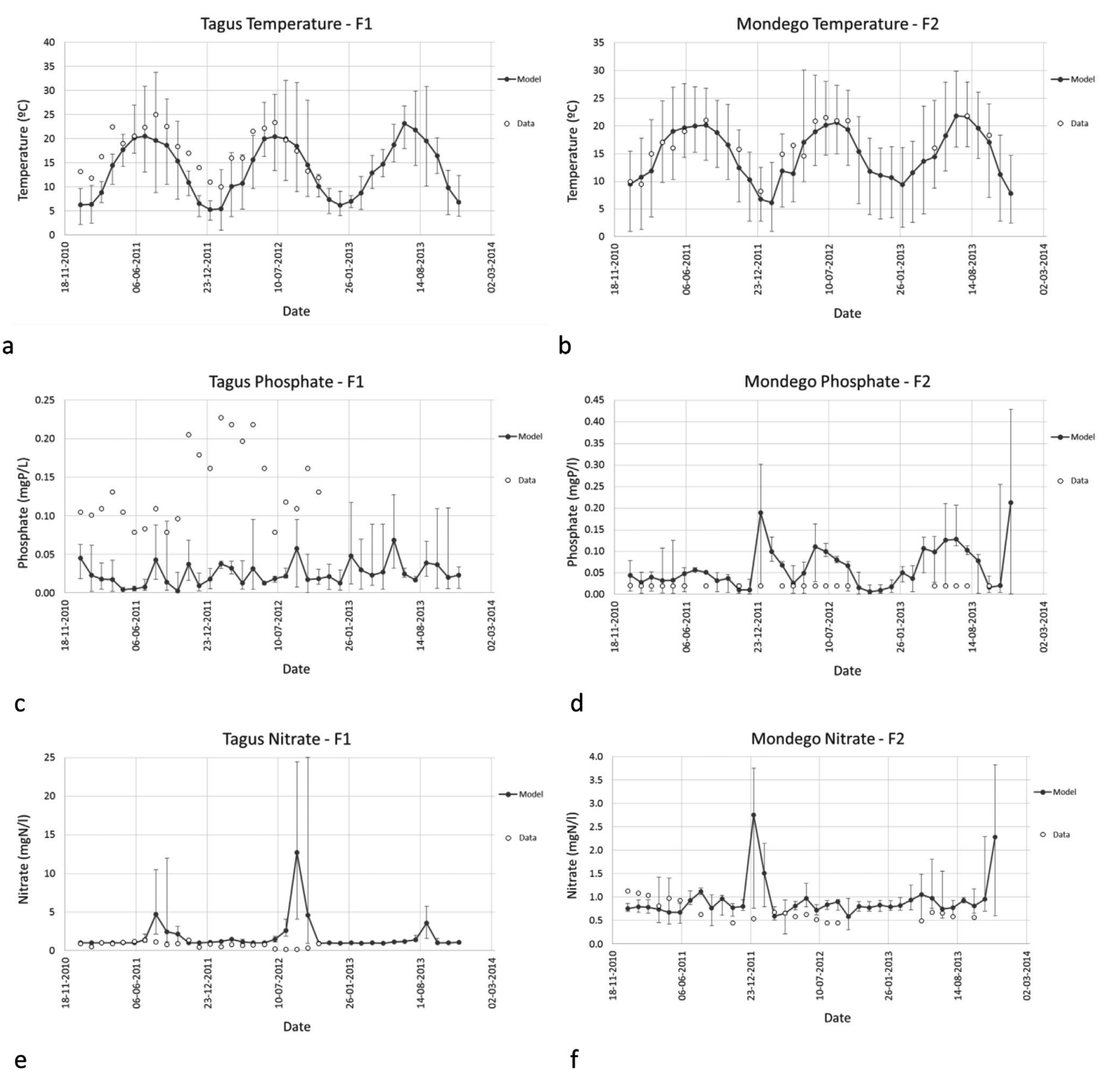

Fig. 6. Monthly averaged modelling results on river water quality (grey line) and station field data (white circles) for the Tagus River (left) and Mondego River (Right); a) and b) temperature (°C); c) and d) orthophosphate (mg P l^{-1}); e) and f) nitrate (mg N l^{-1}). Error bars are only shown for modelling results as the observed values correspond to monthly samples.

Table 3
Simple statistics for the comparison between the observations (Obs.) and modelling results (Mod.) of water properties: temperature (°C), nitrate (mg N l^{-1}) and ortophosphate (mg P l^{-1}) for the 2011–2013 period.

Watershed	Property	Obs. N	Mod. N	Obs. average	Mod. average	R^2	RMSE
Mondego	Temperature (°C)	34	23	16.80	15.10	0.80	5.40
	Nitrate (mg N l^{-1})	36	23	0.70	0.89	0.11	0.38
	Orthophosphate (mg P l^{-1})	32	23	0.02	0.05	0.02	0.05
Tagus	Temperature (°C)	37	23	18.00	14.00	0.75	6.20
	Nitrate (mg N l^{-1})	35	23	0.92	1.80	0.16	2.80
	Orthophosphate (mg P l^{-1})	36	23	0.14	0.02	0.07	0.02

organic matter is able to increase the nutrient concentrations. In the observed nutrients concentrations, the raise was not detected possibly by two reasons: (a) on one hand that high flow was retained by the water reservoirs and (b) in case that part of the organic matter arrived to this reach, the small amount of nutrients could be consumed by benthic primary producers, especially by macrophytes existing along the river bed and not taken into account by this model. The same explanation serves for the peak observed in the Tagus River in August 2012.

4.3. Portuguese river loads

The numerical modelling approach proposed in this study provides the capacity of modelling simultaneously all the watersheds of a certain region delivering an overview of the fresh water reaching the coastal area in terms of flow, temperature and nutrients. Considering that the average volumes and nutrient concentrations for the analysed rivers are correct on average, it was estimated the average annual load for each of the twenty five largest rivers discharging in the Portuguese coast (Table 4). The WI domain was used for most of the Portuguese catchments while the IP domain for the main international rivers: the Douro, Tagus and Guadiana rivers. Table 4 list the fluxes in terms of volume and inorganic nutrients at the end of their watercourse thus obtaining, for the first time, the flow and nutrient budget discharged in the Portuguese coast.

In total, the main twenty five rivers flowing into the Portuguese continental coast discharge in average ca. 82000 H m^3 of fresh water, 215000 Tons of dissolved inorganic Nitrogen and 3300 Tons of dissolved inorganic phosphorus per year. From Table 4 figures, it could be concluded that in natural conditions the Douro River accounts for a third of the nutrients and flow contributions while the Tagus River and the Guadiana River account approximately for the fourth part of the natural contributions to the Portuguese coastal area. All together the small unmonitored rivers represent about 12% of the forecasted discharge for all rivers and thus they also play a relevant role in the coastal areas.

5. Conclusions

Governments worldwide are reducing their efforts in collecting reliable and widespread hydrometric information, which would affect in decision making related to water supply, hydropower, irrigation and other services including drought and flood events warnings or unforeseen adverse impacts on other users (i.e. water logging, salinization, impacts on wetlands, lakes, floodplains, and estuaries) (Mishra and Coulibaly, 2009). This decline, also observed also in Portugal, should be compensated by new methods to complete the information collected by the remaining stations or to produce an estimate value in the watersheds where information is totally absent. In this study, we have explored the use of a numerical model as a valuable tool for completing the observed data.

Table 4
Average river runoff and dissolved inorganic nutrients for the rivers discharging in the Portuguese continental coast during the 2011–2013 period obtained by the MOHID Land simulations. (IP) stands for Iberian Peninsula domain results and (WI) for West Iberia domain results. Rivers are ordered from North to South.

River	Average runoff (Hm^3 y^{-1})	Dissolved nitrogen (Ton y^{-1})	Dissolved phosphorus (Ton y^{-1})
Minho (WI)	7730	15665	172
Lima (WI)	2120	8255	150
Cavado (WI)	1581	3605	27
Ave (WI)	1241	2775	47
Leça (WI)	120	203	4
Douro (IP)	29,359	75049	1119
Vouga (WI)	1869	4447	79
Mondego (WI)	3269	8238	204
Lis (WI)	312	866	23
Alcobaça (WI)	162	334	11
Tornada (WI)	68	176	5
Arnoia (WI)	127	374	11
Grande (WI)	239	399	6
Sizandro (WI)	109	273	9
Lisandro (WI)	67	185	6
Tagus (IP)	16,767	43266	413
Sorraia (WI)	624	1772	52
Sado (WI)	1255	3438	105
Mira (WI)	357	957	18
Odeceixe (WI)	65	150	3
Aljezur (WI)	42	93	2
Arade (WI)	148	411	8
Alcantarilha (WI)	214	495	9
Alcantarilha (WI)	214	495	9
Guadiana (IP)	13,889	42796	843
Total	**81,734**	**214221**	**3327**

The complex pattern of precipitation and hydrology put in evidence the need for sophisticated tools to represent reality and fill conventional data gaps as for the use of modelling. For that reason, we considered that this type of application is valuable tool as a complement to any observing system and also could aid in the explanation of the field data measurements. In this study, the water resource availability in an internationally managed watershed and the fate of rainfall water in a national watershed were used as case studies to show the possible analysis applications that this methodology could support.

Traditionally, watersheds models have been used to reproduce the flow and water properties of a single river catchment while in this new approach the modelling domain could present several outlets that allow to calculate several catchments simultaneously and to obtain the "big picture" of fresh water flow and concentrations for a vast area as the whole Portuguese continental territory or Iberia. This method is generic and could be applied to any region regardless the size or the number of catchments as have been demonstrated with the application with two different horizontal scales to the Portugal and Galicia region and to the complete Iberian Peninsula. With the described architecture, the MOHID Land application is able to estimate the natural flow running in the water lines thus disregarding human consumption, water reservoirs and dams that could influence the amount of water reaching the coastline. These processes would be taken into account in future developments along with further validations in other catchments.

The model was able to represent flow trends and order of magnitude, even at artificialized rivers, of flows and nutrient concentrations and temperature, being a good estimator of the fresh water inputs to the coast. The approach followed to link watershed and coastal models is novel and constitutes a valuable tool for filling data gaps, understanding the nutrient budgets, paths, fate and effect on coastal area and to produce forecast and scenario testing capability, a valuable asset towards an integrated water management. The modelling results are directly used by other downstream models in coastal and estuarine areas producing an original methodology for integrating the water management from the catchment to the open ocean that would be discussed in future research papers (Campuzano et al., 2014).

Acknowledgements

This research was supported by the EMoSEM project, a two-year project (2013–2014) funded by the French National Research Agency (ANR) and the Belgian Science Policy (BELSPO) in the frame of EU FP7 ERA-NET Seas-era. Other papers funded by this project has referred it as SeasERA EMoSEM project (ANR-12-SEAS-0005-01). River flow data were provided by the Portuguese National Institute of Water (INAG) through their portal SNIRH (http://www.snirh.pt). The authors would like to thank the anonymous reviewers for their valuable comments and suggestions to improve the quality of the current manuscript.

References

AEMET, IM, 2011. Atlas climático ibérico/Iberian climate atlas. Agencia Estatal de Meteorología, Ministerio de Medio Ambiente y Rural y Marino, Madrid. Instituto de Meteorologia de Portugal, 80 pp.

Ahuja, L.R., Rojas, K.W., Hanson, J.D., Shaffer, M.J., Ma, L., 2000. Root zone water quality model, modelling management effects on water quality and crop production. Water Resour. Pubns 384.

Allen, R.G., Pereira, L.S., Raes, D., Smith, M., 1998. Crop Evapotranspiration – Guidelines for Computing Crop Water Requirements – FAO Irrigation and Drainage Paper 56. FAO, 1998, ISBN 92-5-104219-5.

Ascione–Kenov, I., de Deus, R., Alves, C.N., Neves, R., 2013. Modelling seagrass biomass and relative nutrient content. J. Coast. Res. 29 (6), 1470–1476.

Campuzano, F.J., Kenov, I., Brito, D., Juliano, M., Fernandes, R., Pinto, L., Neves, R., 2014. Numerical Evaluation of the River Nutrients Influence for the Western Iberian Coastal Region. 3.as Jornadas de Engenharia Hidrográfica. June 2014, Lisbon, Portugal. Extended abstracts: 263-266, pp. 24–26.

Chow, V.T., 1959. Open-channel Hydraulics, 680 pages. McGraw-Hill, 1959.

DGADR, 1997. Código de boas práticas agrícolas para a protecção da água contra a poluição com nitrato de origem agrícola. Direcção Geral Agric. Desenvolv. Rural 1997, 53.

Donigian Jr., A.S., Imhoff, J.C., 2002. From the Stanford Model to BASINS: 40 Years of Watershed Modeling. ASCE Task Committee on Evolution of Hydrologic Methods through Computers. ASCE 150th Anniversary Celebration. November 3–7, 2002. Washington, DC, USA.

EEA, 2007. CLC2006 Technical Guidelines. Technical report, 17. EEA Copenhagen. http://www.eea.europa.eu/publications/technical_report_2007_17.

Ewen, J., Parkin, G., O'Connell, P.E., 2000. SHETRAN: distributed river basin flow and transport modeling system. J. Hydrologic Eng. 5 (3), 250–258.

Farr, T.G., Rosen, P.A., Caro, E., Crippen, R., Duren, R., Hensley, S., Kobrick, M., Paller, M., Rodriguez, E., Roth, L., Seal, D., Shaffer, S., Shimada, J., Umland, J., Werner, M., Oskin, M., Burbank, D., Alsdorf, D., 2007. The shuttle radar topography mission. Rev. Geophys. 45. RG2004.

Feddes, R.A., Hoff, H., Bruen, M., Dawson, T., de Rosnay, P., Dirmeyer, P., Jackson, R.B., Kabat, P., Kleidon, A., Lilly, A., Pitman, A.J., 2001. Modelling root water uptake in hydrological and climate models. Bull. Am. Meteorological Soc. 82, 2797–2809.

Fohrer, N., Eckhardt, K., Haverkamp, S., Frede, H.G., 2001. Applying the SWAT Model as a Decision Support Tool for Land Use Concepts in Peripheral Regions in Germany. Pages 994–999 Sustaining Global Farm. Papers from the 10th International Soil Conservation Organisation Meeting.

Franz, G., Pinto, L., Ascione, I., Mateus, M.D., Fernandes, R., Leitão, P.C., Neves, R., 2014. Modelling of cohesive sediment dynamics in tidal estuarine systems: case study of Tagus estuary, Portugal. Estuarine. Coast. Shelf Sci. 151, 34–44.

Geza, M., McCray, J.E., 2008. Effects of soil data resolution on SWAT model stream flow and water quality predictions. J. Environ. Manag. 88 (3), 393–406.

Green, C.H., van Griensven, A., 2008. Autocalibration in hydrologic modeling: using SWAT2005 in small-scale watersheds. Environ. Model. Softw. 23, 422–434.

Grell, G.A., Dudhia, J., Stauffer, D., 1994. A Description of the Fifth-generation Penn State/NCAR Mesoscale Model (MM5). NCAR Technical Note NCAR/TN-398+STR.

Hoffmann, J., Leake, S.A., Galloway, D.L., Wilson, A.M., 2003. USGS. Open-file Report 03-233, Tucson, USA.

Horn, A.L., Rueda, F.J., Hörmann, G., Fohrer, N., 2004. Implementing river water quality modelling issues in mesoscale watershed models for water policy demands – an overview on current concepts, deficits and future tasks. Phys. Chem. Earth 29 (11–12), 725–737.

Mateus, M., Vaz, N., Neves, R., 2012. A process-oriented model of pelagic biogeochemistry for marine systems. Part II: application to a mesotidal estuary. J. Mar. Syst. 94, S90–S101 (Supplement).

Mishra, A.K., Coulibaly, P., 2009. Developments in hydrometric network design: a review. Rev. Geophys. 47 (2). RG2001.

Neitsch, S.L., Arnold, J.G., Kiniry, J.R., Williams, J.R., 2005. SWAT Theoretical Documentation Version 2005. Temple, TX: Grassland, Soil and Water Research Laboratory, Agricultural Research Service.

Neves, R., 2013. The MOHID concept. In: Mateus, M., Neves, R. (Eds.), Ocean Modelling for Coastal Management – Case Studies with MOHID. IST Press, Lisbon, pp. 1–11.

Paredes, D., Trigo, R.M., García-Herrera, R., Trigo, I.F., 2006. Understanding precipitation changes in Iberia in early spring: weather typing and storm-tracking approaches. J. Hydrometeorol. 7, 101–113.

Partheniades, E., 1965. Erosion and deposition of cohesive soils. J. Hydraulics Div. ASCE 91, 105–139. No. HY1, Proceedings Paper 4204.

Refsgaard, J.C., Storm, B., 1995. In: Singh, V.P. (Ed.), MIKE SHE – Computer Models of Watershed Hydrology. Water Resources Publications, Littleton, Colo, pp. 809–846.

Richards, L.A., 1931. Capillary conduction of liquids through porous mediums. Physics 1 (5), 318–333.

Santos, J.A., Corte-Real, J., Leite, S.M., 2005. Weather regimes and their connection to the winter rainfall in Portugal. Int. J. Climatol. 25, 33–50.

Serrano, A., Garcia, A.J., Mateos, V.L., Cancillo, M.L., Garrido, J., 1999. Monthly modes of variation of precipitation over the Iberian Peninsula. J. Clim. 12, 2894–2919.

Skamarock, W.C., Klemp, J.B., Dudhia, J., Gill, D.O., Barker, D.M., Wang, W., Powers, J.G., 2005. A Description of the Advanced Research Wrf Version 2. Tech. Rep.. National Center for Atmospheric Research.

Trancoso, A.R., Braunschweig, F., Chambel-Leitão, P., Obermann, M., Neves, R., 2009. An advanced modeling tool for simulating complex river systems. Sci. Total Environ. 407, 3004–3016.

Trancoso, A., Saraiva, S., Fernandes, L., Pina, P., Leitão, P., Neves, R., 2005. Modelling macroalgae in estuaries. Ecol. Model. 187 (2–3), 232–246.

Trigo, R.M., Pozo-Vázquez, D., Osborn, T.J., Castro-Díez, Y., Gámiz-Fortis, S., Esteban-Parra, M.J., 2004. North Atlantic Oscillation influence on precipitation, river flow and water resources in the Iberian Peninsula. Int. J. Climatol. 24, 925–944.

Van der Sande, C.I., de Jong, S.M., de Roo, A.P.J., 2003. A segmentation and classification approach of IKONOS-2 imagery for land cover mapping to assist flood risk and flood damage assessment. Int. J. Appl. Earth Observation Geoinformation 4 (3), 217–229.

Wool, T.A., Ambrose Jr., R.B., Martin, J.L., 2001. Water Quality Analysis Simulation Program (WASP). US Environmental Protection Agency, Atlanta, GA.

Yang, P., Ames, D.P., Fonseca, A., Anderson, D., Shrestha, R., Glenn, N.F., Cao, Y., 2014. What is the effect of LiDAR-derived DEM resolution on large-scale watershed model results? Environ. Model. Softw. 58, 48–57.

4 Candidate Work

After the model description and articles/application presented, in this chapter is described what was effectively the authors work in terms of MOHID Land development and in each article/application of the thesis.

4.1 MOHID Land developments

MOHID Land started is development around 2005 with projects Agro727 and TempQSim where the study focus was on soil plots and temporary rivers. The model started by having porous media and river hydraulics developed (e.g. Trancoso et al. 2009) and converged in an explicit integration with simplified runoff (diffuse wave implementation). Before the author thesis MOHID Land simulated only hydrology and in runoff the full St. Venant equation was not yet available. Vegetation was also simulated in a static manner (no vegetation growth).

The author main component developments in MOHID Land are described in next paragraphs. In Figure 7 is presented the processes existing before the thesis (hydrodynamics in all compartments as described in MOHID Land chapter but with runoff simplification to Manning equation) and the ones developed with the thesis.

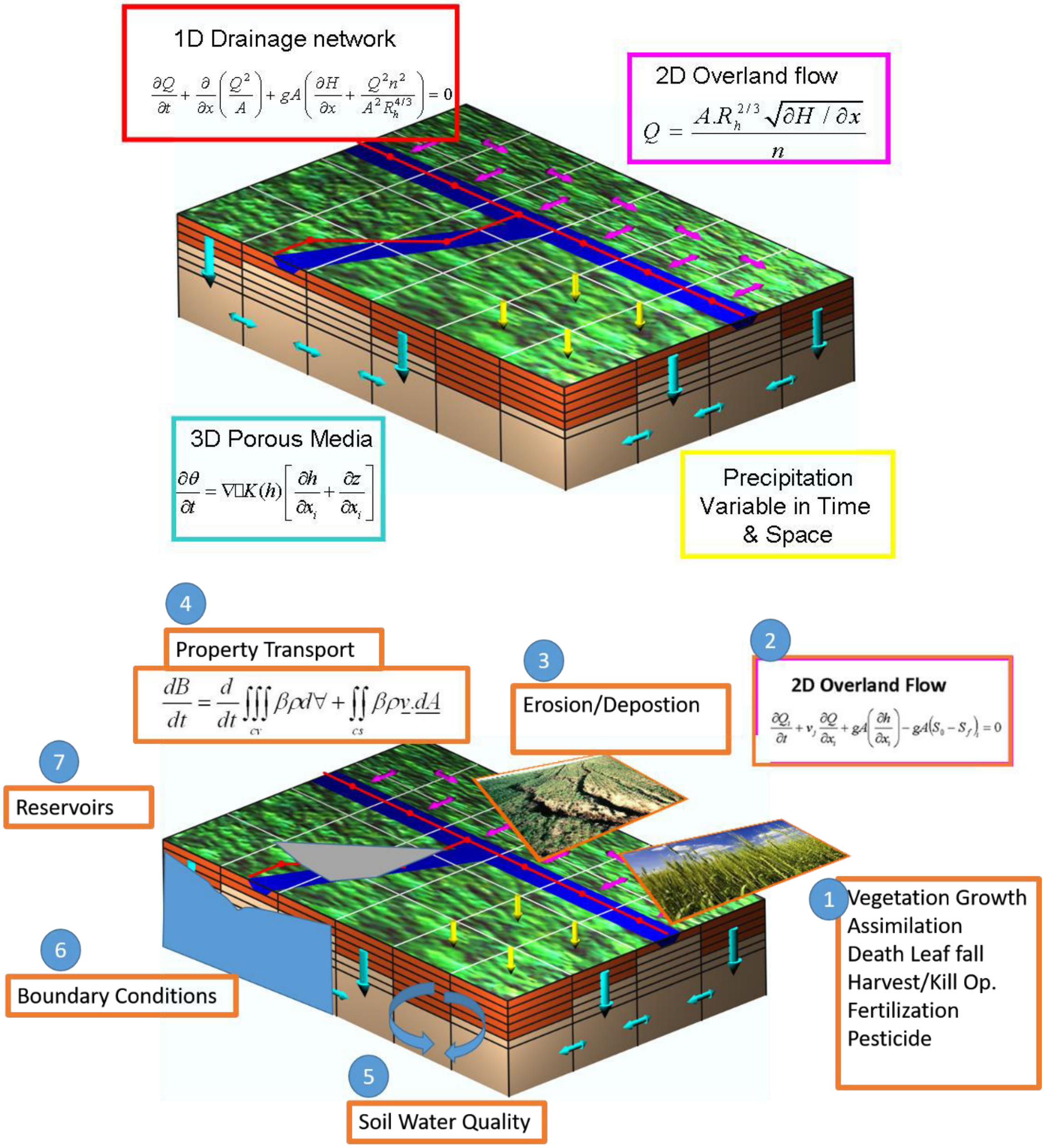

Figure 7 – MOHID Land components before the thesis (above) and the ones added within its scope (below)

Crop Growth Model

Implemented a crop growth model with atmosphere (evapotranspiration, interception) and soil (nutrient uptake, organic matter accumulation) interactions. This work was made by the author adapting from SWAT crop model (that was adapted from EPIC model) that is widely accepted crop growth model. This work made possible to simulate dynamic and realistic plant interactions with soil and management practices (fertilization, pesticide applications, grazing). These processes are the basis for accurate water and nutrient balances (evapotranspiration may represent more then 2/3 of annual precipitated rain and main part of nutrient losses to river come from agricultural practices), providing also the basis for irrigation studies, also a strong area of implementation of the model. For further details see Annex I.

St. Venant Equation

Implemented St. Venant equations in 2D Runoff that are the most complete set of equations for describing flood wave propagation, as described in the model section. This work was made in cooperation with Frank Braunschweig and Action Modulers and was the basis for MOHID Land to be able to represent in detail and in a robust way, flood propagation in surface water (e.g. floodplains, urban areas), now one strong area of implementation of the model.

Erosion/Deposition

Implemented erosion/deposition model in surface runoff. This work was developed by the author following similar implementations made in MOHID Water and MOHD River for consistency (erosion deposition based on critical shear stress and sediment strength thresholds). Splash erosion process was developed in cooperation with David Baily from CNRS, France. These developments made possible to more accurately transport particulated properties (by representing vertical fluxes between water column and sediment) that are the main transport medium for organic matter and phosphorus that can have impact on downstream water bodies (e.g. reservoirs, ditches, etc.). Further description in Trancoso et al. 2009 and Franz et al. 2014).

Property Transport

Implemented property transport in soil and runoff and interaction with river. This work was done by the author first by programming from scratch explicit methods (in a learning approach), and later adapting and improving the work already done for

MOHID Water (Chambel-Leitão, 2003) in this area. This made possible to transport dissolved and particulated properties in these two mediums in order that properties could move in all domains of MOHID Land model (before existed transport only in river). The property transport is the basis for any water quality simulation.

Soil Water Quality

Adapted soil bacteria model (Sediment Quality) to be able to be applied in any study domain (0D, 1D, 2D, 3D), to be dimensional consistent and MOHID “compliant” in terms of describing rates limiting factors explicitly. This work was done by the author following the first developments made by Pedro Galvão (Galvão, 2002) and Lúcia Pinto (Barão, 2007) that adapted RZWQM model but it was not possible to use it beside 0D implementations in MOHID Land model. For further details see Annex II.

Porous Media/Runoff Boundary Conditions

Implemented soil and surface water boundary conditions for water and properties (closed, imposing water levels and concentrations, null gradient, etc.). This work was made by the author to be able to implement the model in plot scale or river stretch scale where imposed lateral levels are known (aquifer levels or surface recorded levels (e.g. flow or tide stations)) and was the basis for several research projects implementations.

Reservoirs

Included reservoir dynamics for volumes and water quality in order to simulate water retention in storage reservoirs that change hydrological conditions downstream. This work was done by the author by interacting with drainage network nodes (inputs and outputs) and by allowing reservoir outflow control rules (based on reservoir volume and outflows or percentage of inflow curves). This development will allow studying artificial watersheds and reservoir impact on hydrology and water quality.

4.2 Applications

In this chapter is described the work done by the author in each article of chapter 3. In Article 1 about Enxoé long term loads using SWAT model the author was responsible for all model implementation and validation and INIAV (Instituto Nacional de Investigação Agrária e Veterinária) responsible for data collection and analysis. In article writing, the author did the major writing and co-authors gave feedback and revision.

In Article 2 about Enxoé flood loads using MOHID Land model the author was responsible for all model implementation and validation and INIAV responsible for data collection and analysis. The author was responsible for automatic sampler implementation and maintenance. In article writing, the author did the major writing and co-authors gave feedback and revision.

In Article 3 about Enxoé reservoir eutrophication management using SWAT and CE-QUAL-W2 models the author was responsible for all model implementation and validation and Universidade de Évora responsible for data collection and analysis. In article writing, the author did the major writing and co-authors gave feedback and revision.

In Article 4 about Póvoa de Santa Iria urban floods management using MOHID Land and SWMM models the author was responsible for MOHID Land model implementation and validation and Hidra responsible for SWMM model implementation and validation and data collection and analysis. OpenMI specific linkage was developed and implemented by Frank Braunschweig and Action Modulers and improved by the candidate. In article writing, the author did the major writing and co-authors gave feedback and revision.

In Article 5 about Iberia Peninsula hydrology and water quality operationalization using MOHID Land model the author was responsible for all model implementation. Model validation was performed mainly from co-authors. In article writing, Francisco

Campuzano was the main driver of the article and writing was distributed amongst co-authors.

5 Conclusions and Recommendations

After the applications, this chapter presents the conclusions about each article/application and globally about work hypothesis, impact of the results and open questions and future recommendations

The integration approach described in the thesis was tested with several models and in several applications ranging from urban flood scale to full water quality in Iberia Peninsula and the tool used to incorporate state-of-the-art knowledge was MOHID Land, a distributed, physically based, variable time step model that solves mass and momentum conservation equations in integral form applying to finite volumes, including 2D surface runoff an 1D river network solving St. Venant Equations, 3D ground water flow solving Richards equation both in saturated and non saturated media. This model integrates in his structure, state-of-the-art coupling with SWAT crop growth model, RZWQM biological driven and PHREEQC chemical driven soil dynamics, and river/reservoir water quality models from WASP, CE-QUAL-W2 and ERSEM models. It is also ready to couple with urban drainage model SWMM and other OpenMI compliant model.

The articles/applications provide complex study sites with different problems to solve where the numerical models were implemented and the hypothesis tested.

Articles/Applications

In the thesis several examples are presented to test the hypothesis that the integration approach is an added value and is consistent in 3 different scales: i) micro scale of urban watershed in Póvoa de Santa Iria using MOHID Land and SWMM models coupled in real time to manage urban floods; ii) small-medium scale in super eutrophic reservoir Enxoé using SWAT, MOHID Land and CE-QUAL-W2 models (coupled offline) to represent actual situation and test management scenarios and iii) large scale in Iberia Peninsula to forecast conditions for estuary and coastal models to improve forecasted fresh water inputs that can impact local circulations and water quality.

The three articles about Enxoé eutrophication (Section 3.1, 0 and 0), showed that the annual load estimated by SWAT model were low and consistent with extensive agricultural use and low point sources loads. However, MOHID Land model results in conjunction with field data showed that the phosphorus load that SWAT estimated to deposit in drainage network, are transported downstream to the reservoir in flood conditions and were used to assess reservoir sediment internal load. The integrated reservoir simulation (CE-QUAL-W2 and SWAT models) showed that high load reductions (around 75%) could not be enough to sustain mesotrophic level and geometry changes (or both) could be used as a solution for trophic level reduction. Here the modelling integration strategy made possible to dynamically compute reservoir input loads in an ungauged watershed and with cross-comparison between models, to quantify the sediment internal load that was key factor for driving reservoir blooms. Future work includes cost-benefit assessment to verify feasibility of the proposed scenarios.

The article about managing urban floods (Section 0) showed that the studied system had some critical pluvial network points with reduced diameter, where the drainage system was not able to fulfil events flow and originated flooding. Moreover, the system seems to be inefficient for return periods higher than 10 years and for those events further work should be done to evaluate infrastructural changes (e.g. general increase in diameters, build reservoirs or use unused infrastructure elements as storage, etc.). The modelling integration in this case is essential since surface preferential flow follows some streets and most of the flooding occurs in a flat area where the surface water is spread-out, and a detailed description of the surface routing processes is needed for describing head pressure that influences drainage system flows. Future work includes testing infrastructural changes (e.g. adding reservoirs, infiltration areas) to make the system more robust.

The article describing MOHID Land operationalization in the Iberia Peninsula (Section 3.5), showed the model ability to represent main hydrology and biogeochemistry processes needed to accurately feed coastal areas with watersheds input and solve the boundary condition problem. When rivers are highly artificialized new approaches need to be studied and recent MOHID Land developments about simulating reservoirs dynamics should be tested to verify its capacity to overcome this limitation. Also in this implementation the integration approach is essential to a coastal forecast system in order to predict possible extraordinary events (e.g. be part of an Early Warning System). Future work relates to testing the new reservoir development.

The articles/applications presented above showed that the integration approach was core to i) represent Enxoé long-term and short-term processes that have both influence the reservoir dynamics; ii) represent surface water-drainage system interactions that influence hydraulic behaviour and originated floods in Póvoa e Santa Iria and iii) represent best forecast conditions to coastal areas that take into consideration all hydrology and biogeochemical interactions in upstream watersheds.

Revisiting Hypothesis and objectives

The thesis hypothesis was that integrated state-of-the art approaches can solve the problems associated to boundary conditions assumptions by combining in one numerical framework the best knowledge of each area describing the main processes and explicitly describing the fluxes between mediums.

The thesis objectives were to i) show integration examples suited to solve specific environmental problems and ii) integrate the best knowledge in each field of study in a state-of-the-art open source framework to be able to continuously improve with time.

The hypothesis seems valid for complex systems with interactions between watershed and reservoir, surface water and drainage system, inland and coastal zones as shown in the study cases (where these consist of examples of validation). The objectives have also been fulfilled by integrating/coupling to MOHID Land different state-of-the-art models and approaches (e.g. integration of SWAT vegetation growth, SWMM coupling, and other formulations not tested in the scope of the applications).

Impact on state-of-the-art

While exist several approaches that appeared in the last years that integrate diverse models to solve the type of problems approached in this thesis, they describe only part of the water cycle problem (reservoir/watershed, river/floodplain, urban drainage/surface). It seems to lack one open-source modelling system that incorporates all this knowledge in different areas and is able to simulate parts of the system and simplify processes when not needed or use the full array of systems and processes when required.

The work presented here built the backbone of a state-of-the-art numerical system that has the main processes associated to hydrology, hydraulics, soil and river water quality (biological and chemical driven) and it has the potential to be a starting point for future fine tuning and validation that can result in several research projects and PhD thesis (see below).

The MOHID Land developments during the thesis allowed for the better description of some processes and specifically:

- The vegetation growth model was a starting point for the creation of a scientific research area in Maretec research group (Instituto Superior Técnico) around agricultural optimization, resulting in several European research projects as Aquapath-Soil, Figaro, MyFarm, etc.
- The implementation of the 2D St. Venant model, created a robust model for flooding and allowed for the implementation of several flood studies namely the one for National Environmental Agency (APA) for 24 areas in Portugal in the scope of the Flood Directive (mapping risk areas) and in Lisbon for the Urban Drainage Plan in the definition of alternatives for flood reduction (in company Action Modulers).
- The property transport in all mediums, soil quality processes and boundary conditions developments allowed the implementations for example at

micro scale (few hectares) for wetland management as research project Attenagua (Maretec – Instituto Superior Técnico).

- All developments related to hydrodynamics and water quality allowed for the MOHID Land and MOHID Water integrations for reservoir management, similar as used in the thesis with SWAT and CE-QUAL-W2, for example in several studies for Agência Pernambucana de Água e Clima, Brazil (in company Action Modulers).

Recommendations

There are three main aspects that should be addressed in the future to manage MOHID Land complex system: i) test and validation of developments; ii) cross-scale implementations and ii) improve model speed.

MOHID Land model has now much of the main state-of-the-art hydrological and biogeochemistry processes and new features or processes are included in a straightforward way since hydrology and property transport/transformation modules are built. MOHID Land with the full hydrology ad water quality processes is producing already a lot of information in several domains so testing and validation should focus on individual processes as contained as possible (e.g. in plot scale examples for specific validations). As example of possible future validation topics/research projects/PhD thesis:

- soil plot for crop growth optimization with different conditions,
- sediment dynamics in erosion plots,
- wetland hydraulics and denitrification processes
- organic matter cycling in contrasting land uses and crops,
- reservoir impacts on watershed management (water and nutrients)

MOHID Land has the ability to simulate both the large-scale watershed as the detailed river-groundwater interactions, and usually very high level of detail is not possible in a wide area and the boundary condition problem appears. In order to tackle examples of different scales (e.g. simulate flood propagation in flat area and also storm event that generates it, miles away in the mountains) without losing information, a nesting approach is needed. In a nesting approach, the higher resolution domain would get its boundary conditions from the father, coarser model, optimizing the number of cells to use. This process is already developed in MOHID Water model and should be replicated in MOHID Land.

With the increasing computational power available every day, and multithreaded approaches, simulation times are able to decrease or more simulations and higher resolutions are possible. However, this tends to be asymptotic and usually is limited by the amount of time each “thread” is actively working compared to the time to manage “threads” or pass information between them or to processor/memory. MOHID Land already uses OpenMP (Open MultiProcessing) technology for parallelizing loops and should explore the feasibility of using MPI (Message Passing Interface) to break down computational grid and run them in separate “threads”. Using a similar approach with graphical card processors instead of CPU should also be explored.

Acknowledgements

The thesis had the direct and indirect contributions that the author wishes to acknowledge.

As direct contributions, would like to thank to supervisor Ramiro Neves for the guidance, revisions, and discussions around modelling and for providing the great workplace conditions. Also to the co-authors of the articles for revision and discussions and INIAV, Universidade de Évora, SIMTEJO and APA for providing field data used in this work.

In terms of indirect contributions wish to thank to Maretec team for developing the MOHID model, mainly Pedro Chambel-Leitão the developer of MOHID Soil, a starter of MOHID Land, Rosa Trancoso that developed river network model, Frank Braunschweig the main developer that reshaped and created most of the MOHID Land version prior to this thesis (hydrology and hydraulic processes) and Eduardo Jauch that coupled soil chemical reaction module (not covered in this thesis) and pushed the model even forward.

A word also for all other MOHID developers for fruitful discussions and guidance in MOHID (especially Pedro Pina, Luis Fernandes and Frank Braunschweig for the support). As final remark thank you to all Action Modulers and Maretec teams for the great spirit and support that enhanced work conditions.

References

Abbot, M. B. and A. W. Minns (1998). Computational Hydraulics (Second ed.). Ashgate.

Barão, A. L. (2007) - Carbon, Nitrogen and Phosphorus Soil Cycle Modelling, Dissertação para a obtenção do Grau de Licenciado em Engenharia do Ambiente, IST Lisboa.

Beasley, D.B.; Huggins, L.F. (1982) - ANSWERS user's manual. Department of Agricultural Engineering, Purdue University, West Lafayette, IN, USA (1982).

Braunschweig F, Chambel P, Fernandes L, Pina P, Neves R. (2004) The object oriented design of the integrated modelling system MOHID. Proceedings of the XVth InternationalConference on Computational Methods in Water Resources (CMWR XV), June 13–17, Chapel Hill, NC, USA; 2004

Cameira, M.R.; Fernando, R.M.; Ahuja, L.R.; Ma, L (2007) - Using RZWQM to simulate the fate of nitrogen in field soil–crop environment in the Mediterranean region, Agricultural Water Management, Volume 90, Issues 1–2, 24 May 2007, Pages 121-136, ISSN 0378-3774, 10.1016/j.agwat.2007.03.002.

Cancino L, Neves R. (1999) Hydrodynamic and sediment suspension modelling in estuarine systems: Part I: Description of the numerical models. J Mar Syst 1999a;22(2–3):105–16

Celia, M. A., Bouloutas, E. T., Zarba, R. L. (1990) - A General Mass-Conservative Numerical Solution for the Unsaturated Flow Equation. Water Resources Research. Vol 26, Nº 7. Pages 1483-1496, July 1990.

Deltares (2008) - Validation Document Delft3D-FLOW. A software system for 3D flow simulations. Deltares documentation.

DHI (2007) MIKE 21 & MIKE 3 Flow Model Hyrodynamic Module. DHI documentation.

Deus R, Brito D, Kenov IA, Lima M, Costa V, Medeiros A, Neves R, Alves CN. Three-dimensional model for analysis of spatial and temporal patterns of phytoplankton in Tucuruí reservoir, Pará, Brazil. Ecological Modelling. 2013; 253: 28-43

Donigian Jr., A.S., Imhoff, J.C., (2002) - From the Stanford model to BASINS: 40 years of watershed modeling. ASCE Task Committee on Evolution of Hydrologic Methods Through Computers. ASCE 150th Anniversary Celebration. November 3–7, 2002. Washington, DC, USA.

EEA, (2009) - Water resources across Europe — confronting water scarcity and drought. European Environment Agency OPOCE (Office for Official Publications of the European Communities). Published: Mar 17, 2009

Ewen, J.; Parkin, G.; O'Connell, P.E. (2000) - SHETRAN: Distributed river basin flow and transport modeling system. Journal of Hydrologic Engineering, Vol. 5, No. 3, July, 2000.

Feddes, R. A., Kowalik, P. J.; Zaradny, H. (1978) - Simulation of field water use and crop yield. Wageningen, The Netherlands. Centre for Agricultural Publishing and Documentation.

Galvão, P. B. (2002) - Solute Dynamics in Unsaturated Soil, Dissertação para a obtenção do Grau de Licenciado em Engenharia do Ambiente, IST Lisboa.

Grünberger, O.; Macaigne, P.; Michelot, J.L.; Hartmann, C.; Sukchan, S. (2008) - Salt crust development in paddy fields owing to soil evaporation and drainage: Contribution of chloride and deuterium profile analysis, Journal of Hydrology, Volume 348, Issues 1–2, 1 January 2008, Pages 110-123, ISSN 0022-1694, 10.1016/j.jhydrol.2007.09.039.

Harbaugh, A.W., Banta, E.R., Hill, M.C., and McDonald, M.G., (2000) - MODFLOW-2000, the U.S. Geological Survey modular ground-water model -- User guide to modularization concepts and the Ground-Water Flow Process: U.S. Geological Survey Open-File Report 00-92, 121 p.

Jeon, Ji-Hong; Yoon, C.G.; Donigian Jr., A.S.; Jung, Kwang-Wook (2007) - Development of the HSPF-Paddy model to estimate watershed pollutant loads in paddy farming regions, Agricultural Water Management, Volume 90, Issues 1–2, 24 May 2007, Pages 75-86, ISSN 0378-3774, 10.1016/j.agwat.2007.02.006.

Jayakrishnan, R.; Srinivasan, R.; Santhi, C.; Arnold, J.G: (2005) - Advances in the application of the SWAT model for water resources management. Hydrological Processes, 19 (3) (2005), pp. 749–762

Krysanova, V.; Müller-Wohlfeil, D.I.; Becker, A. (1998) - Development and test of a spatially distributed hydrological/water quality model for mesoscale watersheds, Ecological Modelling, Volume 106, Issues 2–3, 1 March 1998, Pages 261-289, ISSN 0304-3800, 10.1016/S0304-3800(97)00204-4.

Leitão, P.C.; Chambel-Leitão, P.; Neves, R. (2000) – Modelação numérica da circulação da água no solo, O modelo MOHID. Revista Pedologia, Oeiras 28: 46-55

Chambel-Leitão, P.C. (2003) - Integração de Escalas e de Processos na Modelação no Ambiente Marinho, Dissertação para a obtenção do Grau de Doutor em Engenharia do Ambiente, IST Lisboa

Lindsley Jr, R. K., M. A. Kohler, and J. L. Paulhus (1982). Hydrology for Engineers (Third ed.). International Student Edition, McGrawHill.

Ma, L.; Hoogenboom, G.; Ahuja, L.R.; Ascough II; J.C.; Saseendran, S.A.. (2006) - Evaluation of the RZWQM-CERES-Maize hybrid model for maize production, Agricultural Systems, Volume 87, Issue 3, March 2006, Pages 274-295, ISSN 0308-521X, 10.1016/j.agsy.2005.02.001.

Ma, L.; Ahuja, L.R.; Ascough II, J.C.; Shaffer, M.J.; Rojas, K.W.; Malone, R.W.; Cameira, M.R. (2000) – Integrating system modeling with field research in agriculture: applications of the root zone water quality model (RZWQM). Advances in Agronomy, Volume 71 pp 233-292

Martins, F. (2000). Modelação Matemática Tridimensional de escoamentos costeiros e estuarinos usando uma abordagem de coordenada vertical genérica. Tese de Doutoramento. Instituto Superior Técnico. Universidade Técnica de Lisboa,

Mateus, M. A process-oriented model of pelagic biogeochemistry for marine systems. Part I: Model description. J. Marine Syst. 2012, 94, S78–S89.

Neitsch, S.L., J.G. Arnold, J.R. Kiniry, J.R. Williams, (2005) - SWAT2005 Theoretical Documentation.

Neves, R.J.J. (1985) - Étude Experimentale et Modélisation des Circulations Transitoire et Résiduelle dans l'Estuaire du Sado. Ph. D. Thesis.Univ. Liège, 371 pp.

Obermann, M., 2007. Nutrient dynamics in temporary waters of Mediterraneancatchments. PhD thesis. University of Hannover. March 2007.

Panday, S.; Huyakorn, P. (2004) - A fully coupled physically-based spatially-distributed model for evaluating surface/subsurface flow. Advances in Water Resources 27 (2004) 361–382

Parkhurst, D.L., and Appelo, C.A.J., 2013, Description of input and examples for PHREEQC version 3—A computer program for speciation, batch-reaction, one-dimensional transport, and inverse geochemical calculations: U.S. Geological Survey Techniques and Methods, book 6, chap. A43, 497 p., available only at http://pubs.usgs.gov/tm/06/a43/.

Pietrzak, J (1998) - The use of TVD limiters for forward-in-time upstream-biased advection schemes in ocean modeling, Month. Weather Rev. 126 (1998), pp. 812–830.

Portela, L.I. (1996) - Modelação Matemática dos Processos Hidrodinâmicos e Qualidade da Água no estuário do Tejo. Tese de doutoramento. Instituto Superior Técnico, Univ. Técnica de Lisboa.

Ramos, T.B.; Šimůnek, J.; Gonçalves, M.C.; Martins, J.C.; Prazeres, A.; Castanheira, N.L.; Pereira, L.S. (2011) - Field evaluation of a multicomponent solute transport model in soils irrigated with saline waters, Journal of Hydrology, Volume 407, Issues 1–4, 15 September 2011, Pages 129-144, ISSN 0022-1694, 10.1016/j.jhydrol.2011.07.016.

Refsgaard, J. C., and Storm, B. (1995). MIKE SHE - Computer models of watershed hydrology, V. P. Singh, ed., Water Resources Publications, Littleton, Colo., 809–846.

Silva, A. (1992) - Modelação Matemática Não Linear de Ondas de Superfície e de Correntes Litorais. Tese de doutoramento em Engenharia Mecânica, Instituto Superior Técnico, Univ. Técnica de Lisboa.

Šimůnek, J., Šejna, M.; Saito, H.; Sakai, M.; van Genuchten, M. Th. (2008) - The Hydrus-1D Software Package for Simulating the Movement of Water, Heat, and Multiple Solutes in Variably Saturated Media, Version 4.0, HYDRUS Software Series 3, Department of Environmental Sciences, University of California Riverside, Riverside, California, USA, pp. 315, 2008.

Thomas, L.H. (1949) - Elliptic problems in linear difference equations over a network, Watson Sci. Comput. Lab. Rept., Columbia University, New York, 1949.

Thomee, V (2001) - From finite differences to finite elements: A short history of numerical analysis of partial differential equations, Journal of Computational and Applied Mathematics, Volume 128, Issues 1-2, 1 March 2001, Pages 1-54, ISSN 0377-0427.

Trancoso, A.R.; Braunschweig, F.; Leitão, P.C.; Obermann, M.; Neves, R. (2009) An advanced modelling tool for simulating complex river systems. Science of the Total Environment 407 (2009) 3004–3016

Annexes

Annex 1 – Vegetation Growth Model

This annex describes the vegetation growth model included in MOHID Land, adapted from SWAT model.

In the natural system, vegetation growth is achieved using both its terrestrial and aerial parts. In the terrestrial part, root development is used for water and nutrient uptake and then these constituents distributed along all the plant biomass. Water is used for regulating temperature, cellular processes and helps on nutrient and organic compounds transport (xylem and phloem circulations). In the aerial part (leaves) plant receives solar radiation and exchanges gases with the atmosphere (oxygen and carbon dioxide) to achieve photosynthetic reactions and respiration. All these processes give the plant nutrient, carbon and energy so it can grow (accumulate biomass). Stems connect roots to leaves (distribute water and nutrients through the plant from sources to sinks and allow leaves to reach the sunlight) and depending on plant strategy (annual cycles or perennial) can be absent or compose an important part of plant biomass.

Fallen leaves, stem or dead roots increase detritus or organic matter in soil or river stream. This organic matter can fall naturally (plant growth strategy), be generated because of plant death or by grazing or harvesting. The organic matter is composed by nutrients that plant accumulated during its growth but that can not be used directly by plant. Bacteria in soil and in sediments mineralize organic matter to soluble nutrients. These nutrients can remain in soil, be transported or taken by other plants and sustain other plant generations growth.

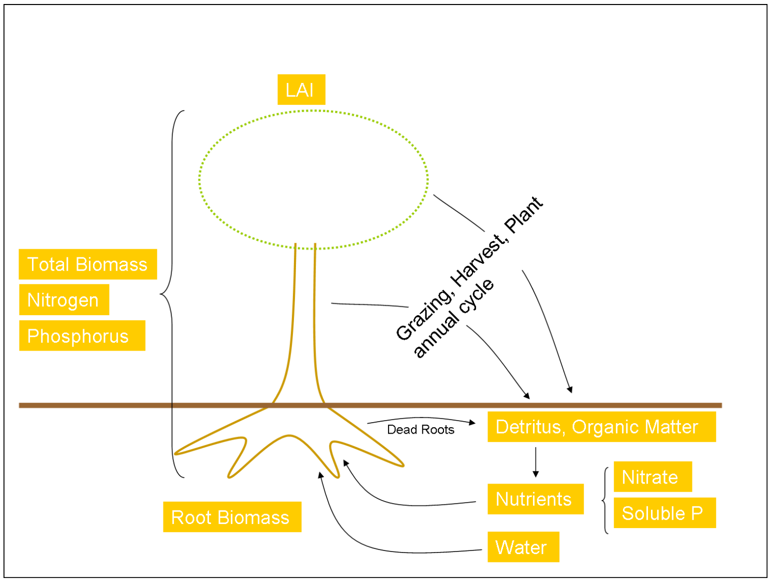

Figure 8 - SWAT state variables (orange rectangles) and vegetation processes (arrows).

MOHID vegetation module (adapted from SWAT) tries to describe the main processes for vegetation growth that are shown in Figure 8. Plant biomass is computed for the entire plant and the distinguishing of roots and leaves is made afterwards based on plant stage. Nutrient pools in the soil are composed by nitrate and soluble phosphorus and carbon is not considered on the organic matter pool.

SWAT is widely used watershed model from USDA (United States Department of Agriculture) and has a large crop and tree database with parameters related to vegetation growth. A great deal of bibliography has be written with successful application worldwide from small to large watershed and for different climatic regions.

Vegetation growth model is explained in next chapters starting with an introductory model's general concepts. It will be presented the model state variables, related processes (that affect state variables) and finally the equations that represent state variables evolution. The equations used are taken from SWAT model (Neitsch et al. 2005).

Model General Concepts

Heat Units

The vegetation growing cycle is based on Heat Units (HU) theory which states that plants have heat needs that can be related to time to maturity.

The HU represent the plant's growing cycle that only occurs if the mean temperature is greater a minimum or base value. In other words, if the mean daily temperature is lower than the plant's base temperature no growing will occur; in the other hand, if it is higher, plant grows and the heat units accumulation is the difference between the air mean daily temperature and the plant's base temperature. When plant reaches maturity heat units, growing ceases.

Thermal time is calculated in SWAT as Heat Units as follows:

$$HU = \overline{T}_{av} - T_{base} \quad \text{when} \quad \overline{T}_{av} > T_{base}$$ **Equation 27**

HU - number of heat units accumulated on a given day (heat units)

T av - mean daily temperature (ºC)

Tbase - plant's base or minimum temperature for growth (ºC)

Vegetation Types

Are considered 7 kinds of vegetation: warm season annual legume, cold season annual legume, perennial legume, warm season annual, cold season annual, perennial, trees.

In terms of simulation differences, perennial crops, trees and cold season annual present a dormancy period when day length reduces below a minimum level. In perennial crops and trees the root depth is the maximum according to the specie and soil; in other hand, for annual crops root depth grows with plant cycle. Legume crops have nitrogen fixation and in trees growing is partitioned between leaves/needles and woody growth.

Model State Variables

The following state variables exist for vegetation growth (refer to Figure 8).

- Water in soil is represented by soil water content.
- The nutrient pool in soil is constituted by nitrate and soluble phosphorus.
- Detritus/Organic matter in the soil
- Biomass, nitrogen and phosphorus plant content is referred for the total plant.
- Leaf Area Index represents leaf biomass.
- Root biomass

Model Processes

Water uptake from soil by plants is computed based on optimal uptake and then updated with effective uptake. Optimal uptake depends on potential evapotranspiration and water uptake distribution in soil (simulating root development with higher density near surface and decay with root depth). Effective water uptake is computed taking in to account that i) if in upper layers water available does not meet potential demand lower layers can compensate; ii) if soil water content decreases, it is increasingly difficult for the plant to extract water from the soil; iii) water uptake for plant ceases when soil water content is at wilting point.

Nitrogen and phosphorus uptakes are based on similar concepts where an optimal uptake and then an effective uptake are computed. Nutrient demand (optimal) is computed based on plant optimal nutrient content (depends on plant stage) and real nutrient content. The effective nutrient uptake is than computed depending on nutrient availability in soil layers. Nitrogen fixation and phosphorus luxurious uptake are also computed.
Nitrogen and phosphorus generation are dependent on sources (precipitation, fertilization) and soil processes (transport, soil biochemical reactions) that are not focused on this text.

Management operations (harvesting, killing, etc.) reduce biomass and form detritus that increase **organic matter pool in soil**. Optimal harvesting is computed based on plant stage and effective harvest takes into account water stresses and harvesting efficiency.

Biomass growth (total plant biomass) is based on optimal growth (radiation use efficiency) and the effective growth is computed taking into account plant stresses (water, nutrient, light and temperature)

Root biomass (important for root growth and water and nutrient uptake) is estimated based on a fraction of total biomass and plant stage.

Leaf Area Index is computed based on a maximum value (database for plant) and plant stage. Once maximum leaf area index is reached, LAI is maintained until leaf senescence begin to exceed leaf growth and LAI decreases.

Model Equations

Water Consumption

Water consumption is computed based on an optimal consumption (depending on transpiration and capacity to remove it from the soil) and the effective available water in the soil.

Optimal

The potential water uptake from the soil surface to any depth in the root zone is estimated with the function:

$$w_{up,z} = \frac{E_t}{\left[1 - \exp(-\beta_w)\right]} \cdot \left[1 - \exp\left(-\beta_w \cdot \frac{z}{z_{root}}\right)\right] \qquad \textbf{Equation 28}$$

where $w_{up,z}$ is the potential water uptake from the soil surface to a specified depth, z, on a given day (mm H2O), E_t is the maximum plant transpiration on a given day (mm H2O), βw is the water-use distribution parameter, z is the depth from the soil surface (mm), and z_{root} is the depth of root development in the soil (mm). The potential water uptake from any soil layer can be calculated by solving Equation 28 for the depth at the top and bottom of the soil layer and taking the difference.

$$w_{up,ly} = w_{up,zl} - w_{up,zu}$$ **Equation 29**

where $w_{up,ly}$ is the potential water uptake for layer ly (mm H2O), $w_{up,zl}$ is the potential water uptake for the profile to the lower boundary of the soil layer (mm H2O), and $w_{up,zu}$ is the potential water uptake for the profile to the upper boundary of the soil layer (mm H2O).

Since root density is greatest near the soil surface and decreases with depth, the water uptake from the upper layers is assumed to be much greater than that in the lower layers. The water-use distribution parameter, βw, is set to 10 in SWAT. With this value, 50% of the water uptake will occur in the upper 6% of the root zone.

If upper layers in the soil profile do not contain enough water to meet the potential water uptake, users may allow lower layers to compensate. The equation used to calculate the adjusted potential water uptake is:

$$w'_{up,ly} = w_{up,ly} + w_{demand} \cdot epco$$ **Equation 30**

Where $w'_{up,ly}$ is the adjusted potential water uptake for layer ly (mm H_2O), $w_{up,ly}$ is the potential water uptake for layer ly calculated with Equation 29 (mm H2O), w_{demand} is the water uptake demand not met by overlying soil layers (mm H2O), and epco is the plant uptake compensation factor. The plant uptake compensation factor can range from 0.01 to 1.00 and is set by the user. As epco approaches 1.0, the model allows more of the water uptake demand to be met by lower layers in the soil. As epco approaches 0.0, the model allows less variation from the depth distribution described by Equation 28 to take place.

As the water content of the soil decreases, the water in the soil is held more and more tightly by the soil particles and it becomes increasingly difficult for the plant to extract water from the soil. To reflect the decrease in the efficiency of the plant in extracting water from dryer soils, the potential water uptake is modified using the following equations:

$$w''_{up,ly} = w'_{up,ly} \cdot \exp\left[5 \cdot \left(\frac{SW_{ly}}{(.25 \cdot AWC_{ly})} - 1\right)\right] \quad \text{when } SW_{ly} < (.25 \cdot AWC_{ly})$$

$$w''_{up,ly} = w'_{up,ly} \quad \text{when } SW_{ly} \geq (.25 \cdot AWC_{ly})$$

Equation 31

Where $w''_{up,ly}$ is the potential water uptake adjusted for initial soil water content (mm H_2O), $w'_{up,ly}$ is the adjusted potential water uptake for layer ly (mm H_2O) calculated with Equation 30 SW_{ly} is the amount of water in the soil layer on a given day (mm H2O), and AWC_{ly} is the available water capacity for layer ly (mm H2O). The available water capacity is calculated:

$$AWC_{ly} = FC_{ly} - WP_{ly}$$

Equation 32

where AWC_{ly} is the available water capacity for layer ly (mm H2O), FC_{ly} is the water content of layer ly at field capacity (mm H2O), and WP_{ly} is the water content of layer ly at wilting point (mm H2O).

Effective

If the water content in the soil layers is lower than the optimal amount, then the effective water uptake will be lower than the optimal.

Effective water uptake can be computed from:

$$w_{actualup,ly} = \min\left[w''_{up,ly}, (SW_{ly} - WP_{ly})\right]$$

Equation 33

where $w_{actualup,ly}$ is the effective water uptake for layer *ly* (mm H_2O), SW_{ly} is the amount of water in the soil layer on a given day (mm H_2O), and WP_{ly} is the water content of layer *ly* at wilting point (mm H_2O). The total water uptake for the day is calculated:

$$w_{actualup} = \sum_{ly=1}^{n} w_{actualup,ly}$$

Equation 34

where $w_{actualup}$ is the total plant water uptake for the day (mm H_2O), $w_{actualup,ly}$ is the effective water uptake for layer *ly* (mm H_2O), and *n* is the number of layers in the soil profile. The total plant water uptake for the day calculated with Equation 34 is also the actual amount of transpiration that occurs on the day.

$$E_{t,act} = w_{actualup}$$ **Equation 35**

where $E_{t,act}$ is the effective amount of transpiration on a given day (mm H_2O) and $w_{actualup}$ is the total plant water uptake for the day (mm H_2O).

Nutrient Consumption

Nutrient consumption is computed based on an optimal consumption (depending on optimal growth and plant stage) and the effective available nutrients in the soil.

Optimal

Plant nutrient uptake is controlled by the plant nutrient equation. The plant nutrient equation calculates the fraction of nitrogen or phosphorus in the plant biomass as a function of growth stage given optimal growing conditions.

$$fr_N = \left(fr_{N,1} - fr_{N,3}\right) \cdot \left[1 - \frac{fr_{PHU}}{fr_{PHU} + \exp\left(n_1 - n_2 \cdot fr_{PHU}\right)}\right] + fr_{N,3}$$ **Equation 36**

$$fr_P = \left(fr_{P,1} - fr_{P,3}\right) \cdot \left[1 - \frac{fr_{PHU}}{fr_{PHU} + \exp\left(p_1 - p_2 \cdot fr_{PHU}\right)}\right] + fr_{P,3}$$ **Equation 37**

where fr_N and fr_P are the fraction of nitrogen and phosphorus in the plant biomass on a given day, $fr_{N,1}$ and $fr_{P,1}$ are the normal fraction of nitrogen and phosphorus in the plant biomass at emergence, $fr_{N,3}$ and $fr_{P,3}$ are the normal fraction of nitrogen and phosphorus in the plant biomass at maturity, fr_{PHU} is the fraction of potential heat units accumulated for the plant on a given day in the growing season, and n1 and p1 and n2 and p2 are shape coefficients.

The shape coefficients are calculated by solving Equation 36 and Equation 37 using two known points ($fr_{N,2}$, $fr_{PHU,50\%}$) or ($fr_{P,2}$, $fr_{PHU,50\%}$) and ($fr_{N,3}$, $fr_{PHU,100\%}$) or ($fr_{P,3}$, $fr_{PHU,100\%}$).

To determine the mass of nitrogen or phosphorus that should be stored in the plant biomass on a given day, the nitrogen and phosphorus fraction is multiplied by the total plant biomass:

$$bio_{N,opt} = fr_N \cdot bio$$ **Equation 38**

$$bio_{P,opt} = fr_P \cdot bio$$ **Equation 39**

where $bio_{N,opt}$ and $bio_{P,opt}$ are the optimal mass of nitrogen and phosphorus stored in plant material for the current growth stage (kg/ha), fr_N and fr_P are the optimal fraction of nitrogen and phosphorus in the plant biomass for the current growth stage, and bio is the total plant biomass on a given day (kg ha-1).

Compute plant nutrient demand:

$$N_{up} = \mathrm{Min}\begin{cases} bio_{N,opt} - bio_N \\ \\ 4 \cdot fr_{N,3} \cdot \Delta bio \end{cases}$$ **Equation 40**

$$P_{up} = 1.5 \cdot \mathrm{Min}\begin{cases} bio_{P,opt} - bio_P \\ 4 \cdot fr_{P,3} \cdot \Delta bio \end{cases}$$ **Equation 41**

where N_{up} and P_{up} are the potential nitrogen and phosphorus uptake (kg /ha), $bio_{N,opt}$ and $bio_{P,opt}$ are the optimal mass of nitrogen and phosphorus stored in plant material for the current growth stage (kg /ha), bio_N and bio_P are the actual mass of nitrogen and phosphorus stored in plant material (kg /ha), $fr_{N,3}$ and $fr_{P,3}$ are the normal fraction of nitrogen and phosphorus in the plant biomass at maturity, and Δbio is the potential increase in total plant biomass on a given day (kg/ha).

The difference between the phosphorus content of the plant biomass expected for the plant's growth stage and the actual phosphorus content is multiplied by 1.5 to simulate luxury phosphorus uptake.

The depth distribution of nitrogen and phosphorus uptake is calculated with the functions:

$$N_{up,z} = \frac{N_{up}}{\left[1 - \exp(-\beta_n)\right]} \cdot \left[1 - \exp\left(-\beta_n \cdot \frac{z}{z_{root}}\right)\right]$$ **Equation 42**

$$P_{up,z} = \frac{P_{up}}{\left[1 - \exp(-\beta_p)\right]} \cdot \left[1 - \exp\left(-\beta_p \cdot \frac{z}{z_{root}}\right)\right]$$ **Equation 43**

where $N_{up,z}$ and $P_{up,z}$ are the potential nitrogen and phosphorus uptake from the soil surface to depth z (kg/ha), N_{up} and P_{up} are the potential nitrogen and phosphorus uptake (kg /ha) computed in Equation 40 and Equation 41, βn and βp are the nitrogen and phosphorus uptake distribution parameter, z is the depth from the soil surface (mm), and zroot is the depth of root development in the soil (mm). The potential nitrogen and phosphorus uptake for a soil layer is calculated by solving Equation 42 and Equation 43 for the depth at the upper and lower boundaries of the soil layer and taking the difference.

$$N_{up,ly} = N_{up,zl} - N_{up,zu}$$ **Equation 44**

$$P_{up,ly} = P_{up,zl} - P_{up,zu}$$ **Equation 45**

Where $N_{up,ly}$ and $P_{up,ly}$ are the potential nitrogen and phosphorus uptake for layer ly (kg /ha), $N_{up,zl}$ and $P_{up,zl}$ are the potential nitrogen and phosphorus uptake from the soil surface to the lower boundary of the soil layer (kg /ha), and $N_{up,zu}$ and $P_{up,zu}$ are the potential nitrogen and phosphorus uptake from the soil surface to the upper boundary of the soil layer (kg /ha).

Root density is greatest near the surface, and nitrogen and phosphorus uptake in the upper portion of the soil will be greater than in the lower portion. The depth distribution of nitrogen and phosphorus uptake is controlled by βn and βp, the nitrogen and phosphorus uptake distribution parameter, a variable users are allowed to adjust. Nitrogen removed from the soil by plants is taken from the nitrate pool and phosphorus from solution phosphorus pool. The importance of the nitrate and phosphorus uptake distribution parameter lies in its control over the maximum amount of nitrate and solution P removed from the upper layers. Because the top 10 mm of the soil profile interacts with surface runoff, the nitrate and phosphorus uptake distribution parameter will influence the amount of nitrate and labile phosphorus available for transport in surface runoff. The model allows lower layers in the root zone to fully compensate for lack of nitrate and solution P in the upper layers, so there should not be significant changes in nitrogen and phosphorus stress with variation in the value used for βp.

Effective

Effective nitrogen and phosphorus uptake take into account optimal consumption (based on plant stage) and available nutrient pools.

The effective amount of nitrogen and phosphorus removed from a soil layer is calculated:

$$N_{actualup,ly} = \min\left[N_{up,ly} + N_{demand}, \quad NO3_{ly}\right]$$ **Equation 46**

$$P_{actualup,ly} = \min\left[P_{up,ly} + P_{demand}, \quad P_{solution,ly}\right]$$ **Equation 47**

where $N_{actualup,ly}$ and $P_{actualup,ly}$ are the effective nitrogen and phosphorus uptake for layer ly (kg /ha), $N_{up,ly}$ and $P_{up,ly}$ are the potential nitrogen and phosphorus uptake for layer ly (kg /ha), N_{demand} and P_{demand} are the nitrogen an phosphorus uptake demand not met by overlying soil layers (kg /ha), and $NO3_{ly}$ and $P_{solution,ly}$ are the nitrate and solution P content of soil layer ly (kg NO3-N/ha and kgP/ha).

Nitrogen Fixation

If nitrate levels in the root zone are insufficient to meet the demand of a legume, SWAT allows the plant to obtain additional nitrogen through nitrogen fixation. Nitrogen fixation is calculated as a function of soil water, soil nitrate content and growth stage of the plant.

$$N_{fix} = N_{demand} \cdot f_{gr} \cdot \min\left(f_{sw}, \quad f_{no3}, \quad 1\right)$$ **Equation 48**

where N_{fix} is the amount of nitrogen added to the plant biomass by fixation (kg N/ha), N_{demand} is the plant nitrogen demand not met by uptake from the soil (kg N/ha), f_{gr} is the growth stage factor (0.0-1.0), f_{sw} is the soil water factor (0.0-1.0), and f_{no3} is the soil nitrate factor (0.0-1.0). The maximum amount of nitrogen that can be fixed by the plant on a given day is N_{demand}.
Growth stage exerts the greatest impact on the ability of the plant to fix nitrogen. The growth stage factor is calculated:

$$\begin{aligned}
f_{gr} &= 0 && \text{when } fr_{PHU} \le 0.15 \\
f_{gr} &= 6.67 \cdot fr_{PHU} - 1 && \text{when } 0.15 < fr_{PHU} \le \\
f_{gr} &= 1 && \text{when } 0.30 < fr_{PHU} \le \\
f_{gr} &= 3.75 - 5 \cdot fr_{PHU} && \text{when } 0.55 < fr_{PHU} \le
\end{aligned}$$ **Equation 49**

where f_{gr} is the growth stage factor and fr_{PHU} is the fraction of potential heat units accumulated for the plant on a given day in the growing season. The growth stage factor is designed to reflect the buildup and decline of nitrogen fixing bacteria in the plant roots during the growing season.

The soil nitrate factor inhibits nitrogen fixation as the presence of nitrate in the soil goes up. The soil nitrate factor is calculated:

$$f_{no3} = 1 \qquad \text{when } NO3 \leq 100$$

$$f_{no3} = 1.5 - 0.0005 \cdot NO3 \qquad \text{when } 100 < NO3 \leq 300 \qquad \textbf{Equation 50}$$

$$f_{no3} = 0 \qquad \text{when } NO3 > 300$$

where f_{no3} is the soil nitrate factor and NO3 is the nitrate content of the soil profile (kg NO3-N/ha).

The soil water factor inhibits nitrogen fixation as the soil dries out. The soil water factor is calculated:

$$f_{sw} = \frac{SW}{.85 \cdot FC} \qquad \textbf{Equation 51}$$

where f_{sw} is the soil water factor, SW is the amount of water in soil profile (mm H2O), and FC is the water content of soil profile at field capacity (mm H2O).

Vegetation Growth

Vegetation growth will be focused on i) Plant total biomass; ii) canopy cover and canopy height and ii) root development. Biomass is computed based on optimal and effective growth (based on plant stresses). Canopy and root partition is computed as a function of plant stage (heat units achieved).

Plant Total Biomass

Optimal

The currently approach used in SWAT and other EPIC-based models is the RUE approach for optimal growth. Interception of photosynthetic active radiation is estimated with Beer's law:

$$H_{phosyn} = 0.5 \cdot H_{day} \cdot \left(1 - \exp\left(k_{\ell} \cdot LAI\right)\right) \qquad \textbf{Equation 52}$$

H_{phosyn} - amount of intercepted photosynthetically active radiation on a given day (MJ m^{-2})

Hday - incident total solar (MJ m-2)

Hday . 0,5 - incident photosynthetically active radiation (MJ m^{-2})

k - Light extinction coefficient

LAI - leaf area index

Potential biomass production per day is estimated with the equation:

$$\Delta bio = RUE \cdot H_{phosyn}$$ **Equation 53**

Δbio - increase in total plant biomass on a given day (kg/ha)

RUE - radiation-use efficiency of the plant (kg/ha $(MJ/m^2)^{-1}$ or g/MJ)

Radiation-use efficiency is sensitive to variations in atmospheric CO_2 concentrations and vapour pressure deficit, equations are taken in account in SWAT.

The daily plant biomass accumulation is determined by:

$$bio = \sum_{i=1}^{d} \Delta bio_i$$ **Equation 54**

bio - total plant biomass on day (kg/ha)

Δbio_i - increase in total plant biomass on day *i* (kg/ha)

Effective

The plant growth factor quantifies the fraction of potential growth achieved on a given day and is calculated:

$$\gamma_{reg} = 1 - \max(wstrs, \quad tstrs, \quad nstrs, \quad pstrs)$$ **Equation 55**

where γ_{reg} is the plant growth factor (0.0-1.0), *wstrs* is the water stress for a given day, *tstrs* is the temperature stress for a given day expressed as a fraction of optimal plant growth, *nstrs* is the nitrogen stress for a given day, and *pstrs* is the phosphorus stress for a given day.

The potential biomass predicted with Equation 53 is adjusted daily if one of the four plant stress factors is greater than 0.0 using the equation:

$$\Delta bio_{act} = \Delta bio \cdot \gamma_{reg}$$ **Equation 56**

where $\Delta bioact$ is the actual increase in total plant biomass on a given day (kg/ha), Δbio is the potential increase in total plant biomass on a given day (kg/ha), and γreg is the plant growth factor (0.0-1.0).

Plant stresses are presented next.

Water stress is simulated by comparing actual and potential plant transpiration:

$$wstrs = 1 - \frac{E_{t,act}}{E_t} = 1 - \frac{w_{actualup}}{E_t}$$ **Equation 57**

wrstrs – water stress for a given day

E_t – maximum plant transpiration on a given day (mm H_2O)

$E_{t,act}$ – actual amount of transpiration on a given day (mm H_2O)

$w_{actualup}$ – total plant water uptake for the day (mm H_2O)

Temperature stress is a function of the daily average air temperature and the optimal temperature for plant growth. The equations used by SWAT to determine temperature stress are:

$$tstrs = 1 \quad \textbf{when} \quad \overline{T_{av}} \le T_{base}$$

$$tstrs = 1 - \exp\left[\frac{-0.1054\left(T_{opt} - \overline{T_{av}}\right)^2}{\left(\overline{T}_{av} - T_{base}\right)^2}\right] \quad \textbf{when} \quad T_{base} < \overline{T}_{av} \le T_{opt}$$

Equation 58

$$tstrs = 1 - \exp\left[\frac{-0.1054\left(T_{opt} - \overline{T_{av}}\right)^2}{\left(2 \cdot T_{opt} - \overline{T}_{av} - T_{base}\right)^2}\right] \quad \textbf{when} \quad T_{opt} < \overline{T}_{av} \le 2 \cdot T_{opt} - T_{base}$$

$$tstrs = 1 \quad \textbf{when} \quad \overline{T}_{av} > 2 \cdot T_{opt} - T_{base}$$

Where:

tstrs – temperature stress for a given day expressed as a fraction of optimal plant growth

$\overline{T}_{av}$ - mean air temperature for day (ºC)

T_{base} – plant's base or minimum temperature for growth (ºC)

T_{opt} - plant's optimal temperature for growth (ºC)

Nitrogen stress is quantified by SWAT comparing actual and optimal plant nitrogen levels. Nitrogen stress varies between 0.0 at optimal nitrogen content and 1.0 when nitrogen content of the plant is 50% or less of the optimal value. It is computed with the equation:

$$nstrs = 1 - \frac{\varphi_n}{\varphi_n + \exp\left[3.535 - 0.02597 \cdot \varphi_n\right]} \qquad \textbf{Equation 59}$$

nstrs - nitrogen stress for a given day

φ_n - scaling factor for nitrogen stress

The scaling factor is calculated:

$$\varphi_n = 200 \cdot \left(\frac{bio_N}{bio_{N,opt}} - 0.5 \right) \qquad \textbf{Equation 60}$$

$bio_{N,opt}$– optimal mass of nitrogen stored in plant material for the current growth stage (Kg N/ha)

bio_N - actual mass of nitrogen stored in plant material (Kg N/ha)

Phosphorus stress is quantified in SWAT by comparing actual and optimal plant phosphorus levels. Phosphorus stress varies between 0.0 at optimal phosphorus content and 1.0 when the phosphorus content of the plant is 50% or less of the optimal value. It is computed with the equation:

$$pstrs = 1 - \frac{\varphi_p}{\varphi_p + \exp\left[3.535 - 0.02597 \cdot \varphi_p\right]} \qquad \textbf{Equation 61}$$

pstrs – phosphorus stress for a given day

φ_p - scaling factor for phosphorus stress

The scaling factor is calculated by:

$$\varphi_P = 200 \cdot \left(\frac{bio_P}{bio_{P,opt}} - 0.5 \right) \qquad \textbf{Equation 62}$$

$Bio_{P,opt}$– optimal mass of phosphorus stored in plant material for the current growth stage (Kg N/ha)

Bio_P - actual mass of phosphorus stored in plant material (Kg N/ha)

Canopy cover and canopy height

In the initial period of plant growth, canopy height and leaf area development are controlled by the optimal leaf area development curve:

$$fr_{LAImx} = \frac{fr_{PHU}}{fr_{PHU} + \exp(\ell_1 - \ell_2 \cdot fr_{PHU})} \quad \textbf{Equation 63}$$

where fr_{LAImx} is the fraction of the plant's maximum leaf area index corresponding to a given fraction of potential heat units for the plant, fr_{PHU} is the fraction of potential heat units accumulated for the plant on a given day in the growing season, and l1 and l2 are shape coefficients. The fraction of potential heat units accumulated by a given date is calculated:

$$fr_{PHU} = \frac{\sum_{i=1}^{d} HU_i}{PHU} \quad \textbf{Equation 64}$$

where fr_{PHU} is the fraction of potential heat units accumulated for the plant on day d in the growing season, HU is the heat units accumulated on day i (heat units), and PHU is the total potential heat units for the plant (heat units).

The shape coefficients are calculated by solving Equation 63 using two known points (fr_{LAI},1,fr_{PHU},1) and (fr_{LAI},2,fr_{PHU},2).

The canopy height on a given day is calculated:

$$h_c = h_{c,mx} \cdot \sqrt{fr_{LAImx}} \quad \textbf{Equation 65}$$

where hc is the canopy height for a given day (m), $h_{c,mx}$ is the plant's maximum canopy height (m), and fr_{LAImx} is the fraction of the plant's maximum leaf area index corresponding to a given fraction of potential heat units for the plant. Once the maximum canopy height is reached, h_c will remain constant until the plant is killed.

For tree stands, the canopy height varies from year to year rather than day to day:

$$h_c = h_{c,mx} \cdot \left(\frac{yr_{cur}}{yr_{fulldev}} \right) \quad \textbf{Equation 66}$$

where h_c is the canopy height for a given day (m), $h_{c,mx}$ is the plant's maximum canopy height (m), yr_{cur} is the age of the tree (years), and $yr_{fulldev}$ is the number of years for the tree species to reach full development (years).

The amount of canopy cover is expressed as the leaf area index. For annuals and perennials, the leaf area added on day i is calculated:

$$\Delta LAI_i = \left(fr_{LAImx,i} - fr_{LAImx,i-1}\right) \cdot LAI_{mx} \cdot \left(1 - \exp(5 \cdot (LAI_{i-1} - LAI_{mx}))\right) \qquad \textbf{Equation 67}$$

while for trees, the leaf area added on day i is calculated:

$$\Delta LAI_i = \left(fr_{LAImx,i} - fr_{LAImx,i-1}\right) \cdot \left(\frac{yr_{cur}}{yr_{fulldev}}\right) \cdot LAI_{mx} \cdot \left(1 - \exp\left(5 \cdot \left(LAI_{i-1} - \left(\frac{yr_{cur}}{yr_{fulldev}}\right) \cdot LAI_{mx}\right)\right)\right) \qquad \textbf{Equation 68}$$

The total leaf area index is calculated:

$$LAI_i = LAI_{i-1} + \Delta LAI_i \qquad \textbf{Equation 69}$$

where ΔLAI_i is the leaf area added on day i, LAI_i and LAI_{i-1} are the leaf area indices for day i and i-1 respectiviely, $fr_{LAImx,i}$ and $fr_{LAImx,i-1}$ are the fraction of the plant's maximum leaf area index calculated with Equation 63 for day i and i-1, LAI_{mx} is the maximum leaf area index for the plant, yr_{cur} is the age of the tree (years), and $yr_{fulldev}$ is the number of years for the tree species to reach full development (years).

The potential leaf area added on a given day is also adjusted daily for plant stress:

$$\Delta LAI_{act,i} = \Delta LAI_i \cdot \sqrt{\gamma_{reg}} \qquad \textbf{Equation 70}$$

where $\Delta LAI_{act,i}$ is the actual leaf area added on day *i*, ΔLAI_i is the potential leaf area added on day *i* that is calculated with Equation 67 or Equation 68, and γ_{reg} is the plant growth factor (0.0-1.0).

Leaf area index is defined as the area of green leaf per unit area of land. Once the maximum leaf area index is reached, LAI will remain constant until leaf senescence begins to exceed leaf growth. Once leaf senescence becomes the dominant growth process, the leaf area index for annuals and perrenials is calculated:

$$LAI = LAI_{mx} \cdot \frac{\left(1 - fr_{PHU}\right)}{\left(1 - fr_{PHU,sen}\right)} \qquad fr_{PHU} > fr_{PHU,sen} \qquad \textbf{Equation 71}$$

While for trees, the calculation is:

$$LAI = \left(\frac{yr_{cur}}{yr_{fulldev}} \right) \cdot LAI_{mx} \cdot \frac{(1 - fr_{PHU})}{(1 - fr_{PHU,sen})} \quad fr_{PHU} > fr_{PHU,sen}$$ **Equation 72**

where LAI is the leaf area index for a given day, LAI_{mx} is the maximum leaf area index, fr_{PHU} is the fraction of potential heat units accumulated for the plant on a given day in the growing season, $fr_{PHU,sen}$ is the fraction of growing season (PHU) at which senescence becomes the dominant growth process, yr_{cur} is the number of years of development the tree has accrued (years), and $yr_{fulldev}$ is the number of years for the tree species to reach full development (years).

Root development

In SWAT the amount of total biomass portioned to the root system is 30-50% in seedlings and decreases to 5-20% in mature plants. SWAT varies the fraction of total biomass in roots, from 0.40 at emergence to 0.20 at maturity.

To calculate the daily root biomass fraction the following equation is used:

$$fr_{root} = 0.40 - 0.20 \cdot fr_{PHU}$$ **Equation 73**

frroot - fraction of total biomass partitioned to roots on a given day in the growing season

frPHU - fraction of potential heat units accumulated for the plant on a given day in the growing season

For perennials and trees, SWAT assumes:

$$z_{root} = z_{root,mx}$$ **Equation 74**

z_{root} - depth of root development in the soil on a given day (mm)

$z_{root,mx}$ - maximum depth for root development in the soil (mm).

For annuals, the simulated root depth varies linearly form 0.0 mm, at the beginning of the growing season, to the maximum rooting depth at *frPHU* = 0.40 using the equation:

$$z_{root} = 2.5 \cdot fr_{PHU} \cdot z_{root,mx} \qquad \text{if } fr_{PHU} \leq 0.40$$
$$z_{root} = z_{root,mx} \qquad \text{if } fr_{PHU} > 0.40$$ **Equation 75**

z_{root} - depth of root development in the soil on a given day (mm) *frPHU* - fraction of potential heat units accumulated for the plant on a given day in the growing season

$z_{root,mx}$ - maximum depth for root development in the soil (mm)

Harvest/Kill

Optimal

When a harvest or harvest/kill operation is performed, a portion of the plant biomass is removed from the HRU as yield. The nutrients and plant material contained in the yield are assumed to be lost from the system (i.e. the watershed) and will not be added to residue and organic nutrient pools in the soil with the remainder of the plant material. In contrast, a kill operation converts all biomass to residue. However, a harvest efficiency can be defined and the remained biomass is converted to residue. The fraction of the above-ground plant dry biomass removed as dry economic yield is called the harvest index. For the majority of crops, the harvest index will be between 0.0 and 1.0. However, plants whose roots are harvested, such as sweet potatoes, may have a harvest index greater than 1.0.

The economic yield of most commercial crops is the reproductive portion of the plant. Decades of crop breeding have led to cultivars and hybrids having maximized harvest indices. Often, the harvest index is relatively stable across a range of environmental conditions.

SWAT calculates harvest index each day of the plant's growing season using the relationship:

$$HI = HI_{opt} \cdot \frac{100 \cdot fr_{PHU}}{\left(100 \cdot fr_{PHU} + \exp\left[11.1 - 10 \cdot fr_{PHU}\right]\right)}$$

Equation 76

where HI is the potential harvest index for a given day, HIopt is the potential harvest index for the plant at maturity given ideal growing conditions, and frPHU is the fraction of potential heat units accumulated for the plant on a given day in the growing season.

Crop yeld is calculated:

$$yld = bio_{ag} \cdot HI \qquad \text{when } HI \leq 1.00$$

Equation 77

$$yld = bio \cdot \left(1 - \frac{1}{(1 + HI)}\right) \qquad \text{when } HI > 1.00$$

where yld is the crop yield (kg/ha), bio_{ag} is the aboveground biomass on the day of harvest (kg ha-1), HI is the harvest index on the day of harvest, and bio is the total plant biomass on the day of harvest (kg ha-1). The aboveground biomass is calculated:

$$bio_{ag} = (1 - fr_{root}) \cdot bio$$

Equation 78

where fr_{root} is the fraction of total biomass in the roots the day of harvest, and bio is the total plant biomass on the day of harvest (kg ha-1).

The amount of nutrients removed in the yield are calculated:

$$yld_N = fr_{N,yld} \cdot yld$$

Equation 79

$$yld_P = fr_{P,yld} \cdot yld$$

where yldN is the amount of nitrogen removed in the yield (kg N/ha), yldP is the amount of phosphorus removed in the yield (kg P/ha), frN,yld is the fraction of nitrogen in the yield, frP,yld is the fraction of phosphorus in the yield, and yld is the crop yield (kg/ha).

Effective

The harvest index predicted with equation for optimal is affected by water deficit using the relationship:

$$HI_{act} = (HI - HI_{min}) \cdot \frac{\gamma_{wu}}{\gamma_{wu} + \exp[6.13 - 0.883 \cdot \gamma_{wu}]} + HI_{min}$$

Equation 80

where HIact is the actual harvest index, HI is the potential harvest index on the day of harvest calculated with equation for optimal HI, HImin is the harvest index for the plant in drought conditions and represents the minimum harvest index allowed for the plant, and γwu is the water deficiency factor. The water deficiency factor is calculated:

$$\gamma_{wu} = 100 \cdot \frac{\sum_{i=1}^{m} E_a}{\sum_{i=1}^{m} E_o}$$ **Equation 81**

where Ea is the actual evapotranspiration on a given day, Eo is the potential evapotranspiration on a given day, i is a day in the plant growing season, and m is the day of harvest if the plant is harvested before it reaches maturity or the last day of the growing season if the plant is harvested after it reaches maturity.

In the harvest only operation, the model allows the user to specify a harvest efficiency. The harvest efficiency defines the fraction of yield biomass removed by the harvesting equipment. The remainder of the yield biomass is converted to residue and added to the residue pool in the top 10 mm of soil. If the harvest efficiency is not set or a 0.00 is entered, the model assumes the user wants to ignore harvest efficiency and sets the fraction to 1.00 so that the entire yield is removed from the HRU.

$$yld_{act} = yld \cdot harv_{eff}$$ **Equation 82**

where yldact is the actual yield (kg ha-1), yld is the optimal crop yield calculated (kg ha-1), and harveff is the efficiency of the harvest operation (0.01-1.00). The remainder of the yield biomass is converted to residue:

$$\Delta rsd = yld \cdot \left(1 - harv_{eff}\right)$$

Equation 83

$$rsd_{surf,i} = rsd_{surf,i-1} + \Delta rsd$$

where Δrsd is the biomass added to the residue pool on a given day (kg ha-1), yld is the optimal crop yield calculated (kg ha-1) and harveff is the efficiency of the harvest operation (0.01-1.00) rsdsurf,i is the material in the residue pool for the top 10 mm of soil on day i (kg ha-1), and rsdsurf,i-1 is the material in the residue pool for the top 10 mm of soil on day i-1 (kg ha-1).

Annex 2 – Sediment Quality Model

This annex describes the main RZWQM equations and the approach to make it dimensional correct yielding similar results as with original formulation.

Soil bacteria are responsible for organic matter decay and nitrification processes that make available dissolved nutrients (ammonia, nitrate, dissolved inorganic phosphorus) to plants and to leaching, and denitrification processes that can be important in wetlands as a nitrogen sink to atmosphere.

Sediment quality model in MOHID Land is a module for bacteria driven activity as mineralization, nitrification and denitrification processes in soil and was adapted from RZWQM (Ma et al., 2000).

Microorganism population has autotrophic, heterotrophic aerobic and anaerobic, and solubilizing bacteria population types where carbon, nitrogen and phosphorus composition are dependent on growth, death and respiration processes:

Equation 84. Carbon, nitrogen and phosphorus content evolution for each microorganism type.

$$\frac{dC_{micro}}{dt} = \left(K_{growth}C - K_{resp}C - K_{death}C\right) * C_{micro}$$

$$\frac{dN_{micro}}{dt} = \left(K_{growth}N - K_{resp}N - K_{death}N\right) * N_{micro}$$

$$\frac{dP_{micro}}{dt} = \left(K_{growth}P - K_{resp}P - K_{death}P\right) * P_{micro}$$

Where C_{micro}, N_{micro}, P_{micro} are carbon, nitrogen and phosphorus content of microorganisms (mg/L), respectively, and K_{growth}, K_{resp} and K_{death}, are growth, respiration and death rates (day^{-1}).

Bacteria growth is obtained trough mineralization, nitrification or denitrification (decay rates). The respiration is dependent on microorganisms efficiency on processing substrate and for microorganism nitrogen and phosphorus, ratios to carbon are used (microorganism need to maintain C:N and C:P ratios and excrete nitrogen or phosphors if above ratio or assimilate them if below).

Next equations show the computation of the microorganisms growth, respiration and death rates.

Equation 85. Rates for growth, rspiration and death of microorganisms.

$$K_{growth}C = K_{decay}$$

$$K_{resp}C = K_{decay} * OrganismEfic$$

$$K_{growth}N = K_{decay} * \frac{1}{OM\_C:N}$$

$$K_{resp}C = K_{decay} * \frac{OrganismEfic}{Organism\_C:N}$$

$$K_{growth}P = K_{decay} * \frac{1}{OM\_C:P}$$

$$K_{resp}P = K_{decay} * \frac{OrganismEfic}{Organism\_C:P}$$

Where K_{decay} is growth, respiration or death rate (day^{-1}), OrganismEfic is the microorganism efficiency to the decay process (-) and is a parameter, and OM_C:N is organic matter carbon to nitrogen ratio, OM_C:P is organic matter C:P ratio, Organism_C:N is microorganism C:N ratio and Organism_C:P is microorganism C:P ratio and are all defined parameters for each organism type.

Base Formulation

The original RZWQM model formulation has decay rates and death rates with and without substrate (organic matter that needs to exist for processes). This formulation is presented next.

Decay rates

For decay rates the generic following equation is used (some process require an organic substrate as denitrification), where aerobiose/anaerosbiose, temperature, oxygen and pH dependence is computed:

Equation 86. RZWQM decay rates.

$$K_{decay} = f_{aer} \times \left(\frac{K_b \times T_p}{h_p} \times A_{decay} \right) \times e^{\left(\frac{-Ea}{Rg \times T_p} \right)} \times \frac{[O_2]}{[H^+]^{Khn}} \times Pop_{micro} \times Adj \times [Substrate]$$

$$Khn = 0.166665 \; if \;\; pH \le 7$$

$$Khn = -0.3333 \; if \;\; pH > 7$$

$$Adj = 1 \; if \;\; pH \le 7$$

$$Adj = 3159.7 \; if \;\; pH > 7$$

Where:

f_{aer} - Aerobic factor

f_{anaer} - Anaerobic factor

K_b - Boltzman constant J × K^{-1}

T_p - temperature K

h_p - Planck constant J × s

Rg - Universal gas constant Kcal / mole / K

A_{decay} - decay coefficient s. day-1.pop-1

Ea - Apparent activation energy Kcal ×$mole^{-1}$

O2 - Oxygen concentration in soil, assuming soil air not limited mol / L

H^+ - Hydrogen mol / L

Khn - exponent for hydrogen ion

pop – microorganisms population #org / kgsoil

Adj - Coefficient dependent of the soil pH

The dimensional analysis of the equation yields inconsistent units between both sides of the equation. In Figure 9 is presented the dimensional analysis of the equation where parameters Khn and Adj make impossible to get consistent unis in both sides of the equation.

$$[day-1]???[subst] = [-] \times \left(\frac{[J.^{\circ}K^{-1}] \times [^{\circ}K]}{[J.s]} \times [s.day^{-1}.pop^{-1}] \right) \times e^{\left(\frac{-[kcal.mole^{-1}]}{[kcal.mole^{-1}.^{\circ}K^{-1}] \times [^{\circ}K]} \right)} \times \frac{[molO_2.L^{-1}]}{[molH^+.L^{-1}]^{[???]}} \times Pop_{micro} \times [???] \times [subst]$$

Figure 9. Dimensional analysis on RZWQM original decay rates.

Death rates

For death rates the generic following equation is used, where aerobiose/anaerosbiose, temperature, oxygen and pH dependence is computed:

Equation 87. RZWQM death rates.

$$K_{death} = \left(\frac{1}{f_{aer} \; or \; f_{anaer}} \right) \times \frac{\left(\frac{K_b \times T_p}{h_p} \times A_{decay} \right)}{e^{\left(\frac{-Ea}{Rg \times T_p} \right)}} \times \frac{[H^+]^{Khn}}{[O_2]} \times Pop_{micro} \, / \, Adj \times \frac{1}{[Substrate]}$$

In **Error! Reference source not found.** is presented the dimensional analysis of the quation where parameters Khn and Adj make impossible to get consistent unis in both sides of the equation.

$$\frac{[day-1]???}{[Subs]} = [-] \times \frac{\left(\frac{[J.^{\circ}K^{-1}] \times [^{\circ}K]}{[J.s]} \times [s.day^{-1}.pop^{-1}] \right)}{e^{\left(\frac{-[kcal.mole^{-1}]}{[kcal.mole^{-1}.^{\circ}K^{-1}] \times [^{\circ}K]} \right)}} \times \frac{[molH^{+}.L^{-1}]^{[???]}}{[molO_2.L^{-1}]} \times Pop_{micro} / [???] \times \frac{1}{[Subs]}$$

Figure 10. Dimensional analyses on RZWQM on original death rates

The dimensional inconsistencies in original formulation led to a reformulation of the equations.

New Formulation

Due to the difficulty to verify dimensional analysis in the original RZWQM ecay and death equations, the base formulation was changed in the scope of this thesis to a general approach where a maximum rate exists (the optimum rate, only affected by temperature) and then multipliers (between 0 and 1) to account for aerobiose/anaerobiose, oxygen, nutrient, pH and substrate effect on maximum rate (maintenance in case of optimum conditions or reduction in case of less optimum conditions). This approach is similar to a general approach in water quality models as for example “Water Quality” in MOHID framework.

Decay rates

The decay rate was changed to have a maximum rate and multipliers to account limiting factors as water content (aerobiose/anaerobiose), oxygen, pH, substract, etc.) - Equation 88.

Equation 88. Adapted decay rates.

$$K_{decay} = MaximumRate \times \psi(aer/anaer) \times \psi(Oxigen) \times \psi(pH) \times \psi(Substrate\_Decay)$$

Figure 11 shows the decay rates dimensional analysis very straightforward with the resulting rate (day^{-1}) is the maximum rate (day^{-1}) multiplied by adimensional multipliers between 1 and 0 where 1 is optimal conditions and 0 worst conditions (no decay).

$$\left[day^{-1}\right]=\left[day^{-1}\right]\times\left[0-1\right]\times\left[0-1\right]\times\left[0-1\right]\times\left[0-1\right]$$

Figure 11 . Adapted decay rates units.

The maximum rate is only temperature dependent (activation energy process computation taken from RZWQM) - Equation 89 and Figure 12.

Equation 89. Adapted decay rates maximum rate.

$$MaximumRate=\left[\left(\frac{K_b\times T_p}{h_p}\times A_{decay}\right)\times e^{\left(\frac{-Ea}{Rg\times T_p}\right)}\right]\times Pop_{micro}$$

$$\left[day^{-1}\right]=\left[\left(\frac{\left[J.^{\circ}K^{-1}\right]\times\left[^{\circ}K\right]}{\left[J.s\right]}\times\left[s.day^{-1}.pop^{-1}\right]\right)\times e^{\left(\frac{-\left[kcal.mole^{-1}\right]}{\left[kcal.mole^{-1}.^{\circ}K^{-1}\right]\times\left[^{\circ}K\right]}\right)}\right]\times Pop_{micro}$$

Figure 12. Adapted decay rate maximum rate dimensional analysis.

Death rates

Death rates in the adapted version have a similar concept but the multipliers have a complementary value to decay rates (1 is worst conditions – higher death rate, and 0 is best condition – no death rate) as expressed in Equation 90 and Figure 13.

Equation 90. Adapted death rates maximum rate.

$$K_{decay}=MaximumRate\times\frac{1}{\psi(aer/anaer)}\times(1-\psi(Oxigen))\times(1-\psi(pH))\times\psi(Substrate\_Death)$$

$$MaximumRate=\left[\frac{\left(\frac{K_b\times T_p}{h_p}\times A_{decay}\right)}{e^{\left(\frac{-Ea}{Rg\times T_p}\right)}}\right]\times Pop_{micro}$$

Figure 13. Adapted death rates maximum rate dimensional analysis.

In the following points are presented the computations of rates multipliers that were introduced.

pH term - ψ(pH)

The pH term computation follows the same concept already in RZWQM where a optimum pH exists for the microorganisms and lower or higher values interfere with microorganisms optimum activity (Equation 91 and Figure 14) resulting in similar behaviour.

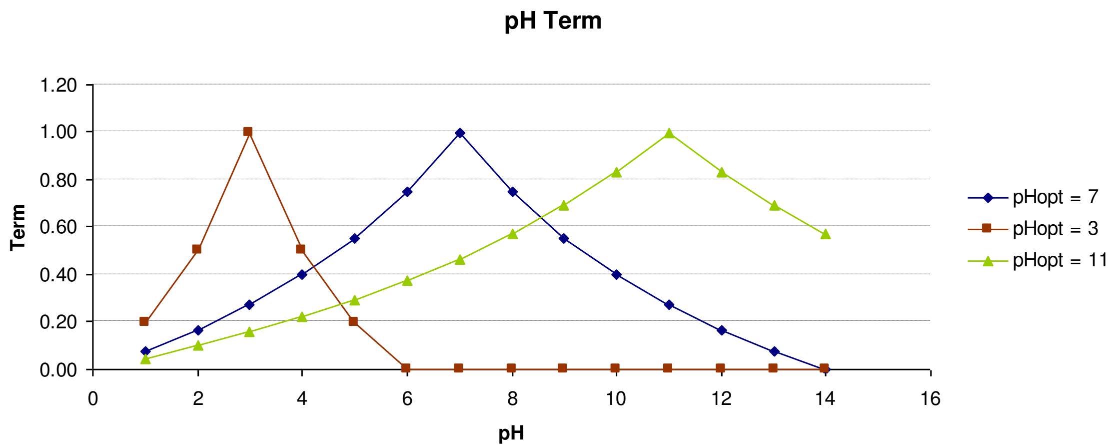

Figure 14. pH term variation with diferent optimum values.

The equations for pH term is described in Equation 91 and give a symmetric triangle around optimum. The original formulation from RZWQM tends to decrease highly the term for basic pH, meaning that in the original model the microorganisms tend to stress out more with basic than acid pH. The new model may be changed in the future to adapt to that behaviour.

Equation 91. pH term computation.

$$if\ \ pH > pHopt \Rightarrow pHused = 2 \times pHopt - pH$$

$$term = \frac{pHused}{2 \times pHopt - pHused}$$

Oxygen Term and decay substrate term - ψ(Oxygen) and ψ(substrate_Decay)

The oxygen and substrate terms (for decay) express the need of these substances for the decay processes (that need oxygen and substrate) and so are 1 if the concentration is higher than the optimum and linearly reduce if lower (Figure 15 and Equation 92). These curves can be dynamically changed in the future to implement exponential or other type of reduction.

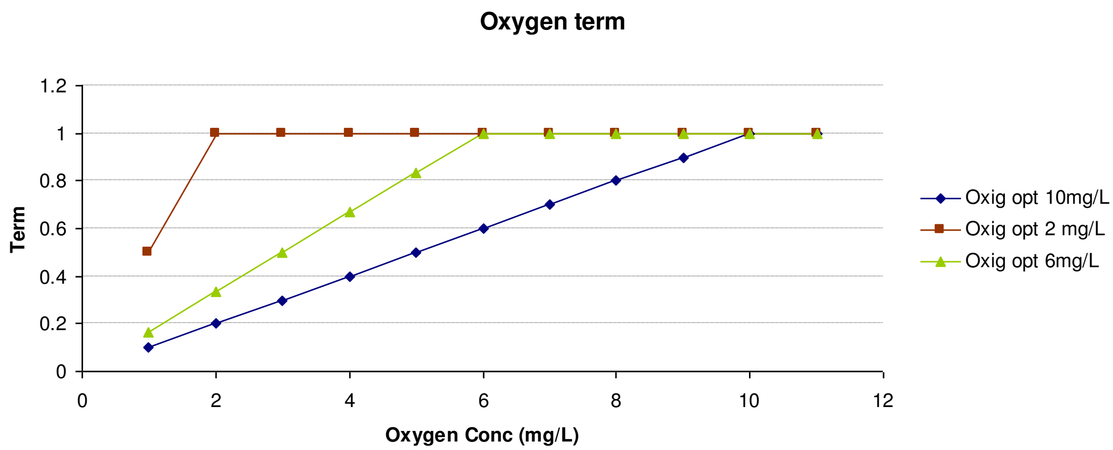

Figure 15. Oxygen and substrate term variation for diferente optimum values.

Equation 92. Oxygen and substrate term computation.

$$term = \min\left(\frac{Conc}{OptConc};1\right)$$

For concentrations lower than optimum the term will be lower as the concentration lows. For concentrations higher than optimum there will not be “food” stress and term is 1. This assumes that the concentrations are not toxic at high values (this formulation is used in the model for soil carbon and oxygen).

Death substrate term - ψ(substrate_Death)

The substrate term for death express the need of this substances for the decay processes (that need substrate) but because is for death computation are inversed of the previous one and so are 0 if the concentration is higher than the optimum and linearly reduce if lower (higher substrate limitation and death rates) - Equation 93 and Figure 16.

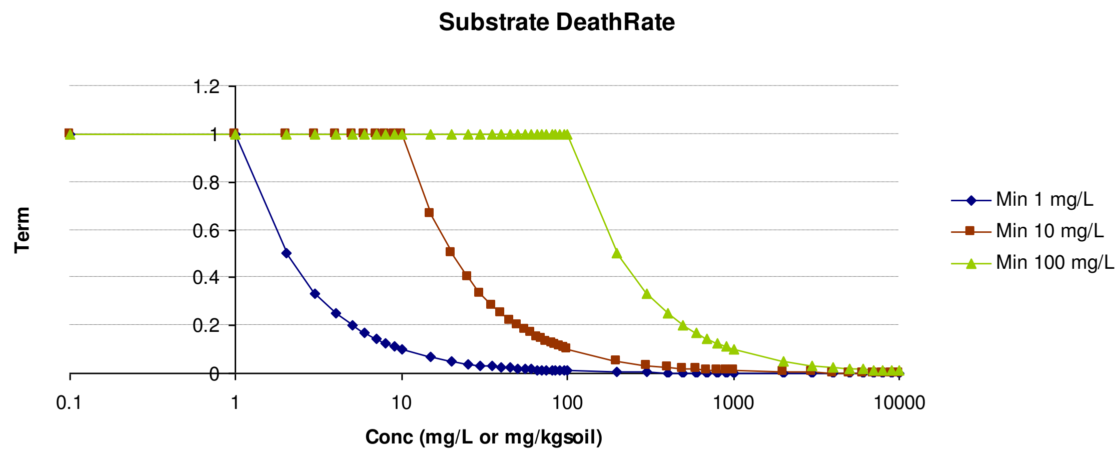

Figure 16. Substrate term variation in death rates for diferente optimum values.

Equation 93. Substrate term variation in death rates computation.

$$term = \min\left(\frac{MinConc}{Conc};1\right)$$

For concentrations lower than minimum the term will be 1 meaning that death rate will be maximum from this component. As concentration rises above minimum, “food” is more available and decreases limitation and term lowers. At really high concentration the term is almost zero making the death rate also close to zero.